CONSOLIDATION OF FIBER-REINFORCED COMPOSITES WITH THERMOPLASTIC MATRICES

A Thesis

Presented to

The Academic Faculty

By

Jurron Bradley

In Partial Fulfillment

Of the Requirements for the Degree

Doctor of Philosophy

School of Chemical Engineering

Georgia Institute of Technology

January 2001

CONSOLIDATION OF FIBER-REINFORCED COMPOSITES WITH THERMOPLASTIC MATRICES

Approved by:

Dr. John Muzzy, Chairman

Dr. Jonathan Colton

Dr. Karl Jacob

Dr. Jeffrey Morris

Dr. Mary Rezac

Date Approved: 2/24/01

dedicated to the little people

ACKNOWLEDGEMENTS

I am greatly indebted to my thesis advisor, Dr. John D. Muzzy, for his guidance, patience, and support. Furthermore, I would like to thank Dr. Jonathan Colton, Dr. Jeffrey Morris, Dr. Mary Rezac, and Dr. Karl Jacob for serving on my thesis reading committee. In addition, I would like to thank Dr. Colton for help with the Wabash press.

I also would like to thank Dr. Satish Kumar for use of rheometer equipment, Yolande Berta for the use and help with SEM equipment, and Dr. Haskell Bechkham for use of TGA equipment.

Next, I am grateful for the financial support from the National Science Foundation Composite Traineeship. I would also like to thank John Manville, Inc. for donating glass mat and Vetrotex for donating Twintex®.

I am obliged to the entire Center for Polymer Processing group for helpful suggestions and assistance. Specifically, I would like to thank Jeff Toke for assistance with DSC analysis and mold design. Furthermore, I am very grateful for the work of several undergraduate assistants: Nathan Williams, Susan Fangmann, Jeff Pfaendtner, and Terrence Byrd.

I would like to acknowledge my friends for all their support, good times, and memories: Mark Abbett, Gabe Banks, Esq., Mechelle Barnes, Dr. Paul Canatella, Terra Chaney, George Davidson, Timmy Duncan, Scottie Eggleston, Dr. Tonya Hall, Tony Holloway, George Hill, Henry Hipps, Scottie Jackson, Derrick Kidani, Willie Maul, Dr.

Devin McCallister, Katina McKinney, Jonathan Pettigrew, Patric Quinney, Travis Reed, Dr. Kip Sturgill, Marcus Thomas, Tremell Watson, Dr. Kim Webb, Terry White, Stephanie Williams, and William Wyatt.

Finally, I would like to thank my parents, Julius and Deborah Bradley, my sister, Juronica Bradley, and the Jones, Bradley, and Young families for their unconditional love, support, and prayers.

TABLE OF CONTENTS

LIST OF TABLES

LIST OF FIGURES

LIST OF SYMBOLS

A	=	surface area, m^2
A_{mold}	=	cross sectional area of mold, m^2
A_w	=	area weight of fiber mat, g/m^2
d	=	distance between cylinder centers, m
D_f	=	diameter of single fiber filament, m
E	=	percent deviation, %
h	=	gap width, m
K_1	=	tortuosity, dimensionless
m	=	power-law consistency index, $Pa\text{-}s^n$
m_f	=	mass of mats, kg
n	=	power-law flow index
P	=	dimensionless pressure
p	=	number of experimental observations
P	=	pressure, Pa
P_c	=	capillary pressure, Pa
Q	=	flow rate through cell, m^2/s
R	=	cylinder radius, m
r	=	dimensionless radial coordinate
R	=	fiber radius, m
r	=	radius of cylinder, m

R_e = Reynolds number, dimensionless

R_∞ = radius of fluid envelope, m

r_f = radius of fiber, m

r_h = hydraulic radius, m

s_X = standard deviation of X, mm

s_n = standard deviation of n

s_m = standard deviation of m

s_ε = standard deviation of ε

s_Λ = standard deviation of Λ

t = time, s

U = average fluid velocity in tube, m/s

v_f = fiber volume fraction, dimensionless

V = average flow rate per unit area, m/s

V = superficial velocity, m/s

V_f = volume of fibers, m^3

V_m = volume of mold, m^3

V_o = superficial velocity, m/s

V_r = dimensionless velocity in r-direction

v_{void} = void content, dimensionless

v_{void} = void content of the composite, dimensionless

v_{voidi} = initial void content, dimensionless

V_θ = dimensionless velocity in θ-direction

W_c = weight of composite sample, g

W_{fc} = weight of fibers in composite sample, g

W_{ca} = weight of composite sample in air, kg

W_{ce} = weight of composite sample in ethanol, kg

w_f = weight percent of fiber in the composite, %

w_r = weight percent of resin in the composite, %

X = distance from inlet of cell, m

X = penetration depth, permeation depth, mm

X = thickness of fiber bed, m

X_c = thickness of fiber bed available for flow, m

X_{exp} = experimental penetration depth, mm

X_{pred} = predicted penetration depth, mm

Δh = thickness change, mm

ΔP = fluid pressure drop, Pa

Γ = gamma function

Π = second invariant of the rate of deformation tensor

δ = thickness of mat under pressure, m

ε = porosity, dimensionless

γ_w = wall shear rate, 1/s

$\dot{\gamma}$ = shear rate, 1/s

ε_{ij} = components of the rate of deformation tensor, 1/s

γ = experimental specific gravity of composite, dimensionless

η = viscosity, Pa-s

ρ = density, kg/m^3

ρ_{ce} = experimental density of the composite, kg/m^3

ρ_{ct} = theoretical density of the composite, kg/m^3

ρ_e = density of ethanol, kg/m^3

ρ_f = density of fiber, g/m^3

ρ_r = density of resin, kg/m^3

σ = surface tension of polymer, Pa-m

τ_{ij} = components of stress tensor, Pa

SUMMARY

A continuous fiber-reinforced polymer (CFRP) composite is a material composed of reinforcing fibers that are held together with a polymer matrix. Thermoplastics are rarely used in CFRP composites. Two reasons for this include the high viscosity of thermoplastic materials and the lack of processing information available for continuous fiber-reinforced thermoplastics. Because of the high viscosity of thermoplastics, the rate-limiting step in producing continuous fiber-reinforced thermoplastics is the slow permeation of the resins through the fiber bed. Therefore, it is important to quantify the permeation process.

There is little experimental or theoretical work reported on the transverse permeation of thermoplastics through beds of fibers. With this in mind, the fundamental objective of this thesis was to answer three questions:

1. Can the transverse permeation process during thermoplastic composite processing be modeled with semi-empirical and theoretical models?
2. Which model more accurately models the permeation process?
3. Are the models valid for different materials and processing conditions?

To answer these questions, several permeation experiments were performed, and semi-empirical and mechanistic models were used to describe the permeation process. A variety of thermoplastics, fibers, preforms, and processing conditions were used in the

permeation experiments. The semi-empirical model was referred to as the Semi-empirical model, and the mechanistic models were referred to as the Vijaysri and Bruschke models, respectively. Compression molding, a common composite processing technique, was used to study the permeation.

There was good agreement between all the models and the experimental results. The Semi-empirical and Bruschke models gave matching predictions that were slightly better than the Vijaysri model. With this in mind, it was recommended to use the Bruschke model to quantify the transverse permeation of thermoplastic through beds of fibers. The reason for this recommendation was that the Bruschke model, unlike the Semi-empirical model, did not require an empirical constant as an input parameter.

Another goal of this thesis was to derive a model to predict the void content of thermoplastic composites. The Bruschke model was used as a basis for the void content model. There was good agreement between the theoretical and experimental void contents.

CHAPTER I
INTRODUCTION

1.1 Introduction

A continuous fiber-reinforced polymer (CFRP) composite is a material composed of reinforcing fibers that are held together with a polymer matrix. Thermoplastics are rarely used in CFRP composites. Two reasons for this include the high viscosity of thermoplastic materials and the lack of processing information available for continuous fiber reinforced thermoplastics. Because of the high viscosity of thermoplastics, the rate-limiting step in producing continuous fiber reinforced thermoplastics is the slow permeation of the resins through the fiber bed. Therefore, it is important to quantify the permeation process.

The permeation process can be described as flow through a porous medium. In the case of CFRP composite processing, the porous medium is a fiber bed. Because of the cylindrical shape of fibers, the fiber beds can be viewed as a bed of long, solid cylinders. Furthermore, the fibers in the beds can be arranged in many directions relative to each other. To illustrate this point, Figure 1.1 is a schematic of two common arrangements of the fiber bed: unidirectional and random.

There is little experimental or theoretical work reported on the transverse flow of non-Newtonian fluids through beds of cylinders. Figure 1.2 is a schematic to illustrate transverse permeation.

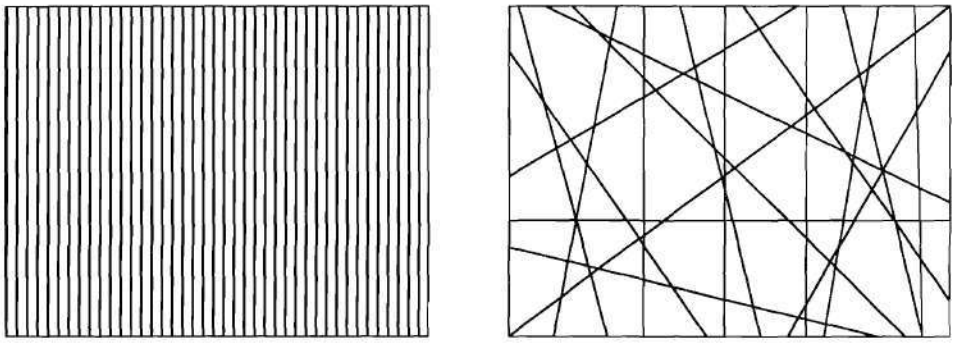

Figure 1.1: Illustration of unidirectional and random fiber arrangements.

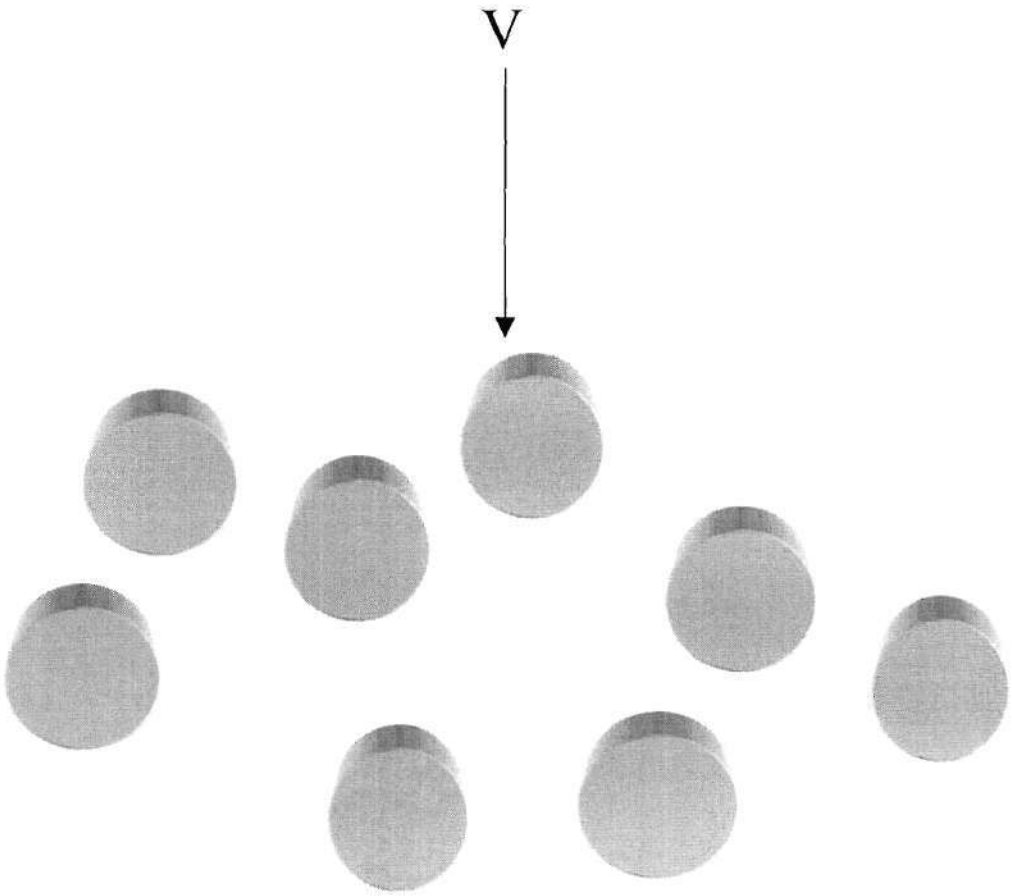

Figure 1.2: Illustration of transverse permeation of a fluid through a bed of cylinders where V is the superficial velocity of a fluid permeating through the bed.

Most of the experimental studies that are reported are on the flow of non-Newtonian polymer solutions normal to aluminum and steel cylinders arranged in a specific manner, such as a square array. These experimental studies were conducted in the porosity range of 0.4-0.7. In addition, the diameters of the metal cylinders were 100-9,525 μm. In contrast, the common porosity range in CFRP processing is 0.25-0.7, and the fibers in CFRP composites are not perfectly arranged. Furthermore, the diameters of the fibers are usually about 7-16 μm. A review of the literature suggests that there is a need for a comprehensive experimental study on the transverse permeation of thermoplastics through beds of fibers.

Also, there is little theoretical work reported on the transverse permeation of non-Newtonian fluids through beds of cylinders. The theoretical approaches reported are based on idealized periodic arrangements or unit cells of the bed of cylinders. Figure 1.3 is a schematic of the typical square unit cell assumption. In the literature, numerical and analytical methods were used to solve the momentum equations for the two dimensional flow of a power-law fluid through the unit cells. In terms of CFRP processing, a possible disadvantage of this approach could be the highly idealized nature of the fiber arrangement assumption. The fiber beds used in composite processing do not have perfect arrangements. The advantage of this idealized approach is that no empirical constants are needed.

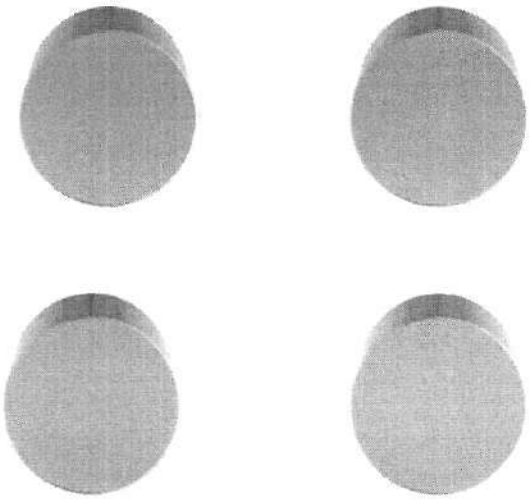

Figure 1.3: Illustration of a square arrangement of cylinders or fibers.

Because of the complexity of fiber beds, a semi-empirical approach may be more successful at describing the transverse permeation. The semi-empirical approach is based on the equation for the flow of a power-law fluid through a straight, circular tube. This equation is corrected for the tortuosity and the geometry of the fiber bed by using an empirical constant. A possible disadvantage of this model is that the constant may vary with material and processing condition selections. The advantage of this model is its simplicity. The validity of the theoretical equations and the semi-empirical equation for CFRP composite processing needs to be studied.

1.2 Motivation, Objectives and Project Description

The motivation behind this work was the lack of processing information available for the transverse permeation of thermoplastics through a bed of fibers. The fundamental objective of this thesis was to answer three questions:

1. Can the transverse permeation process during thermoplastic composite processing be modeled with semi-empirical and theoretical models?
2. Which model more accurately models the permeation process?
3. Are the models valid for different materials and processing conditions?

To answer these questions, a semi-empirical model and two mechanistic models were used to describe the permeation process, and several experiments were run to test the models. Another goal of this thesis was to use materials and processing conditions

commonly used in the composite industry. With this in mind and because of the need for experimental data on transverse permeation during thermoplastic composite processing, a variety of fibers, resins, preforms, and processing conditions were used to answer question number three above. In this work, carbon, glass, and sisal fibers were used for the fiber beds. Polypropylene, nylon 6, and polyphenylene sulfide were used as the resins. In addition, three types of composite preforms were studied: random mat, powder-coated towpreg, and commingled fibers. The random mat was composed of fibers that were randomly arranged to each other. The powder-coated towpreg and commingled fibers were composed of fibers arranged unidirectionally. The porosity range studied was 0.24-0.71. Compression molding, a common thermoplastic composite processing technique, was used to study the transverse permeation process.

Finally, another goal of this research was to model the void content of the composites made from the permeation experiments with the towpreg and commingled fiber preforms as a function of processing pressure and temperature and material parameters. Void content refers to empty space in a composite. For example, if a polymer does not completely fill the empty spaces in a fiber bed during the permeation process, the composite will contain voids. The presence of voids in a composite can be detrimental to its mechanical properties and its resistance to environmental effects like moisture. Therefore, it is essential to use the proper processing and material conditions to minimize voids.

1.3 Summary

The motivation behind this work is the lack of processing information available for the transverse permeation of thermoplastics during CFRP processing. A general, predictive permeation model would aid in reducing the number of trial and error experiments required to determine optimum thermoplastic composite processing conditions. In addition, a large database of experimental results of the transverse permeation of thermoplastics during CFRP processing would be beneficial.

1.4 Thesis Outline

In Chapter II of this thesis the following are discussed: definitions of composite terms, composite processing, composite materials, and a literature review on transverse permeation of non-Newtonian fluids through beds of cylinders. In Chapter III, the theory used to describe the transverse permeation process in this research is detailed. Chapter IV lists the materials and methods used to study transverse permeation. A discussion of results is given in Chapter V. Conclusions and recommendations are presented in Chapter VI.

CHAPTER II

BACKGROUND

2.1 Introduction

In Section 2.2 the following are discussed: definition of composites, fibers, resins, preforms, and processing. In Section 2.3 a literature review on transverse permeation through beds of cylinders is discussed. In Section 2.4 a summary is given. References are listed in Section 2.5.

2.2 Definition of Composite

A composite is a multi-phase material where the interaction of the phases usually produces properties different from the individual phases. A continuous fiber-reinforced polymer (CFRP) composite contains two phases. These two phases are referred to as the reinforcement phase and the matrix phase. The reinforcement phase is a fiber, and the matrix phase is a polymer. The fiber carries the load, whereas the matrix binds the fiber, protects the fiber from environmental damage, and transfers the load.

2.2.1 Fibers

Fibers often constitute the largest volume fraction of the composite. Therefore it is essential to properly select the fiber in these composites because the fibers influence many characteristics and properties of the composite. Some of these characteristics and properties are specific gravity, tensile strength and modulus, compressive strength and

modulus, fatigue strength, electrical and thermal conductivities, and cost. The most commonly used fibers are glass and carbon. In addition, fibers are typically sold in tow form or mat form. A tow is a collection of single fiber filaments, and a mat is composed of single fiber filaments or tows bound together in the form of a mat. An important feature of a fiber bed in a composite is the arrangement of fibers relative to each other. Typical arrangements of the fibers are unidirectional and random. Figure 2.1 is a simple orthogonal view of typical fiber arrangements and a schematic of a fiber tow. In this research, glass, carbon, and sisal fibers were used.

2.2.2 Matrix

In CFRP composites, the matrix phase is a polymer. Polymers can be divided into two categories: thermoset and thermoplastic.

Thermosets are produced by curing and are chemically joined by crosslinks. Because of these links, thermosets are composed of rigid three-dimensional networks. In general, thermosets are thermally stable and are resistant to many chemicals. In comparison to thermoplastics, they experience less creep and stress relaxation. Disadvantages of thermosets include limited shelf life at room temperature before curing, long fabrication times due to curing requirements, and low strain-to-failure. Another disadvantage is their inability to be melted and reshaped.

The CFRP composites industry utilizes thermosets more frequently than thermoplastics. The reason for this is because thermosets are easier to process and are well understood and documented. Typical thermosets used in CFRP composites are epoxies, polyesters, and vinyl esters.

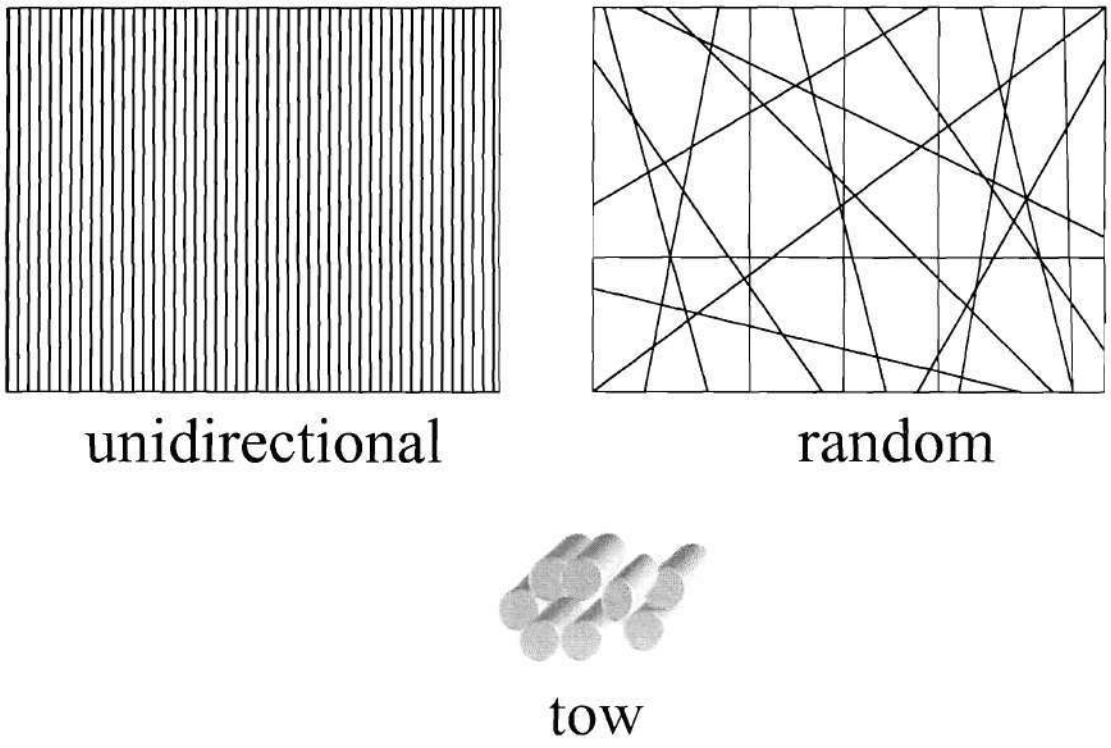

Figure 2.1: Fiber arrangements and fiber tow.

Thermoplastics are linear chain molecules and do not contain crosslinks. The chains are held together by weak secondary bonds. Because of this, thermoplastics can be melted and reshaped. Other advantages of thermoplastics over thermosets include unlimited storage life, shorter processing times, high impact strength, fracture resistance, ease of repair, and ease of handling. The primary disadvantage of thermoplastics is their high melt viscosities. Because of this, thermoplastics are difficult to combine with fibers and difficult to process. CFRP composites with thermoplastic matrices usually require higher processing pressures and temperatures. Therefore, production costs are higher. Other disadvantages of thermoplastic composites include lack of processing experience and limited databases. The thermoplastics used in this research were polypropylene (PP), nylon-6 (N6), and polyphenylene sulfide (PPS). All three of these thermoplastics are commonly used in the composites industry.

2.2.3 Preforms

A preform is a partially consolidated composite, and thus it is an intermediate step in producing a composite part. Figure 2.2 is a schematic of typical thermoplastic composite preforms. Preforms are produced as intermediates to reduce the processing costs of composites. Three common preforms are random mat preforms, powder-coated towpreg, and commingled fibers. The simplest and oldest preform is the mat preform. Combining resin sheets and fiber mats composed of fibers arranged randomly produces random mat preforms. The porosities of the fiber beds in mat preforms are generally

~0.5-0.7. In an effort to reduce processing time, researchers developed additional preforms to reduce the resin permeation distance required to fill the fiber bed. Two results of this research are the powder-coated towpreg and commingled fiber preforms. A powder-coated towpreg is a unidirectional fiber tow with a layer of resin primarily on the outer surface of the tow. A commingled fiber is a collection of unidirectional resin fibers and reinforcement fibers. Typical porosities of the fiber beds in these two preforms are ~0.24-0.4. (Gutowski, 1997; Mallick, 1993; Beland, 1990)

Random mat preforms, powder-coated towpreg, and commingled fibers were used in this research. The mat preform geometry is easy to model since there is a distinct arrangement between the resin and fibers. The other two preforms are more difficult to model since their geometry is not as simple as that of the mat preform. The preforms and the modeling of the permeation through the preforms are discussed in greater detail in Chapters IV and V, respectively.

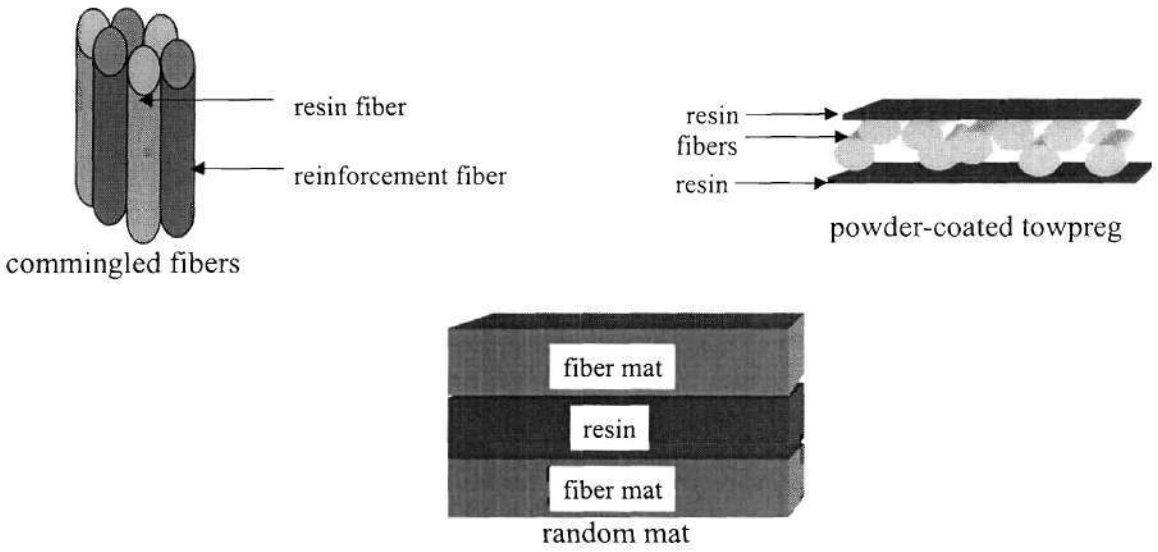

Figure 2.2: Illustration of common thermoplastic preforms.

2.2.4 Processing

The processing of continuous fiber-reinforced thermoplastics can be divided into two main steps. The first step is to combine the fiber and resin to make a preform. Some commercial processes used to combine fibers with thermoplastic matrices to make preforms include hot-melt impregnation, solution impregnation, liquid impregnation, film stacking, commingling, and dry powder coating (Mallick, 1993). The final step after shaping a composite part is the utilization of heat and pressure to force the resin into the void spaces of the fiber bed. Several commercial methods are used to consolidate CFRP composites. These methods include filament winding, pultrusion, hand lay-up, resin transfer molding, and compression molding (Mallick, 1993). Compression molding was used in this research. Compression molding is a very simple processing technique consisting of placing the preform in a heated mold and applying pressure to force the resin into the void spaces of the fiber bed (Beland, 1990). The heated mold is typically placed between two platens of a hydraulic press, which is used to apply the force. This processing technique can be operated in either batch or continuous modes. Figure 2.3 is a simple schematic of compression molding.

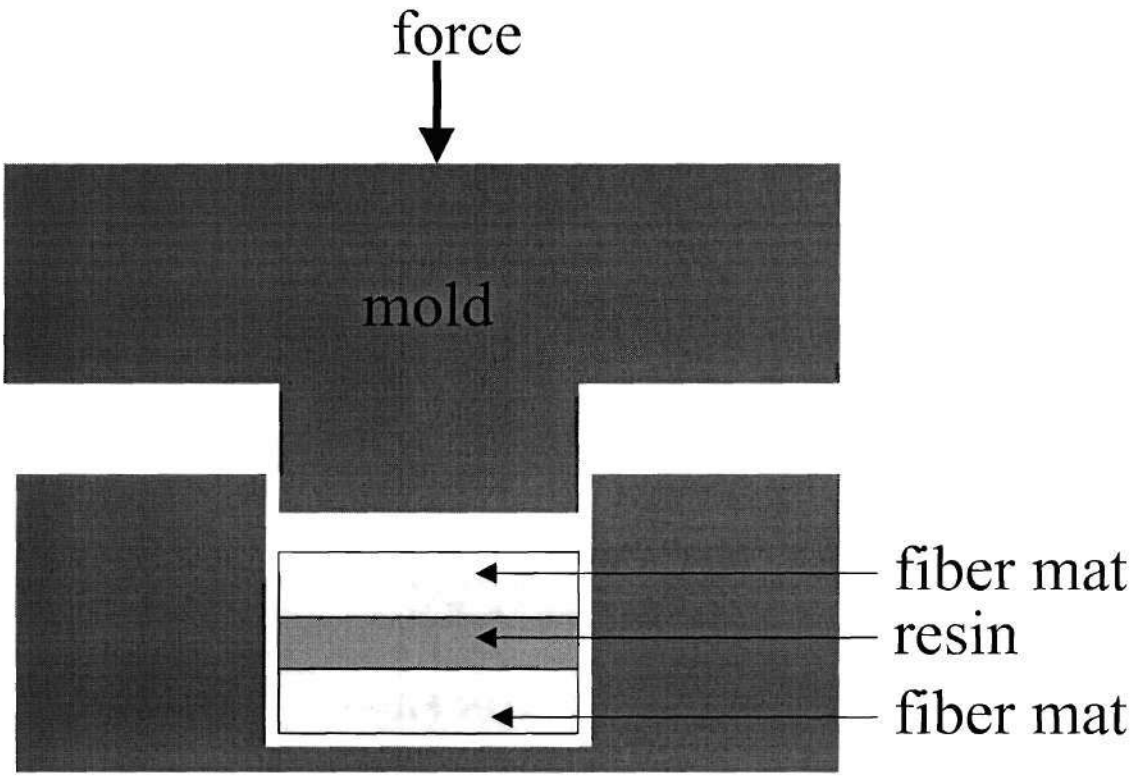

Figure 2.3: Illustration of compression molding technique and a mat preform during compression molding experiment.

The parameter that needs to be controlled during composite processing is the permeation depth of resin into the fiber bed. Variables that may affect the transient permeation depth are listed below. The first four variables are well known to affect the permeation rate, but the last four variables are less known.

1. Processing pressure
2. Processing temperature (viscosity)
3. Porosity of fiber bed
4. Fiber radius
5. Fiber bed geometry
6. Weight percents of resin and fiber
7. Fiber type
8. Fluid type

2.2.5 Applications

CFRP composites are replacing traditional metallic materials in several applications. The strength and modulus of CFRP composites are comparable to traditional metallic materials. The main advantages of CFRP composites over metallic materials are their low specific gravities, higher strength-to-weight ratios, and higher modulus-to-weight ratios. Markets for CFRP composites include the aircraft, military, space, automotive, sporting goods, and marine markets. Examples of applications of CFRP composites are given in Table 2.1.

Table 2.1: Applications of CFRP composites

Sporting Goods	Marine	Automotive	Aircraft and Military
skis	decks	hood	rotor blades
hockey sticks	hulls	bumper	elevator facesheets
surfboards	frames	drive shafts	rudders
javelins	masts	door panels	ailerons

2.3 Literature Review

In this section, the experimental and theoretical work on the transverse permeation of fluids through beds of cylinders is reviewed. In Section 2.3.1, a very brief review on the transverse flow of Newtonian fluids through porous media is discussed. *Section 2.3.2 is a detailed discussion on the flow non-Newtonian fluids through beds of* cylinders.

2.3.1 Newtonian Fluids

Most of the work on flow through porous media has been conducted on media composed of spherical particles with water or light weight oils as the permeants (Mashelkar et al., 1989). Darcy's law, an empirical model, has been used extensively to model the flow in these spherical systems (Åstrom et al., 1992). Darcy's law was established by studying the flow of water through sand. The drawback of this model is that it requires an empirical constant. A semi-empirical model, similar in form to Darcy's law, has also been used by researchers to model the flow of Newtonian fluids through porous media (Åstrom et al., 1992). The basis of this semi-empirical model is the equation for the average flow rate of a Newtonian fluid through a straight, circular tube.

The average flow rate was modified by replacing the radius of the tube with a hydraulic radius and by making corrections for tortuosity with an empirical constant called the Kozeny constant. Like Darcy's law, the disadvantage of this semi-empirical model is the need of an empirical constant. This semi-empirical model was derived for beds of spherical particles, but researchers have used the model for beds of cylindrical objects by adjusting the hydraulic radius (Åstrom et al., 1992). Åstrom et al. (1992) and Skartsis et al. (1992c) presented reviews of Darcy's law and the similar semi-empirical model.

Experiments on the transverse flow of Newtonian fluids, such as water, through beds of carbon fibers were conducted by Skartsis et al. (1992a), Skartsis et al. (1992b), Skartsis and Kardos (1990), Lam and Kardos (1988), and Gutowski et al. (1987). The flow of Newtonian fluids through perfectly arranged beds of metal cylinders was experimentally studied by Sadiq et al. (1995), Skartsis et al. (1992b), Skartsis and Kardos (1990), Chmielewski et al. (1990), Kirsch and Fuchs (1967), and Bergelin et al. (1950). Sangani and Yao (1988), Larson and Higdon (1986), Drummond and Tahir (1984), Sangani and Acrivos (1982), Keller (1964), Happel (1959), Hasimoto (1959), and Kuwabara (1959) presented theoretical work on the transverse flow of Newtonian fluids through arrays of cylinders. Most of these theoretical models are in excellent agreement with each other. The comparison of the theoretical models and the semi-empirical model, discussed above, with reported experimental results obtained using perfectly arranged metal cylinders is good, but comparisons with experimental results obtained using real fiber beds are poor. Åstrom et al. (1992), Skartsis et al. (1992c), and Jackson and James

(1986) presented reviews on the theoretical and experimental work available in the literature on the transverse flow of Newtonian fluids through beds of cylinders.

2.3.2 Non-Newtonian Fluids

There has been very little experimental or theoretical work on the transverse flow of non-Newtonian fluids through beds of cylindrical objects. More specifically, there are only a few experimental studies that used actual fiber beds (Miller et al., 1998; Skartsis et al., 1992; Seo and Lee, 1990). The studies of non-Newtonian fluids through perfectly arranged arrays of metal cylinders are also limited (Sabiri and Comiti, 1997; Sadiq et al., 1995; Skartsis et al., 1992; Prakash et al., 1987; Adams and Bell et al., 1968). Vijaysri et al. (1999), Bruschke and Advani (1993), Skartsis et al. (1992b), Bafna and Baird (1992), and Tripathi and Chhabra (1992) presented theoretical work on the transverse flow of non-Newtonian fluids through beds of cylinders. These experimental and theoretical studies are discussed below. It should be noted that in most of the experimental and the theoretical studies, the power-law model, shown in Equation 2.1, was used to describe viscosity.

$$\eta = m\dot{\gamma}^{n-1} \tag{2.1}$$

Where:

η = Non-Newtonian viscosity, Pa-s

m = power-law consistency index, Pa-s^n

n = power-law flow index, dimensionless

γ = shear rate, 1/s

2.3.2.1 Experimental

Skartsis et al. (1992b) studied the transverse flow of polymeric solutions through beds of cylindrical aluminum rods and carbon fibers. The radius of the aluminum rods was 0.119 cm, and they were arranged in a square arrangement to obtain porosities of 0.43, 0.45, and 0.68. Aqueous solutions of polyacrylamide and an aqueous solution of xanthan gum were used as the permeants through the bed of aluminum cylinders. The measured power-law constants of the solutions were: n = 0.33-0.53 and m = 0.11-0.18 Pas^n. The radius of the carbon fibers was 7.5 μm, and the unidirectional carbon fiber bed had a porosity of 0.68. An aqueous solution of polyacrylamide was used as the permeant through the carbon fiber bed. The measured power-law constants of polyacrylamide solution were: n = 0.41 and m = 0.0.001 $Pas^{0.41}$. Skartsis et al. (1992b) also numerically solved for the two dimensional flow of a power-law fluid through a square array of cylinders. They compared their numerical results on permeation rate with their experimental data obtained with the aluminum rods and found an error of about 40 %. They did not report results for the experiments conducted with the carbon fibers.

Sadiq et al. (1995) studied the flow of Carbopol, a polymer manufactured by B.F. Goodrich, in solution normal to 0.1588 cm diameter aluminum rods. The

rods were arranged in a square arrangement to obtain porosities of 0.6, 0.5, and 0.4. The measured power-law constants of the Carbopol solution were: m = 23-28 Pas^n and n = 0.39-0.54. They calculated percent differences of about 30 % between their permeation rate results and the theoretical results of Bruschke and Advani, (1993), which are discussed below.

Prakash et al. (1987) and Adams and Bell (1968) studied the flow of carboxymethylcellulose (CMC) solutions transverse to a bed of 0.95 cm diameter copper cylinders. The cylinders were arranged in a square array, and the porosity of the bed was about 0.5. The measured power-law constants were: n = 0.5-0.830 and m = 0.0001-2 Pas^n. Prakash et al. (1987) linearly regressed their data to develop an empirical model for the permeation rate. Prakash et al. (1987) compared the results of Adams and Bell (1968) with their empirical model and found errors of about 10 %.

Sabiri and Comiti (1997) studied the transverse flow of an aqueous solution of CMC normal to 0.01 cm diameter stainless steel cylinders. The rheological characteristics of the solution were: n = 0.6-0.9 and m = 0.06-0.26 Pas^n. The porosity of the bed of cylinders was 0.39. They used a semi-empirical equation to predict the permeation rate to within 10 % of their experimental data.

Two studies by Seo and Lee (1991) and Miller et al. (1998) that are reported in the literature implicitly studied the transverse permeation of thermoplastics through real fibers. Neither study measured the permeation rate, but both studies measured the degree of impregnation, which is defined below.

Seo and Lee (1991) placed a single fiber tow in a mold, and then filled the mold with PEEK resin. They heated the mold to temperatures above the melt temperature, and applied pressure in the range of 0.1-1 MPa. The applied pressures were held for a specific amount of time, and these times were 5-30 minutes. After the specified time, the pressure was removed and the degree of impregnation was calculated by counting how many fibers were not exposed to the resin. The measured power-law constants of the PEEK were: n = 0.9163 and m = 200-944 Pas^n. They developed a semi-empirical equation to calculate the degree of impregnation. The error between the model and the data was on average 8 %. Miller et al. (1998) also studied the degree of impregnation using commingled glass and polypropylene fibers. Like Seo and Lee, (1991) they placed a collection of the commingled fibers in a mold and heated the mold to a temperature above the melt temperature. Pressure was applied to the mold for specific times, and after this time duration the pressure was removed and the degree of impregnation was assessed. Miller et. al. (1998) linearly regressed their data to develop an empirical model that relates the degree of impregnation to applied pressure and time. They did not measure the rheological parameters of the resin. The rheology of the resin and the physical properties of the fibers were lumped into the empirical constants of the model. The error between the empirical model and the data was on average 13 %.

2.3.2.2 Theoretical

Vijaysri et al. (1999) theoretically studied the two-dimensional flow of inelastic, incompressible, power-law fluids normal to an array of cylinders. Inertia effects were ignored. They did not assume a formal arrangement of the cylinders relative to each other, but they did assume a concentric envelope of fluid surrounded each cylinder. This geometric assumption is commonly referred to as a cell model. The boundary conditions applied were no slip on the cylinder surface, zero vorticity on the outer surface of the hypothetical concentric envelope of fluid, and symmetry on the remaining surfaces. The momentum equations were solved numerically using the finite difference method. They presented results in the range of n = 0.5-1 and porosity = 0.4-0.9. They concluded that their results were accurate to within 0.5 to 1%. They did not experimentally verify their model; however, they did use the scant results available in literature to compare their results. They found that the error between their theoretical permeation rate and the experimental results of Skartsis et al. (1992b) obtained for the ideal arrangement of aluminum rods described above was roughly 18 %. They also reported differences of about 3 % with the experimental results of Adams and Bell (1968) and Prakash et al. (1987), which were described above. They also compared their results with the Newtonian experimental results of Sadiq et al. (1995), which were obtained by studying the flow of corn syrup normal to an array of aluminum and nylon rods. Vijaysri et al. (1999) found that their model predicts the Newtonian experimental results of Sadiq et al. (1995) well at

porosities greater than 0.5. In this porosity range, they calculated errors on average of 17 %. However, at porosities less than 0.5, they calculated errors on average of 66 %. They stated that this difference was due to the assumption of each cylinder being surrounded by an envelope of fluid and that their model is more valid for high porosity systems.

Tripathi and Chhabra (1992) and Bruschke and Advani (1993) also used the same cell model approach as Vijaysri et al. (1999). Bruschke and Advani (1993) used the same boundary conditions as Vijaysri et al. (1999), but they did not numerically solve the equations. Instead, they obtained an approximate solution by using simplifying assumptions. Because of these assumptions, they admitted that their results are only valid for mildly shear thinning fluids. Taking a slightly different approach than Vijaysri et al. (1999), Tripathi and Chhabra (1992) assumed zero shear stress instead of zero vorticity on the outer surface of the envelope of the fluid. Because of this difference in boundary condition, permeation rates of Tripathi and Chhabra (1992) are about 1.14 times higher than those of Vijaysri et al. (1999).

Like Vijaysri et al. (1999), Tripathi and Chhabra (1992) compared their theoretical results with the experimental results of Adams and Bell (1968) and Prakash et al. (1987), and they calculated differences of about 15 %. Both Bruschke and Advani (1993) and Tripathi and Chhabra (1992) agreed with Vijaysri et al. (1999) in that the cell model is probably only valid for high porosity systems.

Bruschke and Advani (1993) developed a model for the two dimensional flow of an inelastic, incompressible, power-law fluid normal to a square array of cylinders. The square array geometry assumption is commonly referred to as a unit cell model. For boundary conditions, they assumed no slip on the cylinder surface, constant pressure at the inlet and outlet of the unit cell, and symmetry conditions on the remaining surfaces. In addition, inertia effects were ignored. The power-law index was varied between 0.5 and 1, and the porosity range was 0.3-0.95. They used a numerical flow simulation package to solve the flow equations, and they determined the accuracy of their numerical results were about 0.7 %. They also verified their results with the Newtonian numerical results of Sangani and Acrivos (1982). Skartsis et al. (1992b) used the same square unit cell modeling approach as Bruschke and Advani (1993), and hence their results are in agreement. Bruschke and Advani (1993) also derived an analytical solution for the flow using the lubrication approximation. The analytical results agreed well with the numerical results up to a porosity of about 0.7. As expected, the best agreement between the analytical results and the numerical results were at low porosities. Bruschke and Advani (1993) did not report any experimental results. However, as discussed above, Sadiq et al. (1995) compared their experimental permeation rate results with the theoretical results of Bruschke and Advani (1993) and calculated differences of about 30 %. Bafna and Baird (1992) also developed an analytical solution like Bruschke and Advani (1993) based on the lubrication approximation. They too did not run any experiments.

In this thesis, the theoretical equations of Vijaysri et al. (1999) and Bruschke and Advani (1993) and a semi-empirical equation were used to model the transverse permeation. The lubrication approximation of Bruschke and Advani (1993) was used since the common porosity range of CFRP composites is 0.3-0.7, and the approximation was in good agreement with their numerical results up to a porosity of about 0.7. The model that Bruschke and Advani (1993) proposed was chosen over the other unit cell models because they presented both a numerical and analytical solution. The model by Vijaysri et al. (1999) was chosen over the other cell models because it did a better job at predicting the experimental data available in literature and because it had the broadest validity in terms of porosity and shear index. However, it was only used for the random mat preform processing because of its limitation to high porosity systems. The porosity of mat preforms are typically greater than 0.5, and the porosity of powder-coated towpreg and commingled fibers are commonly about 0.25-0.4. The model proposed by Bruschke and Advani (1993) and a semi-empirical equation were used for all three preforms. All three models are discussed in greater detail in Chapter III.

2.4 Summary

In this chapter, CFRP composite terms were defined. The experimental and theoretical work reported in literature on the transverse flow of non-Newtonian fluids through beds of cylinders was discussed. It was shown that there is there is a need for a

comprehensive study on the transverse permeation of non-Newtonian fluids, like thermoplastics, through real fiber beds. In addition, there is a need to test the validity of theoretical models with experimental permeation results. In Chapter 3, the equations used to model transverse permeation in this research will be detailed.

2.5 References

Adams and Bell, 1968: Adams, D. and Bell, K., "Fluid Friction and Heat Transfer For Flow of Sodium Carboxymethylcellulose Solutions Across Banks of Tubes", *Chem. Eng. Prog. Symp. Ser.,* 1968, n 82, v 64, p 133-145.

Åstrom et al., 1992: Åstrom, B., Pipes, B., Advani, S., "On Flow Through Aligned Fiber Beds and Its Application to Composites Processing", *Journal of Composite Materials*, 1992, v 26, n 9, p 1351-1373.

Bafna and Baird, 1992: Bafna, S and Baird, D., "An Impregnation Model for the Preparation for Thermoplastic Prepregs", *Journal of Composite Materials*, 1992, v 26, n 5, p 683-707.

Beland, 1990: Beland, S., *High Performance Thermoplastic Resins and Their Composites*, Noyes Publication, New Jersey, 1990.

Bergelin et al., 1950: Bergelin, O., Brown, G., Hull, J., Sullivan, F., "Heat Transfer and Fluid Friction During Viscous Flow Across Banks of Tubes-III: A Study of Tube Spacing and Tube Size", *Trans. ASME*, 1950, p 881-888.

Bruschke and Advani, 1993: Bruschke, M, and Advani, S., " Flow of Generalized Newtonian Fluids Across a Periodic Array of Cylinders", *J. Rheol.*, 1993, v 37, n 3, p 479-497.

Chmieleski et al., 1990: Chmielewski, C., Petty, C., Jayaraman, K., "Crossflow of Elastic Liquids Through Arrays of Cylinders", Journal of Non-Newtonian Fluid Mechanics, 1990, v 35, p 309-325.

Drummond and Tahir, 1984: Drummond, J. and Tahir, M., "Laminar Viscous Flow Through Regular Arrays of Parallel Solid Cylinders", *Int. J. Multiphase Flow*, 1984, v 10, n 5, p 515-540.

Gutowski, 1997: Gutowski, T., *Advanced Composites Manufacturing*, John Wiley & Sons, Inc., New York, 1997.

Gutowski et al., 1987: Gutowski, T., Cai, Z., Bauer, S., Boucher, D., Kingery, J., Wineman, S., " Consolidation Experiments for Laminate Composites", *Journal of Composite Materials*, 1987, v 21, p 650-669.

Happel, 1959: Happel, J, "Viscous Flow Relative to Arrays of Cylinders", *AICHE Journal*, 1959, v 5, n 2, 174-177.

Jackson and James, 1986: Jackson, G. and James, D., "The Permeability of Fibrous Porous Media", *The Canadian Journal of Chemical Engineering*, 1986, v 64, p 364-374.

Keller, 1964: Keller, J., "Viscous Flow Through a Grating or Lattice of Cylinders", *J. Fluid Mech.*, 1964, v 18, p 94-96.

Kirsch and Fuchs, 1967: Kirsch, A. and Fuchs, N., " Studies on Fibrous Aerosol Filters-II. Pressure Drops in Systems of Parallel Cylinders", Ann. Occup. Hyg., 1967, v 10, p 23-30.

Kuwabara, 1959: Kuwabara, S., "The Forces Experienced by Randomly Distributed Parallel Cylinders or Spheres in a Viscous Flow at Small Reynolds Numbers", *Journal of Physics Society of Japan*, 1959, v 14, n 4, p 527-532.

Lam and Kardos, 1986: Lam, R., and Kardos, J., "The Permeability of Aligned and Cross-Plied Fiber Beds During Processing of Continuous Fiber Composites", *ASC Ann. Tech. Conf.*, 1986, v3, p 3-11.

Larson and Higdon, 1987: Larson, R. and Higdon, J., "Microscopic Flow Near the Surface of Two-Dimensional Porous Media. Part 2. Transverse Flow", *J. Fluid Mech.*, 1987, v 178, p 119-136.

Mallick, 1993: Mallick, P., *Fiber-Reinforced Composites: Materials, Manufacturing, and Design, Second Edition*, Marcel Dekker, New York, 1993.

Mashelkar et al., 1989: Mashelkar, R., Mujumdar, A., Kamal, R., *Transport Phenomena in Polymeric Systems*, Ellis Horwood Limited, Chichester, 1989.

Miller et al., 1998: Miller, A., Dodds, J, Gibson, A, "High Speed Pultrusion of Thermoplastic Matrix Composites", *Composites Part A*, 1998, p 773-782.

Prakash et al., 1987: Prakash, O., Gupta, N., Mishra, P., " Newtonian and Inelastic Non-Newtonian Flow Across Tube Banks", *Ind. Eng. Chem. Res.*, 1987, v 26, p 1365-1372.

Sabiri and Comiti, 1997: Sabiri, N. and Comiti, J., "Experimental Validation of A Model Allowing Pressure Gradient Determination for Non-Newtonian Purely Viscous Fluid-Flow Through Packed Beds", *Chemical Engineering Science*, 1997, v 52, n 20, p 3589-3592.

Sadiq, 1995: Sadiq, T., Advani, S., Parnas, R., "Experimental Investigation of Transverse Flow Through Aligned Cylinders", *Int. J. Multiphase Flow*, 1995, v 21, n5, p 755-774.

Sangani and Acrivos, 1982: Sangani, A. and Acrivos, A., "Slow Flow Past Periodic Arrays of Cylinders with Application to Heat Transfer", *Intl, J. Multiphase Flow*, 1982, v 8, n 3, p 193-206.

Sangani and Yao, 1988: Sangani, A. and Yao, C, " Transport Processes in Random Arrays of Cylinders. II. Viscous Flow", *Phys. Fluid*, 1988, v 31, n 9, p 2435-2444.

Seo and Lee, 1991: Seo, J and Lee, W, "A Model of the Resin Impregnation in Thermoplastic Composites", *Journal of Composite Materials*, 1991, v 25, p 1127-1141.

Skartsis et al. 1992a: Skartsis, L, Khomami, B., Kardos, J., "Resin Flow Through Fiber Beds During Composite Manufacturing Processes. Part II: Numerical and Experimental Studies of Newtonian Flow Through Fiber Beds", *Polymer Engineering and Science*, 1992, v 32, n4, p 231-238.

Skartsis et al, 1992b: Skartsis, L, Khomami, B., Kardos, J., " Polymeric Flow Through Fibrous Media", *J. Rheol.*, 1992, v 36, n 4, p 589-620.

Skartsis et al., 1992c: Skartsis, L, Kardos, J., Khomami, B., "Resin Flow Through Fiber Beds During Composite Manufacturing Processes. Part I: Review of Newtonian Flow Through Fiber Beds", *Polymer Engineering and Science*, 1992, v 32, n4, p 221-230.

Skartsis and Kardos, 1990: Skartsis, L. and Kardos, J., " The Newtonian Permeability and Consolidation of Oriented Carbon Fiber Beds", *Proceedings of American Society of Composites*, p 548-552.

Tripathi and Chhabra, 1992: Tripathi, A. and Chhabra, R, "Slow Power-law Fluid Flow Relative to an Array of Infinite Cylinders", *Ind. Chem. Res.*, 1992, v 31, p 2754-2759.

Vijaysri et al., 1999: Vijaysri, M, Chhabra, R., Eswaran, V., "Power-law Fluid Flow Across an array of Infinite Circular Cylinders: A Numerical Study", *J. Non-Newtonian Fluid Mech.*, 1999, v 87, p 263-282.

CHAPTER III

THEORY

3.1 Introduction

In this chapter, the equations used in this research to describe transverse permeation are detailed. In Section 3.2, the theory behind the semi-empirical equation is outlined. In Sections 3.3 and 3.4, the mechanistic equations are detailed. In Section 3.5, it is shown how the transverse permeation models can be used to calculate void content of a composite. A summary is given in Section 3.6, and references are listed in Section 3.7.

3.2 Semi-empirical Model

The basis of the semi-empirical equation is the average fluid velocity of a power-law fluid through a straight, circular tube as shown in Equation 3.1. The power-law model, shown in Equation 2.1, was used to describe the viscosity.

$$U = \frac{n}{1+3n}\left(\frac{1}{2m}\right)^{\frac{1}{n}}\left(\frac{\Delta P}{X_e}\right)^{\frac{1}{n}} R^{\frac{(1+n)}{n}} \tag{3.1}$$

Where:

U = average fluid velocity in tube, m/s

n = power-law flow index

m = power-law consistency index, Pa-s^n

ΔP = fluid pressure drop, Pa

X_e = effective path traveled by fluid, m

R = radius of tube, m

Inertia is neglected since the Reynolds numbers in this research are about 10^{-12}-10^{-11} in magnitude. Sample calculations for the Reynolds numbers are located in Appendix A. Because the Reynolds numbers are so low, the flow is considered fully developed. Brodkey and Hershey (1988) and Whitaker (1992) showed that the entry length for laminar pipe flow is on the order of $10^{-2}DR_e$, where D is the diameter and R_e is the Reynolds number. The diameters of the fibers used in this research are on the order of 10^{-6} μm, and thus the pore diameters available for flow are on the order of 10^{-6} μm, because transverse flow is being studied. Furthermore, capillary pressure was neglected since the applied processing pressures are at least one order of magnitude greater than the capillary pressure estimates, which are located in Appendix A.

While Equation 3.1 is for flow through a straight, circular tube, it can be generalized for porous media using the same approach used by Åstrom et al. (1992), Kozeny (1927), and Carman (1956) for flow through spherical particles. Since the geometry of a fiber bed in a composite is more complicated than a circular tube, the radius, R, was replaced with a hydraulic radius, r_h, and a shape factor, K_o, term to generalize Equation 3.1 for various capillary shapes. The hydraulic radius is defined in Equation 3.2. For circular capillaries, K_o equals 2, and for parallel plate cross sections,

K_o equals 3 (Åstrom et al., 1992 and Carman, 1956). For the mat preforms it was assumed that the fibers were arranged such that circular capillaries were available for flow. Therefore, a shape factor of 2 was used for the mat preform processing.

$$r_h = \frac{\text{flow volume}}{\text{wetted area}} = \frac{AX\varepsilon}{\left(\frac{2AX(1-\varepsilon)}{r_f}\right)} = \frac{r_f}{2}\frac{\varepsilon}{1-\varepsilon} \tag{3.2}$$

Where:

r_h	=	hydraulic radius, m
A	=	surface area, m^2
X	=	thickness of fiber bed, m
ε	=	porosity of fiber bed
r_f	=	radius of fiber, m

Figure 3.1 is a schematic of the geometry assumptions in this research for the capillaries formed in the fiber beds. For the towpreg and commingled fibers, it was assumed that the pores were of the parallel plate geometry shown in Figure 3.1. Therefore, a shape factor of 3 was used for the towpreg and commingled fibers.

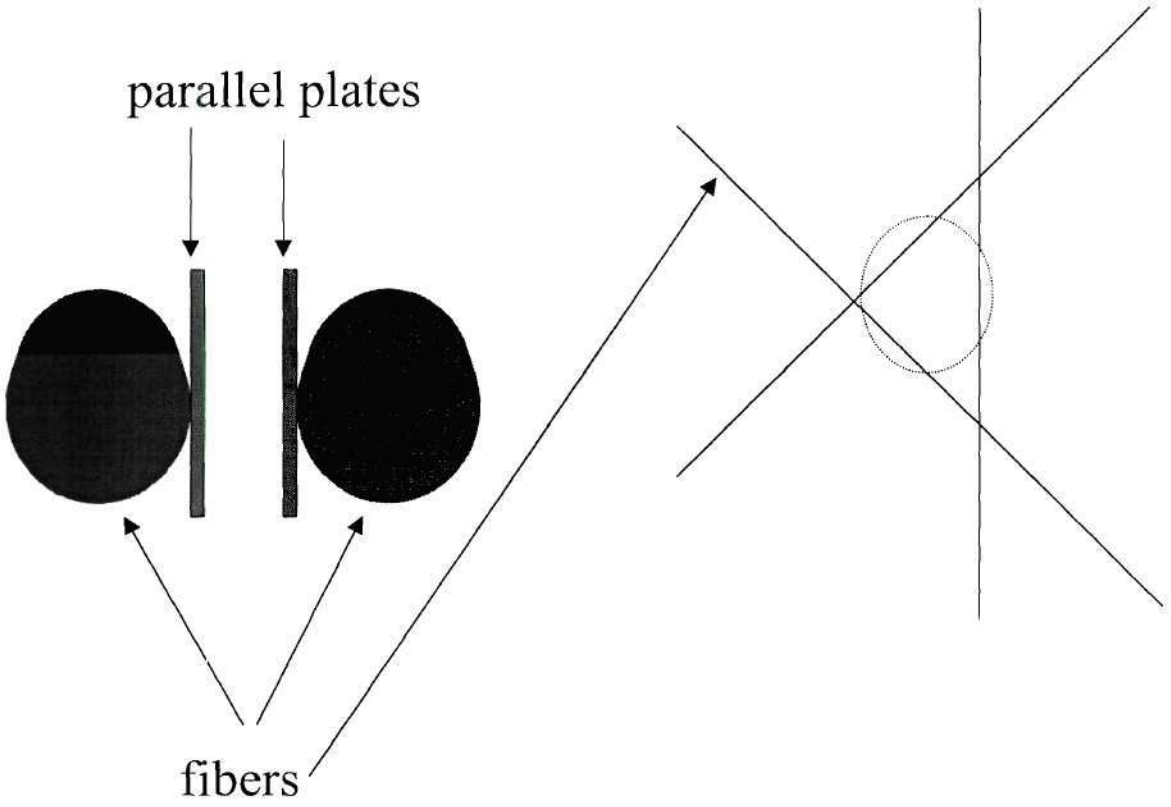

Figure 3.1: Schematic of capillary assumption for Semi-empirical model.

The tortuosity, K_1, of the fiber bed was accounted for by Equations 3.3 and 3.4 (Åstrom et al., 1992; Kozeny, 1927; Carman, 1956).

$$K_1 = \frac{X_e}{X} \tag{3.3}$$

Where:

K_1 = tortuosity

$$VK_1 = U\varepsilon \tag{3.4}$$

Where:

V = average flow rate per unit area, m/s

Kozeny, (1927) argued that the path traveled by the fluid is greater than the thickness of the porous medium. Carman (1956) argued that because of the tortuosity of porous media, the velocity of the fluid in the capillary has to be corrected.

After inserting Equations 3.2-3.4 into Equation 3.1, the result is Equation 3.5.

$$V = \left(\frac{4n}{1+3n}\right)\left(\frac{1}{2}\right)^{\frac{1+n}{n}}\left(\frac{\varepsilon^{2n+1}}{(1-\varepsilon)^{1+n}}\right)^{\frac{1}{n}}\left(\frac{1}{K_o(K_1)^{\frac{1+n}{n}}}\right)\left(r_f^{\frac{1+n}{n}}\right)\left(\frac{\Delta P}{mX}\right)^{\frac{1}{n}} \tag{3.5}$$

$$K = K_o K_1^2 \tag{3.6}$$

The combination of the shape factor, K_o, and the tortuosity, K_1, above in Equation 3.6 is commonly referred to as the Kozeny constant, K, which has to be determined experimentally.

Equation 3.5 was transformed into terms of transient permeation depth using Equation 3.7. The resulting equation to determine permeation depth is Equation 3.8.

$$V = \frac{dX}{dt} \tag{3.7}$$

Where:

X = permeation depth, m

t = time, s

$$X = \left[\left(\frac{1+n}{1+3n} (2)^{\frac{n-1}{n}} \left(\frac{\varepsilon^{2n+1}}{(1-\varepsilon)^{1+n}} \right)^{\frac{1}{n}} \left(\frac{1}{K_o K_1^{\frac{1+n}{n}}} \right) \right) \left(r_f^{\frac{1+n}{n}} \left(\frac{\Delta P}{m} \right)^{\frac{1}{n}} t \right) \right]^{\frac{n}{1+n}} \tag{3.8}$$

Where:

X = permeation depth, m

It is essential to select the proper power-law constants for Equation 3.8. Therefore, Equation 3.9 was used to estimate the shear rate range during the composite processing in this research (Åstrom et al., 1992). Estimates of the shear rates are discussed in Chapter V. The rheology experiments described in Chapter IV were conducted in the estimated range.

$$\gamma_w = \frac{1+3n}{4n}\frac{K_o U}{r_h} \tag{3.9}$$

Where:

γ_w = wall shear rate, 1/s

A possible drawback of Equation 3.8 is that the Kozeny constant may vary with material and processing conditions. The advantage of this model is its simplicity. In the remainder of this thesis, Equation 3.8 will be referred to as the Semi-empirical model.

3.3 Vijaysri Model

Vijaysri, et al. (1999) solved the equations of motion for the two dimensional flow of an incompressible, power-law fluid normal to an array of cylinders. As with the Semi-empirical equation, inertia was ignored. They assumed a concentric envelope of fluid surrounded each cylinder. This geometric assumption is illustrated in Figure 3.2.

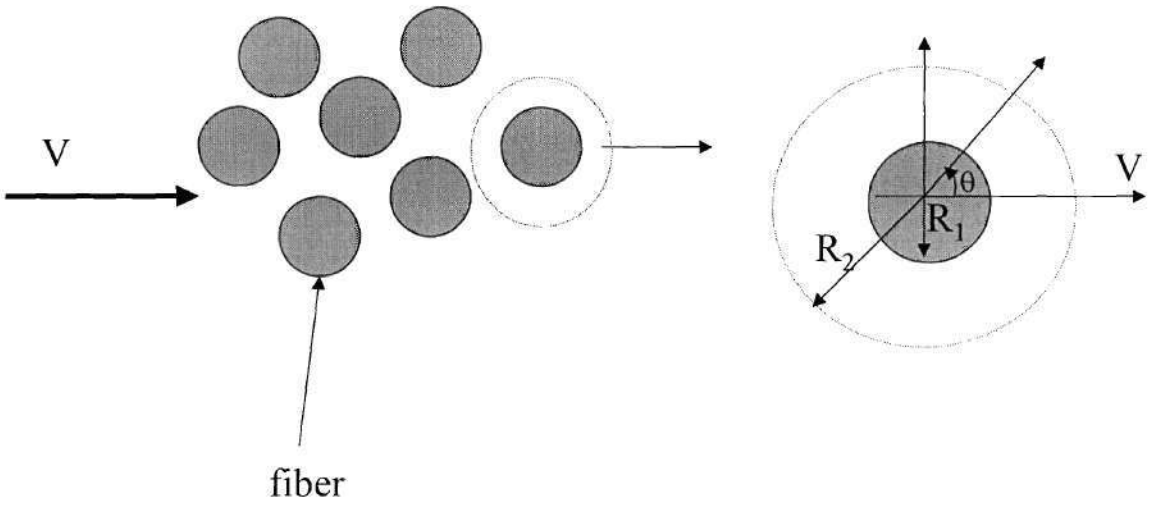

Figure 3.2: Schematic of geometry assumption for Vijaysri model. The dotted circle refers to the hypothetical envelope of fluid.

Using cylindrical coordinate systems, they assumed $V_z = 0$, $V_r = V_r(r,\theta)$, and $V_\theta = V_\theta(r,\theta)$. In cylindrical coordinates, they listed the continuity and momentum balance as shown in Equations 3.10-3.12.

$$\frac{1}{r}\frac{\partial(rV_r)}{\partial r} + \frac{1}{r}\frac{\partial V_\theta}{\partial \theta} = 0 \tag{3.10}$$

Where:

V_r = dimensionless velocity in r-direction

V_θ = dimensionless velocity in θ-direction

r = dimensionless radial coordinate

$$\frac{DV_r}{Dt} = -\frac{1}{2}\frac{\partial P}{\partial r} + \frac{2^n}{R_e}\left[\frac{1}{r^2}\frac{\partial\left(r^2\tau_{rr}\right)}{\partial r} + \frac{1}{r}\frac{\partial \tau_{r\theta}}{\partial \theta} - \frac{\tau_{\theta\theta}}{r}\right] \tag{3.11}$$

Where:

P = dimensionless pressure

R_e = Reynolds number

n = power-law flow index

τ_{ij} = components of stress tensor, Pa

$$\frac{DV_\theta}{Dt} = -\frac{1}{2r}\frac{\partial P}{\partial \theta} + \frac{2^n}{R_e}\left[\frac{1}{r^2}\frac{\partial\left(r^2\tau_{r\theta}\right)}{\partial r} + \frac{1}{r}\frac{\partial \tau_{\theta\theta}}{\partial \theta}\right] \tag{3.12}$$

They used Equation 3.13 for the rheological equation of state for a power-law fluid. The apparent viscosity was expressed with Equation 3.14.

$$\tau_{ij} = 2\eta\varepsilon_{ij} \tag{3.13}$$

Where:

ε_{ij} = components of the rate of deformation tensor, 1/s

$$\eta = (2\Pi)^{\frac{(n-1)}{2}} \tag{3.14}$$

Where:

η = viscosity, Pa-s

Π = second invariant of the rate of deformation tensor

In Equations 3.10-3.14, the velocity components were scaled using the superficial velocity, V, and the pressure was scaled using $1/(2\rho_f V^2)$. The radial distance was scaled using the cylinder radius, R, and the extra stress components were scaled using $m(V/R)^n$. The constant m is the power-law consistency index. Equation 3.15 was scaled using $(V/R)^2$. It was written in terms of velocity components as shown in Equations 3.16.

$$\Pi = \varepsilon_{rr}^2 + \varepsilon_{\theta\theta}^2 + 2\varepsilon_{r\theta}^2 \tag{3.15}$$

$$\begin{aligned} \varepsilon_{rr} &= \frac{\partial V_r}{\partial r} \\ \varepsilon_{\theta\theta} &= \frac{1}{r}\frac{\partial V_\theta}{\partial \theta} + \frac{V_r}{r} \\ \varepsilon_{r\theta} &= \frac{1}{2}\left[r\frac{\partial\left(\frac{V_\theta}{r}\right)}{\partial r} + \frac{1}{r}\frac{\partial V_r}{\partial \theta} \right] \end{aligned} \tag{3.16}$$

Because of the two dimensional nature of the flow, they introduced the stream and vorticity functions. The stream function, ψ, was scaled using VR, and the vorticity

function, ω, was scaled using V/R. The stream and vorticity functions are shown in Equations 3.17-3.19.

$$V_r = \frac{1}{r}\frac{\partial \psi}{\partial \theta} \tag{3.17}$$

$$V_\theta = -\frac{\partial \psi}{\partial r} \tag{3.18}$$

$$\omega = -B^2 \psi \tag{3.19}$$

Where:

$$B^2 = \left(\frac{\partial^2}{\partial r^2} + \frac{1}{r}\frac{\partial}{\partial r} + \frac{1}{r^2}\frac{\partial^2}{\partial \theta^2}\right)$$

By combining the above equations and eliminating the pressure terms using cross-differentiation, they listed the generalized form of the Navier-Stokes equation in terms of the stream function and vorticity for axisymmetric flow of power-law fluids in polar coordinates as shown in Equation 3.20.

$$\frac{\partial \omega}{\partial t} + \frac{1}{r}\left[\left(\frac{\partial \omega}{\partial r}\frac{\partial \psi}{\partial \theta}\right) - \left(\frac{\partial \omega}{\partial \theta}\frac{\partial \psi}{\partial r}\right)\right] = \frac{2^n \eta}{R_e} B^2 \omega + \frac{2^{n+1}}{R_e}\left[\begin{array}{l} \left(\frac{\partial \omega}{\partial r} + \frac{1}{n}\frac{\omega}{r} + \frac{1}{r}\frac{\partial^2 \psi}{\partial r^2}\right)\frac{\partial \eta}{\partial r} \\ + \frac{1}{r^2}\left(\frac{\partial \omega}{\partial \theta} - \frac{2}{r^2}\frac{\partial \psi}{\partial \theta} + \frac{2}{r}\frac{\partial^2 \omega}{\partial r \partial \theta}\right)\frac{\partial \eta}{\partial \theta} \\ - \left(\frac{\partial^2 \psi}{\partial r^2} + \frac{\omega}{r}\right)\left(\frac{\partial^2 \eta}{\partial r^2} - \frac{1}{r^2}\frac{\partial^2 \eta}{\partial \theta^2}\right) \\ + \frac{2}{r^2}\left(\frac{\partial^2 \psi}{\partial r \partial \theta} - \frac{1}{r}\frac{\partial \psi}{\partial \theta}\right)\frac{\partial^2 \eta}{\partial r \partial \theta} \end{array}\right] \tag{3.20}$$

They assumed steady state conditions, but they included the transient term in Equation 3.20, since the false transient technique was used to numerically solve the equations. The boundary conditions are listed below in Equations 3.21-3.24.

$$r = 1, V_r = 0, V_\theta = 0$$
$$r = r_\infty, \omega = 0, V_r = \cos\theta \tag{3.21}$$

$$r = 1, \omega = -\frac{\partial^2 \psi}{\partial r^2}, \psi = 0$$
$$r = r_\infty, \omega = 0, \psi = -r_\infty \sin\theta \tag{3.22}$$

$$r_\infty = (1-\varepsilon)^{-\frac{1}{2}} = \frac{R_\infty}{R} \tag{3.23}$$

Where:

R = cylinder radius, m

R_∞ = radius of fluid envelope, m

$$\theta = 0, \omega = 0, \psi = 0$$
$$\theta = 180, \omega = 0, \psi = 0 \tag{3.24}$$

They solved the flow equations with a finite difference scheme using the false transient time-stepping method to obtain the steady state solution. A detailed description of the numerical solution procedure and validation can be found in Vijaysri et al. (1999). They stated that their results were accurate to within 0.5-1%. Results were presented in the following ranges: n = 0.5-1 and ε = 0.4-0.95. They reported their results in the form of a loss coefficient, Λ, which is a function of porosity and power-law flow index. The

loss coefficient is equal to $C_D R_e$, where C_D is the drag coefficient and R_e is the Reynolds number. The loss coefficient was defined using Equation 3.25.

$$\Lambda = 2^n \left(\frac{\pi}{(1-\varepsilon)} \right) \left(\frac{1}{V^n} \right) R^{n+1} \left(\frac{\Delta P}{mX} \right) \tag{3.25}$$

In this research, Equation 3.25 was modified using Equation 3.7 to determine the transient permeation depth, X, and the result is Equation 3.26. Furthermore, the fiber radius, r_f, is equal to the cylinder radius, R. Values of Λ at different porosities, ε, and power-law flow index values, n, are found in Vijaysri et al. (1999).

$$X = \left[\left(2 \left(\frac{1+n}{n} \right) \left(\frac{\pi}{(1-\varepsilon)\Lambda} \right)^{\frac{1}{n}} \right) \left(r_f^{\frac{n+1}{n}} \left(\frac{\Delta P}{m} \right)^{\frac{1}{n}} t \right) \right]^{\frac{n}{n+1}} \tag{3.26}$$

A possible disadvantage of this model is the highly idealized nature of the geometry. Also, because of the geometry assumption, the model is primarily valid for high porosity systems. Therefore, its use is limited primarily to the processing of random fiber mats. The advantage of this model is that no empirical constants are needed. In the remainder of this thesis, Equation 3.26 will be referred to as the Vijaysri model.

3.4 Bruschke Model

Bruschke and Advani (1993) developed a numerical and analytical solution for the two dimensional flow of an incompressible, power-law fluid through a square unit cell. Like the other models, inertia effects were ignored. Figure 3.3 is a schematic of the square unit cell.

The analytical solution was derived using the lubrication approximation, and it compares well with the numerical solution, especially at lower porosities. In this research, the analytical solution was used. The details of the analytical solution are discussed below. The details of the numerical solution are located in Bruschke and Advani (1993).

Figure 3.4 is a schematic of the unit cell used for the analytical solution. The basis of the analytical solution is the equation for flow of a power-law fluid between two parallel plates as given by Equation 3.27.

$$\frac{dP}{dX} = Q^n m \left(\frac{1+2n}{2n}\right)^n \left(\frac{2}{h}\right)^{2n+1} \tag{3.27}$$

Where:

Q	=	flow rate through cell, m^2/s
n	=	power-law flow index
m	=	power-law consistency index, $Pa\text{-}s^n$
h	=	gap width, m
P	=	pressure, Pa
X	=	distance from inlet of cell, m

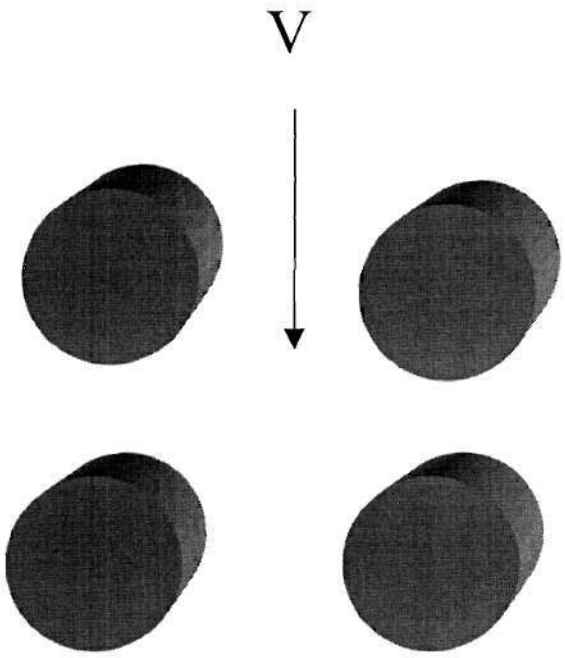

Figure 3.3: Illustration of square unit cell where V is the superficial velocity.

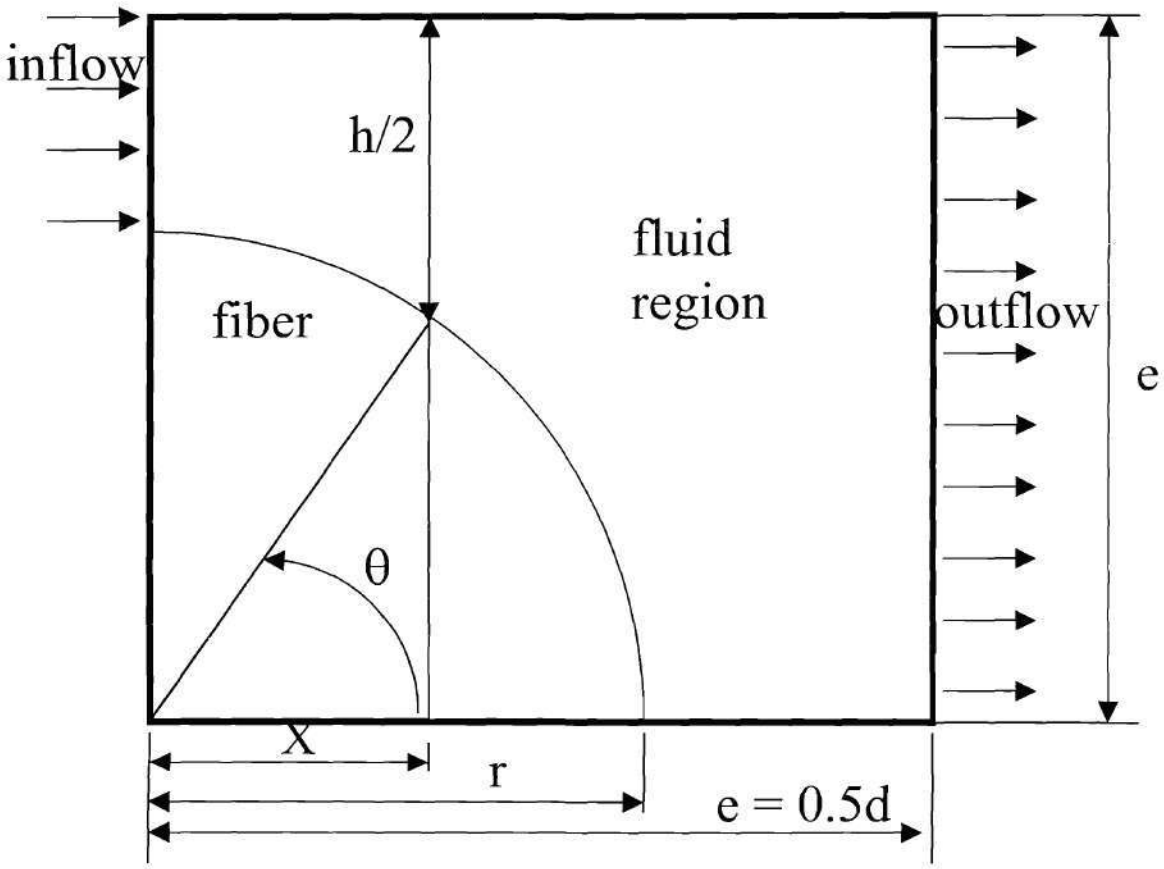

Figure 3.4: Illustration of geometry used for Bruschke model where X is the distance from the inlet of the cell, r is cylinder radius, h is the gap width, d is the distance between the centers of the cylinders, and e is half the distance between the centers of cylinders.

Using Figure 3.3, the gap width was expressed as Equation 3.28

$$h = d - 2\sqrt{r^2 - X^2} \tag{3.28}$$

Where:

d = distance between cylinder centers, m

r = radius of cylinder, m

Substituting Equation 3.28 for the gap width and changing to radial coordinates, Equation 3.27 was rearranged as Equation 3.29.

$$dP = Q^n m\left(\frac{1+2n}{2n}\right)^n e^{-2n}\left[(1-l\cos\theta)^{-(2n+1)}d\theta - (1-l\cos\theta)^{-2n}d\theta\right] \tag{3.29}$$

Where:

$$e = 0.5d \tag{3.30}$$

$$l = \frac{r}{e} \tag{3.31}$$

$$l = \sqrt{\frac{4}{\pi}(1-\varepsilon)} \tag{3.32}$$

and

ε = porosity

They used mathematical tables by Beyer (1984) to evaluate Equation 3.29, and they presented the result in the form of a variable called flow mobility or M. The flow mobility is defined in Equation 3.33.

$$M = \frac{1}{2} Q^{1-n} \frac{1}{m} \left(\frac{2n}{1+2n} \right)^n e^{2n} \frac{1}{\sqrt{\pi}} \left[\begin{array}{l} (1+l)^{-(2n+1)} \left(\cos^2 \alpha \right)^{2n+1} \alpha^{-4n-1} \dfrac{\Gamma\left(2n+\frac{1}{2}\right)}{\Gamma(2n+1)} \\ -(1+l)^{-2n} \left(\cos^2 \alpha \right)^{2n} \alpha^{-4n+1} \dfrac{\Gamma\left(2n-\frac{1}{2}\right)}{\Gamma(2n)} \end{array} \right]^{-1} = \frac{VX}{\Delta P} \tag{3.33}$$

Where:

V = superficial velocity, m/s

Γ = gamma function

$$\alpha = \arctan \sqrt{\frac{1-l}{1+l}} \tag{3.34}$$

For small α, the second term in Equation 3.33 was neglected since it is at least two orders of magnitude less than the first term. The result was Equation 3.35.

$$M = \frac{1}{2} Q^{1-n} \frac{1}{m} \left(\frac{2n}{1+2n} \right)^n e^{2n} \frac{1}{\sqrt{\pi}} \left[(1+l)^{-(2n+1)} \left(\cos^2 \alpha \right)^{2n+1} \alpha^{-4n-1} \frac{\Gamma\left(2n+\frac{1}{2}\right)}{\Gamma(2n+1)} \right]^{-1} = \frac{VX}{\Delta P} \tag{3.35}$$

Where:

$$Q = Vd \tag{3.36}$$

In this research, Equation 3.35 was modified using Equation 3.7 to obtain the transient permeation depth, X, and the result is Equation 3.37. The radius of the cylinder, r, is equal to the radius of the fiber, r_f, in this research.

$$X = \left[\left(\frac{1+n}{n} \right) \left(\frac{1}{2^n} \right)^{\frac{1}{n}} \left\{ \frac{\frac{1}{\sqrt{\pi}} \left(\frac{2n}{1+2n} \right)^n \left[(1+l)^{-(2n+1)} \left(\cos^2 \alpha \right)^{2n+1} \alpha^{-4n-1} \frac{\Gamma\left(2n+\frac{1}{2}\right)}{\Gamma(2n+1)} \right]^{-1}}{l^{n+1}} \right\}^{\frac{1}{n}} \left\{ r_f^{\frac{1+n}{n}} \left(\frac{\Delta P}{m} \right)^{\frac{1}{n}} t \right\} \right]^{\frac{n}{n+1}} \quad (3.37)$$

A possible disadvantage of this model is the highly idealized nature of the square unit cell. The advantage of this model is that no empirical constants are needed. In the remainder of this thesis Equation 3.37 will be referred to as the Bruschke model. Table 3.1 lists all the input parameters for the Semi-empirical, Vijaysri, and Bruschke models and how they were determined.

Table 3.1: Parameters in the model equations

Model	Parameters	Method of Determination	Chapter Discussed
Semi-*empirical*	X	LVDT	4 & 5
	n	parallel plate rheometer	4 & 5
	m	parallel plate rheometer	4 & 5
	P	hot press	4
	t	data acquisition card	4
	ε	SEM(towpreg and commingled fibers); compression experiments(mats)	4 & 5
	r_f	manufacturer	4
	K_o	equals 2 for mat preform processing; equals 3 for towpreg and commingled fiber processing	3
	K_1	non-linear regression of experimental data	5
Vijaysri	X	LVDT	4 & 5
	n	parallel plate rheometer	4 & 5
	m	parallel plate rheometer	4 & 5
	P	hot press	4
	t	data acquisition card	4
	ε	SEM(towpreg and commingled fibers); compression experiments(mats)	4 & 5
	r_f	manufacturer	4
	Λ	Vijaysri et al. (1999)	3,5
Bruschke	X	LVDT	4 & 5
	n	parallel plate rheometer	4 & 5
	m	parallel plate rheometer	4 & 5
	P	hot press	4
	t	data acquisition card	4
	ε	SEM(towpreg and commingled fibers); compression experiments(mats)	4 & 5
	r_f	manufacturer	4
Void content	v_{void}	density measurement	4 & 5
	v_{voidi}	density measurement	4 & 5
	X_c	SEM	4 & 5
	X	LVDT	4 & 5

3.5 Void Content Equation

The quality of a composite part is determined by its void content, where void content refers to areas in the composite not occupied by resin or fiber. The presence of voids in a composite can be detrimental to its mechanical properties and its resistance to environmental effects like moisture. Therefore, it is important to minimize void content. With this in mind, it would be beneficial to be able to model void content as a function of processing conditions and material parameters. The models described above can be used to predict the void content. Equation 3.38 was used to calculate the void content of the powder-coated towpreg and the commingled fibers. The calculated value was compared to the experimental void content, which is discussed in Chapter IV. Figure 3.5 is a schematic of the geometry used to determine the void content equation. At time, t, equal to zero, the composite has an initial void content v_{voidi}. As time progresses, the resin flows into the pores of the fiber bed reducing the void content.

$$v_{void}(t) = v_{voidi}\left(1 - \frac{X(t)}{X_c}\right) \tag{3.38}$$

Where:

v_{void} = void content

v_{voidi} = initial void content

X = permeation depth, m

X_c = thickness of fiber bed available for flow, m

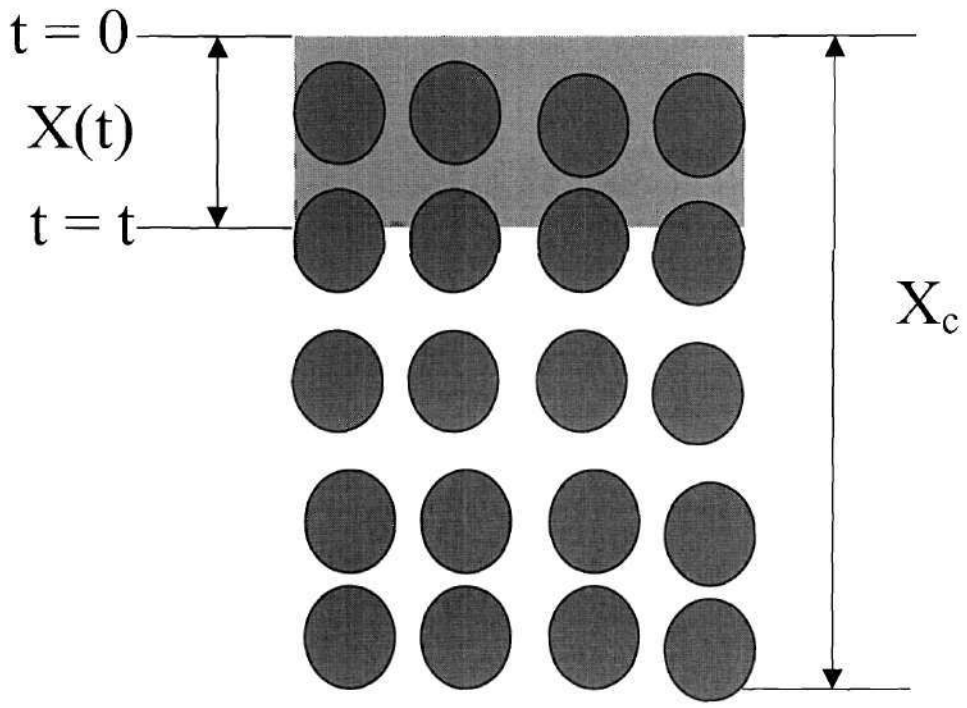

Figure 3.5: Schematic used to derive void content equation.

3.6 Summary

In this chapter, the three models used to describe the transverse permeation process in this research were detailed. The Semi-empirical model was derived using the equation for the average flow rate of a power-law fluid through a circular tube. The equation was modified by introducing a hydraulic radius and an empirical constant called the Kozeny constant. This model was used for the processing of all the preforms. A possible drawback of this model is that the Kozeny constant will vary with material and processing conditions. An advantage of this model was its simplicity. The Vijaysri model was developed by numerically solving for the flow of a power-law fluid normal to an array of cylinders. It was assumed that a concentric envelope of fluid surrounded each cylinder. Because of this geometric assumption, this model was limited to high porosity systems. Therefore, in this research it was only used for the mat preforms, which had porosities of ~0.6-0.7. An advantage of this model is that no empirical constants are needed. The Bruschke model is based on a square unit cell arrangement of fibers. An analytical solution was derived using the lubrication approximation. Like the Vijaysri model, an advantage of Bruschke model is that no empirical constants were needed. Disadvantages of this model include the ideal geometric assumption. The Bruschke model was used for the processing of all the preforms. Finally, an equation to predict void content was introduced.

3.7 References

Åstrom et al., 1992: Åstrom, B., Pipes, B., Advani, S., "On Flow Through Aligned Fiber Beds and Its Application to Composites Processing", *Journal of Composite Materials*, 1992, v 26, n 9, p 1351-1373.

Beyer, 1984: Beyer, W., *CRC Standard Mathematical Tables*, CRC Press, Florida, 27th Edition, 1984.

Brodkey and Hershey, 1988: Brodkey, R. and Hershey, H., *Transport Phenomena: A Unified Approach*, McGraw-Hill Book Company, New York, 1988.

Bruschke and Advani, 1993: Bruschke, M, and Advani, S., " Flow of Generalized Newtonian Fluids Across a Periodic Array of Cylinders", *J. Rheol.*, 1993, v 37, n 3, p 479-497.

Carman, 1956: Carman, P., *Flow of Gases Through Porous Media*, Butterworths Publications, London, 1956.

Kozeny, 1927: Kozeny, J., *Sitzungsberichte Akademie der Wissenshaft, Wien*, Abt. IIa, 136, p. 271-306, 1927.

Vijaysri et al., 1999: Vijaysri, M, Chhabra, R., Eswaran, V., "Power-law Fluid Flow Across an array of Infinite Circular Cylinders: A Numerical Study", *J. Non-Newtonian Fluid Mech.*, 1999, v 87, p 263-282.

Whitaker, 1992: Whitaker, S., *Introduction to Fluid Mechanics*, Krieger Publishing Company, Florida, 1992.

CHAPTER IV

MATERIALS AND METHODS

4.1 Introduction

In Section 4.2, the materials used in this research are discussed. In Section 4.3, the experiments conducted to determine the input variables for the models detailed in Chapter III are discussed. In Section 4.4, the experiments conducted to determine the validity of the models, presented in Chapter III, for continuous fiber-reinforced polymer (CFRP) processing are discussed. In Section 4.5, the design of experiments is outlined.

4.2 Materials

As stated earlier, one goal of this thesis was a comprehensive study of thermoplastic composites processing. Therefore, different fibers, resins, and preforms were used. In addition, practical resins and fibers were selected. This section is divided into three areas based on the three preforms: random mat, powder-coated towpreg, and commingled fibers.

4.2.1 Mat Preforms

Polypropylene and nylon 6 sheets were used as the matrix in the fiber mat preforms. The polypropylene sheet was Resinol Type O® from Allied Resinous Products, and the nylon sheet was Nylatron® 907 from DSM. The properties of the resins are located in Table 4.1.

Glass, carbon, and sisal mats were used for the reinforcement mat. The glass mat was type 8447 from John Manville. Technical Fibre supplied the carbon mat and Georgia Composites supplied the sisal mat. The mats were composed of single fiber filaments that were arranged randomly. Figure 4.1 displays the scanning electron microscopy photograph (SEM) pictures of the mats. The properties of the mats are located in Table 4.1.

4.2.2 Towpreg

Applied Fiber Systems supplied the towpreg. Nylon 6 and polyphenylene sulfide (PPS) were used as the matrices in the powder-coated towpreg. The specific grade of the resins is proprietary information. Properties of the resins are located in Tables 4.2.

E-glass and carbon were used as the reinforcement in the towpreg. Figure 4.2 is a collection of SEM pictures of the towpreg. For each resin and fiber combination for the towpreg, two different weight percents were used, and these values are located in Table 4.2.

4.2.3 Commingled Fibers

Vetrotex supplied the commingled fibers under the tradename Twintex®. The properties of Twintex® are listed in Tables 4.3. Polypropylene fibers were used as the matrix in the commingled fibers, and glass fibers were used as the reinforcement. Two different resin weight percentages were used. Figure 4.3 is a SEM photograph of the Twintex®.

Table 4.1: Properties of Resin and Fiber: Mat Preforms

	Fiber Radius [μm]	Fiber Length [cm]	Area Weight [g/cm^2]	Density [g/cm^3]	Thickness as Received [cm]
Resin					
polypropylene	-		-	0.905	0.635
nylon 6	-		-	1.13	0.635
Fiber					
glass	8	3.81	0.0229	2.54	0.203
sisal	125	5.08	0.0245	1.45	0.317
carbon	4	3.81	0.0279	1.70	0.152

Table 4.2: Properties of Resin and Fiber: Towpreg

	Fiber Radius [μm]	Fiber* Length [cm]	Resin Weight Percent [%]	Fiber Density [g/cm^3]	Resin Density [g/cm^3]	Thickness as Received [cm]	Width as Received [cm]
carbon/N6	3.5	25.4	33 & 43	1.78	1.13	0.033	0.469
glass/N6	8	25.4	34 & 26	2.58	1.13	0.035	0.355
carbon/PPS	3.5	25.4	38 & 48	1.78	1.35	0.030	0.469

*The towpreg was manually cut to this length. This is explained in greater detail in Section 4.4.1.

Table 4.3: Properties of Resin and Fiber: Commingled Fibers (Twintex®)

	Fiber Radius [μm]	Fiber* Length [cm]	Resin Radius [μm]	Resin Weight Percent [%]	Fiber Density [g/cm^3]	Resin Density [g/cm^3]
glass/PP	9	25.4	12.5	25 & 40	2.61	0.905

*The commingled fibers were manually cut to this length. This is explained in greater detail in Section 4.4.1.

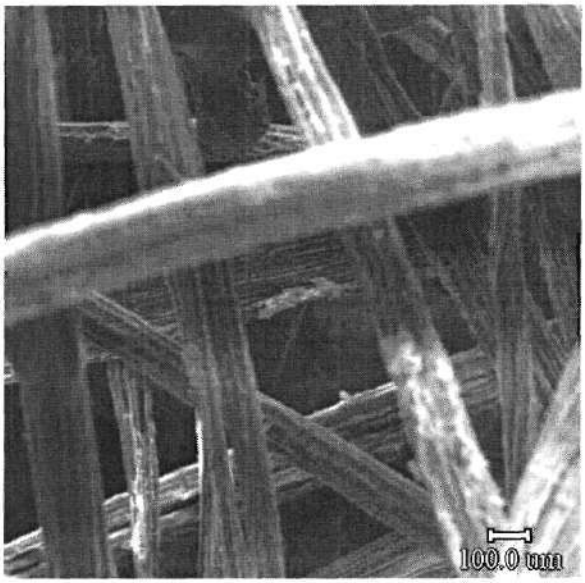

A

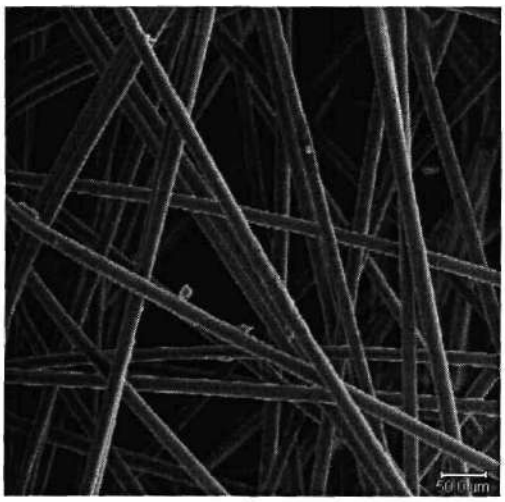

B

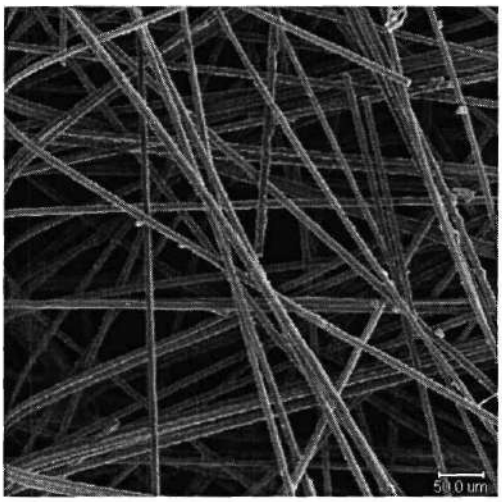

C

Figure 4.1: SEM photographs of fiber mats where A, B, and C refer to sisal mat, glass mat, and carbon mat, respectively. The micron bars on the photos A, B, and C are 100 μm, 50 μm, and 50 μm, respectively.

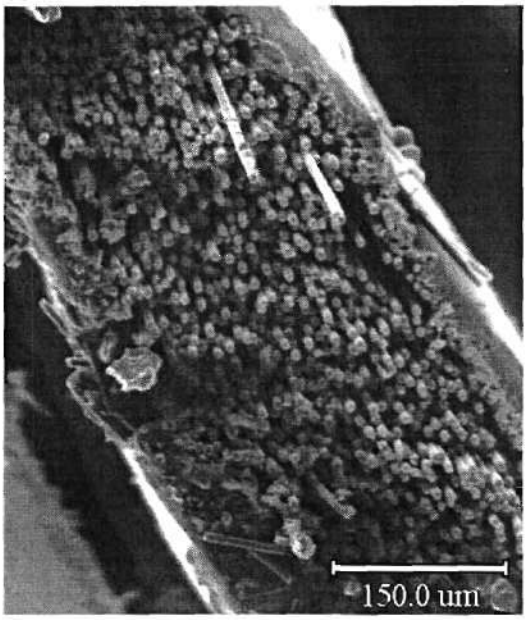

B

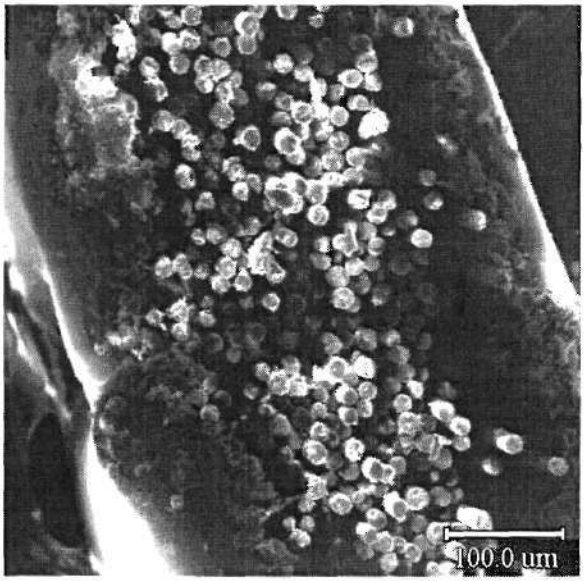

C

Figure 4.2: SEM photographs of towpreg where A, B, and C refer to carbon/N6, carbon/PPS, and glass/N6 glass, respectively.

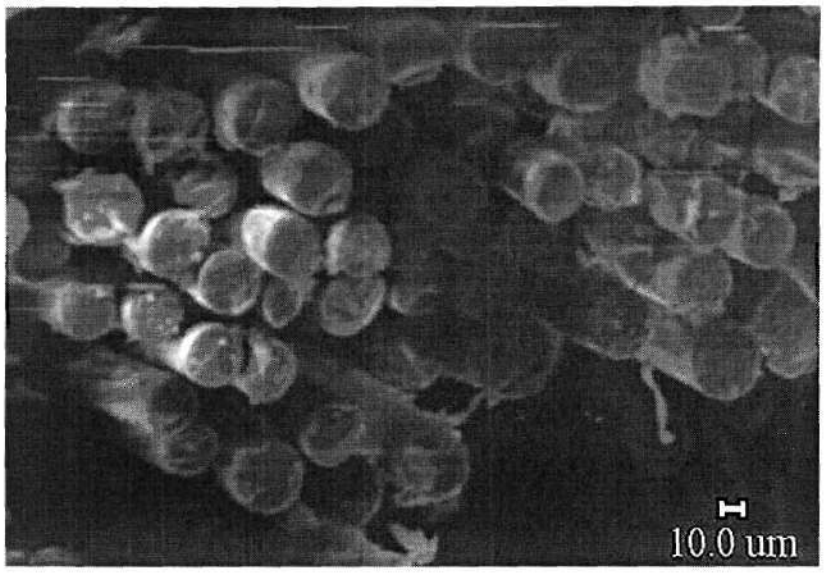

Figure 4.3: SEM photograph of commingled fibers (Twintex®).

4.3 Experimental: Input Parameters for Chapter III Models

The procedures used to determine the input parameters listed in Table 3.1 in Chapter III are described in this Section.

4.3.1 Melt Temperature

The melt temperature was needed to determine the minimum composite processing temperature. A TA Instruments Differential Scanning Calorimetry (DSC) (Model #2920) was used to determine the melt temperature of the polymers.

The resins were dried according to vendor instructions. The N6 used in the mat preforms and the towpreg was dried at 85 °C for 4 hours. The PP used in the mat preforms and towpreg was dried at 85 °C for 1 hour. The PPS was dried at 120 °C for 3 hours. Next, a small amount of dried resin was placed in an aluminum pan and covered. Then, the resin was heated at a rate of 20 °C/min. Next, it was cooled down to room temperature and reheated at the same rate. The first heating removed the thermal history of the sample. The experiment was conducted under a nitrogen atmosphere.

4.3.2 Degradation Temperature

The degradation temperature was needed to determine the maximum processing temperature. Thermal gravimetric analysis (TGA) was used to determine the degradation temperature. A Seiko TG/DTA (Model #320) was used to perform the analysis.

The resins were dried according to vendor instructions, as described above. Next, a small amount of resin was placed in an aluminum pan. Then, the resin was heated at a rate of 20 °C/min up to about 600°C. During composite processing, the resin is exposed

to elevated temperatures for specific time periods. Because of this, isothermal experiments also were conducted in which the resin was held at the processing temperature for specific time periods to assess the affect of holding time at temperature on the resin stability. All of the tests were conducted under an air purge.

4.3.3 Rheology

Viscosity versus shear rate data was needed to obtain power law constants. A Haake RS 150 with 20 mm parallel plates was used. Before each test, the resins were dried according to vendor specifications, as described above. The dried resin was placed between the heated parallel plates and viscosity versus shear rate data was recorded. Two tests were run for each polymer and each processing temperature.

4.3.4 Void Content

Void content is used to quantify the quality of a composite part. The void content was calculated by using the experimental and theoretical density of the composite and Equation 4.1. The theoretical density was calculated with Equation 4.2. Method A of ASTM-D792 standard was used as a guideline to calculate the experimental density of the composite.

$$v_{void} = \frac{\rho_{ct} - \rho_{ce}}{\rho_{ct}} \tag{4.1}$$

Where:

v_{void} = void content of the composite

ρ_{ct} = theoretical density of the composite, kg/m^3

ρ_{ce} = experimental density of the composite, kg/m^3

$$\rho_{ct} = \frac{100}{\left(\frac{w_r}{\rho_r} + \frac{w_f}{\rho_f}\right)} \tag{4.2}$$

Where:

w_f = weight percent of fiber in the composite, % , discussed in Section 4.3.5

w_r = weight percent of resin in the composite, % , discussed in Section 4.3.5

ρ_r = density of resin, kg/m^3

ρ_f = density of fiber, kg/m^3

As stated above, method A of ASTM-D792 was used to calculate the experimental density, ρ_{ce}, of the composite. Five 2.54 cm by 2.54 cm samples were cut from the composite using a diamond blade saw. Next, a Mettler Toledo (Model AG245) density determination kit was used to weigh the sample in air and in a beaker of ethanol to obtain the specific gravity of the sample using Equation 4.3

$$\gamma = \frac{W_{ca}}{W_{ca} - W_{ce}} \tag{4.3}$$

Where:

γ = experimental specific gravity of composite

W_{ca} = weight of composite sample in air, kg

W_{ce} = weight of composite sample in ethanol, kg

The density of the composite is determined using the specific gravity and the density of ethanol with Equation 4.4.

$$\rho_{ce} = \gamma \rho_e \tag{4.4}$$

Where:

γ = experimental specific gravity of composite

ρ_e = density of ethanol, kg/m^3

4.3.5 Fiber and Resin Weight Percents

The weight percentages of the components of the composites are needed to calculate the theoretical density, and the theoretical density is needed to calculate void content. The void content, discussed in Section 4.3.4 above, is used to assess the quality of a composite part. A liquid digestion method and a resin burn-off method were used to determine the weight percentages. ASTM-D3171-76 and ASTM-2584-94 were used as guidelines. In both methods, resin is removed from the composite, and the weight of the remaining fibers is measured. In the liquid digestion method, a small sample of the composite is placed in a solvent that dissolves the matrix. In the resin burn-off method, a small sample of the composite is placed in a furnace, and the resin is burned off. The weight percentage of the fiber is calculated using Equation 4.5.

$$w_f = 100\left(\frac{W_{fc}}{W_c}\right) = (1 - w_r) \tag{4.5}$$

Where:

w_f = weight percent of fiber in the composite, %

w_r = weight percent of resin in the composite, %

W_{fc} = weight of fibers in the composite sample, g

W_c = weight of composite sample, g

To determine the weight percentages, five 2.54 cm by 2.54 cm samples were cut from composite. For the glass composites, the burn-off method was used. The sample was placed in a furnace, which was heated to 1050 °F, for 1 hour. Next, the weight of the remaining fiber was recorded after the sample was cooled to room temperature. For the carbon fiber and nylon 6 composites, the matrix digestion method was used, since carbon fibers can not withstand the high temperatures required for the burn-off method. The carbon and nylon 6 composite sample was placed in formic acid and allowed to sit over night. Next, the sample was filtered, washed with acetone and water, dried, and then weighed. For the carbon fiber and PPS composites, the sample was dissolved in hot sulfuric acid at 75 °C. Next, the sample was filtered, washed with water and acetone, dried, and then weighed.

4.3.6 SEM

SEM was used to verify the permeation depth of resin into the mat preforms and to determine the porosity of the towpreg and commingled fibers. Small samples were cut from the composite, and the cross section was ground smooth and polished. Next, the sample was glued to a SEM sample holder and coated with gold in a sputter coater. Finally, the sample was placed in the scanning electron microscope (Hitachi S-800) and viewed.

4.3.7 Porosity

The models detailed in Chapter III require porosity, ε, as an input variable. Figure 4.4 is an illustrative definition of porosity in the towpreg and commingled fiber preforms. The porosity, ε, is the porosity that is seen by the advancing flow front. Referring to Figure 4.4 again, as the flow front passes through the fiber bed, the porosity seen by the flow front remains constant. The porosity should not be confused with overall void content of the composite, which does decrease as the resin flows into the fiber bed. The porosity of the fiber bed in the powder-coated towpreg and the commingled fibers was calculated from SEM images using Iridium software (Version 5.14N) installed as an accessory to the SEM equipment described above. Since the contrast between the matrix and the fiber is great enough, the software uses the distribution of pixels in the image to calculate the fraction of the SEM image occupied by fibers, and the porosity can be calculated from this value by subtracting one. More detail about the porosity of the towpreg and commingled fiber preforms are discussed in Chapter V.

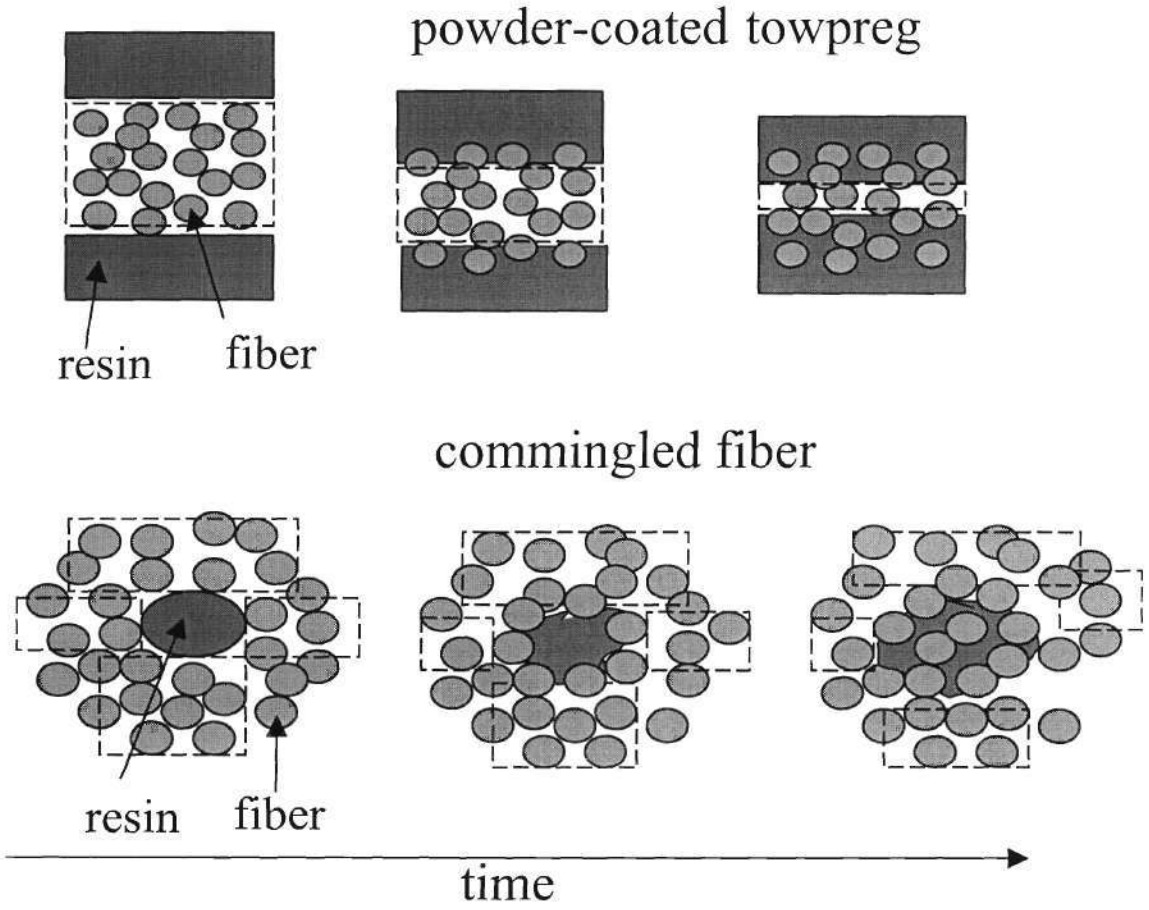

Figure 4.4: Illustration of porosity available for flow for the towpreg and commingled fiber preforms. The porosity, ε, is equal to one minus the fiber volume fraction inside the dotted box of fibers.

In the mat preforms, as described above, the porosity refers to the porosity seen by the advancing flow front. The porosity, as shown in Equation 4.6, is equal to one minus the fiber volume fraction. First, a stack of mats was weighed to obtain m_f. Next, the weighed mats were placed in an empty mold. The area of the mold is 25.4 cm by 25.4 cm. Next, the thickness of the mats under pressure, δ, was obtained using the experimental apparatus described in Section 4.4. The processing pressures used during the permeation tests, which are discussed in Section 4.5, were used to compress the mats. The density of the fibers, ρ_f, in the mats was obtained from the vendor.

$$v_f = \frac{V_f}{V_{mold}} = \frac{\frac{m_f}{\rho_f}}{A_{mold}\delta} = 1 - \varepsilon \tag{4.6}$$

Where:

v_f	=	fiber volume fraction, dimensionless
V_f	=	volume of fibers, m^3
V_{mold}	=	volume inside mold, m^3
ε	=	porosity
A_{mold}	=	cross sectional area of mold, m^2
ρ_f	=	density of fiber, g/m^3
δ	=	thickness of mats under pressure, m
m_f	=	mass of mats, kg

4.4 Experimental: Permeation Apparatus and Procedure

4.4.1 Preform Preparation

For the mat preforms, resin sheets were placed between sheets of mats to make a "sandwich" form. The following number of sheets was used on each side of the resin sheet: 5-8 sheets for glass mat, 3 sheets for carbon mat, 6-7 sheets for sisal mat. For the towpreg, the tows were wound onto a 25.4 cm by 25.4 cm mandrel using a filament winder, and the ends were spot welded to make 25.4 cm by 25.4 cm sheets. Then 12 sheets of the wound towpreg were stacked to make the preform. The same procedure used for the towpreg above was used for the commingled fibers.

4.4.2 Permeation Apparatus and Procedure

A simple schematic of the experimental set-up for permeation is shown in Figure 4.5. A Wabash (Model #V50-1818-2TMX) hot press was used to study the transverse permeation. A 25.4 cm by 25.4 cm mold was used to house the preforms. The temperature of the mold was monitored with an Omega (Model TJ120-CAIN-316U-12-GG) thermocouple. The displacement of the mold, which was used to monitor the transient permeation, was monitored with a linear variable differential transformer (LVDT) from Lucas Control Systems Products (Model 4000HR-006-010). The LVDT was attached to a lever on the Wabash press that moved with the bottom platen of the press. The movement of the platen was due to the displacement of the mold, which in turn was due to the resin permeating into the fiber bed. The accuracy of the LVDT reading is ± 1 %. The temperature and LVDT data was collected using an Omega data

acquisition card (Model WB-Dynares-8-Ultra), which was installed into a DELL (Model Dimension XPS D333) PC.

The procedure below was used to study the permeation of the resin in the towpreg and commingled fiber preforms. For the mat preforms, step 5 and step 6 were reversed. For the towpreg and commingled fibers, the pressure was held during the cooling period to prevent void formation. Figure 4.6 is a schematic of the transverse permeation process.

1. The mold is placed between the platens of the press.
2. The hot press is heated to the processing temperature.
3. The mold is allowed to reach the processing temperature. The temperature of the mold is monitored with a thermocouple. The sample is placed in the hot mold. The sample is allowed to reach processing temperature. The times required to reach the processing temperatures are: carbon mat preforms (30 minutes), sisal mat preforms (45 minutes), glass mat preforms (60 minutes), towpreg and commingled fibers preforms (10 minutes).
4. Force is applied to the mold for a specific amount of time.
5. After the specified time has been reached, cooling water and cooling air are used to cool the mold.
6. The force is removed.
7. The mold with the sample is removed from the press. The composite is removed from the mold and prepared for measurement of properties.

8. Mold compliance was obtained by compressing the mold without a preform inside.

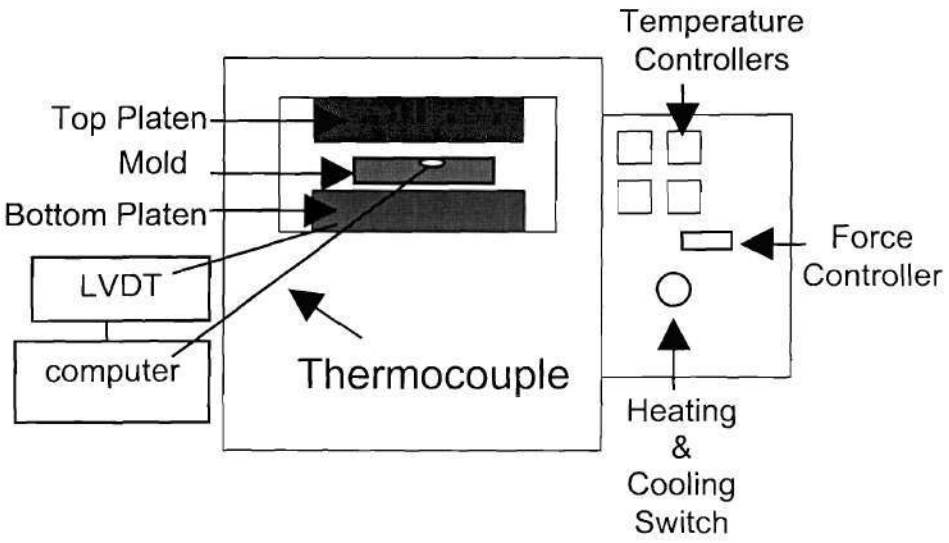

Figure 4.5: Schematic of permeation apparatus.

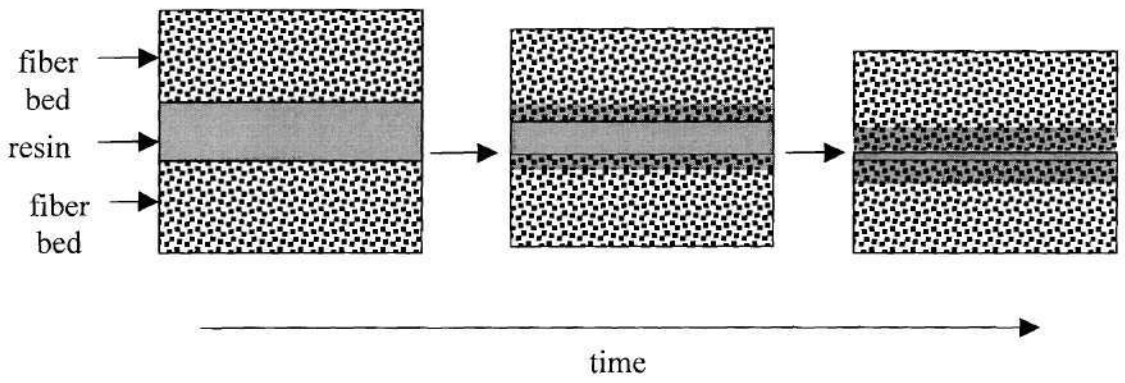

Figure 4.6: Schematic of a mat preform during transverse permeation process.

As was discussed in Chapter I, one goal of this thesis was to model the void content of towpreg and commingled fiber composites as a function of processing and material parameters. The void content model was discussed in Chapter III. In the model, the initial void content of the composite is needed. To obtain the initial void contents, composites were made using the same permeation procedure described above except, step 4 was excluded. After step 3 above and after cooling, the composite was removed and the initial void content was calculated using the procedures discussed earlier in Section 4.3.4.

4.5 Design of Experiments

Because a goal of this thesis was to conduct a comprehensive experimental study of thermoplastic composite processing, a vast array of fibers, resins, and processing conditions were chosen. In addition, practical materials and practical operating conditions were selected. The designs of experiments are located in Tables 4.4-4.6. Two tests were run at each condition in the tables. The experiments were designed so that the permeation flow front would not completely fill the void spaces in the fiber beds. Because of this, in each preform there were resin rich layers. For example, in the mat preforms, the top stack of mats and the bottom stack of mats never touched. Therefore, there was a layer of resin left in the "sandwich" style mat preform at the end of the permeation experiment described in Section 4.4.

Table 4.4: Experimental Design: Mat

Experiment	Fiber mat	Resin	Pressure [MPa]	Temperature [°C]	Pressure Hold Time [min]
M1	glass	polypropylene	1.38	170	5.5
M2	glass	polypropylene	1.38	190	5.5
M3	glass	polypropylene	2.76	170	5.5
M4	glass	polypropylene	2.76	190	5.5
M5	glass	nylon 6	1.38	230	5.5
M6	glass	nylon 6	2.76	230	5.5
M7	carbon	polypropylene	1.38	170	4
M8	carbon	polypropylene	1.38	190	4
M9	carbon	polypropylene	2.76	170	4
M10	carbon	polypropylene	2.76	190	4
M11	carbon	nylon 6	1.38	230	4
M12	carbon	nylon 6	2.76	230	4
M13	sisal	polypropylene	0.34	170	4
M14	sisal	polypropylene	0.34	190	4

*Note: Shorter pressure hold times were used for carbon and sisal mats because of limited product supply and cost.

Table 4.5 Experimental Design: Towpreg

Experiment	Towpreg	Resin Weight Percent [%]	Pressure [MPa]	Temperature [°C]	Pressure Hold Time [min]
T1	carbon/nylon 6	43	0.52	230	2.5
T2	carbon/nylon 6	43	0.52	260	2.5
T3	carbon/nylon 6	43	1.03	230	2.5
T4	carbon/nylon 6	43	1.03	260	2.5
T5	carbon/nylon 6	33	0.52	230	2.5
T6	carbon/nylon 6	33	0.52	260	2.5
T7	carbon/nylon 6	33	1.03	230	2.5
T8	carbon/nylon 6	33	1.03	260	2.5
T9	glass/nylon 6	34	0.52	230	2.5
T10	glass/nylon 6	34	0.52	260	2.5
T11	glass/nylon 6	34	1.03	230	2.5
T12	glass/nylon 6	34	1.03	260	2.5
T13	glass/nylon 6	26	0.52	230	2.5
T14	glass/nylon 6	26	0.52	260	2.5
T15	glass/nylon 6	26	1.03	230	2.5
T16	glass/nylon 6	26	1.03	260	2.5
T17	carbon/PPS	48	0.52	310	2.5
T18	carbon/PPS	48	1.03	310	2.5
T19	carbon/PPS	38	0.52	310	2.5
T20	carbon/PPS	38	1.03	310	2.5
T21	carbon/nylon 6	43	*	230	*
T22	carbon/nylon 6	43	*	260	*
T23	carbon/nylon 6	33	*	230	*
T24	carbon/nylon 6	33	*	260	*
T25	glass/nylon 6	34	*	230	*
T26	glass/nylon 6	34	*	260	*
T27	glass/nylon 6	26	*	230	*
T28	glass/nylon 6	26	*	260	*
T29	carbon/PPS	48	*	310	*
T30	carbon/PPS	38	*	310	*

*Note: Experiments to determine initial void content. No pressure was applied

Table 4.6: Experimental Design: Commingled

Experiment	Twintex®	Resin Weight Percent [%]	Pressure [MPa]	Temperature [°C]	Pressure Hold Time [s]
C1	glass/PP	25	0.34	180	80
C2	glass/PP	25	0.34	210	80
C3	glass/PP	25	0.69	180	80
C4	glass/PP	25	0.69	210	80
C5	glass/PP	40	0.34	180	80
C6	glass/PP	40	0.34	210	80
C7	glass/PP	40	0.69	180	80
C8	glass/PP	40	0.69	210	80
C9	glass/PP	25	*	180	*
C10	glass/PP	25	*	210	*
C11	glass/PP	40	*	180	*
C12	glass/PP	40	*	210	*

*Note: Experiments to determine initial void content. No pressure was applied

CHAPTER V

RESULTS and DISCUSSION

5.1 Introduction

In Section 5.2, the results of the material characterization and model input parameters experiments are discussed. In Sections 5.3-5.6, the experimental and theoretical permeation results are presented and discussed. Uncertainty and limitations of the permeation results are discussed in Section 5.7. References are listed in Section 5.8.

5.2 Material Characterization and Input Parameters for Chapter III Models

5.2.1 Melt Temperature

The melt temperatures of the polymers used in this research were needed to determine the minimum composite processing temperature. Differential scanning calorimetry (DSC) analysis was performed to determine the melt temperatures. Figures 5.1-5.5 are the DSC second heating curves of the polymers. The melting points determined for the polypropylene (PP) and nylon 6 (N6) that were used during the mat processing were 160 °C and 219 °C, respectively. The manufacturers of these two polymers reported melting temperatures of 165 °C for the PP and 216 °C for the N6. Figures 5.1 and 5.2 are the DSC curves of the PP and N6 used with the mat preforms.

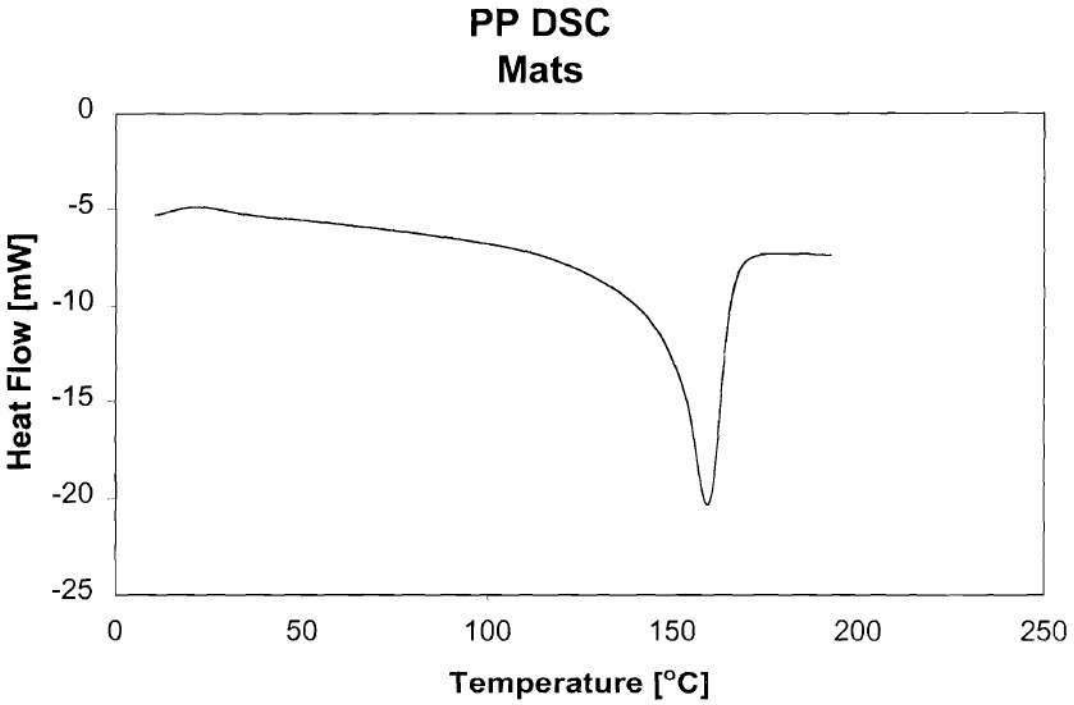

Figure 5.1: DSC curve of PP used for mat preforms.

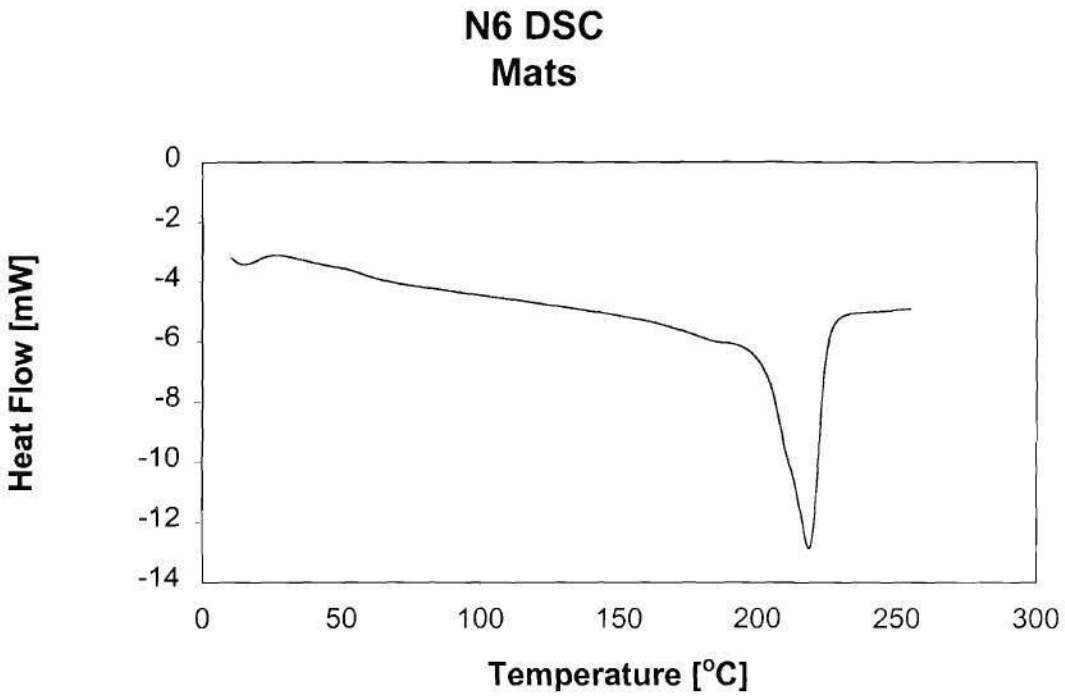

Figure 5.2: DSC curve of N6 used for mat preforms.

The melt temperatures obtained for the N6 and polyphenylene sulfide (PPS) used in the towpregs were 222 °C and 284 °C, respectively. These melting points also agreed well with the melt temperatures reported by the manufacturers. The manufacturers of these two resins reported melting points of 220 °C for the N6 and 280 °C for the PPS. Figures 5.3 and 5.4 are the DSC curves of these two polymers. A melt temperature of 160 °C was found for the PP used in the commingled fibers. Like the other resins discussed above, this melting point compared well with the value listed by the manufacturer. The manufacturer listed a melt temperature of 159 °C. Figure 5.5 is the DSC curve for the PP used in the commingled fiber preform. As discussed earlier, the melt temperatures of the resins were used as a guideline to select the minimum processing temperatures used in this research.

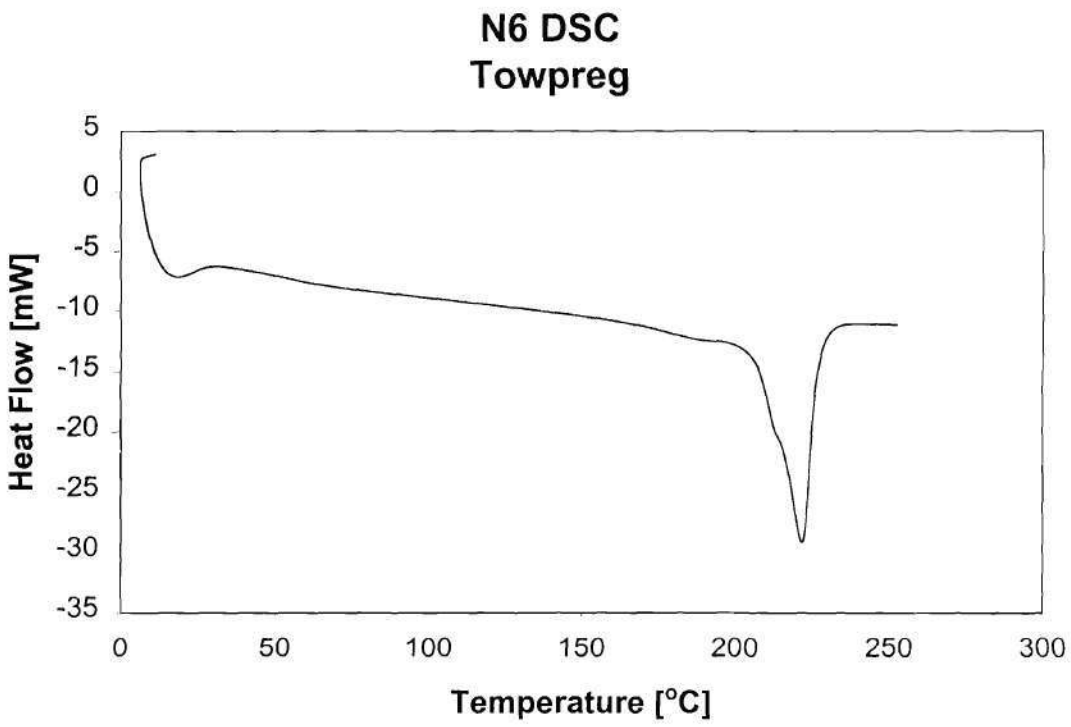

Figure 5.3 DSC curve of N6 used in towpreg.

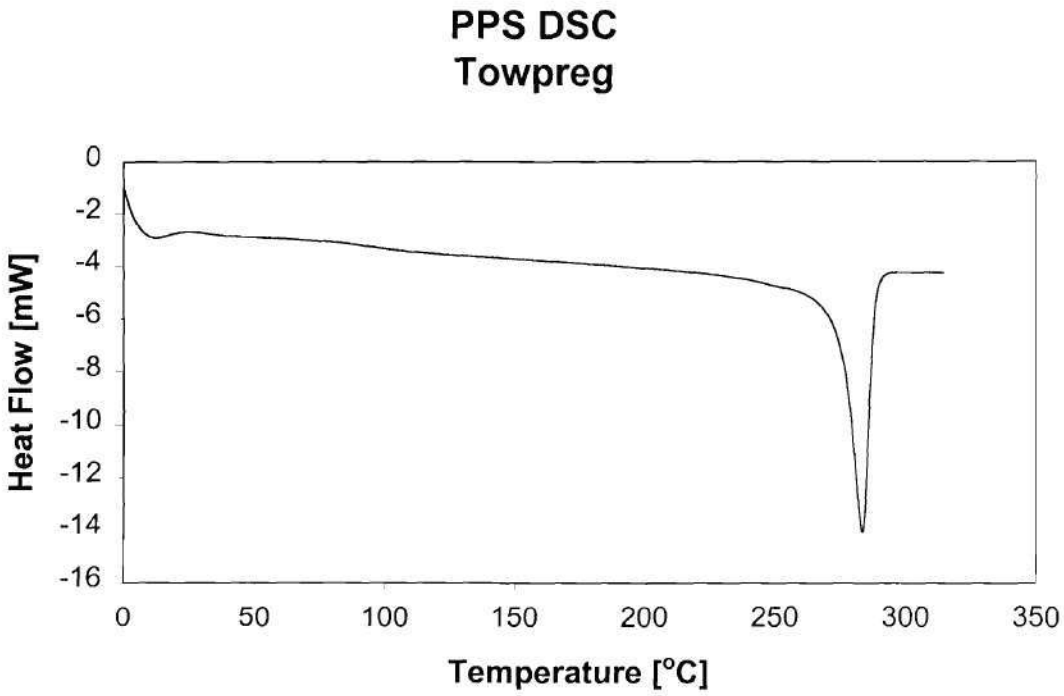

Figure 5.4: DSC curve of PPS used in towpreg.

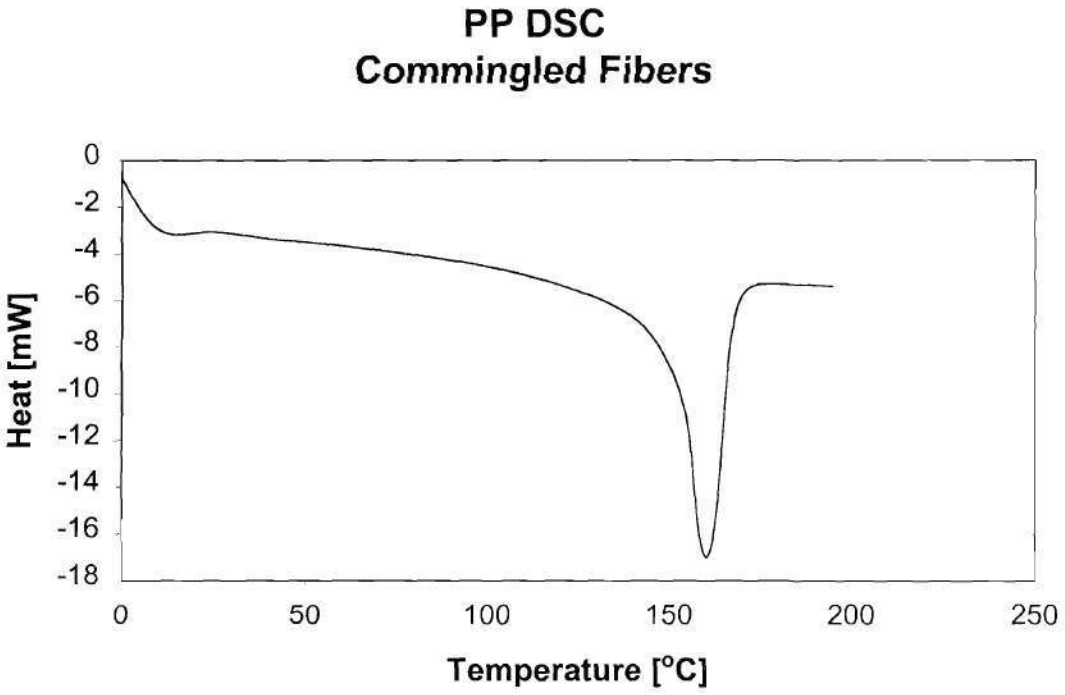

Figure 5.5: DSC curve of PP used in commingled fibers.

5.2.2 Degradation Temperature

The degradation temperatures of the polymers used in this research were needed to determine the maximum processing temperature. TGA analysis was performed to determine the degradation temperatures. Temperature ramp and isothermal experiments were conducted. Figures 5.6-5.10 are the TGA curves for the polymers. The degradation temperature is recorded as the point at which the polymer loses 5 % of its weight. As shown in Figures 5.6 and 5.7, the degradation temperatures found for the PP and N6 used in the mat preforms were 290 °C and 380 °C, respectively.

Since the heating times required to reach the processing temperatures for mat processing were 0.5-1 hour, 1 hour isothermal TGA experiments were conducted at temperatures ~30 °C higher than the maximum composite processing temperature. As shown in Figure 5.6 for the PP, there was no degradation during this time period. For the N6 as shown in Figure 5.7, there was about 1.4 % degradation, where about 0.7 % of this degradation was due to moisture. This was expected since it is well documented that N6 retains moisture and will degrade if exposed to elevated temperatures and air (Floyd, 1966). Since N6 is so sensitive to processing conditions, only one processing temperature of 230 °C was used for its processing with the mat preforms.

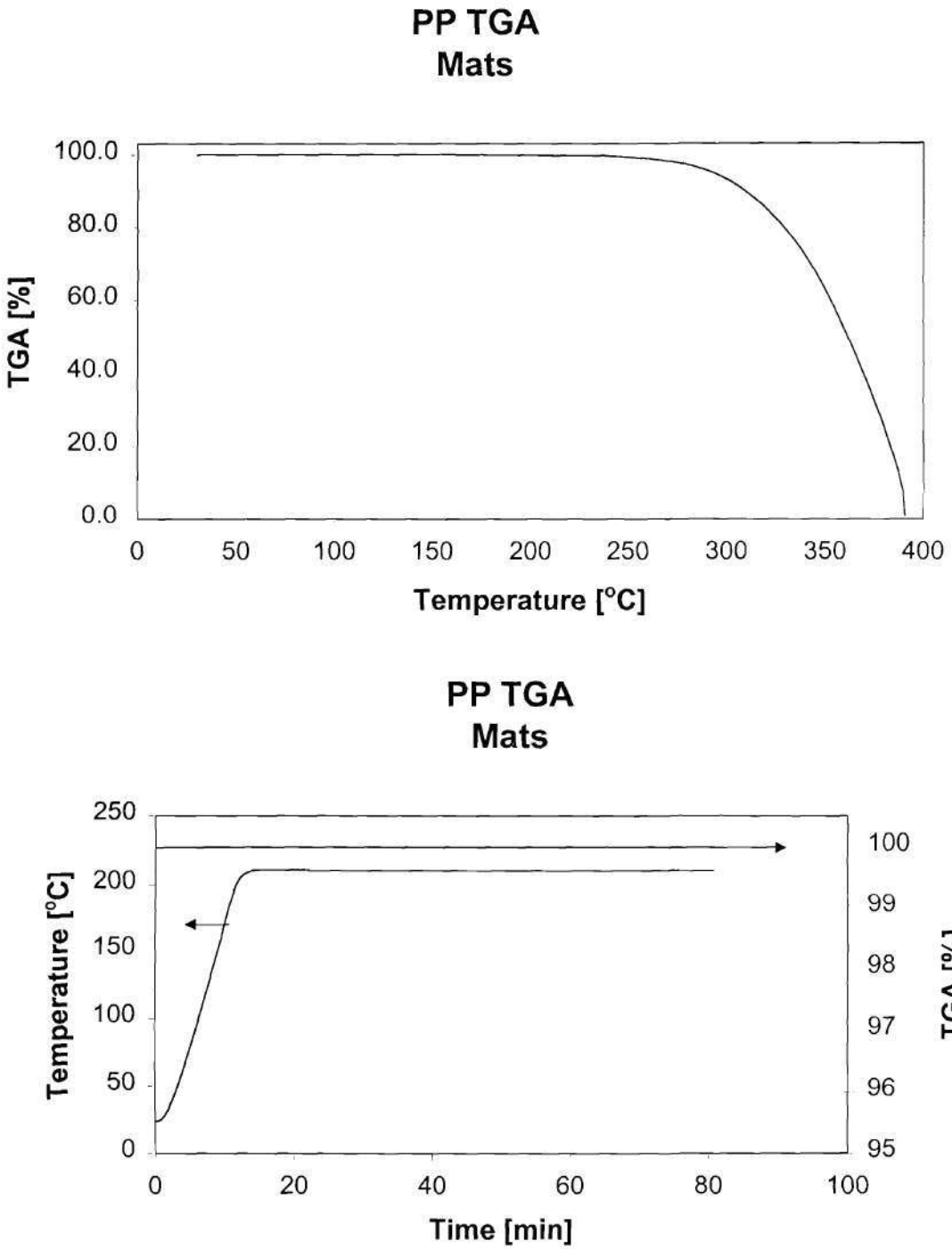

Figure 5.6: TGA of PP used in mats. In the top graph the heating rate is 20 °C/min and in the bottom graph the temperature is held at ~210 °C for 1 hour.

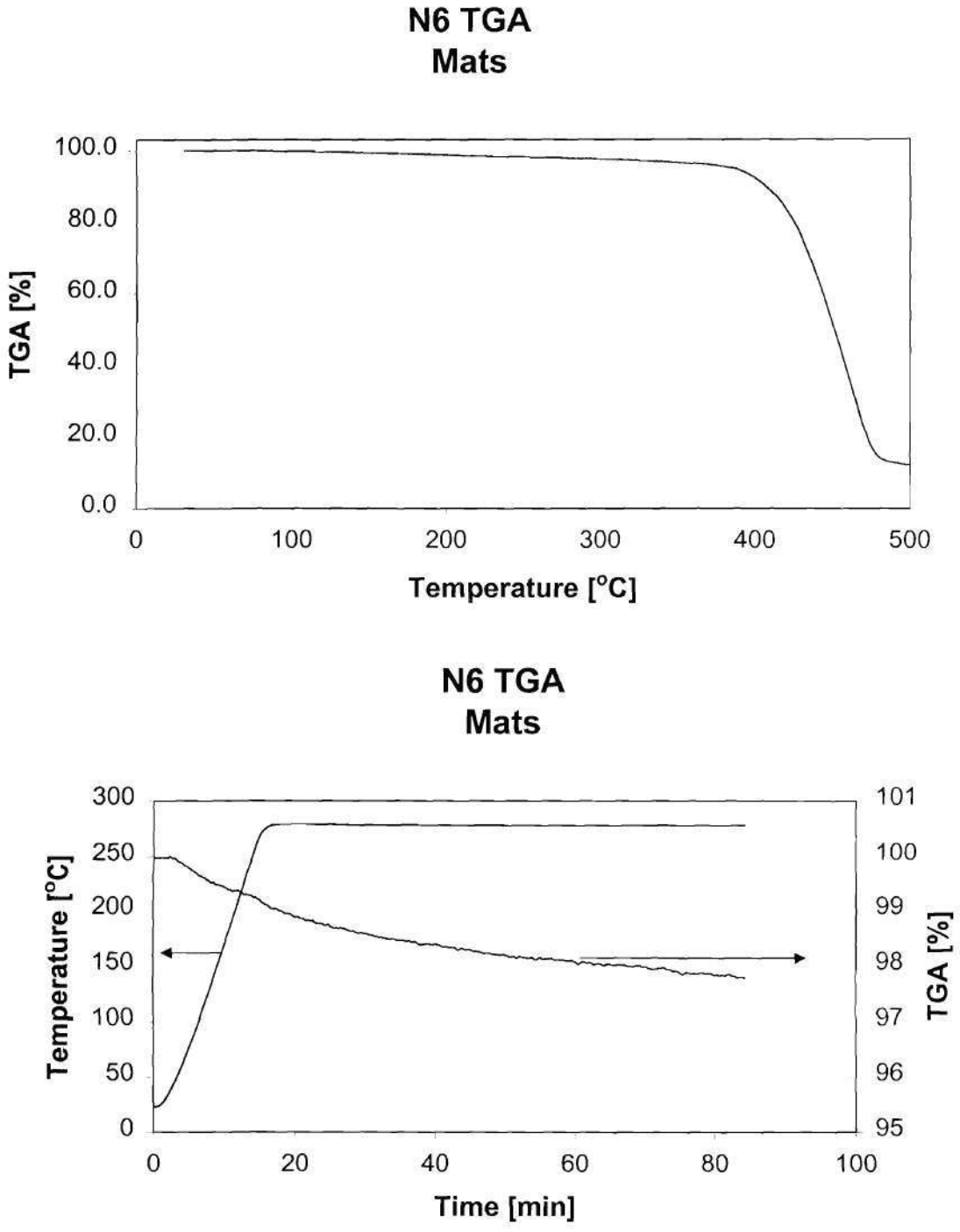

Figure 5.7: TGA curves of N6 used in mat preforms. In the top graph the heating rate is 20 °C/min and in the bottom graph the temperature is held at ~275 °C for 1 hour.

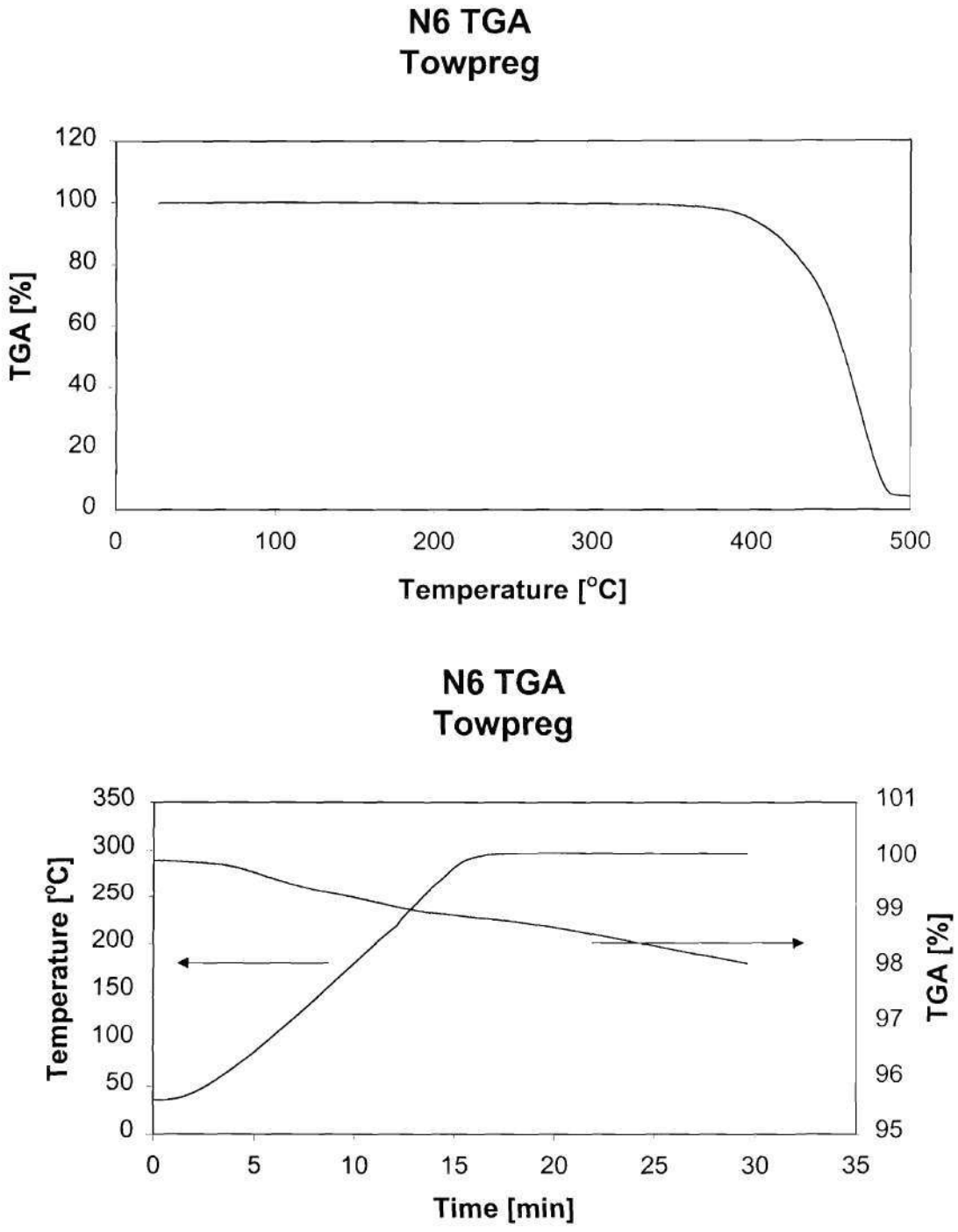

Figure 5.8: TGA curves of N6 used in towpreg. In the top graph the heating rate is 20 °C/min and in the bottom graph the temperature is held at ~297 °C for 15 minutes.

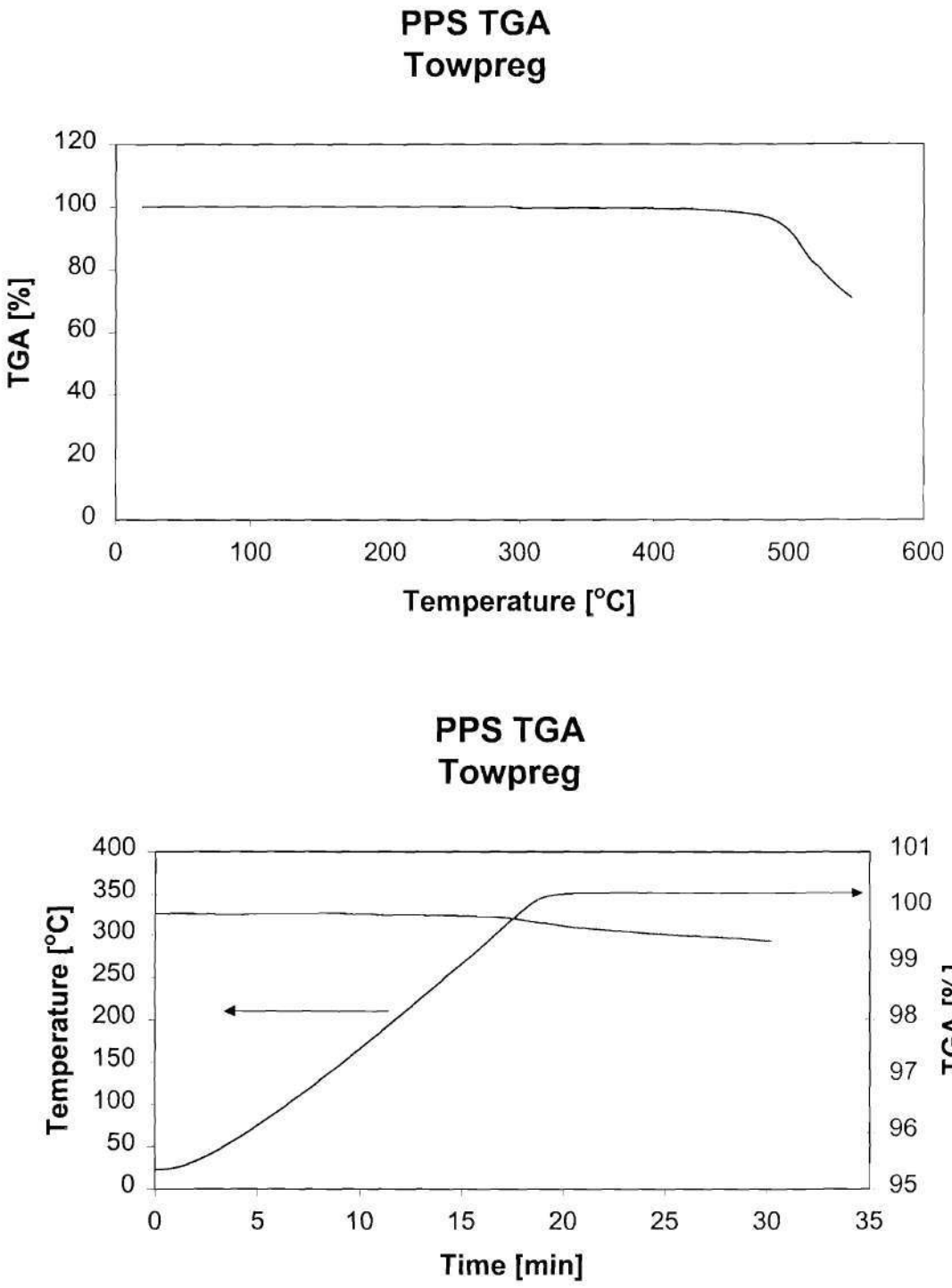

Figure 5.9: TGA curves of PPS used in towpreg. In the top graph the heating rate is 20 °C/min and in the bottom graph the temperature is held at ~350 °C for 15 minutes.

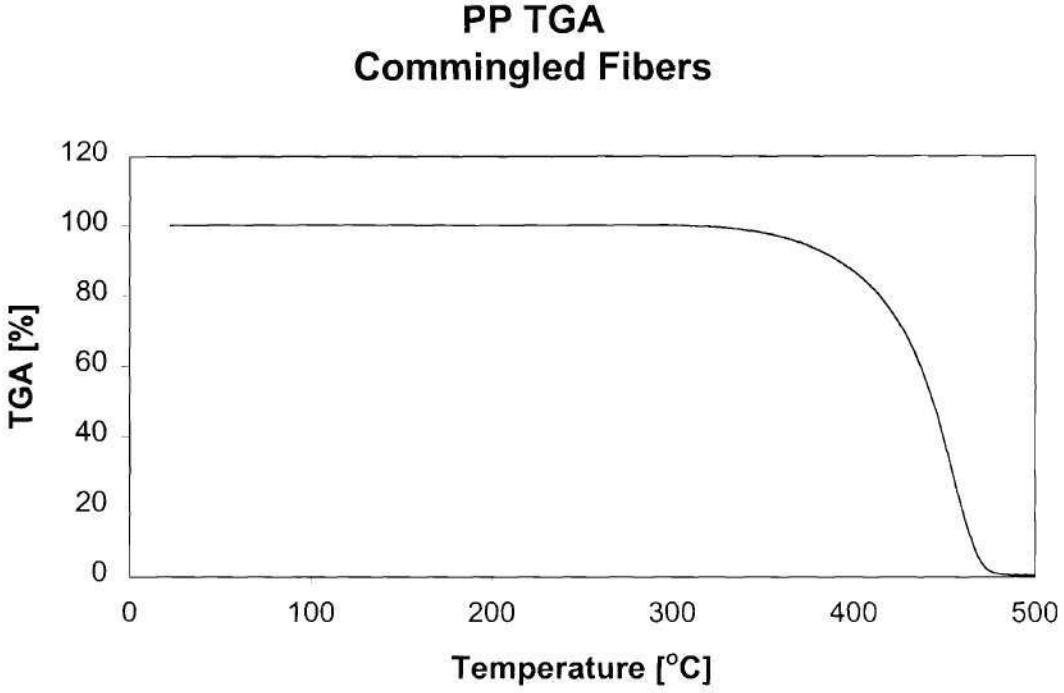

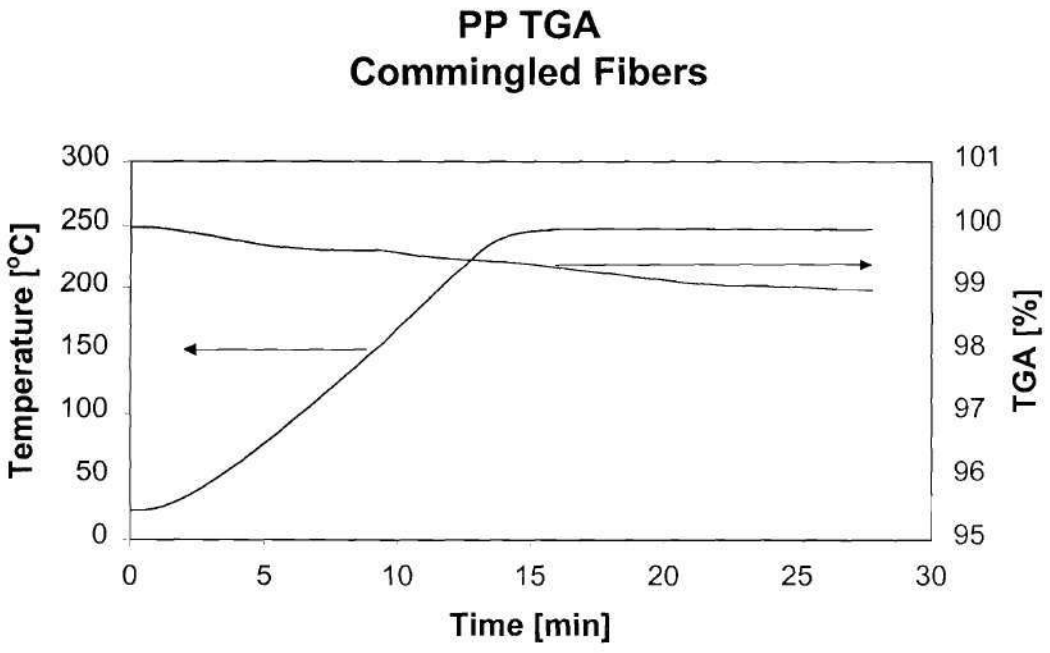

Figure 5.10: TGA curves of PP used in commingled fibers. In the top graph the heating rate is 20 °C/min and in the bottom graph the temperature is held at ~248 °C for 15 minutes.

As displayed in Figures 5.8 and 5.9, degradation temperatures of 400 °C and 490°C were obtained for the N6 and PPS used in the towpreg. Isothermal experiments of 15 minutes were conducted at temperatures ~30 °C higher than the maximum composite processing temperatures. As shown in Figure 5.8, N6 lost about 1.4 % of its weight during this duration. About 0.7 % of the loss was probably attributed to moisture. As shown in Figure 5.9, PPS lost about 0.6 % of its weight.

Referring to Figure 5.10, the degradation temperature found for the PP used in the commingled fiber preform was 370 °C. Isothermal experiments of 15 minutes were conducted at temperatures ~30 °C higher than the maximum composite processing temperature. During this time period, the PP lost about 1 % of its weigh where about 0.5 % of this loss was probably due to moisture.

As stated earlier, the degradation temperatures obtained and discussed above were used to help select the maximum composite operating temperatures. Table 5.1 lists the melt temperatures, composite processing temperatures, and degradation temperatures.

Table 5.1: Thermal properties of polymers

Polymer	Preform	Experimental Melt Temperature [°C]	Vendor Melt Temperature [°C]	Composite Processing Temperature [°C]	Degradation Temperature [°C]
PP	Mat	160	165	170 & 190	290
N6	Mat	219	216	230	380
N6	Towpreg	222	220	230 & 260	400
PPS	Towpreg	284	280	310	490
PP	Commingle	160	159	180 & 210	370

5.2.3 Rheology

The power-law constants, n and m, were needed as inputs to the model equations discussed in Chapter III. A parallel plate rheometer was used to obtain viscosity versus shear rate data. The data was corrected using the Weissenberg-Rabinowitsch correction. The shear rates were estimated using Equation 3.9, and the rheology experiments were conducted in this estimated range. The estimated shear rates during the mat preform processing are 0.4-1.5 1/s, and the estimated shear rates during the towpreg and commingled fiber preforms processing are 1.4-5.8 1/s and 1.3-1.6 1/s, respectively. These calculated shear rates were expected, since compression molding of thermoplastic composites is a low shear rate process. Sample calculations for the shear rates are located in Appendix B. Figures 5.11-5.15 are the curves for the viscosity data. Simple linear regression of the power-law equation for viscosity was used to calculate the power-law constants.

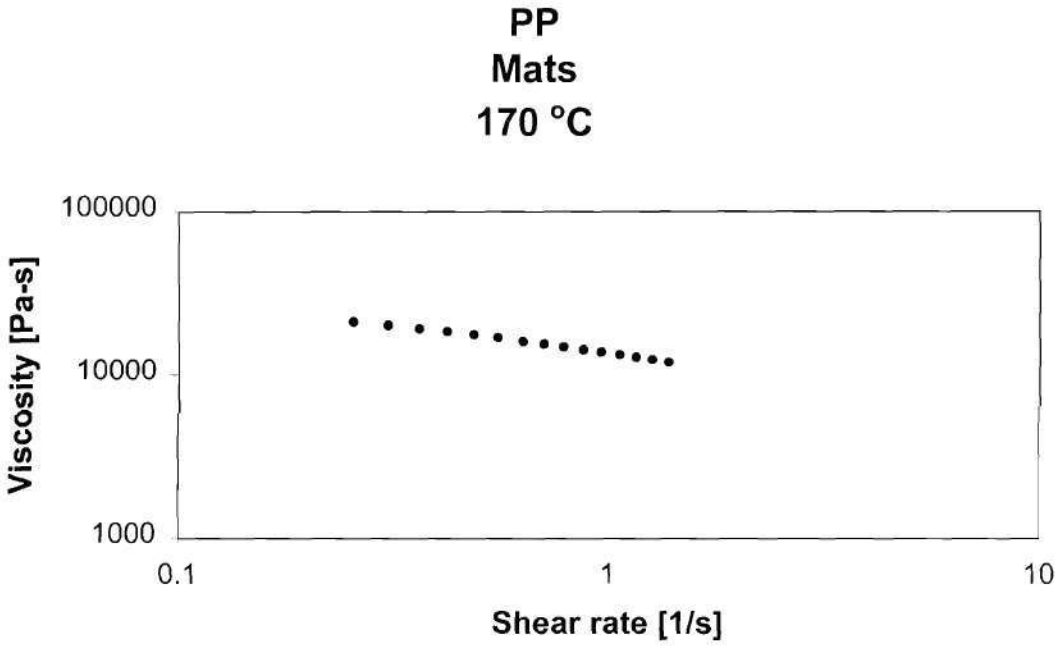

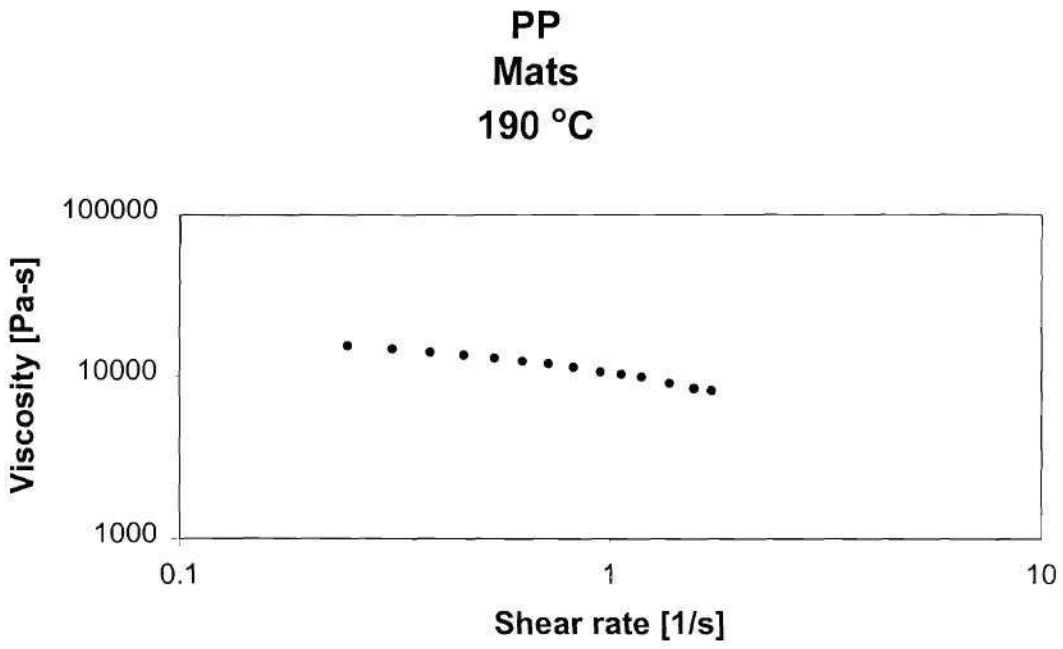

Figure 5.11: Viscosity versus shear rate curves for PP used in mat preforms. The top graph is at 170 °C and the bottom graph is at 190 °C.

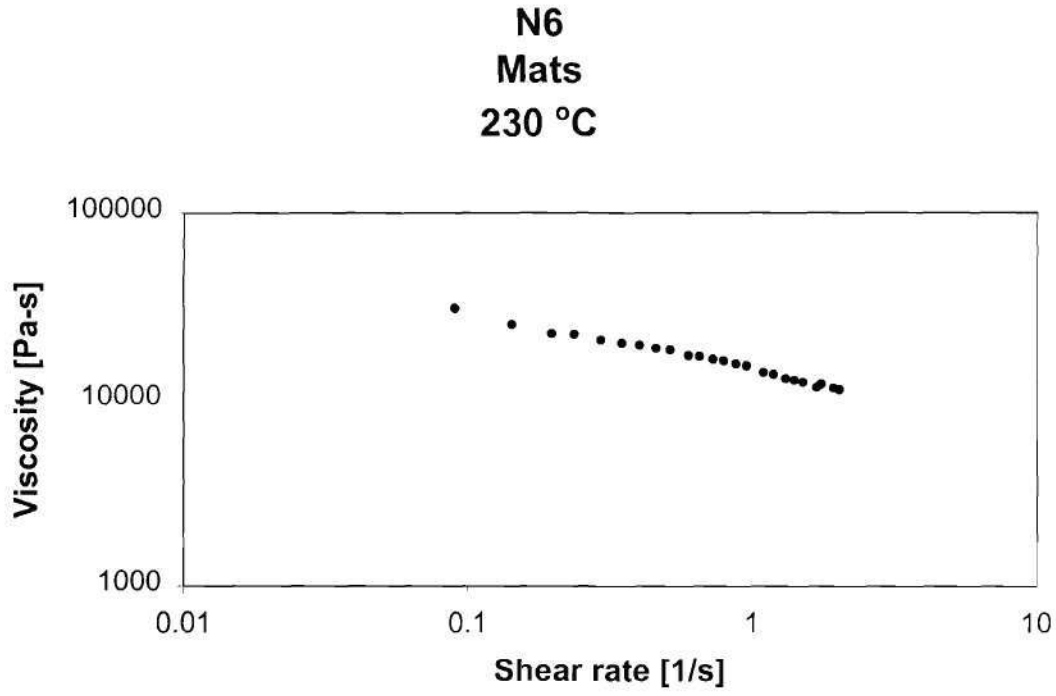

Figure 5.12: Viscosity versus shear rate curve for N6 used in mat preforms.

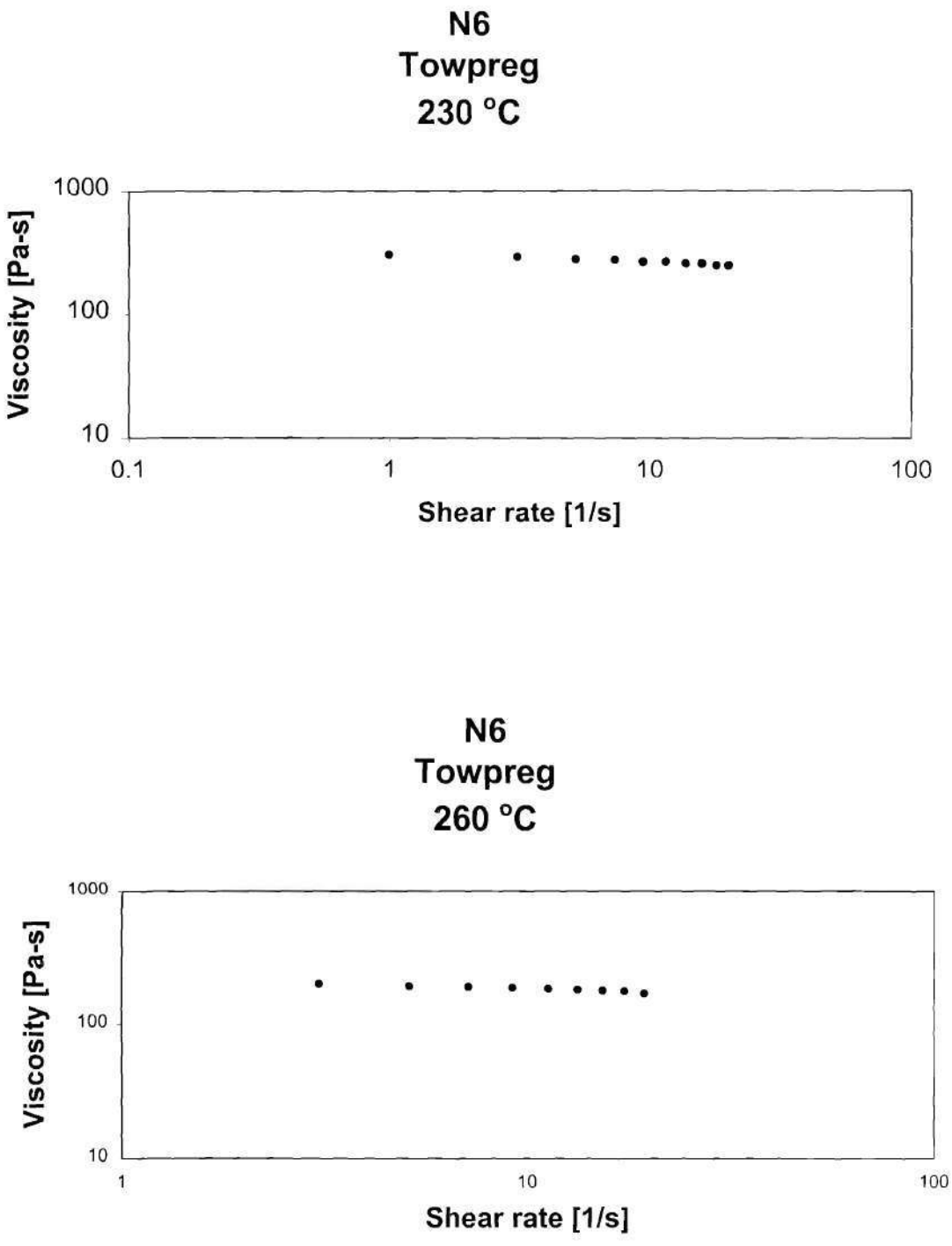

Figure 5.13: Viscosity versus shear rate curve for N6 used in towpreg. The top graph is at 230 °C and the bottom graph is at 260 °C.

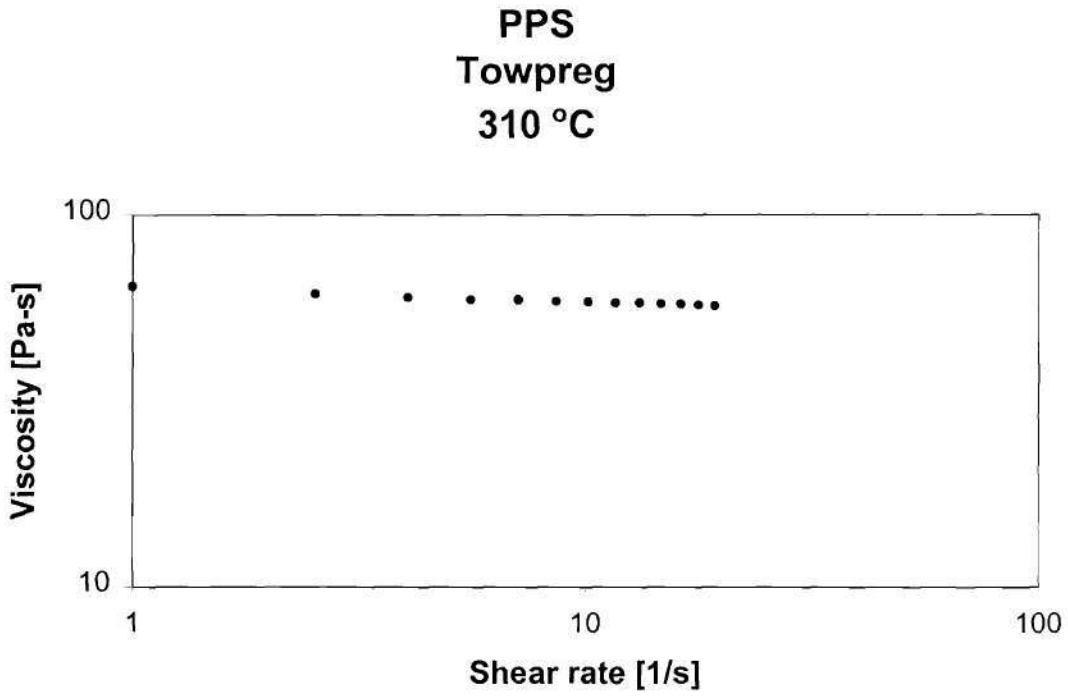

Figure 5.14: Viscosity versus shear rate for PPS used in towpreg.

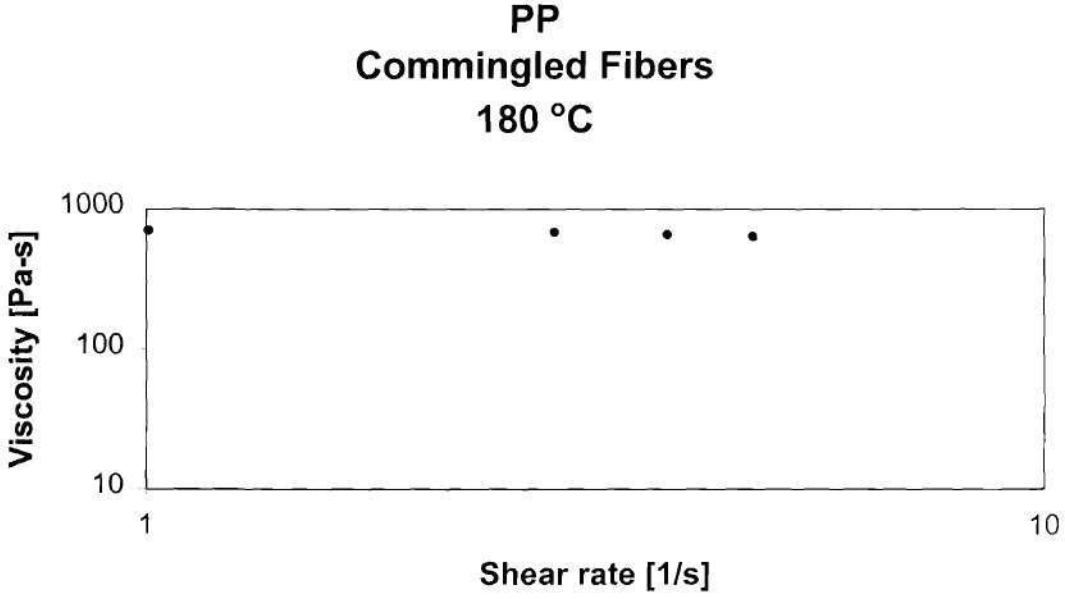

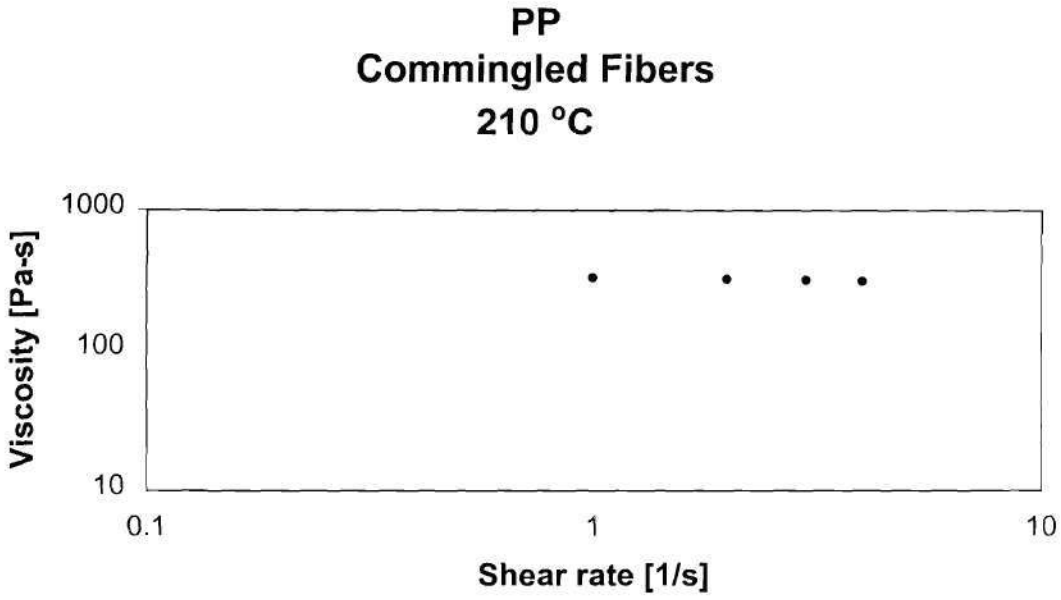

Figure 5.15: Viscosity versus shear rate curve for PP used in commingled fiber preforms. The top graph is at 180 °C and the bottom graph is at 210 °C.

For the PP and N6 used in the mat preforms, the power-law flow index values calculated were 0.65 and 0.71, respectively. The power law-consistency values for the PP were 10,300 Pa-s^n and 13,400 Pa-s^n, and the consistency value for the N6 was 14,400 Pa-s^n. As expected, both PP and N6 exhibited shear-thinning behavior as shown in Figures 5.11 and 5.12.

For the N6 and PPS used in the towpreg, the power-law flow index values calculated were 0.93 and 0.96, respectively. The m values for N6 were 186 Pa-s^n and 304 Pa-s^n. The m value for PPS was 63 Pa-s^n. Figures 5.13 and 5.14 depict the slight shear-thinning behavior of the two resins.

An n value of 0.94 was calculated for the PP used in the commingled fibers. Values of 320 Pa-s^n and 732 Pa-s^n were calculated for the consistency index. Figure 5.15 displays the viscosity versus shear rate curves for the PP. The power law constants for all the resins described above are listed in Table 5.2.

Table 5.2: Power-law parameters of the polymers used in this research

Polymer	Preform	Temperature [°C]	m [Pa-s^n]	n
PP	Mat	170	13,400	0.65
		190	10,300	
N6	Mat	230	14,400	0.71
N6	Towpreg	230	304	0.93
		260	186	
PPS	Towpreg	310	63	0.96
PP	Commingled fibers	180	732	0.94
		320	320	

5.2.4 Porosity

The porosities of the fiber beds, ε, were needed as inputs to the model equations presented in Chapter III. As stated in Chapter IV, the porosities of the mat preforms were obtained using Equation 4.6 and the compression procedure outlined in Section 4.4.2. The resulting porosities are located in Table 5.3, where δ is the thickness of the mat. The porosities calculated for the glass and carbon fiber mats were 0.68-0.71. The porosity of the sisal mat was 0.58. The other parameters needed to calculate the porosity in Equation 4.6 are located in Table 4.1. The porosities did not change drastically by doubling the pressure. This is understandable since it has been shown that an infinite amount of pressure is needed to substantially decrease the porosity below a certain asymptotic porosity value (Gutowski, 1997). Also, once the applied pressure was reached during the compression experiments to determine the porosity, the porosity of the mats did not change. Therefore, the porosity is assumed to be constant during the permeation tests.

Table 5.3: Mat porosity results

Mat	Processing Pressure [MPa]	δ [cm]	ε
Carbon	1.38	0.049±0.0007	0.71
	2.76	0.0461	0.69
Glass	1.38	0.031±0.0003	0.71
	2.76	0.028±0.0001	0.68
Sisal	0.34	0.045±0.0003	0.58

As discussed in Chapter IV, the porosities of the towpreg and commingled fiber preforms were determined using scanning electron microscopy (SEM) analysis. The results are located in Table 5.4. The average porosity was determined by taking six SEM pictures of the fiber bed from a composite sample. As shown in Table 5.4, an average porosity of 0.24 was calculated. In addition, this porosity value of 0.24 did not vary with fiber selection, processing temperature, processing pressure, weight percent, or preform. It is believed that this is a result of the fibers being well compacted as received in the unprocessed tow or commingled fiber, as shown in Figures 4.2 and 4.3. Also, the value of 0.24 for the porosity corresponds well with values reported in literature for the porosity of carbon and glass fiber beds obtained using transverse compression pressures similar to the processing pressures used in this research (Gutowski, 1997 and Skartsis et al., 1992). Figures 5.16-5.18 are SEM photographs showing the low porosity of the fiber beds.

Also, shown in Figure 5.19 is a SEM photograph of a carbon/N6 composite from experiment T21. As discussed in Chapter IV, the composite in this experiment was produced by heating the preform to the processing temperature, allowing the sample to reach the processing temperature, and then cooling the sample. No pressure was applied. The photograph in Figure 5.19 illustrates how the fiber bed looks just before applying pressure to force the resin into the pores. As shown in the figure, the porosity is already very low before the pressure is even applied. In fact, a porosity of 0.24 was calculated for the fiber bed.

Unlike the clear contrast between the fiber and resins in Figures 5.16-5.18, the SEM photographs of the PPS composites did not show any contrast between the fibers and resins. Therefore, it was not possible to obtain porosity values for the PPS composites. The possible reason for this is that the SEM porosity analysis package could not distinguish between the fiber and resin. The SEM analysis is based on different intensity levels of each species in a sample. Since the structure of PPS includes a benzene ring and more specifically the cyclical carbon ring, it is hard to distinguish between the resin and the carbon fibers. However, it is believed that the porosity of the carbon bed in the carbon and PPS composites would not be significantly different than 0.24. The geometry of the carbon and PPS towpreg and all the processing conditions of their composites were the same as the other fiber/resin systems. The only difference is the resin itself.

Table 5.4: Towpreg and commingled fiber bed porosity results

Experiment	Material	Resin Weight [%]	Processing Pressure [MPa]	Processing Temperature [°C]	ε
T2	carbon/N6	43	0.52	260	0.24±0.03
T10	glass/N6	34	0.52	260	0.24±0.02
T4	carbon/N6	33	1.03	260	0.24±0.02
T16	glass/N6	26	1.03	260	0.24±0.05
C1	commingled fibers	25	0.34	180	0.24±0.02
C6	commingled fibers	40	0.34	210	0.24±0.05
C7	commingled fibers	40	0.69	180	0.24±0.02
C4	commingled fibers	25	0.69	210	0.24±0.01
T3	*carbon/N6	43	1.03	230	0.24
T5	*carbon/N6	33	0.52	230	0.24±0.004
T11	*glass/N6	34	1.03	230	0.24±0.01

*Note: Only 2 SEM pictures were taking for these samples

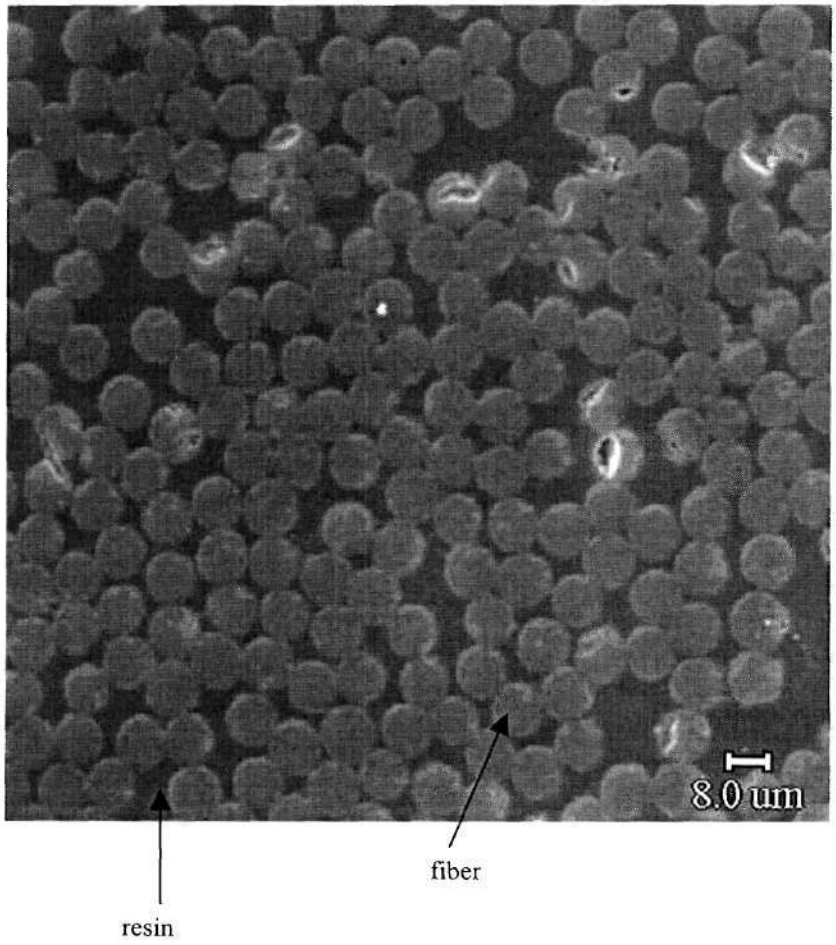

Figure 5:16: SEM photograph of a carbon/N6 composite.

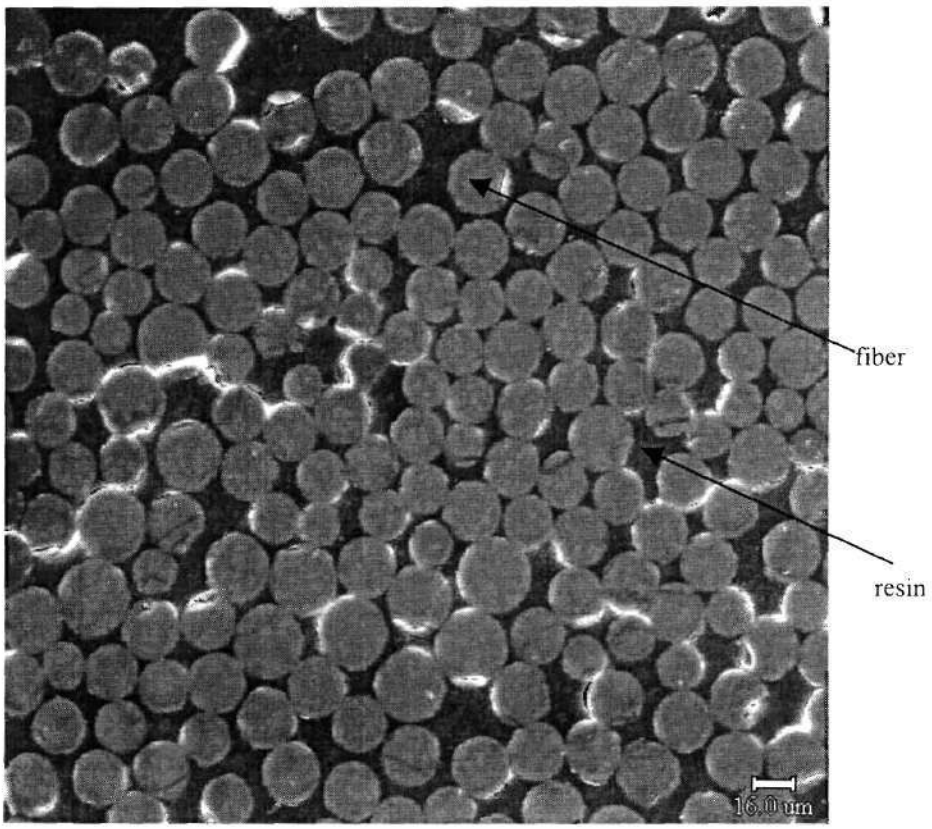

Figure 5:17: SEM photograph of glass/N6 composite.

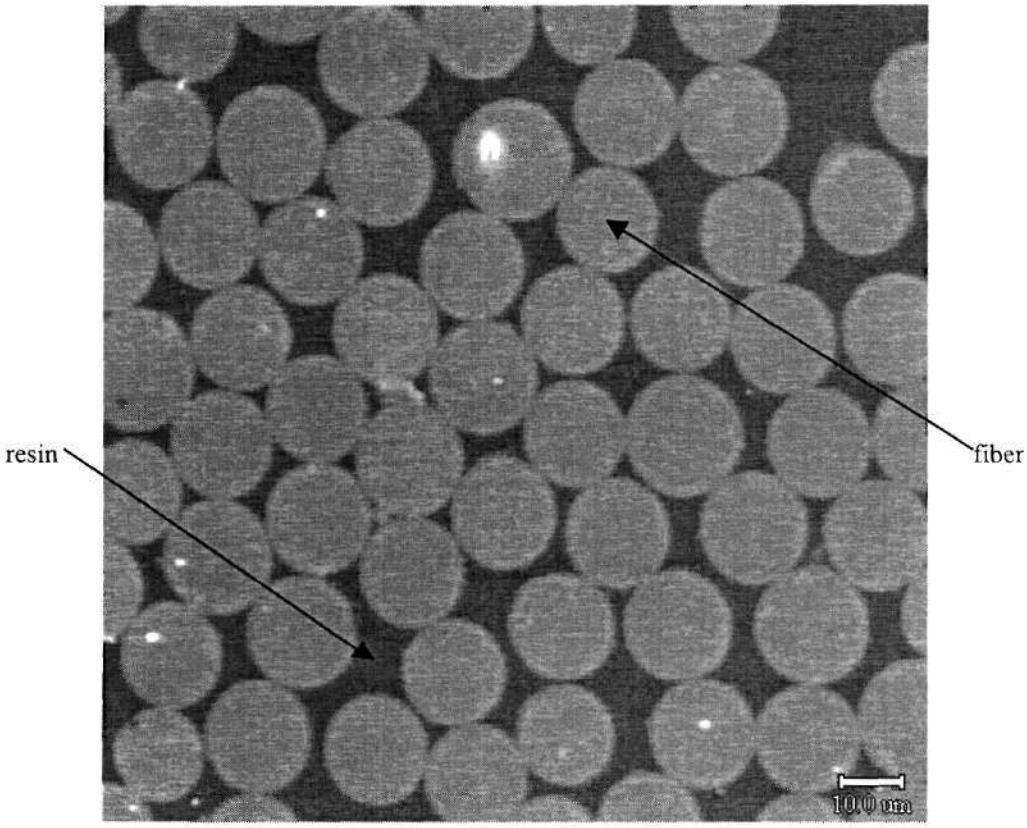

Figure 5:18: SEM photograph of commingled fiber composite.

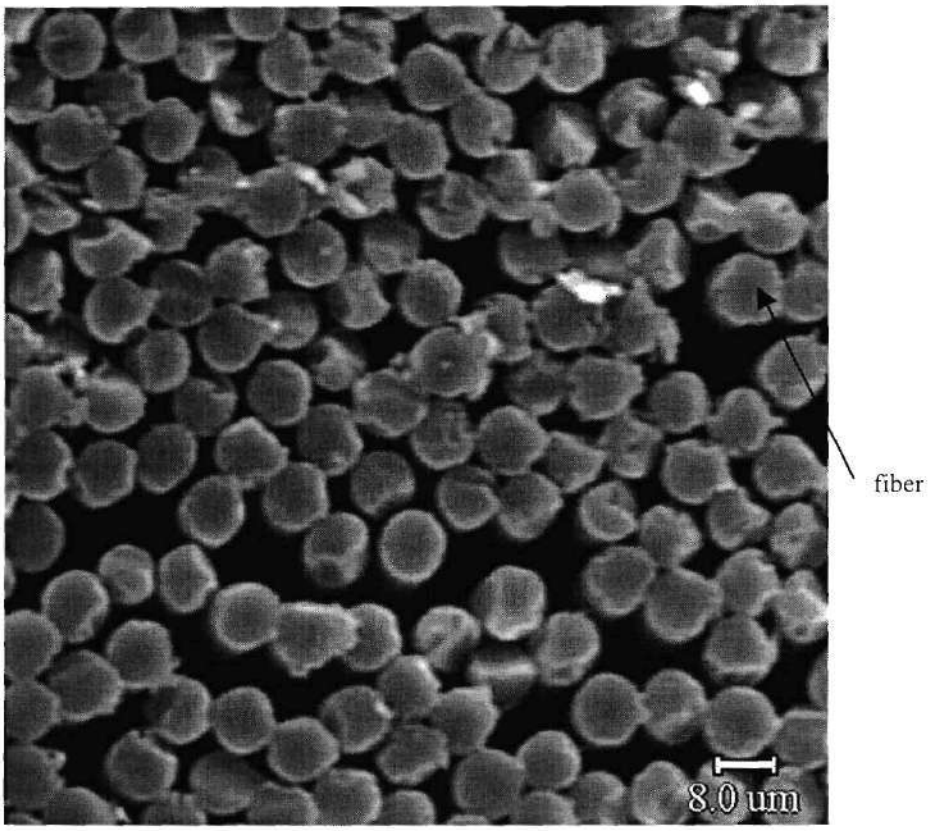

Figure 5.19: SEM photograph of carbon/N6 composite from experiment T21 The resin weight percent is 43 and the processing temperature is 230 °C. The spaces between the fibers are empty and are available for flow.

5.3 Introduction to Model Results

In the following Sections, experimental permeation results are compared to the theoretical equations developed in Chapter III. In Section 5.4, the permeation experiments with mat preforms are presented and discussed. In Section 5.5, the results with the towpreg are discussed. Finally, the commingled fiber results are analyzed in Section 5.6.

5.4 Mat Results

5.4.1 Introduction

In this section, the experimental permeation results with the mat preforms are presented, discussed, and compared to the model equations, Equations 3.8, 3.26, and 3.37, which were detailed in Chapter III. These three equations are listed below. As stated in Chapter III, Equation 3.8 will be referred to as the Semi-empirical model, Equation 3.26 as the Vijaysri model, and Equation 3.37 as the Bruschke model (Vijaysri et al., 1999 and Bruschke and Advani, 1993). All the parameters in the equations were described in Chapter III.

$$X = \left[\left(\frac{1+n}{1+3n} (2)^{\frac{n-1}{n}} \left(\frac{\varepsilon^{2n+1}}{(1-\varepsilon)^{1+n}} \right)^{\frac{1}{n}} \left(\frac{1}{K_o K_1^{\frac{1}{n}}} \right) \right) \left(r_f^{\frac{1+n}{n}} \left(\frac{\Delta P}{m} \right)^{\frac{1}{n}} t \right) \right]^{\frac{n}{1+n}} \tag{3.8}$$

$$X = \left[\left(2 \left(\frac{1+n}{n} \right) \left(\frac{\pi}{(1-\varepsilon)\Lambda} \right)^{\frac{1}{n}} \right) \left(r_f^{\frac{n+1}{n}} \left(\frac{\Delta P}{m} \right)^{\frac{1}{n}} t \right) \right]^{\frac{n}{n+1}} \tag{3.26}$$

$$X = \left[\left(\frac{1+n}{n} \right) \left(\frac{1}{2^n} \right)^{\frac{1}{n}} \left(\frac{\frac{1}{\sqrt{\pi}} \left(\frac{2n}{1+2n} \right)^n \left[(1+l)^{-(2n+1)} \left(\cos^2 \alpha \right)^{2n+1} \alpha^{-4n-1} \frac{\Gamma\left(2n+\frac{1}{2}\right)}{\Gamma(2n+1)} \right]^{-1}}{l^{n+1}} \right)^{\frac{1}{n}} \left(r_f^{\frac{1+n}{n}} \left(\frac{\Delta P}{m} \right)^{\frac{1}{n}} t \right) \right]^{\frac{n}{n+1}} \quad (3.37)$$

In all three of the model equations, the variable of interest is X, the transient penetration depth. In the Semi-empirical equation, another important parameter is the tortuosity, K_1, which is the only unknown in Equation 3.8. Therefore, the experimental permeation data was non-linearly regressed using a statistical analysis package, SAS, to determine K_1 (SAS Institute, Inc., 1989). Once K_1 was known, Equation 3.6 was used to calculate the Kozeny constant. The parameter K_1 was converted into terms of the Kozeny constant because the latter is a "standard" parameter used by many researchers when discussing permeation through porous media. Referring to the experimental design for mat preforms in Table 4.4, an average of the 14 calculated Kozeny constants was found and this average value was used in Semi-empirical model.

In the Vijaysri model, the loss coefficient, Λ, was obtained from Vijaysri, et al. (1999). The loss coefficient is a function of porosity and power law index. The authors presented a range of coefficients corresponding to various porosities and power-law indices. Their results are listed in Table C.1 in Appendix C. Unfortunately, they did not present results at the exact porosity and power-law index values used in this research. Therefore, their data in Table C1 was regressed to determine the loss coefficients at the

porosities and power-law indices used this research. While it is understood that extrapolation can be dangerous, the values of porosities and power law indices in this research fall within the range of porosities and power-law indices reported by the authors. The new loss coefficients are shown with an asterisk in Table C1. In comparison with the author's data, the new coefficients appear to be qualitatively correct. Also, in Appendix C are the regressed curves and the resulting equations.

The experimental penetration depth was calculated using the LVDT and the experimental set-up described in Section 4.2.2. The LVDT measured the thickness change of the sample. The thickness change was due to the transient resin permeation through the pores of the fiber mat. Referring to Figure 5.20, a mass balance was used to determine the transient penetration depth. The resulting equation for the transient penetration depth is Equation 5.1.

$$X(t) = \frac{\Delta h(t)}{2\varepsilon} \tag{5.1}$$

Where:

X	=	penetration depth, mm
Δh	=	thickness change, mm
ε	=	porosity
t	=	time, s

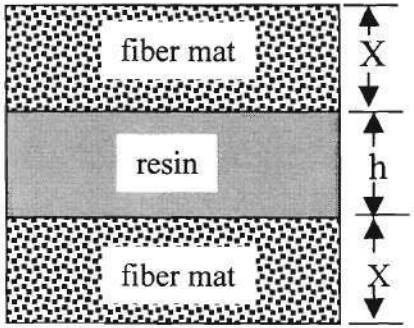

A

$t_i=0$

- mat preform inside mold during heating stage
- no pressure has been applied
- very small changes in h
  - -data not included in calculations

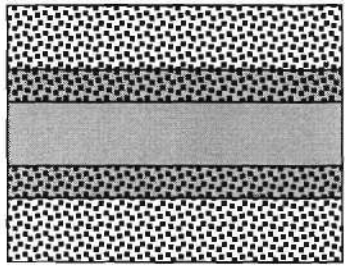

B

t=0

- mat preform at processing temperature
- pressure increased to the processing pressure
  - -time to reach the processing pressure: ~6-10 s
- fiber mats fully compressed after ~6-10 s
- t=0 refers to the time at which the mats have just been fully compressed
  - -penetration depth data collection is started
  - -penetration depth from heating stage not included in data

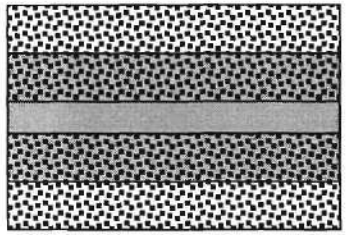

C

t>0

- some processing time greater than zero
- constant applied pressure forces resin into pores
- resin rich layer throughout process
- resin flow front is free
  - -the fiber mat is not completely wet out

Figure 5.20: Schematic used to calculate experimental penetration depth of resin, X, from the transient thickness change, h.

The experimental penetration depth was compared to the theoretical depth by using Equation 5.2.

$$E = 100 \frac{\sum_{i=1}^{p} \frac{\left| X_{exp_i} - X_{pred_i} \right|}{X_{exp_i}}}{p} \tag{5.2}$$

Where:

E	=	percent deviation, %
p	=	number of experimental observations
X_{exp}	=	experimental penetration depth, mm
X_{pred}	=	predicted penetration depth, mm

The affects of processing pressure, temperature, fiber, porosity, and resin on the Kozeny constant were assessed graphically and by an analysis of variance (ANOVA) (Hayter, 1996).

5.4.2 Calculated Kozeny Constants

As shown in Table 5.5, the average calculated Kozeny constant is 7.9 for the mat preform processing. Furthermore, the constant did not vary greatly across the vast array of material and processing conditions as is evident by the small standard deviation of 0.3. The p-values of the ANOVA on the Kozeny constant are displayed in Table 5.6. As shown in Table 5.6, all of the p-values are greater than 0.05, and thus none of the factors have an effect on the Kozeny constant. The full table of the SAS results for the Kozeny constants are located in Appendix D and the full ANOVA is located in Appendix E.

Using Newtonian fluids such as water, and porous media composed of randomly arranged cylindrical objects, such as steel and copper wire, nylon fibers, and filter mats, some researchers calculated Kozeny constant values of 4-16 in the porosity range of 0.5-0.8 (Skartsis et al., 1992).

Table 5.5: Kozeny constant results for mat preform processing

Experiment	Fiber mat	Resin	Pressure [MPa]	Temperature [°C]	Kozeny constant K
M1	glass	PP	1.38	170	7.8
M2	glass	PP	1.38	190	7.7
M3	glass	PP	2.76	170	8.3
M4	glass	PP	2.76	190	7.8
M5	glass	N6	1.38	230	8.3
M6	glass	N6	2.76	230	8.2
M7	carbon	PP	1.38	170	7.8
M8	carbon	PP	1.38	190	7.5
M9	carbon	PP	2.76	170	7.5
M10	carbon	PP	2.76	190	7.8
M11	carbon	N6	1.38	230	7.8
M12	carbon	N6	2.76	230	7.8
M13	sisal	PP	0.34	170	8
M14	sisal	PP	0.34	190	7.8
				Average	7.9
				Standard Deviation	0.3

Table 5.6: p-values from the ANOVA on the Kozeny constant

Factor	p-value
Polymer	0.102
Fiber	0.1
Temperature	0.175
Porosity	0.222
Pressure	0.835

5.4.3 Comparison of Experimental and Theoretical Mat Preform Permeation Results

As stated earlier, the Semi-empirical model, with a Kozeny constant of 7.9, and the Vijaysri and Bruschke models were compared to the experimental data using Equation 5.2. The percent errors between the experimental data and the models are shown in Table 5.7. As shown in Table 5.7, the deviation between the experimental data and the Semi-empirical and Bruschke models was on average 4 %, and the deviation between the experimental results and the Vijaysri model was on average 6 %. Graphs of the experimental and theoretical transient penetration depth are shown in Figures 5.21-5.25. Raw data for all of the processing conditions are located in Appendix F.

As shown in Table 5.7 and Figures 5.21-5.25, all three models predict the penetration depth well. It was expected that the Semi-empirical model would predict the data well. However, the exceptional validity of both the Bruschke and Vijaysri models was a surprise since both are based on highly idealized geometric assumptions. It is believed that the models predicted the experimental data well because the experimental procedures, materials, and set-up in this research did not violate the model assumptions. For example, in this research the Reynolds numbers were $\sim 10^{-11}$ for the mat preform processing. Therefore, the creeping flow assumption in the model equations was applicable. In addition, because the flow was so slow, the quasi-steady state assumption was valid. Furthermore, the length to diameter ratios of the fibers in the mats were ~203-4,762. Because of these large aspect ratios, the assumptions of infinite cylinder lengths and of negligible end effects was legitimate. Another plausible reason for the good fit is

due to the experimental set-up in this research. The length of the sides of the square mold was 25.4 cm. This large side length, in comparison to the small thickness of the fiber beds, minimized wall effects and longitudinal flow along the fibers. Also, additional prevention of flow along the fiber axis was achieved by enclosing the sides of the mold. Finally, good estimates of the shear rates were essential to obtain the correct power-law constants.

Table 5.7: Comparison of deviations for experimental and theoretical permeation results for mat preform processing

Experiment	Fiber mat	Resin	Pressure [MPa]	Temperature [°C]	Semi-empirical E [%]	Bruschke E [%]	Vijaysri E [%]
M1	glass	PP	1.38	170	4.4	4.3	6.4
M2	glass	PP	1.38	190	2.2	2.2	6.9
M3	glass	PP	2.76	170	3.6	4.1	4.3
M4	glass	PP	2.76	190	1.5	1.8	5.7
M5	glass	N6	1.38	230	6.7	5.8	7.6
M6	glass	N6	2.76	230	8.3	8.4	7.7
M7	carbon	PP	1.38	170	1.9	1.8	5.7
M8	carbon	PP	1.38	190	4.1	4.2	7.4
M9	carbon	PP	2.76	170	5.8	5.6	8.6
M10	carbon	PP	2.76	190	3.9	3.9	5.4
M11	carbon	N6	1.38	230	3.0	3.6	4.8
M12	carbon	N6	2.76	230	4.3	4.4	8
M13	sisal	PP	0.34	170	3.2	4.4	4.5
M14	sisal	PP	0.34	190	3.4	4.6	4.3
				Average	4.0	4.3	6.3
				Standard Deviation	1.9	1.7	1.5

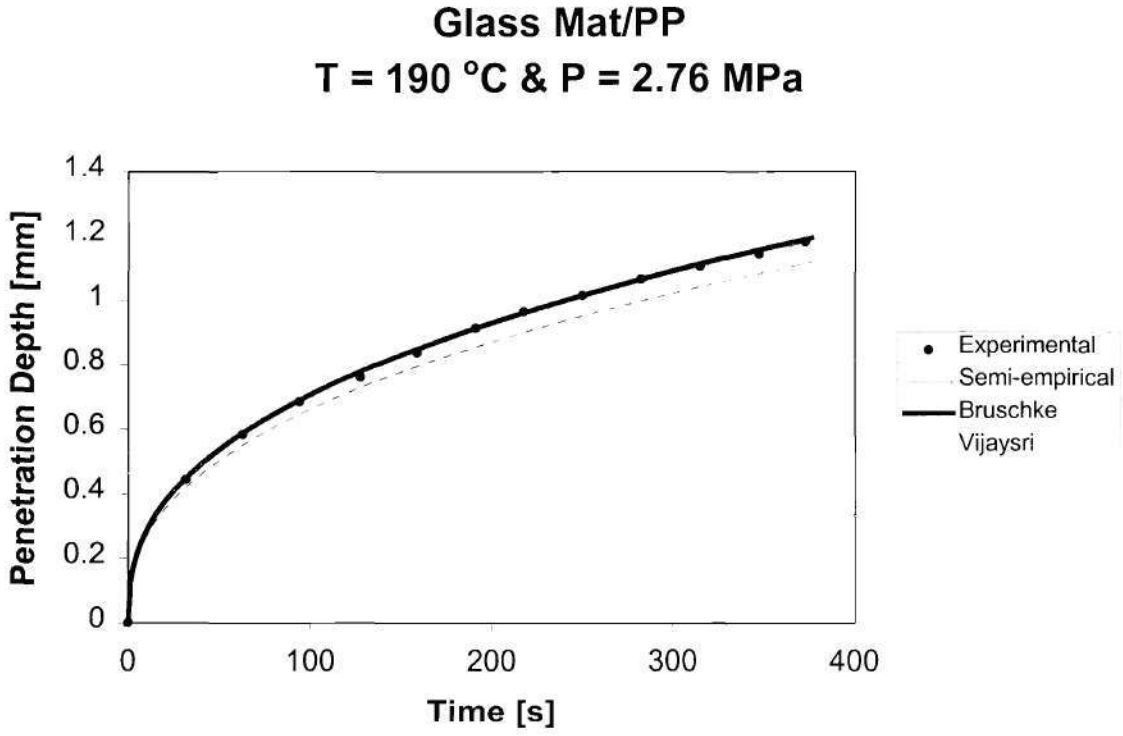

Figure 5.21: Penetration depth versus time for experiment M4. The material is glass mat/PP. The processing pressure is 2.76 MPa and the processing temperature is 190 °C. The standard deviation of the penetration depth is ~0.004 mm. The error bars are too small to be visible on the graph.

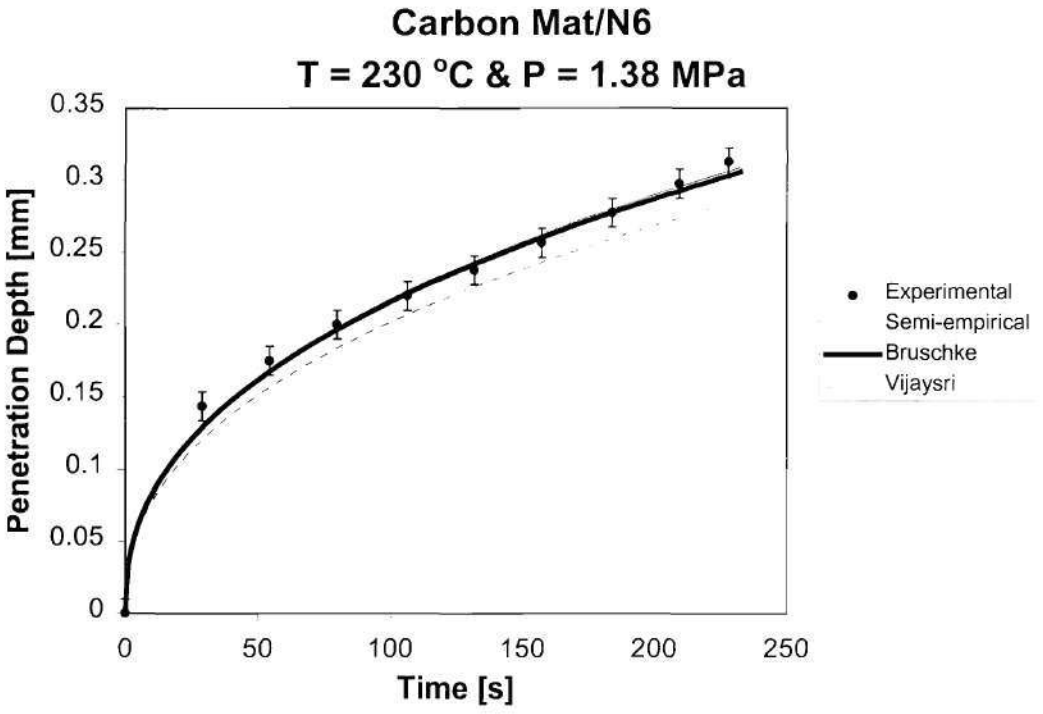

Figure 5.22: Penetration depth versus time for experiment M11. The material is carbon mat/N6. The processing pressure is 1.38 MPa and the processing temperature is 230 °C. The standard deviation of the penetration depth is ~0.01mm.

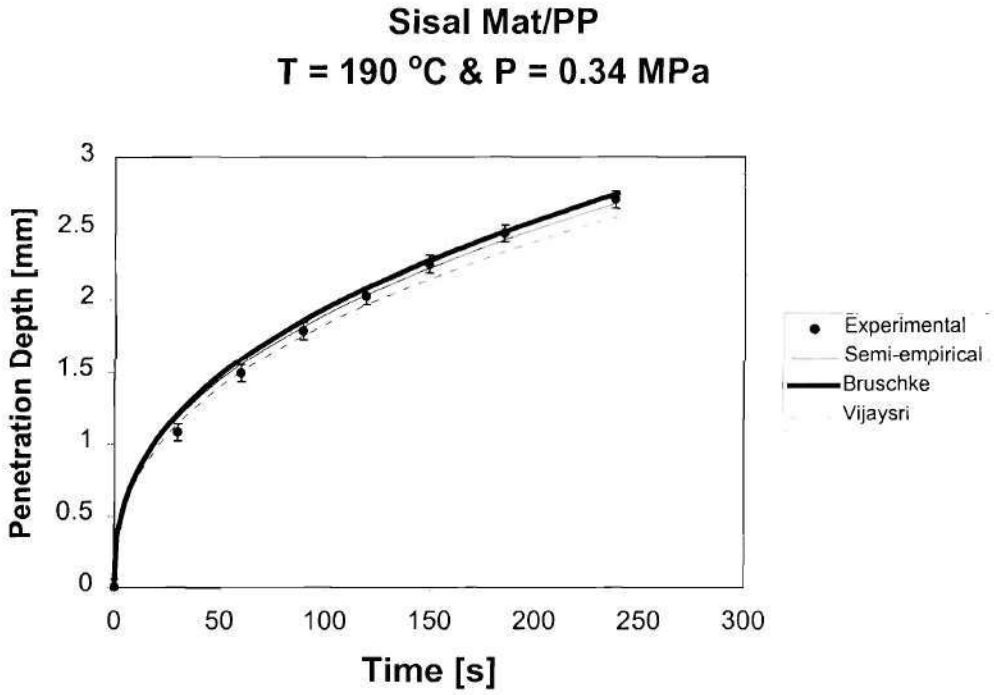

Figure 5.23: Penetration depth versus time for experiment M14. The material is sisal mat/PP. The processing pressure is 0.34 MPa and the processing temperature is 190 °C. The standard deviation of the penetration depth is ~0.06 mm.

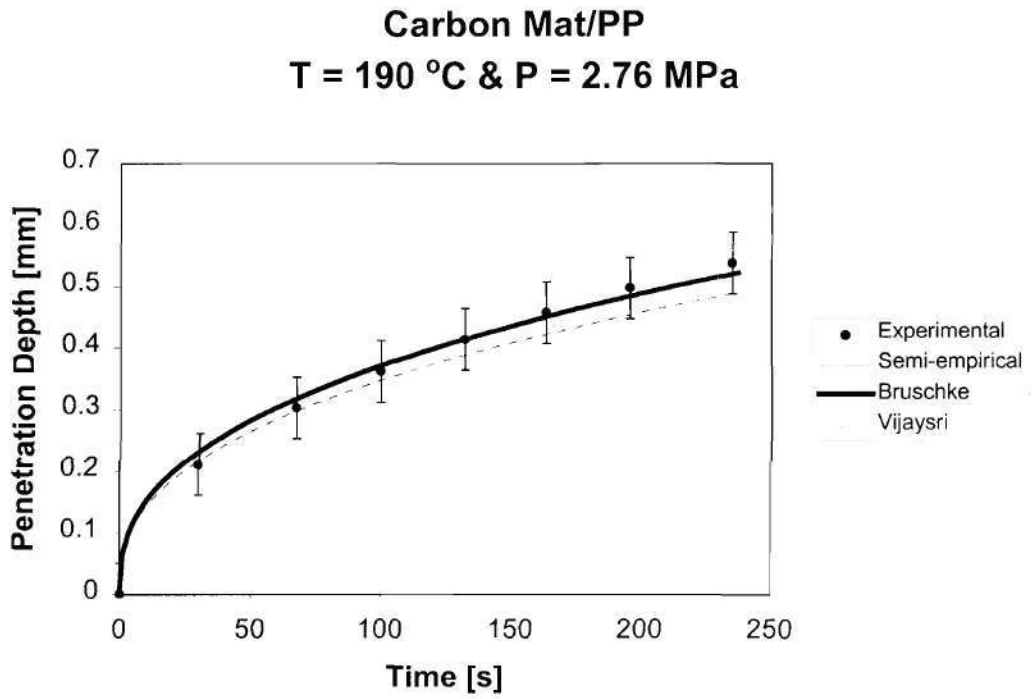

Figure 5.24: Penetration depth versus time for experiment M10. The material is carbon mat/PP. The processing pressure is 2.76 MPa and the processing temperature is 190 °C. The standard deviation of the penetration depth is ~0.05 mm.

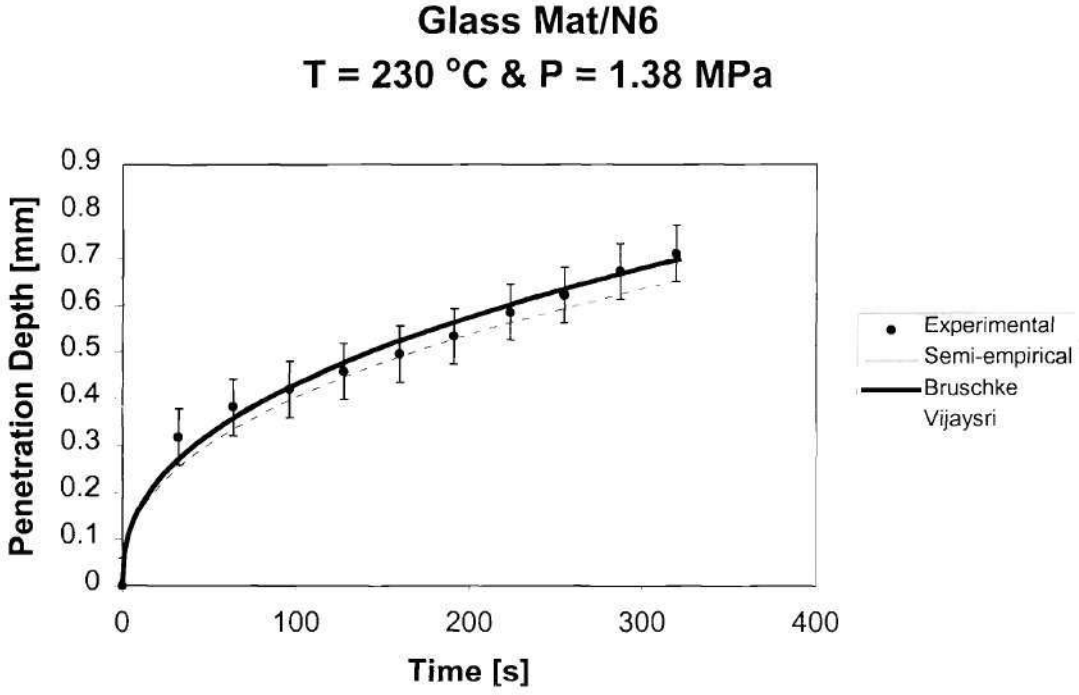

Figure 5.25: Penetration depth versus time for experiment M5. The material is glass mat/N6. The processing pressure is 1.38 MPa and the processing temperature is 230 °C. The standard deviation of the penetration depth is ~0.06 mm.

It is very interesting to note that the Bruschke and Semi-empirical models have about the same percent deviation. In addition, as shown in Figures 5.21-5.25, the two curves tend to coincide. This seems to suggest that the Bruschke model can be used to calculate the Kozeny constant. With this in mind, the Bruschke and Semi-empirical models were equated to each other, and the resulting equation for the theoretical Kozeny constant is Equation 5.3.

$$K = K_o \left(\left(\frac{2^{\frac{2n-1}{2}}}{K_o} \frac{n}{1+3n} \left(\frac{\varepsilon^{2n+1}}{(1-\varepsilon)^{1+n}} \right)^{\frac{1}{n}} \left(\frac{l^{n+1}}{\frac{1}{\sqrt{\pi}} \left(\frac{2n}{1+2n} \right)^{n} \left[(1+l)^{-(2n+1)} \left(\cos^2 \alpha \right)^{2n+1} \alpha^{-4n-1} \frac{\Gamma\left(2n+\frac{1}{2}\right)}{\Gamma(2n+1)} \right]^{-1}} \right)^{\frac{1}{n}} \right)^{\frac{n}{n+1}} \right)^2 \tag{5.3}$$

As shown in Equation 5.3, the Kozeny constant appears to be a function of porosity and power-law index. Using Equation 5.3, Figure 5.26 is a graph of the Kozeny constant as a function of porosities and power-law indices commonly encountered during random mat preform processing with thermoplastics.

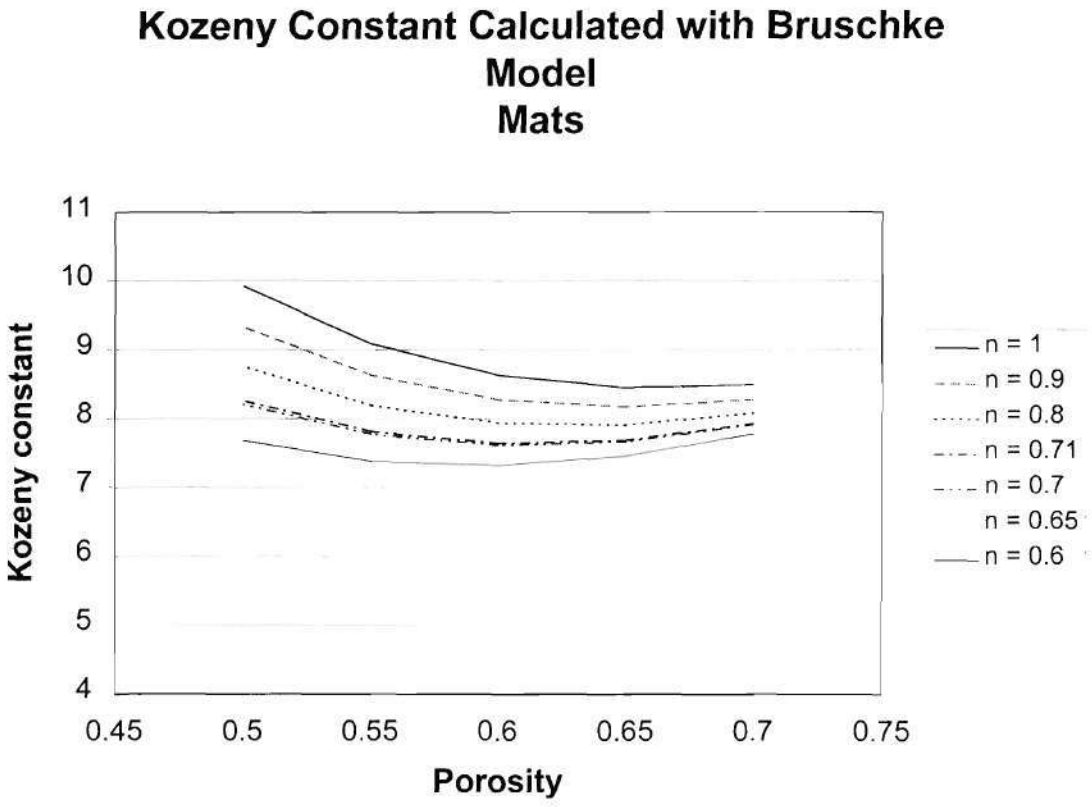

Figure 5.26: Graph of Kozeny constant, calculated from Equation 5.3, versus porosity with power-law flow index as a parameter.

According to Figure 5.26, the Kozeny constant does not vary greatly at the porosities and power-law indices used in this research. This observation lends support to the consistent Kozeny constants found during the processing of thermoplastic mat preforms in this research. However, it should be noted that as the porosity decreases below ~0.55, the Kozeny constant begins to increase significantly and the effect of the power-law flow index is enhanced.

While it is understood that it is not practical to use a semi-empirical model when a valid mechanistic model is available, it is interesting to note the similarity between the very simple Semi-empirical and the more complex Bruschke model. Another interesting observation is that the Bruschke model is based on the square unit cell model, yet it predicted the experimental data well. This can be explained using an analysis by Åstrom et al. (1992). Åstrom et al. (1992) analyzed two theoretical models that were based on the transverse flow of a Newtonian fluid through a porous medium composed of cylinders. In one of the models, the cylinders were assumed to be in a square arrangement, and in the other model the cylinders were assumed to be randomly arranged. Åstrom et al. 1992 showed that at porosities of ~0.6-0.8, the average transverse velocities are equal for both systems. In this research the porosities of the fiber mats were 0.58-0.71.

To check the validity of the experimental penetration depth, SEM photographs were taking of a sample after a permeation test. Referring to Table 5.7, SEM photographs were taking from experiment M5. The experimental permeation depth for

one of the experiments from condition M5 is 1092 μm and the value of the depth in Figure 5.27 is ~1100 μm. Therefore, the experimental penetration depth calculated using the transient thickness data from the LVDT is validated. It should be noted that the actual processing time of this particular experiment, M5, was seven minutes; however, only the first five minutes of the data was used to compare with theoretical calculations.

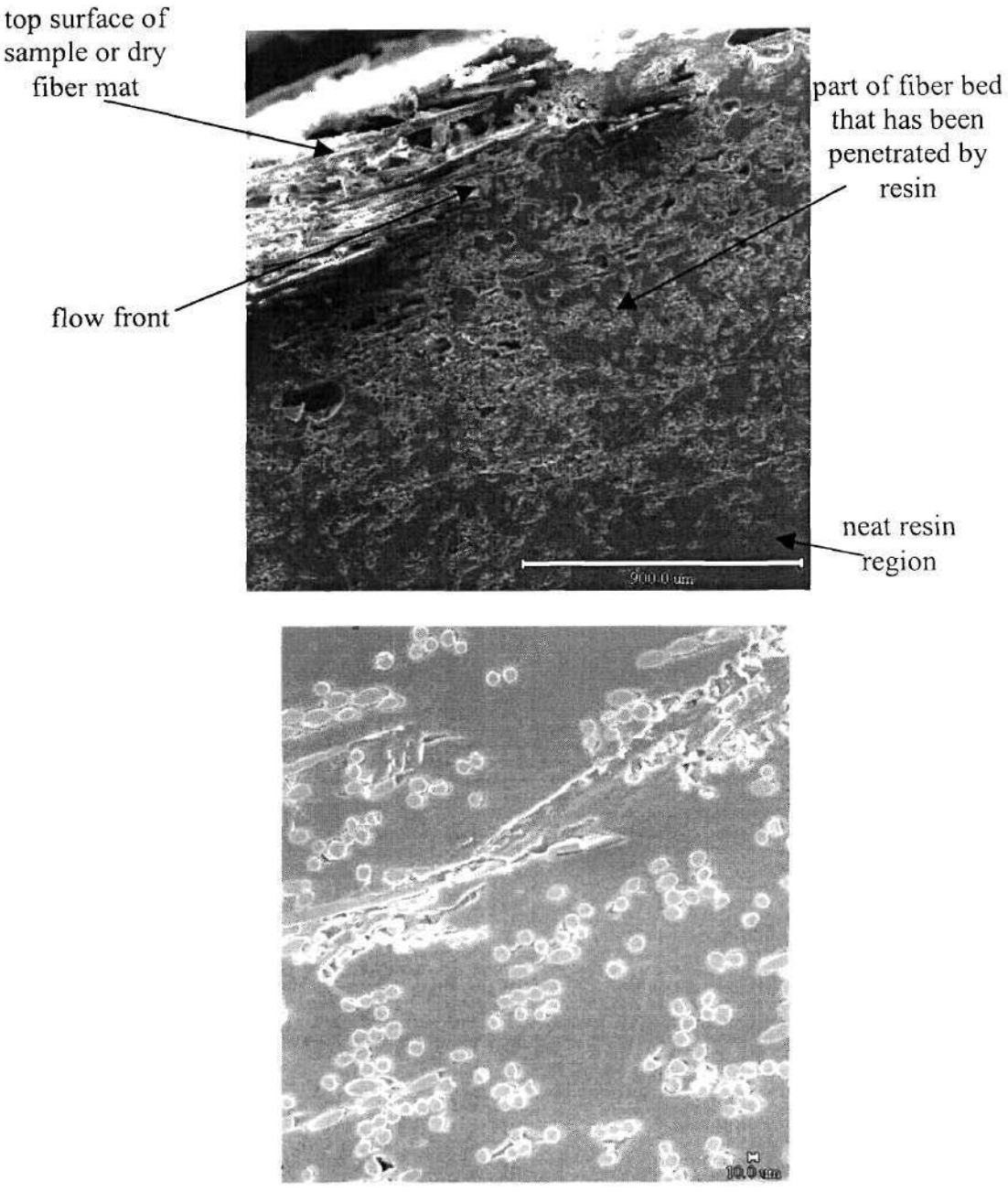

Figure 5.27: SEM photographs of sample from experiment M5 to validate penetration depth. The material is glass mat/N6. The processing pressure is 1.38 MPa and the processing temperature is 230 °C. The micron bar on the top photograph is 900 μm and the micron bar on the bottom photograph is 10 μm. The top photo is at 40X and the bottom photo is at 100X. Both photos are slightly tilted to the left.

5.4.4 Summary

In Section 5.4, the experimental mat preform permeation results were compared to the predictions of the Semi-empirical, Bruschke, and Vijaysri equations. First, an average Kozeny constant of 7.9 was calculated. In addition, the calculated Kozeny constant did not vary with material or processing conditions. Next, it was shown that the Semi-empirical and Bruschke models predicted the transient penetration depth to within about 4 %, and the Vijaysri model predicted the transient depth to within about 6 %. It was also shown the Kozeny constant is a function of porosity and power-law index.

After analyzing the permeation results, it is recommended to that the Bruschke model be used to describe the permeation of thermoplastic through random fiber mats. There are three reasons for this recommendation. First, the percent deviation between the experimental data and the model is lower than the Vijaysri model and equal to the Semi-empirical model. Secondly, the model does not require an empirical constant. Finally, at this point, it does not appear that the Bruschke model is limited to specific ranges of processing and material conditions.

5.5 Towpreg Results

5.5.1 Introduction

In this section, the experimental permeation results with the powder-coated towpreg preforms are presented, discussed, and compared to the Semi-empirical and Bruschke equations. As discussed in Chapter II, the Vijaysri equation was not used because it is valid for porosities greater than ~0.5. The porosity of the fiber beds in the towpreg is 0.24.

Like the mat preform analysis in Section 5.3, the variable of interest in the model equations is X, the transient penetration depth. As with the mat preforms, first the experimental towpreg permeation data was non-linearly regressed using a statistical analysis package, SAS, to determine K_1 (SAS Institute, Inc., 1989). Once K_1 was known, Equation 3.6 was used to calculate the Kozeny constant. Referring to the experimental design for towpreg preforms in Table 4.5, an average of the 20 calculated Kozeny constants was found and this average Kozeny constant was used in the Semi-empirical model. The calculated Kozeny constants are discussed in Section 5.5.2

Like the mat preforms, the experimental penetration depth was calculated using the LVDT and the experimental set-up described in Section 4.2.2. The LVDT measured the thickness change of the sample. The thickness change was due to the transient resin permeation through the pores of the fiber bed. Referring to Figure 5.28, a mass balance was used to determine the transient penetration depth. The resulting equation for the transient penetration depth is the same as Equation 5.1 used for mat preform processing. The experimental and theoretical penetration depth results are discussed in Section 5.5.3.

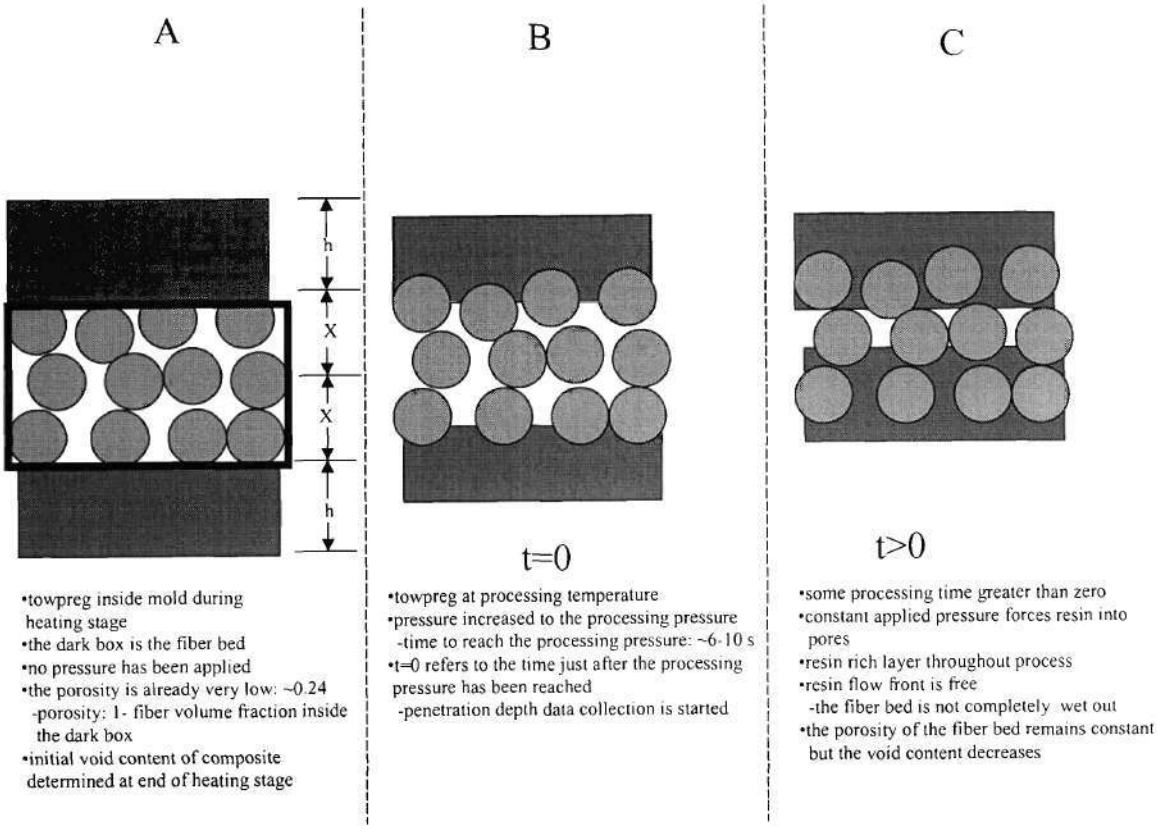

Figure 5.28: Schematic used to calculate penetration depth during towpreg processing. The cylinders represent the fibers and the rectangles represent the resin.

As discussed in Chapter III, the model equations also were used to calculate a theoretical void content. In Section 5.5.4, the experimental and theoretical void content results are discussed.

5.5.2 Calculated Kozeny Constants

As shown in Table 5.8, the average calculated Kozeny constant is 362. In calculating this average, the Kozeny constants calculated at the T10, T11, T12, and T16 conditions were not included. The reason the constants at these conditions were not included was because in these experiments one of the model assumptions was violated. In the model equations, it is assumed that the flow front is free, hence there is no boundary to stop the flow front. At the four conditions listed above, the flow front did reach its boundary. Evidence to support this claim will be discussed in Section 5.5.5. Recommendations to deal with this issue also will be discussed in 5.5.5. As expected, the calculated Kozeny constants at these three conditions were greater than the other conditions, since the Kozeny constant can be viewed as a parameter that describes resistance to flow. As the resistance to flow increases, the Kozeny constant should increase.

With the exception of the four discarded points, the constant did not vary greatly with the different material and processing conditions. The p-values of the ANOVA on the Kozeny constant are listed in Table 5.9. As shown in Table 5.9, p-values for the factors pressure, fiber, and resin weight percent are greater than 0.05. Therefore, none of these factors have an effect on the Kozeny constant. However, the factors of temperature and

resin have p-values less than 0.05. Therefore, they affect the Kozeny constant. This is understandable and will be explained in more detail in Section 5.5.3. It will be shown in Section 5.5.3 that the Kozeny constant is in fact a function of porosity and power-law index, as shown earlier in Section 5.4.3 using Equation 5.3. The effect of temperature on the Kozeny constant is caused by using higher temperatures to process the PPS. As shown in Table 5.2, PPS has a slightly higher power-law index value than N6. The full table of the SAS results for the Kozeny constants are located in Appendix G and the full ANOVA is located in Appendix H.

It should also be noted that the Kozeny constant calculated for the towpreg is significantly greater than that calculated for the fiber mats. The reason for this is the difference in porosities for the two systems. In the mat preforms, the porosity was 0.58-0.71 whereas the porosity was 0.24 for the towpreg. A lower porosity creates a more tortuous path and hence an increase in the Kozeny constant.

As shown in Chapter II, there appears to be no studies reported on the transverse permeation of Non-Newtonian through low porosity beds of unidirectional carbon or glass fibers. However, Gutowski et al. (1987) and Lam and Kardos (1988) conducted transverse permeation studies using Newtonian fluids, such as water and silicone oil, and unidirectional carbon fiber beds. Using a bed porosity of 0.3, Gutowski et al. (1987) calculated a Kozeny constant of 17.9. Lam and Kardos (1988) calculated a Kozeny constant of 11 using a porosity of 0.25. As will be shown in Section 5.5.3, these Kozeny constant values calculated by the authors are significantly lower than the theoretically

calculated values. One possible reason for the authors' results is the use of an incorrect porosity in their calculations.

The use of the Bruschke model to calculate the Kozeny constant, as a function of porosity and power-law index, will be discussed in Section 5.5.3 along with the experimental and theoretical towpreg permeation results.

Table 5.8: Experimentally determined Kozeny constants for towpreg

Experiment	Towpreg	Resin Weight Percent [%]	Pressure [MPa]	Temperature [°C]	Kozeny constant
T1	carbon/N6	43	0.52	230	358
T2	carbon/N6	43	0.52	260	353
T3	carbon/N6	43	1.03	230	353
T4	carbon/N6	43	1.03	260	353
T5	carbon/N6	33	0.52	230	381
T6	carbon/N6	33	0.52	260	362
T7	carbon/N6	33	1.03	230	355
T8	carbon/N6	33	1.03	260	352
T9	glass/N6	34	0.52	230	347
T10	glass/N6	34	0.52	260	411*
T11	glass/N6	34	150	230	387*
T12	glass/N6	34	150	260	689*
T13	glass/N6	26	0.52	230	357
T14	glass/N6	26	0.52	260	351
T15	glass/N6	26	150	230	372
T16	glass/N6	26	150	260	423*
T17	carbon/PPS	48	0.52	310	361
T18	carbon/PPS	48	150	310	380
T19	carbon/PPS	38	0.52	310	366
T20	carbon/PPS	38	150	310	387
				Average	362
				Standard Deviation	12.2

*Note: Data not included in average

Table 5.9: p-values for ANOVA of Kozeny constant for towpreg

Factor	p-value all data
Pressure	0.440
Temperature	0.04
Resin	0.019
Fiber	0.374
Resin Weight Percent	0.2

5.5.3 Comparison of Experimental and Theoretical Towpreg Permeation Results

The percent deviation, E, between the experimental and model results was calculated with Equation 5.2, which was described earlier. As shown in Table 5.10, the deviation between the experimental results and both models is ~6 %. Surprisingly, both models did an excellent job at predicting the penetration depth. The reasons for the good predictions are attributed to the same factors discussed in Section 5.4 for the good predictive results with the mat preforms. For one, Reynolds numbers of $\sim 10^{-11}$ were estimated. In addition, the same large square mold was used to process the towpreg preforms. Finally, the aspect ratios of the fibers in the towpreg preforms were 15,875-36,285.

Graphs of the transient penetration depth are shown in Figures 5.29-5.33. Raw data for each experimental condition are presented in Appendix I. Again, as shown in the Figures 5.29-5.33, there is a very good fit between the data and the models. The standard deviation of the experimental penetration depth is ~0.002 mm. Also, as shown in Figures 5.29-5.33, both of the theoretical curves tend to coincide. Like the mat preform analysis, this suggests that the Bruschke model can be used to assess the Kozeny constant. As stated earlier, it is understood that it would not be practical to use a semi-empirical model when a valid mechanistic model is available. However, it is interesting to note the similarity between the two models. Equation 5.3, with a shape factor of 3, was used to plot the Kozeny constant versus porosity and power-law flow index. The results are shown in Figure 5.34. As can be seen in Figure 5.34, the Kozeny constant increases

drastically with a decrease in porosity. This is reasonable since as the porosity decreases, the tortuosity increases.

Table 5.10: Percent deviation between experimental and theoretical penetration depth results for towpreg processing

Experiment	Towpreg	Resin Weight Percent [%]	Pressure [MPa]	Temperature [°C]	Semi-empirical E [%]	Bruschke E [%]
T1	carbon/nylon 6	43	0.52	230	3.9	4.1
T2	carbon/nylon 6	43	0.52	260	3.2	3.6
T3	carbon/nylon 6	43	1.03	230	5.3	5.7
T4	carbon/nylon 6	43	1.03	260	3.5	4.1
T5	carbon/nylon 6	33	0.52	230	5.4	5.0
T6	carbon/nylon 6	33	0.52	260	3.6	3.7
T7	carbon/nylon 6	33	1.03	230	4.6	4.7
T8	carbon/nylon 6	33	1.03	260	9.3	9.4
T9	glass/nylon 6	34	0.52	230	6.1	6.5
T10	glass/nylon 6	34	0.52	260	*	*
T11	glass/nylon 6	34	150	230	*	*
T12	glass/nylon 6	34	150	260	*	*
T13	glass/nylon 6	26	0.52	230	3.8	4.2
T14	glass/nylon 6	26	0.52	260	5.2	5.5
T15	glass/nylon 6	26	150	230	6.3	6.2
T16	glass/nylon 6	26	150	260	*	*
T17	carbon/PPS	48	0.52	310	6.6	8.1
T18	carbon/PPS	48	150	310	7.9	8.0
T19	carbon/PPS	38	0.52	310	7.1	7.2
T20	carbon/PPS	38	150	310	5.8	6.1
				Average	5.5	5.8
				Standard Deviation	1.7	1.7

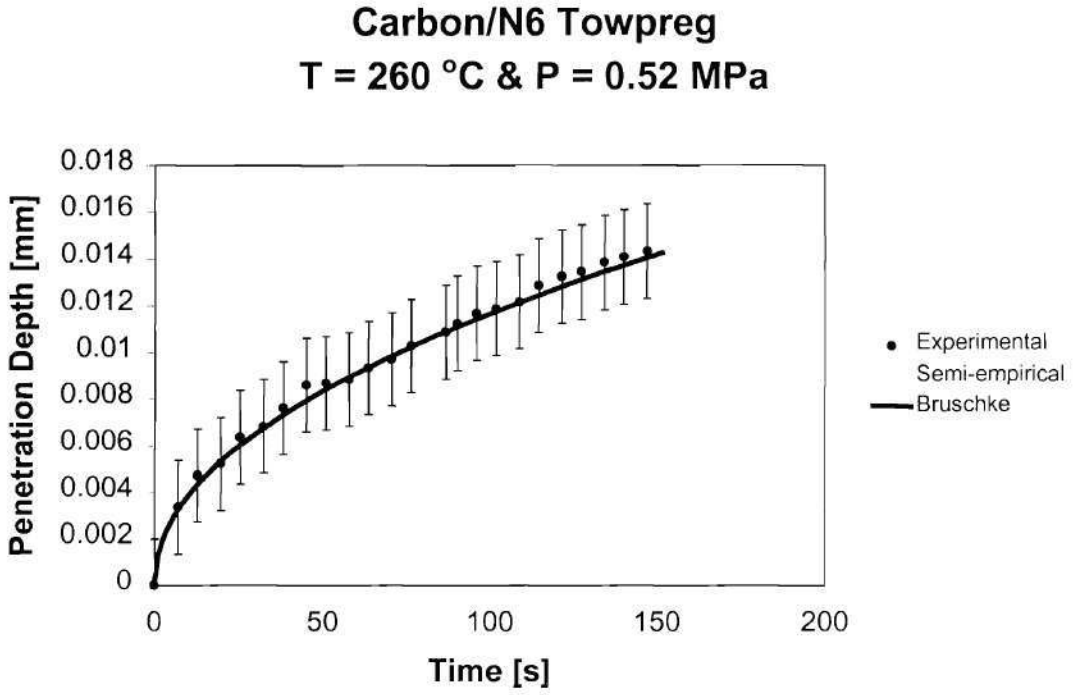

Figure 5:29: Penetration depth versus time for experiment T2. The material is carbon/N6 towpreg. The resin weight percent is 43. The processing pressure is 0.52 MPa and the processing temperature is 260 °C. The standard deviation of the penetration depth is ~0.002 mm.

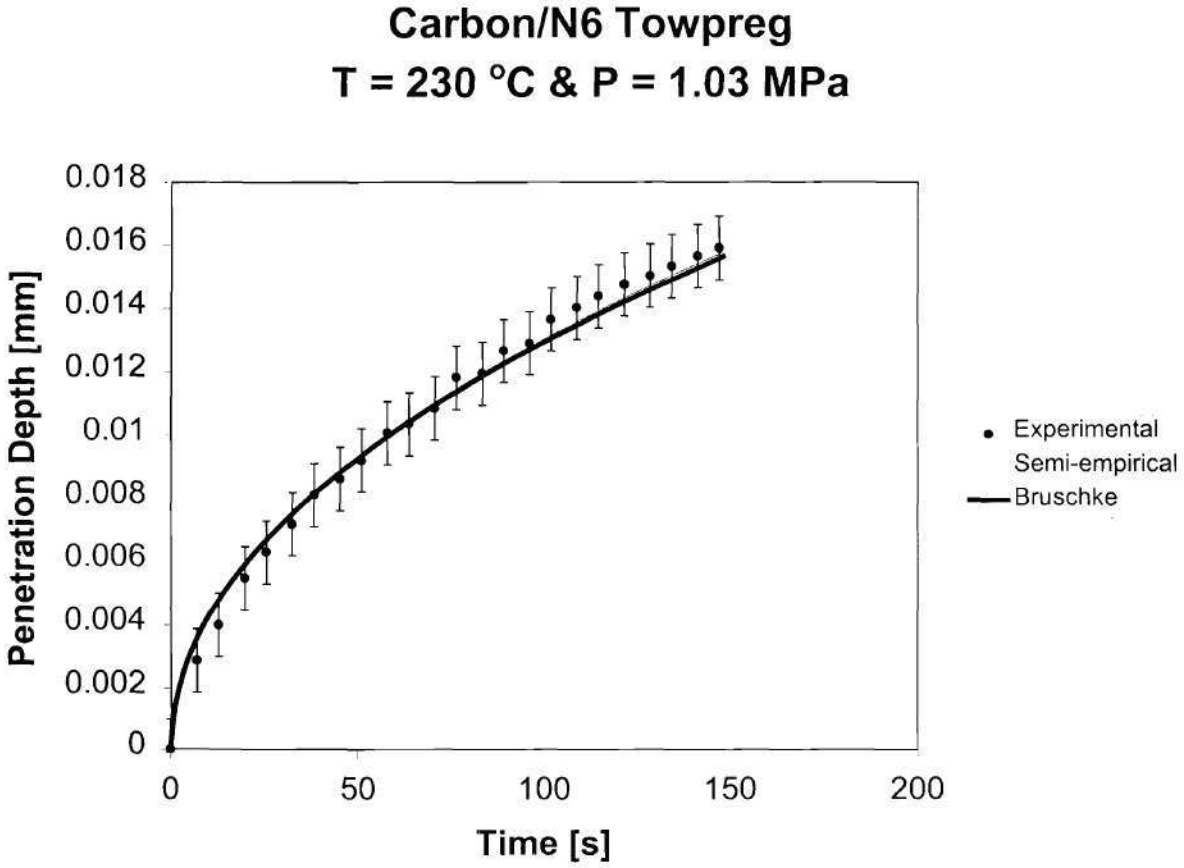

Figure 5:30: Penetration depth versus time for experiment T7. The material is carbon/N6 towpreg. The resin weight percent is 33. The processing pressure is 1.03 MPa and the processing temperature is 230 °C. The standard deviation of the penetration depth is ~0.001 mm.

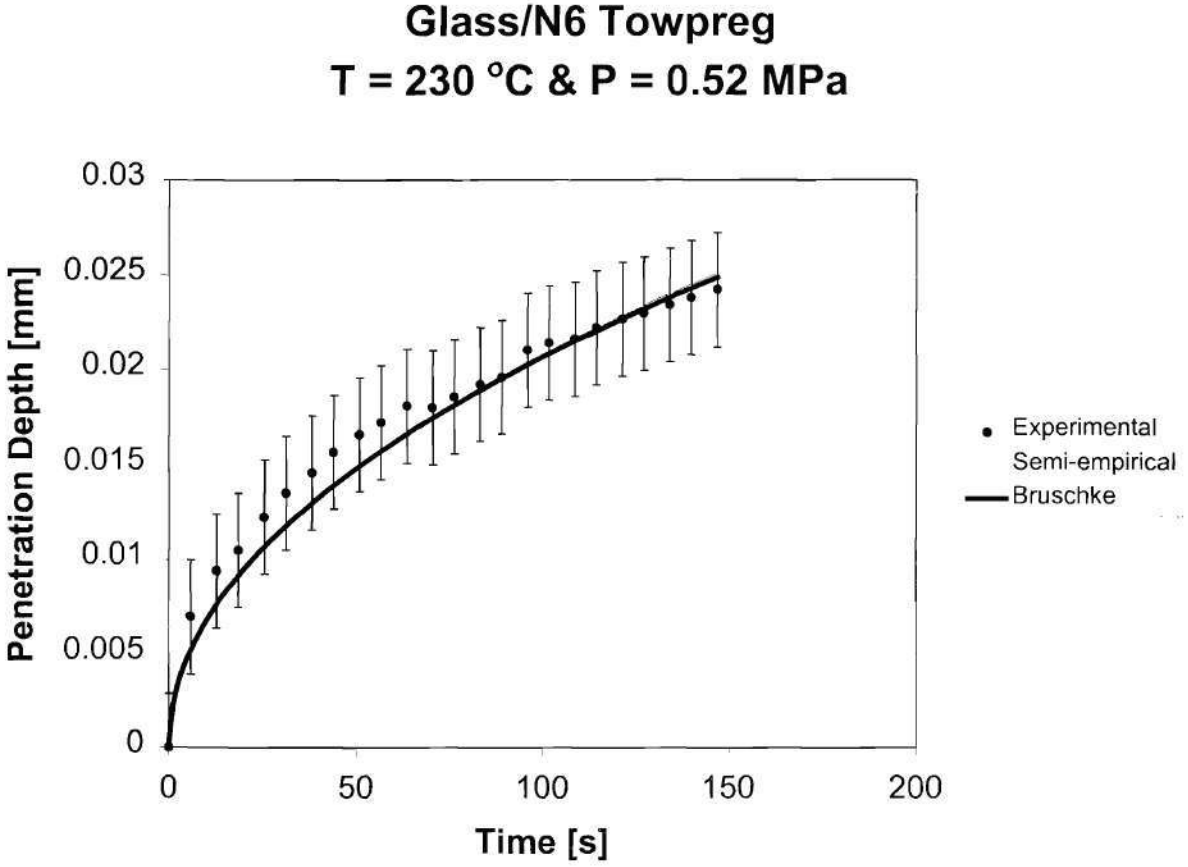

Figure 5:31: Penetration depth versus time for experiment T9. The material is glass/N6 towpreg. The resin weight percent is 34. The processing pressure is 0.52 MPa and the processing temperature is 230 °C. The standard deviation of the penetration depth is ~0.003 mm.

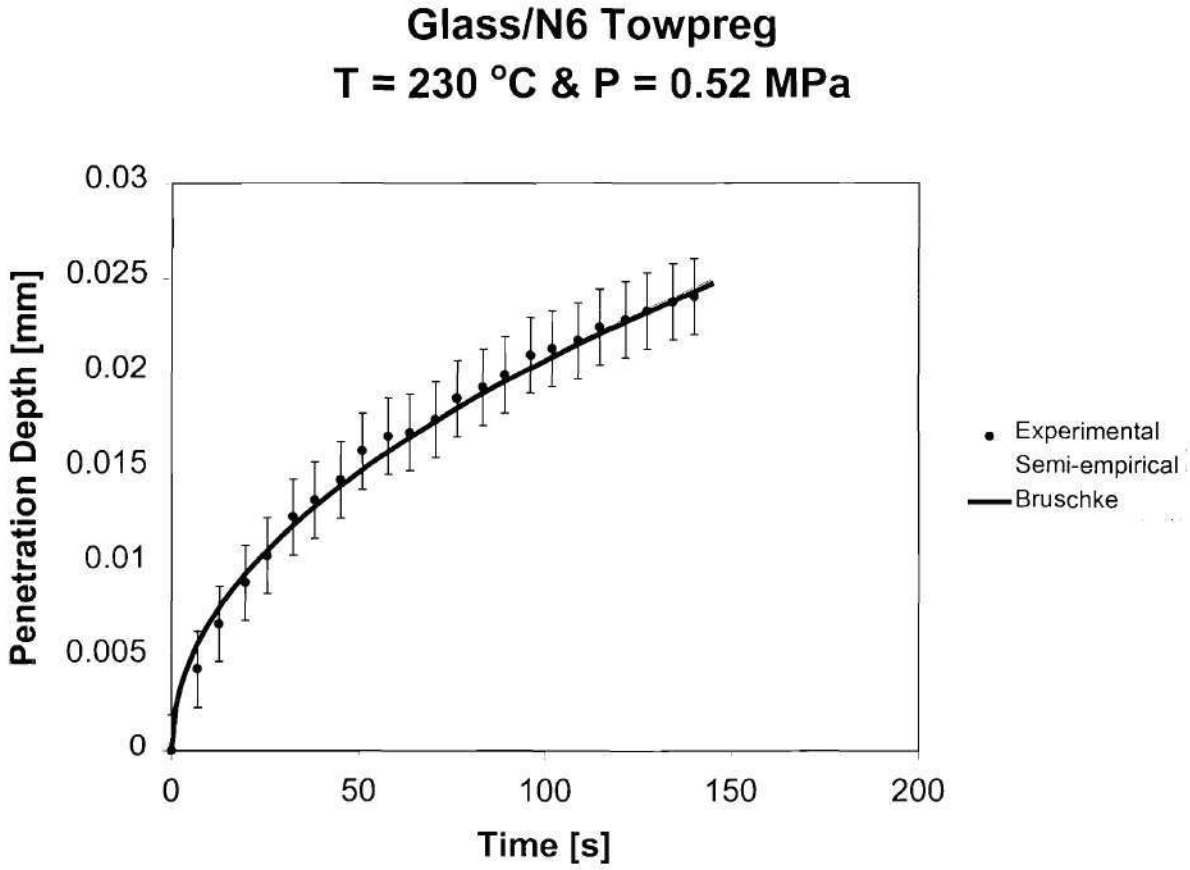

Figure 5:32: Penetration depth versus time for experiment T13. The material is glass/N6 towpreg. The resin weight percent is 26. The processing pressure is 0.52 MPa and the processing temperature is 230 °C. The standard deviation of the penetration depth is ~0.002 mm.

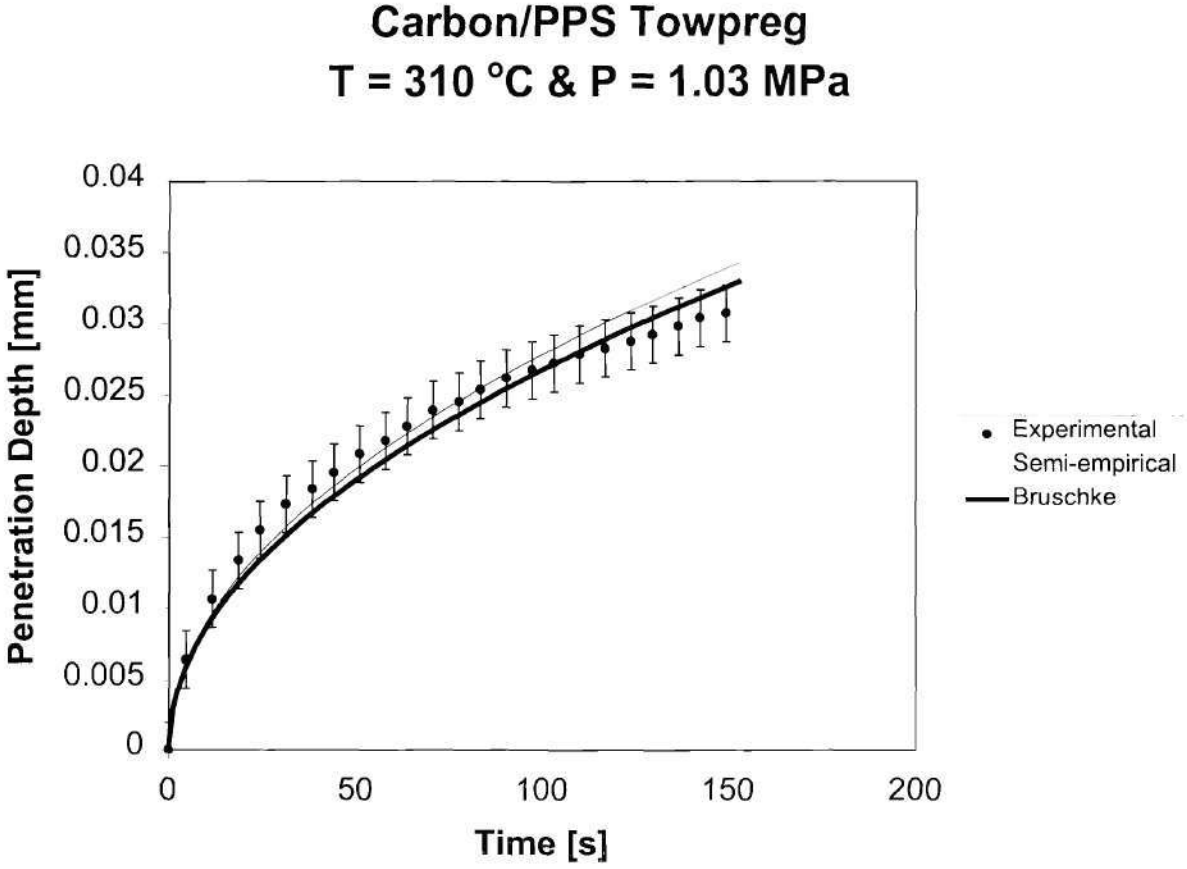

Figure 5:33: Penetration depth versus time for experiment T20. The material is carbon/PPS towpreg. The resin weight percent is 38. The processing pressure is 1.03 MPa and the processing temperature is 310 °C. The standard deviation of the penetration depth is ~0.002 mm.

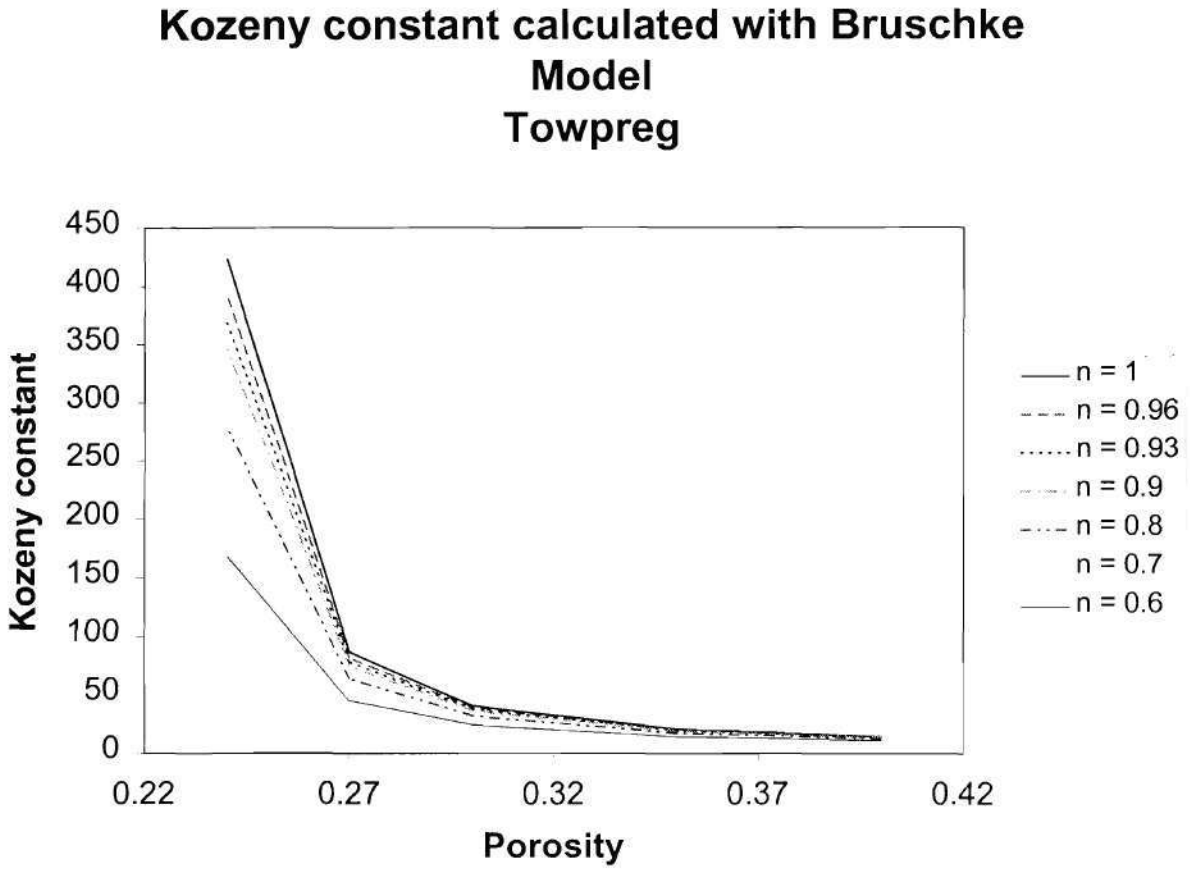

Figure 5.34: Graph of Kozeny constant, calculated from Equation 5.3, versus porosity with power-law flow index as a parameter

5.5.4 Comparison of Experimental and Theoretical Void Content

As discussed in Chapter III, void content in a composite is an important parameter because it can affect the mechanical properties of composites. The equation to calculate the theoretical void content, Equation 3.38, was discussed in Chapter III.

$$v_{void}(t) = v_{voidi}\left(1 - \frac{X(t)}{X_c}\right) \tag{3.38}$$

The Bruschke model was used to calculate X(t). The processing time, t, for the composites, as shown in Table 4.5, was 150 s. To calculate the theoretical void content, the initial void content, v_{voidi}, and the distance available for flow, X_c, were needed. The method to determine the initial void content was discussed in Chapter IV. The composites from experiments T21-T30 in Table 4.5 were used to obtain the initial void content. SEM analysis, as discussed in Chapter IV, was used to determine X_c. The experimental void content was calculated using the density of the composite as outlined in Chapter IV. The results of the experimental and theoretical void content are displayed in Table 5.11. The data used to calculate the experimental void content is listed in Appendix J.

A sample SEM photograph used to determine X_c is shown in Figure 5.35. As expected, X_c is a function of processing temperature and weight percent of resin in the tow. Referring to Table 5.11, as processing temperature increased, X_c decreased. This is plausible since viscosity decreases with increasing temperature. As resin weight percent

increased, X_c decreased. Referring to Table 5.11 again, this is reasonable since it is more likely that more fibers will be covered as the amount of resin content increases.

Table 5.11: Experimental and theoretical void content of composites manufactured from powder-coated towpreg

Experiment	Towpreg	Resin Weight Percent [%]	Pressure [MPa]	Temperature [°C]	Xc [μm]	X(150s) [μm] Bruschke	v_{voidi} [%] Initial	v_{void} [%] Theoretical	v_{void} [%] Experimental
T1	carbon/N6	43	0.52	230	41.0±12.4	10.9	4.9±0.7	3.6	3.1±0.9
T2	carbon/N6	43	0.52	260	35.0±13.1	14.1	3.3±0.3	2.0	1.6±0.7
T3	carbon/N6	43	1.03	230	41.0±12.4	15.7	4.9±0.7	3.0	1.8±0.5
T4	carbon/N6	43	1.03	260	35.0±13.1	20.3	3.3±0.3	1.4	1.0±0.7
T5	carbon/N6	33	0.52	230	47.6±12.7	10.9	4.9±1.0	3.8	3.4±0.4
T6	carbon/N6	33	0.52	260	38.4±14.9	14.1	3.4±1.0	2.1	2.1±1.5
T7	carbon/N6	33	1.03	230	47.6±12.7	15.7	4.9±1.0	3.3	2.3±1.3
T8	carbon/N6	33	1.03	260	38.4±14.9	20.3	3.4±1.4	1.6	1.1±0.9
T9	glass/N6	34	0.52	230	32.5±7.8	25.1	2.8±1.6	0.6	0.4±0.7
T10	glass/N6	34	0.52	260	29.3±7.3	32.4	2.1±1.7	0*	0.4±0.7
T11	glass/N6	34	1.03	230	32.5±7.8	36.0	2.8±1.6	0*	0.3±0.4
T12	glass/N6	34	1.03	260	29.3±7.3	46.4	2.1±1.7	0*	0.1±0.2
T13	glass/N6	26	0.52	230	49.6±11.2	25.1	4.7±1.4	2.3	2.2±1.5
T14	glass/N6	26	0.52	260	39.6±9.3	32.4	4.3±1.6	0.8	1.2±0.9
T15	glass/N6	26	1.03	230	49.6±11.2	36.0	4.7±1.4	1.3	1.3±0.7
T16	glass/N6	26	1.03	260	39.6±9.3	46.4	4.3±1.6	0*	0.5±0.8

*Note: The theoretical void content should be 0 since X(150 s) is greater than X_c

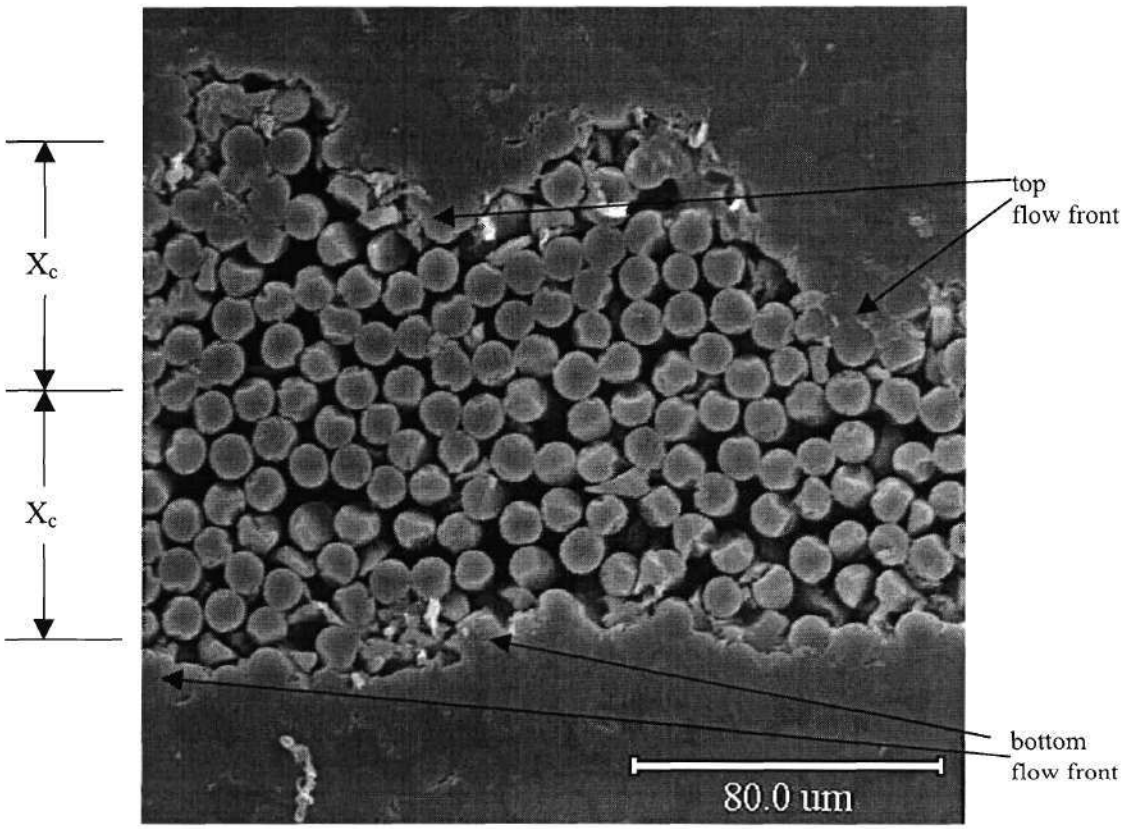

Figure 5.35: SEM photograph used to determine X_c for a towpreg preform. X_c is half the distance between the top and bottom flow front. This SEM photograph is of a sample from experiment T24. The material is carbon/N6 towpreg. The resin weight percent is 33. The processing temperature is 260 °C. It should be noted that the average X_c of the fiber bed in the figure was used since the flow front is uneven.

As shown in Table 5.11, Equation 3.38 predicted the void content of the composites well. As expected, the void percentage decreased with increasing processing pressure and processing temperature. As stated above, higher temperatures result in lower viscosity. Lower viscosity results in larger X(t) and hence a smaller void percentage. Furthermore, when increasing processing pressure, X(t) increases and hence the void content should decrease. It should be noted that the experimental void percentage calculated for the carbon and PPS composites were not included in Table 5.11 because the X_c values could not be determined because of the difficulty in obtaining SEM photographs for this resin/fiber combination as discussed in Section 5.2.3.

5.5.5 Explanation of Discarded Experiments T10, T11, T12, and T16

The data in Table 5.11 can also be used to explain the results of the four discarded experiments of T10, T11, T12, and T16. As shown in the Table 5.11, the X_c values at these conditions are less than the theoretical X(t). Therefore, the transient experimental penetration depth should only equal the transient theoretical penetration depth up to a value of $\sim X_c$. Figure 5.36 illustrates this point. Figure 5.36 is the penetration depth curve for condition T10. It shows that the experimental data follows the theoretical curves up to about 0.024 mm and then begins to level off. Referring to Table 5.11, the X_c at experiment T10 is 0.0293 ± 0.007 mm. The data tapers off because there is no additional flow space. In addition, as shown in Table 5.11, the void contents at the four discarded conditions are less than 1 %. This low void content is evidence of the polymer filling all the void spaces in the fiber bed. It should be mentioned that it is difficult to get void percents much lower than ~0.5 % because of the nature of the fiber bed. In some areas

of the fiber bed, fibers will touch each other or cluster together. In these areas the porosity is too low for resin infiltration. Therefore, it is understood that a void percentage of zero is probably not attainable, especially in low porosity systems.

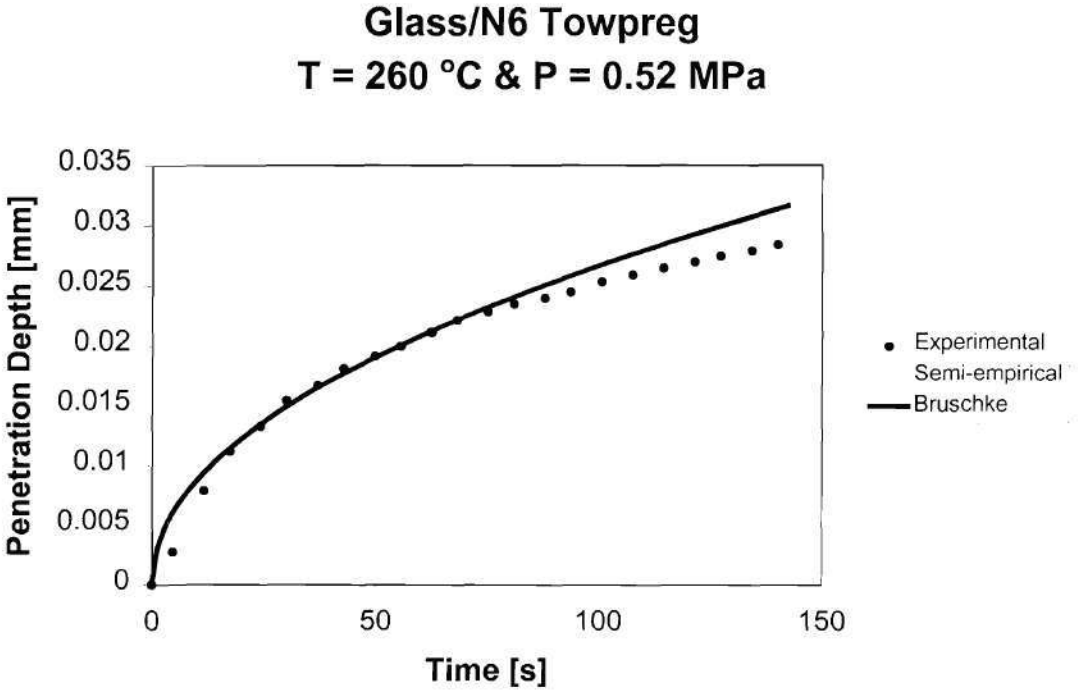

Figure 5.36: Penetration depth versus time for experiment T10. The material is glass/N6 towpreg. The resin weight percent is 34. The processing pressure is 0.52 MPa and the processing temperature is 260 °C. The standard deviation of the penetration depth is ~0.0008 mm.

Three possible ways to modify the model equations to include a provision for the flow front reaching the boundary of X_c are discussed next. The simplest method is to change the limits of integration of Equation 3.7. Instead of integrating from t = 0 to t = t and X = 0 to X = X(t), Equation 3.7 can be integrated from t = t to t = t_c and X = X(t) to X = X_c, where t is the processing time and t_c is the time when X(t) = X_c. The drawback of this approach is that at times greater than t_c negative values of X(t) are possible. A second method is the use of Laplace transforms to solve Equation 5.4 below.

$$X(t) = \begin{cases} \text{Semi - empirical or Bruschke or Vijaysri model} & 0 \le t \ge t_c \\ X_c & t \ge t_c \end{cases} \qquad (5.4)$$

The final method is more complex. In this third method, the time derivative terms in the momentum equations can be retained and the resulting equations solved numerically using appropriate boundary conditions to take into account the boundary X_c. In reality, during practical situations the investigator should know X_c and hence the need for the model equations to include a provision for the boundary may not be necessary.

5.5.6 Summary

In Section 5.5, the permeation results with towpreg preforms were analyzed. A Kozeny constant of 362 was calculated. It was found that the Kozeny constant did not vary with fiber, processing pressure, or resin weight percent. However, it did vary with processing temperature and resin. This variation was explained using the Bruschke

model to calculate the Kozeny constant. Using this method to calculate the Kozeny constant, it was shown that the Kozeny constant increases drastically with decreasing porosity beginning at porosities less than ~0.3. This porosity effect explains the stark difference between the value of 7.9 calculated for the high porosity mat preforms and the high value calculated for the low porosity towpreg. It was also shown that the power-law index has a significant effect on the Kozeny constant as the porosity decreases.

Both the Semi-empirical and Bruschke models predicted the penetration depth to within 6 %. Furthermore, it was illustrated that the Bruschke model can be used to calculate the void content of a composite. The theoretical void contents compared very well with the experimental void percentages.

After analyzing the permeation results, it is recommended to utilize the Bruschke model to describe the permeation of thermoplastic during powder-coated towpreg consolidation. There are three reasons for this recommendation. First, the percent deviation is the same for both the Semi-empirical and Bruschke equations. Secondly, the Bruschke model does not require an empirical constant. Finally, at this point, it does not appear that the Bruschke model is limited to specific ranges of processing and material conditions.

5.6 Commingled Fiber Results

5.6.1 Introduction

In the mat and towpreg preforms, the geometry of the fiber and resin arrangement was relatively easy to model since there were distinct neat resin and neat fiber regions. With commingled fibers, the task is more difficult. In the commingled fiber preforms, there is no distinct arrangement between the resin and reinforcing fibers. However, to simplify the situation, it was assumed that resin fibers were surrounded by a collection of reinforcing fibers. Figure 5.37 is a simple schematic of this assumption, and Figure 5.38 is a SEM photograph of a composite made from the commingled fibers. The geometric arrangement between reinforcing fibers and resin fibers was needed in order to calculate the penetration depth. Figure 5.37 was used to calculate the experimental penetration depth. Referring to Figure 5.37 and by performing a mass balance, Equation 5.5 was used to calculate the penetration depth. As with the mat and towpreg preforms, the LVDT discussed in Chapter IV was used to calculate the thickness change.

$$X(t) = \frac{\Delta h(t)}{4\varepsilon} \tag{5.5}$$

Where:

X	=	penetration depth, mm
Δh	=	thickness change, mm
ε	=	porosity
t	=	time, s

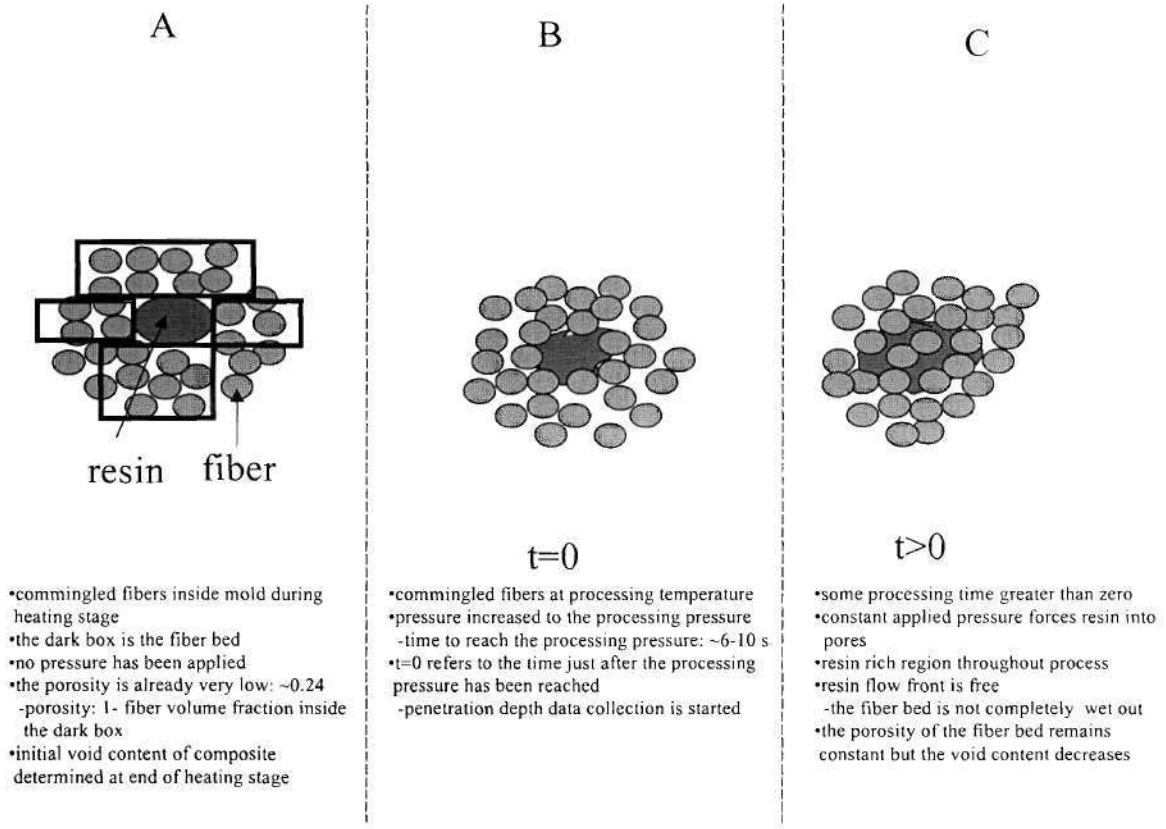

Figure 5.37: Schematic used to calculate the experimental penetration depth. It should be noted that while there is only one square "wall" of glass fibers shown surrounding the larger PP fiber, there might be more glass fibers outside the first square of glass fibers.

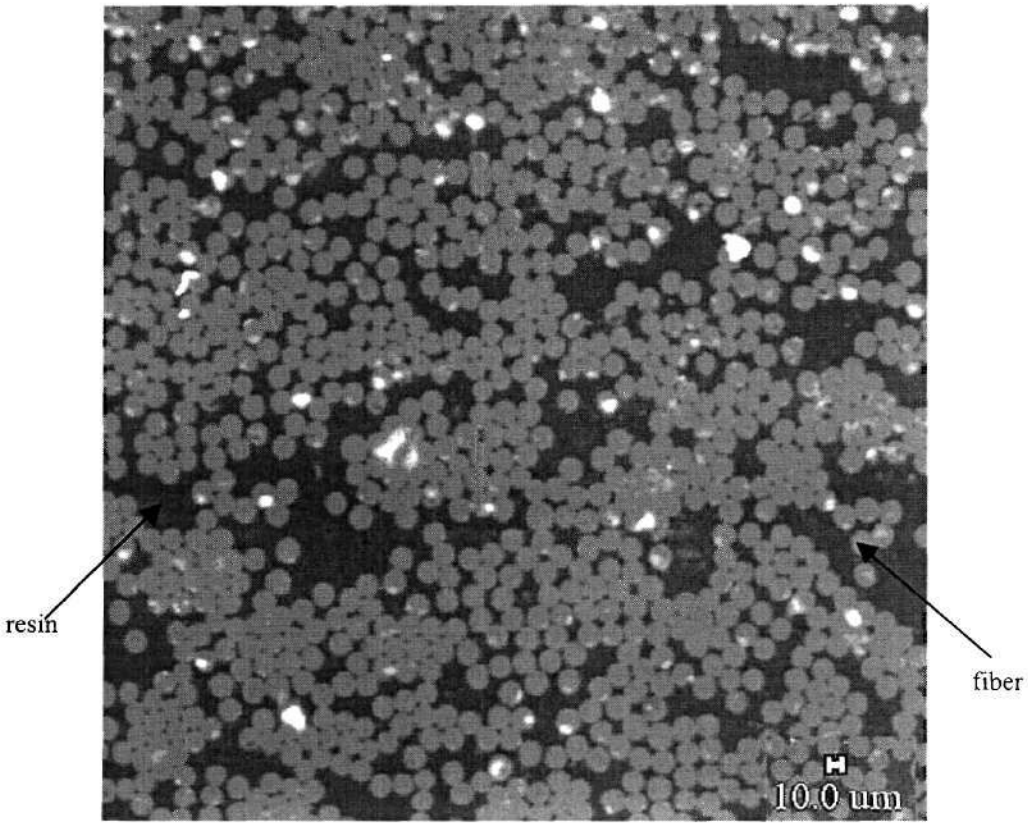

Figure 5.38: SEM photograph of composite from experiment C1. The material is commingled glass/PP fibers. The resin weight percent is 25. The processing pressure is 0.34 MPa and the processing temperature is 180 °C.

Since it has been shown in Sections 5.4 and 5.5 that the Bruschke model can be used to calculate the Kozeny constant, the Bruschke model was used to calculate the Kozeny constant for the commingled fiber processing. The calculated Kozeny constant value was used in the Semi-empirical model. The percent deviations between the experimental and theoretical results were calculated with Equation 5.2. The results are discussed in Section 5.6.2.

Next, the Bruschke model was used to calculate the void content of the composites made from the permeation tests using the commingled fibers. The theoretical void content was compared to the experimental void content. The void content results are analyzed in Section 5.6.3.

5.6.2 Comparison of Experimental and Theoretical Permeation Results

Using Equation 5.3, a Kozeny constant of 376 was calculated for use in the Semi-empirical model. Referring to Table 5.12, the deviation for the two models were both 4.3 %. It was expected that both would have the same deviation. The data from experiments C2, C4, C6, and C8 were not included because of the same reasons discussed in Section 5.5.5 for why the experiments at some of the towpreg experiments were discarded.

Graphs of the penetration depth curves are shown in Figures 5.39-5.42. The standard deviation of the experimental penetration depth is ~0.001 mm. As shown in Figures 5.39-5.42 and in Table 5.12, the models predicted the penetration depth exceptionally well. In addition, the predictions are good across the different processing pressures and resin weight percents. Considering the complexity of the arrangement between the reinforcing and resin fibers, the good predictions are a surprise. The reasons

for the good predictions may be attributed to the same factors discussed in Sections 5.4.3 and 5.5.3 for the good predictive results with the mat and towpreg preforms. For one, the Reynolds numbers during the commingled fiber preform processing were on the order of 10^{-12}. In addition, the same large square mold was used to process the commingled fiber preforms. Finally, the aspect ratio of the fibers in the commingled fiber preforms was 14,111. Raw data for each experiment are located in Appendix K.

Out of curiosity, the data from experiments C1, C3, C5, and C7 were non-linearly regressed using a statistical analysis package, SAS, to determine the Kozeny constant (SAS Institute, Inc., 1989). A Kozeny constant of 369±17.1 was calculated. This value compares well with the value of 376 calculated using the Bruschke model.

Table 5.12: Percent deviation between experimental and theoretical penetration depth results for commingled fibers processing

Experiment	Commingled Fibers	Resin Weight Percent [%]	Pressure [MPa]	Temperature [°C]	Semi-Empirical E [%]	Bruschke E [%]
C1	glass/PP	25	0.34	180	5.5	5.5
C2	glass/PP	25	0.34	210	*	*
C3	glass/PP	25	0.69	180	3.9	3.9
C4	glass/PP	25	0.69	210	*	*
C5	glass/PP	40	0.34	180	5.0	5.0
C6	glass/PP	40	0.34	210	*	*
C7	glass/PP	40	0.69	180	2.8	2.8
C8	glass/PP	40	0.69	210	*	*
				Average	4.3	4.3
				Standard Deviation	1.2	1.2

*Note: The data for these experiments were not included

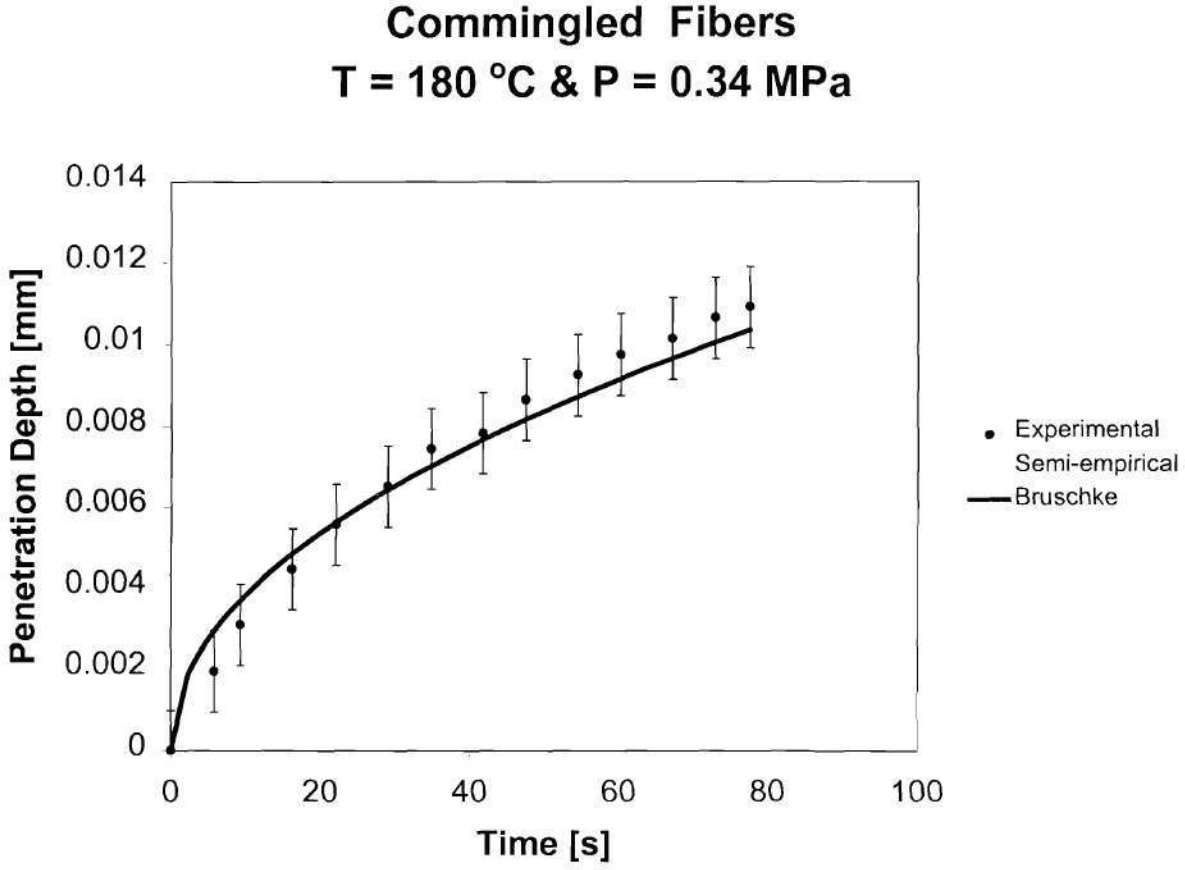

Figure 5.39: Penetration depth curve for experiment C1. The material is commingled glass/PP fibers. The resin weight percent is 25. The processing pressure is 0.34 MPa and the processing temperature is 180 °C. The standard deviation at each penetration depth is ~0.001 mm.

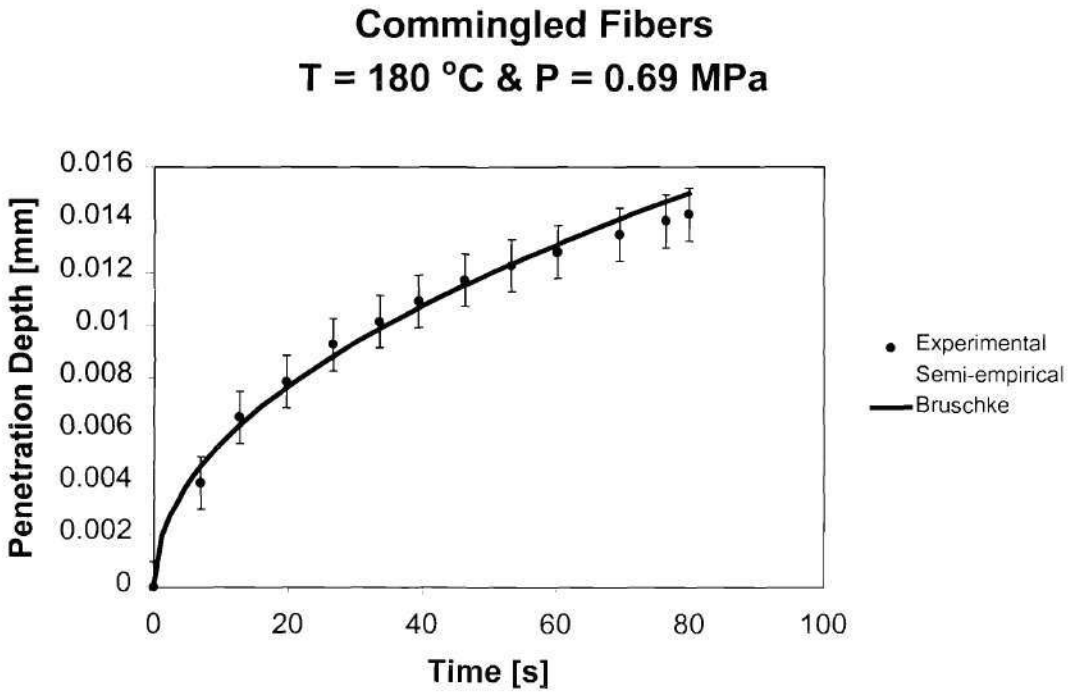

Figure 5.40: Penetration depth curve for experiment C3. The material is commingled glass/PP fibers. The resin weight percent is 25. The processing pressure is 0.69 MPa and the processing temperature is 180 °C. The standard deviation of the penetration depth is ~0.001 mm.

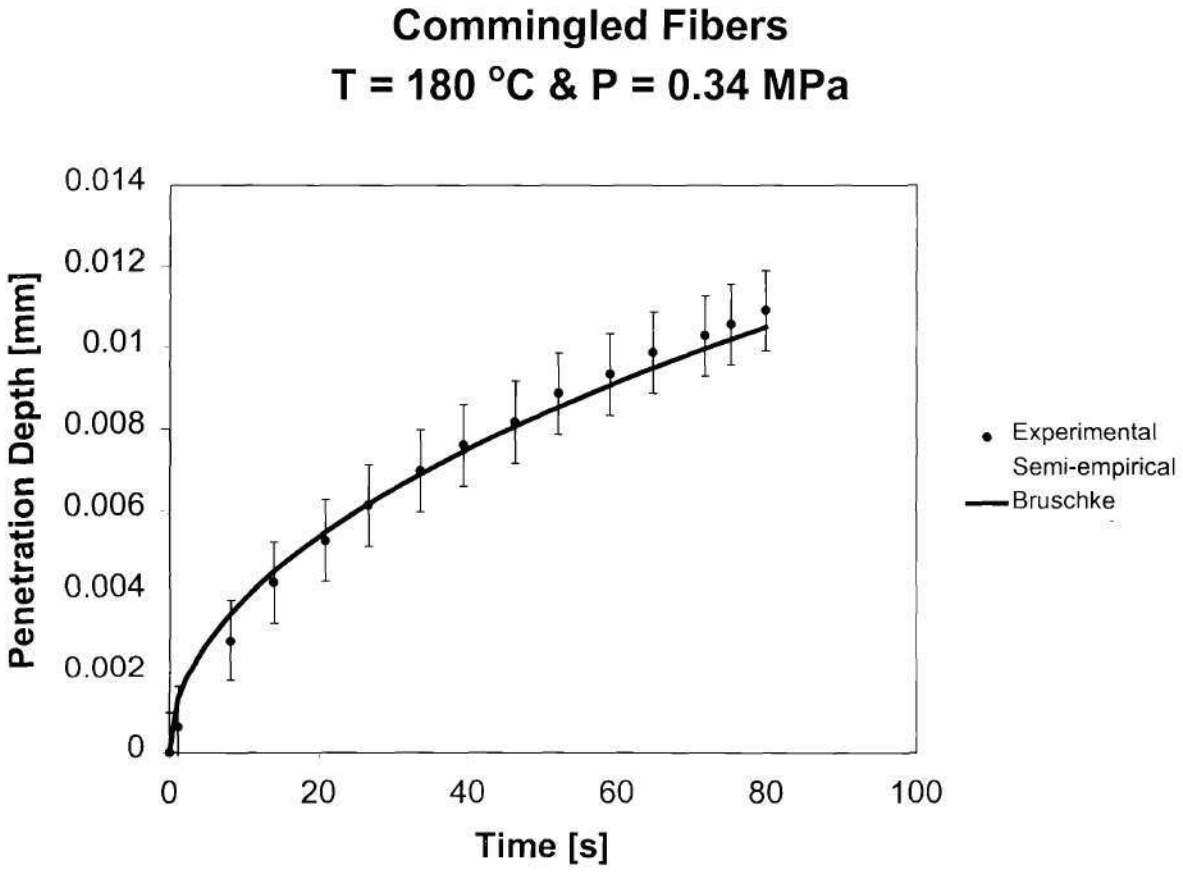

Figure 5.41: Penetration depth curve for experiment C5. The material is commingled glass/PP fibers. The resin weight percent is 40. The processing pressure is 0.34 MPa and the processing temperature is 180 °C. The standard deviation of the penetration depth is ~0.001 mm.

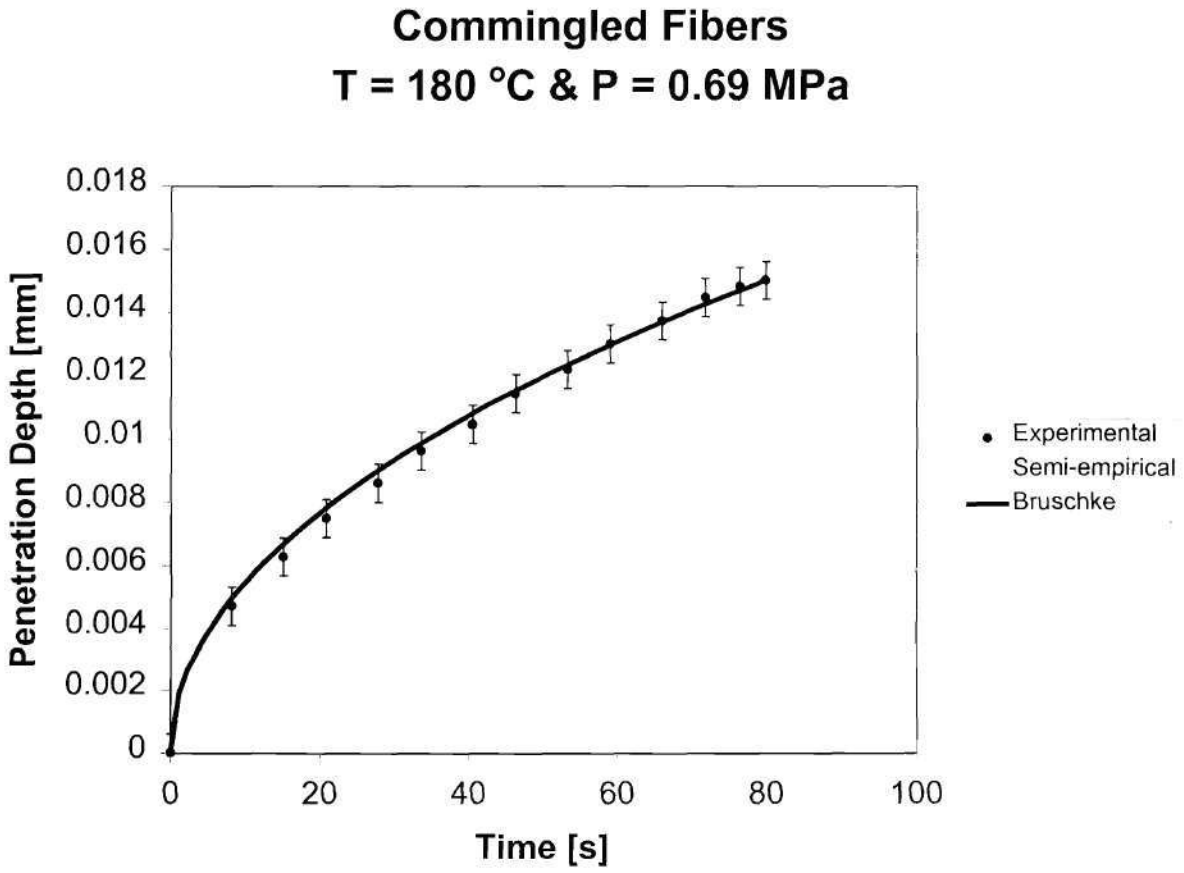

Figure 5.42: Penetration depth curve for experiment C7. The material is commingled glass/PP fibers. The resin weight percent is 40. The processing pressure is 0.69 MPa and the processing temperature is 180 °C. The standard deviation of the penetration depth is ~0.0006 mm.

5.6.3 Comparison of Experimental and Theoretical Void Content

The same method used to determine the theoretical void content as discussed in Section 5.5.4 for the towpreg preforms was used to calculate the theoretical void content for the commingled fibers. The composites from experiments C9-C12 in Table 4.6 were used to obtain the initial void content, and SEM analysis was used to obtain X_c. Raw data used to calculate the experimental void content are located in Appendix J.

As shown in Table 5.13, the theoretical and experimental void contents are in good agreement. As expected, the void percentages decreased with increasing processing pressures and temperatures. The reasons for this trend were discussed in Section 5.5.4. Referring to Table 5.13, it was also expected that the void percentages of the discarded experiments C2, C4, C6, and C8 would be low since the X_c at these conditions are less than the X(80 s) at the conditions.

5.6.4 Summary

In Section 5.6 the permeation results with commingled fibers were analyzed. An experimental Kozeny constant of 369±17.1 and a theoretical Kozeny constant of 376 was calculated. Both the Semi-empirical and Bruschke models predicted the penetration depth to within 4 %. Furthermore, it was illustrated that the Bruschke model can be used to calculate the void content of a composite manufactured with commingled fibers. The theoretical void contents compared very well with the experimental void percentages.

Table 5.13: Experimental and theoretical void content for composites manufactured from commingled fibers

Experiment	Commingled Fibers	Resin Weight Percent [%]	Pressure [MPa]	Temperature [°C]	X_c [μm]	X(80 s) [μm] Bruschke	v_{voidi} [%] Initial	v_{void} [%] Theoretical	v_{void} [%] Experimental
C1	glass/PP	25	0.34	180	37.7±13.2	10.5	2.9±0.4	2.1	2.3±0.2
C2	glass/PP	25	0.34	210	8.6±2.2	16.0	2.6±1.1	0*	0.3±0.3
C3	glass/PP	25	0.69	180	37.7±13.2	15.0	2.9±0.4	1.7	1.4±1.1
C4	glass/PP	25	0.69	210	8.6±2.2	22.9	2.6±1.1	0*	0.8±0.7
C5	glass/PP	40	0.34	180	36.3±15.5	10.5	2.8±1.5	2.0	2.0±0.8
C6	glass/PP	40	0.34	210	9.0±4.5	16.0	1.7±0.8	0*	0.9±0.8
C7	glass/PP	40	0.69	180	36.3±15.5	15.0	2.8±1.5	1.6	1.4±1.2
C8	glass/PP	40	0.69	210	9.0±4.5	22.9	1.7±0.8	0*	0.6±0.5

*Note: The theoretical void content should be 0 since X(80 s) is greater than X_c

After analyzing the permeation results, it is recommended to use the Bruschke model to describe the permeation of thermoplastic during commingled fiber preform consolidation. There are three reasons for this recommendation. First, the percent deviation between the experimental penetration depth and the Bruschke equation is very low. Secondly, the Bruschke model does not require an empirical constant. Finally, at this point, it does not appear that the Bruschke model is limited to specific ranges of processing and material conditions.

5.7 Error Analysis, Limitations, and General Comments

5.7.1 Error Analysis

The standard deviation between the two permeation experiments for each condition was shown in the figures in this chapter with error bars. Also, the standard deviation is listed in the raw data tables in the appendix.

In this thesis, averaged values of the penetration depth were used because of the complexity of the fiber beds. Furthermore, deviation in the flow front for each permeation experiment was not measured. However, Figures 5.27 and 5.35 give some insight into the deviation.

Experimentally determined porosities and power-law constants were needed as inputs to the model equations. In addition, for the Vijaysri model, the loss coefficient, Λ, was needed as an input. The uncertainties of the porosity, power-law constants, and loss coefficient were ~ 9 %, ~ 2 %, and ~ 1 %, respectively. The uncertainty in the theoretical penetration depth, X, can be found using Equation 5.6. (Doebelin, 1995 and Box et al.,

1978). In the case of the Bruschke model, the term involving Λ would not be included in Equation 5.6.

$$s_X = \sqrt{\left(\frac{\partial X}{\partial n} s_n\right)^2 + \left(\frac{\partial X}{\partial m} s_m\right)^2 + \left(\frac{\partial X}{\partial \Lambda} s_\Lambda\right)^2 + \left(\frac{\partial X}{\partial \varepsilon} s_\varepsilon\right)^2} \qquad (5.6)$$

Where:

s_X = standard deviation of X, mm

s_n = standard deviation of n

s_m = standard deviation of m

s_Λ = standard deviation of Λ

s_e = standard deviation of ε

To obtain an idea of the uncertainty in the theoretical penetration depth, the uncertainty of X from the Vijaysri model was found using Equation 5.6. However, the term involving n in Equation 5.4 was omitted due to the difficulty in obtaining a reasonable expression for the partial derivative of X in terms of n. An uncertainty of ~ 6 % was found for X. Figure 5.43 is a graph, with error bars on the theoretical curve, of penetration depth versus time for a mat preform.

5.7.2 Limitations

At the minimum porosity of a fiber bed, there is no space available for flow and hence the models should not predict any resin flow. The minimum porosity available for a square arrangement of cylinders is ~0.22. In the Bruschke model, the penetration depth

goes to zero as ε goes to 0.216. Furthermore, the Kozeny constant calculated from Equation 5.3 goes to infinity, as it should, as ε goes to 0.216. Loss coefficients, Λ, at the maximum available porosity are not available, thus the limitation of the Vijaysri model cannot be accessed.

5.7.3 General Comments

As stated earlier, it is believed that the good predictions of the model equations were due to the experimental procedures used in this research. Furthermore, the good fit between the mechanistic models and the random mat experimental results was a surprise. As discussed earlier, a possible reason for the good predictions was the low porosity of the random fiber mats. Another possible reason for the good predictions was the cylindrical shape of the fibers. As shown in Chapter III, the models were based on flow transverse to long cylinders. It may be that the shape of the fibers is the most significant factor in the good fit between experimental and theoretical results. Studies to test these issues are discussed in Chapter VI.

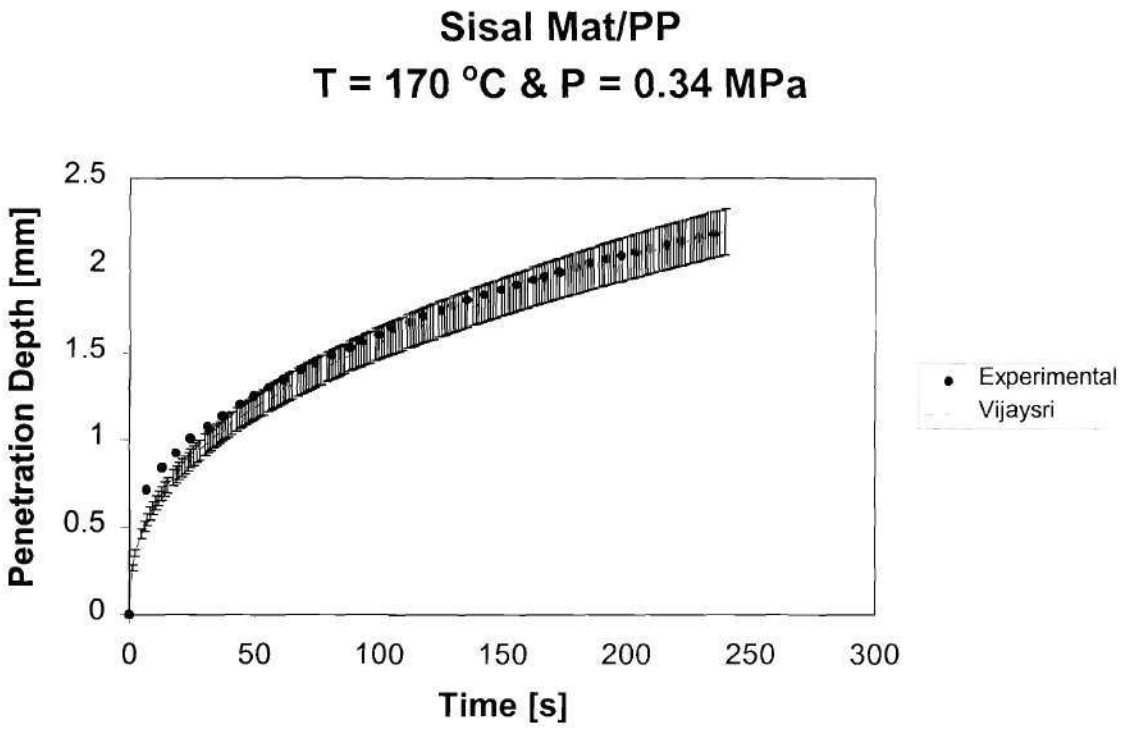

Figure 5.43: Penetration depth versus time for experiment M13. The material is sisal mat/PP. The processing pressure is 0.34 MPa and the processing temperature is 170 °C. The standard deviation of the experimental penetration depth is ~0.04 mm. The error bars are for the theoretical curve.

5.8 References

Åstrom et al., 1992: Åstrom, B., Pipes, B., Advani, S., "On Flow Through Aligned Fiber Beds and Its Application to Composites Processing", *Journal of Composite Materials*, 1992, v 26, n 9, p 1351-1373.

Box et al., 1978: Box, G., Hunter, W., Hunter, J., "Statistics for Experimenters: An Introduction to Design, Data Analysis, and Model Building", Wiley, New York, 1978.

Bruschke and Advani, 1993: Bruschke, M, and Advani, S., " Flow of Generalized Newtonian Fluids Across a Periodic Array of Cylinders", *J. Rheol.*, 1993, v 37, n 3, p 479-497.

Doebelin, 1995: Doebelin, E., "Engineering Experimentation: Planning, Execution, Reporting", McGraw Hill, New York, 1995.

Floyd, 1966: Floyd, F., *Polyamide Resins*, Reinhold Publishing Corporation, New York, 1966.

Gutowski et al., 1987: Gutowski, T., Cai, Z., Bauer, S., Boucher, D., Kingery, J., Wineman, S., "Consolidation Experiments for Laminate Composites", *Journal of Composite Materials*, 1987, v 21, p650-669.

Gutowski, 1997: Gutowski, T., *Advanced Composites Manufacturing*, John Wiley & Sons, Inc., New York, 1997.

Hayter, 1996: Hayter, A., *Probability and Statistics for Engineers and Scientists*, PWS, Boston, 1996.

Lam and Kardos, 1988: Lam, R., and Kardos, J., "The Permeability of Aligned and Cross-Plied Fiber Beds During Processing of Continuous Fiber Composites", *ASC Ann. Tech. Conf.*, 1988, v3, p 3-11.

SAS Institute Inc., 1989: SAS Institute Inc. *SAS/STAT User's Guide, Fourth Edition*, Vol. II. SAS Institute Inc., Cary, NC, 1989

Skartsis et al., 1992: Skartsis, L, Kardos, J., Khomami, B., "Resin Flow Through Fiber Beds During Composite Manufacturing Processes. Part I: Review of Newtonian Flow Through Fiber Beds", *Polymer Engineering and Science*, 1992, v 32, n4, p 221-230.

Vijaysri et al., 1999: Vijaysri, M, Chhabra, R., Eswaran, V., "Power-law Fluid Flow Across an Array of Infinite Circular Cylinders: A Numerical Study", *J. Non-Newtonian Fluid Mech.*, 1999, v 87, p 263-282.

CHAPTER VI

CONCLUSIONS AND RECOMMENDATIONS

6.1 Introduction

In Section 6.2, general conclusions from this research are presented. In addition, the results of this research are matched against the research goals, which were discussed in Chapter I. In Section 6.3, additional research on the topic of transverse permeation of thermoplastics through fiber reinforcements is recommended. References are listed in Section 6.4.

6.2 Conclusions

As stated in Chapter I, the motivation behind this work was the lack of processing information available for the transverse permeation of thermoplastics during continuous fiber-reinforced polymer (CFRP) composite processing. It was shown in Chapter II that there was a need for a comprehensive study on the transverse permeation of thermoplastics through real fiber beds. In addition, it was shown that there was a need to test the validity of theoretical models with experimental permeation results. A general, predictive permeation model would aid in reducing the number of trial and error experiments required to determine optimum thermoplastic composite processing conditions. In addition, a large database of experimental results of the transverse permeation of thermoplastics during CFRP composite processing would be beneficial.

As stated in Chapter I, the fundamental goal of this thesis was to answer three questions. The first question deals with the validity of a semi-empirical or mechanistic model for the transverse permeation of thermoplastics through beds of reinforcing fibers. It was illustrated in this research that the Semi-empirical, Bruschke, and Vijaysri models can be used to predict the transient permeation depth during thermoplastic composite processing. For the mat preform processing, the Semi-empirical and Bruschke models predicted the experimental penetration depth to within 4 % and the Vijaysri model predicted the depth within 6 %. For the towpreg preform processing, the Semi-empirical and Bruschke models predicted the experimental permeation data to within 6 %. Finally, for the commingled fiber preforms, the Bruschke and Semi-empirical models predicted the penetration depth to within 4 %. Therefore, it is safe to conclude that the Semi-empirical model or the mechanistic Bruschke and Vijaysri models can be used to model the transverse permeation of thermoplastic through porous media composed of fibers.

The second question deals with the accuracy of the models. As discussed above, all three models predicted the experimental penetration depth to within 10 %, which is very good. It was expected that the Semi-empirical would give good predictions, but the validity of the two mechanistic equations was unexpected. Considering the ideal geometric assumptions of the two mechanistic models, it was expected that the deviation between the experimental and the theoretical data of these two models would be considerably higher than the Semi-empirical model.

The third question deals with the robustness of the models. All three models gave good predictions across the different processing pressures, temperatures, porosities,

fibers, resins, and preforms. The standard deviations of the deviation, E, were ~1.5 % for all three models and for all three preforms.

It is believed that the good predictions of the model equations were due to the experimental procedures used in this research. The estimated Reynolds numbers in this research were 10^{-11}-10^{-12}. These low Reynolds numbers support the creeping flow assumption. In addition, because of these low Reynolds numbers, inertia effects were negligible, the quasi-steady state assumption was legitimate, and the flow could be considered fully developed. Furthermore, the aspect ratios of the fibers in this research were 202-36,285. Therefore, end effects and longitudinal flow were minimized. Longitudinal flow was also minimized because of the geometric arrangement of the resin and fiber in the preforms. In the mat preforms, a 25.4 cm by 25.4 cm sheet of resin was placed between 25.4 cm by 25.4 cm sheets of fiber mats. For the towpreg, the resin was primarily on the top and bottom surface of the tow. For the commingled fibers, the resin and reinforcing fibers were the same length and they were arranged unidirectionally. Wall effects and longitudinal flow were further minimized by the mold design. A 645 cm^2 square mold, with all sides enclosed, was used to process the preforms.

After analyzing the data, it is recommended to use the Bruschke model for the transverse permeation of thermoplastics through beds of fibers. There are three main reasons for this recommendation. First, the predictions of the Bruschke model are just as accurate as the Semi-empirical model. Secondly, the model does not require an empirical constant. Finally, the model appears to be accurate for a variety of preforms, processing pressures, processing temperatures, porosities, fibers, and resins.

As far as it is known, prior to this study there were no transverse permeation data available for the flow of PP, N6, or any other thermoplastic through glass, sisal, or carbon mats composed of randomly arranged single fibers. In addition, by using the towpreg and commingled preforms, permeation data at the low porosity of 0.24 was obtained. There are no permeation studies reported at porosities this low, and this includes studies with Newtonian fluids and metal cylinders.

Another goal of this research was to model the void content of a composite as a function of processing and material parameters. In this research, it was shown that the Bruschke model could be used to predict the void content of the composite. The theoretically calculated void contents compared well with the experimental void content of the composites manufactured from the towpreg and commingled fibers.

After analyzing the results of this research, interesting questions arose that could be used to initiate further research on the topic of transverse permeation of thermoplastics through beds of fibers. These ideas are discussed below.

6.2 Recommendations

After reviewing the results of this research, six additional studies are recommended. First, it would be beneficial to obtain more experimental data using a variety of resins, fibers, porosities, and preforms to further validate the models. The same experimental procedure and apparatus could be used for this study.

The second recommendation is similar to the first but more specific. It was shown in this research that the Bruschke model could be used to model the transverse

permeation of thermoplastics through a random fiber mat. This is interesting considering that the Bruschke model is based on the square unit cell assumption. As discussed in Chapter V, the reasoning for the good predictions was attributed to the low porosities of the fiber mats. With this in mind, it is recommended to conduct a study of this issue. For example, two different fiber beds could be used: a random fiber mat and a bed composed of unidirectional towpreg. The most important factor to study is the porosity. The porosity range for both types of fiber beds should be 0.24-0.7. It is recommended to determine the validity of the Bruschke model for both systems across the entire porosity range. Since it is relatively inexpensive and readily available, PP could be used as the permeant, and glass fibers could be used for the reinforcement for the same reasons. The same experimental procedure and apparatus used in this research could be used to study the permeation. However, it should be noted that it might be difficult to find commercially available random fiber mats that are composed of single fibers at porosities much lower than 0.6.

The third recommendation deals with using fiber beds composed of fiber bundles. In this research, the mats, towpreg, and commingled fibers were composed of single fibers. Unlike the porous media used in this research, fiber beds also can be composed of fiber bundles. Figure 6.1 is a schematic that illustrates the difference between beds composed of single fibers or fiber bundles. By using media composed of fiber bundles, an additional complexity is added to the permeation process. With fiber beds composed of fiber bundles, two areas of flow are available: flow into the fiber bundle or flow around the fiber bundle. There are some works reported on this issue of fiber bundles

(Ranganathan et al., 1996; Sadiq et al., 1995; Chen et al., 1995; Gebart, 1992). In these studies Newtonian fluids were used as the permeant. Little work is reported on the permeation of thermoplastics through these types of fiber beds. Zhang (1999) studied the flow of PP through a glass mat composed of fiber bundles. According to Zhang (1999), the porosity of the fiber bundles was so low that it did not affect the permeation. Therefore, Zhang (1999) assumed that the PP permeated around the fiber bundles and not into the fiber bundles. It is recommended to conduct a study using PP as the permeant and a glass mat composed of fiber bundles. Furthermore, the effects of the porosity inside the fiber bundle and the overall porosity of the fiber mat on the permeation should be investigated. It is also recommended to test the validity of the Bruschke model on the permeation data. The same experimental procedure and apparatus used in this research could be used for the permeation tests.

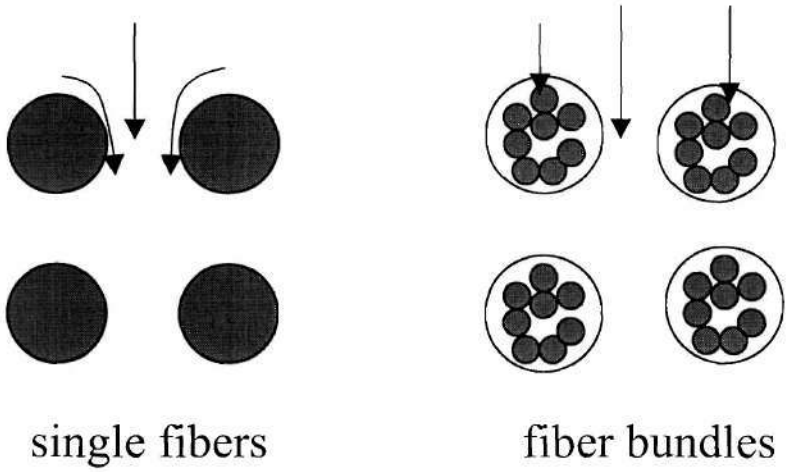

Figure 6.1: Schematic to illustrate the difference between fiber beds composed of single fibers or fiber bundles.

A fourth recommendation deals with using fiber beds composed of a mixture of fibers with different diameters. For example, a bi-directional mat could be composed of glass fibers in one direction and carbon fibers in the other. It is recommended to determine the validity of the Bruschke model for the permeation of a thermoplastic, such as PP, through this type of fiber bed. The effect of the concentration of each fiber should be investigated. As with the earlier recommendations, the same experimental procedure and apparatus could be used for these permeation experiments.

The fifth recommendation deals with elastic effects of resins. During practical composite manufacturing, polymer elastic effects are usually negligible since the flow and shear rates are so small. However, it would be interesting to determine the conditions at which elastic effects do become important. There is little research on the effect of fluid elasticity on the transverse permeation of fluids through beds of fibers. Skartsis, et al., 1992 studied the effects of elasticity using a polymer solution and a unidirectional carbon fiber bed. However, most of the studies reported are on the transverse flow of elastic polymer solutions through metal cylinders (Dyakonova, et al., 1996; Skartsis, et al., 1992; Georgiou et al., 1991; Pilitsis et al, 1991; Chmielewski, et al., 1990;). The common method used in these studies to determine the onset of elastic effects is the use of a friction factor, f, and a Reynolds number, Re. In the studies, fRe is plotted as a function of Re or a Deborah number, De. It should be noted that fRe is equal to some constant, c. Therefore, for purely viscous flow, the plot should be a horizontal line. Onset of elasticity is marked by an increase in the friction factor or flow resistance from the horizontal line. This additional resistance is attributed to elastic effects. It is

understood that there may be concern that the increase in flow resistance may not be solely due to elastic effects. It has been argued that the additional resistance could be due to inertial or a combination of both inertial and elastic effects (Pilitsis et al., 1991). With this in mind, it is recommended to assess the importance of elastic effects by normalizing the data against the predictions obtained for an inelastic fluid with a matching viscosity.

In this new study on the effects of elasticity, a friction factor, f, can be determined by using the Bruschke equation. Next, an appropriate expression for the Reynolds number and the Deborah number needs to be determined. While it may be experimentally difficult because of the high viscosity of thermoplastics, it is recommended to use thermoplastics as the permeant and glass fibers for the reinforcement. A new experimental apparatus would have to be built. The apparatus would have to be capable of pumping the thermoplastics through the fiber bed and capable of measuring the pressure drop across the fiber bed. Some factors that should be investigated include porosity of the fiber bed and fiber arrangement in the bed.

The sixth and final recommendation deals with the shapes of fibers used in the fiber bed. In this research, cylindrical fibers were used. Furthermore, as discussed above, it was found that the Bruschke model predicted the penetration depth well for the random mat preform processing. As mentioned earlier, one possible reason for the good fit was the cylindrical shape of the fibers. It is possible that the shape of the fibers was the major factor in the agreement between experimental and theoretical data. To study the effect of fiber shape on the validity of the Bruschke model, it is recommended to perform permeation studies using textile fibers with different shapes. As with the earlier

recommendations, the same experimental procedure and apparatus could be used for these permeation experiments.

6.4 References

Chen et al., 1995: Chen, Y., Macosko, C., Davis, H., "Wetting of Fiber Mats for Composites Manufacturing: II. Air Entrapment Model", *AIChE Journal*, 1995, v 41, n 10, 2274-2281.

Chmielewski et al., 1990: Chmielewski, C., Petty, C., Jayaraman, K., "Crossflow of Elastic Liquids Through Arrays of Cylinders", Journal of Non-Newtonian Fluid Mechanics, 1990, v 35, p 309-325.

Dyakonova et al., 1996: Dyakonova, N., Odell, J., Brestkin, Y., Lyulin, A., Saez, A., "Macromolecular Strain in Periodic Models of Porous Media Flows", *Journal of Non-Newtonian Fluid Mechanics*, 1996, v 67, p 285-310.

Gebart, 1992: Gebart. B, "Permeability of Unidirectional Reinforcements for RTM", *Journal of Composite Materials*, 1992, v 26, n 8, p 1100-1133.

Georgiou et al., 1991: Georgiou, G., Momani, S., Crochet, M., Walters, K., "Newtonian and non-Newtonian Flow in a Channel Obstructed by an Antisymmetric Array of Cylinders", *Journal of Non-Newtonian Fluid Mechanics*, 1991, v 40, p 231-260.

Pilitsis et al., 1991: Pilitsis, S., Souvaliotis, A., Beris, A., "Viscoelastic Flow in a Periodically Constricted Tube: The Combined Effect of Inertia, Shear thinning, and Elasticity", *Journal of Rheology*, 1991, v 35, n 4, p 605-645.

Ranganathan et al., 1996: Ranganathan, S., Phelan, F., Advani, S., "A Generalized Model for the Transverse Fluid Permeability in Unidirectional Fibrous Media", *Polymer Composites*, 1996, v 17, n 2, p 222-230.

Sadiq et al., 1995: Sadiq, T., Advani, S., Parnas, R., "Experimental Investigation of Transverse Flow Through Aligned Cylinders", *Int. J. Multiphase Flow*, v 21, n5, p 755-774.

Skartsis et al., 1992: Skartsis, L, Khomami, B., Kardos, J., " Polymeric Flow Through Fibrous Media", *J. Rheol.*, 1992, v 36, n 4, p 589-620.

Zhang, 1999: Zhang, Y., "Manufacturing of Glass Mat Reinforced Thermoplastics From Carpet Waste", PhD Thesis, Georgia Institute of Technology, 1999.

APPENDIX A

REYNOLDS NUMBER AND CAPILLARY PRESSURE ESTIMATES

A.1 Reynolds Number

The Semi-empirical, Vijaysri, and Bruschke models were based on creeping flow. Therefore, it was essential to estimate Reynolds numbers. Equation A.1 was used to estimate the Reynolds numbers in this research (Tripathi and Chhabra, 1992). The estimated Reynolds numbers are shown in Table A.1.

$$R_e = \frac{\rho V_o^{2-n} (2R)^n}{m} \tag{A.1}$$

Where:

R_e	=	Reynolds number
ρ	=	density, kg/m^3
V_o	=	superficial velocity, m/s
R	=	fiber radius, m
m	=	power-law consistency, Pas^n
n	=	power-law flow index

Table A.1 Reynolds number estimates

Experiment*	R [m]	ρ [kg/m3]	V_o [m/s]	n	m Pas^n	Re
M13	125E-6	725	8E-6	0.65	13,400	3E-11
T20	3.5E-6	1160	1.9E-7	0.96	63	1E-11
C1	9E-6	725	1.5E-7	0.94	732	2E-12

*Note: Refer to the experimental design tables in Chapter IV for descriptions of these experiments.

A.2 Capillary Pressure

Equation A.2 was used to estimate the capillary pressures in this research (Ahn et al., 1991). The estimated capillary pressures are shown in Table A.2. A conservative value of 0° was used for the contact angle. The surface energies of most polymers are 0.030-0.045 Pa-m (Gutowski, 1997). The capillary pressure estimates in Table A.2 compare well the values obtained by Ahn et al. (1991).

$$P_c = \frac{2(1-\varepsilon)(\sigma \cos\theta)}{D_f \varepsilon} \qquad (A.2)$$

Where:

P_c = capillary pressure, Pa

ε = porosity of fiber bed

σ = surface tension of polymer, Pa-m

D_f = diameter of single fiber filament, m

Table A.2 Capillary pressure estimates

Experiment*	D_f [m]	σ [Pa-m]	θ [°]	ε	P_c [MPa]
M13	250E-6	0.045	0	0.58	0.00026
T20	7E-6	0.045	0	0.24	0.041
C1	18E-6	0.045	0	0.24	0.016

*Note: Refer to the experimental design tables in Chapter IV for descriptions of these experiments.

A.3 References

Ahn et al., 1991: Ahn, K., Seferis, J., Berg, J., "Simultaneous Measurements of Permeability and Capillary Pressure of Thermosetting Matrices in Woven Fabric Reinforcements", *Polymer Composites*, 1991, v 12, n 3, p 156-152.

Gutowski, 1997: Gutowski, T., *Advanced Composites Manufacturing*, John Wiley & Sons, Inc., New York, 1997, p 20.

Tripathi and Chhabra, 1992: Tripathi, A. and Chhabra R., "Slow Power Law Fluid Flow Relative to an Array of Infinite Cylinders", *Ind. Eng. Chem.*, 1992, v 31, p 2754-2759.

APPENDIX B

SHEAR RATE ESTIMATES

Equation 3.9 was used to estimate the shear rates in this research. Sample calculations are shown in Table B.1. The parameters in Equation 3.9 were discussed in Chapter III.

$$\dot{\gamma}_w = \frac{1+3n}{4n}\frac{K_o U}{r_h} \tag{3.9}$$

Table B.1 Shear rate estimates

Experiment*	n	U [m/s]	K_o	r_h [m]	$\dot{\gamma}_w$ [1/s]
M13	0.65	1.4E-5	2	8.6E-5	0.40
T20	0.96	7.9E-7	3	5.5E-7	4.4
C1	0.94	6.2E-7	2	1.4E-6	1.3

*Note: Refer to the experimental design tables in Chapter IV for descriptions of these experiments.

APPENDIX C

VIJAYSRI MODEL LOSS COEFFICIENTS

C.1 Introduction

In the Vijaysri model, the loss coefficient, Λ, was obtained from Vijaysri et al. (1999). The loss coefficient is equal to $C_D Re$, where C_D is the drag coefficient and Re is the Reynolds number. The loss coefficient is a function of porosity and power-law index and this can be represented as $\Lambda(\varepsilon, n)$. Vijaysri et al. (1999) presented a range of Λ values corresponding to various porosities and power-law flow indices. Their results are listed in Table C.1. Unfortunately, they did not present results at the exact porosity and power-law index values used in this research. Loss coefficients at the following porosities and power-law indices were needed for this research: $\Lambda(0.58, 0.65)$, $\Lambda(0.68, 0.65)$, $\Lambda(0.68, 0.71)$, $\Lambda(0.69, 0.65)$, $\Lambda(0.69, 0.71)$, $\Lambda(0.71,0.65)$, $\Lambda(0.71,0.71)$. To obtain these loss coefficients, the data from Vijaysri et al. (1999) was regressed. First, while holding power-law flow index constant, their loss coefficients were plotted as a function of porosity. Using Excel®, the graphs were regressed. These graphs, along with the equations obtain from the regression, are shown in Figures C.1-C.5. Next, the equations from the regression were used to calculate new loss coefficients, $\Lambda(\varepsilon^*, n)$, where ε^* refers to the porosity values in this research. Next, while holding ε^* constant, the new loss coefficients were plotted as a function of n. These graphs are shown in Tables C.6-C.9. The curves in these graphs were regressed using Excel®. The resulting equations from the

regression were used to calculate the loss coefficients at the conditions in this research. The loss coefficients from this regression are referred to as $\Lambda(\varepsilon^*, n^*)$, where ε^* and n^* are the porosities and power-law flow indices in this research.

While it is understood that extrapolation can be dangerous, the values of porosities and power-law indices in this research fall well within the range of porosities and power-law indices reported by the authors. The new loss coefficients are shown in Table C1. In comparison with the original data, the new coefficients appear to be qualitatively correct.

Table C.1: Loss coefficient, Λ, results from Vijaysri et al., (1999). The starred Λ are the results from regression of the original data. The parameters n, ε, and ε* are the power-law flow index, porosity used by Vijaysri, et al., (1999), and the porosities of this research, respectively.

Original Data			New Data		
n	ε	Λ	n	ε*	Λ*
1	0.4	1629.7	1	0.58	404.30
1	0.5	736.86	0.9	0.58	317.44
1	0.7	193.99	0.8	0.58	260.73
1	0.8	102.66	0.5	0.58	99.87
1	0.9	50.37	0.6	0.58	141.26
			0.65*	0.58	171.57
0.9	0.4	1123.12			
0.9	0.5	541.11	1	0.68	217.08
0.9	0.7	163.46	0.9	0.68	181.31
0.9	0.8	88.94	0.8	0.68	148.14
0.9	0.9	47.24	0.5	0.68	67.16
			0.6	0.68	90.14
0.8	0.4	743.65	0.71*	0.68	120.48
0.8	0.5	416.26	0.65*	0.68	103.39
0.8	0.7	132.17			
0.8	0.8	77.13	1	0.69	205.16
0.8	0.9	43.2	0.9	0.69	171.94
			0.8	0.69	140.28
0.6	0.4	350.35	0.5	0.69	64.64
0.6	0.5	208.35	0.6	0.69	86.29
0.6	0.7	82.53	0.71*	0.69	114.23
0.6	0.8	53.03	0.65*	0.69	98.44
0.6	0.9	35.37			
			1	0.71	183.23
0.5	0.4	235.21	0.9	0.71	154.43
0.5	0.5	142.57	0.8	0.71	125.91
0.5	0.7	62.17	0.5	0.71	59.87
0.5	0.8	42.16	0.6	0.71	79.09
0.5	0.9	30.72	0.71*	0.71	102.91
			0.65*	0.71	89.38

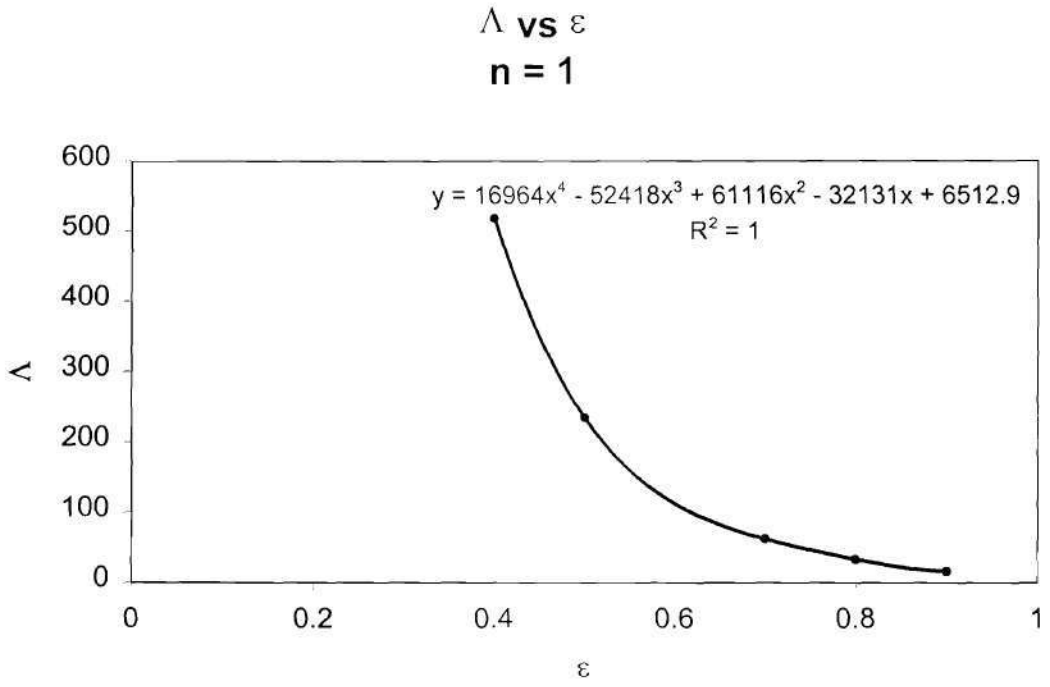

Figure C.1: Plot of Λ from Vijaysri et al., (1999) versus porosity. The power-law flow index is 1.

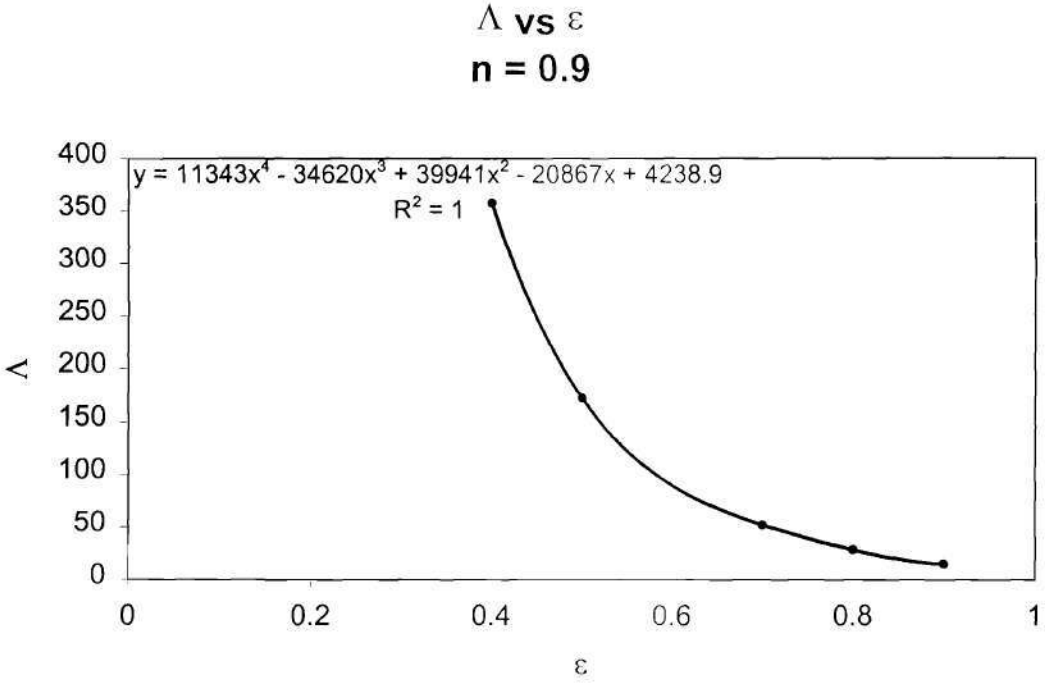

Figure C.2: Plot of Λ from Vijaysri et al., (1999) versus porosity. The power-law flow index is 0.9.

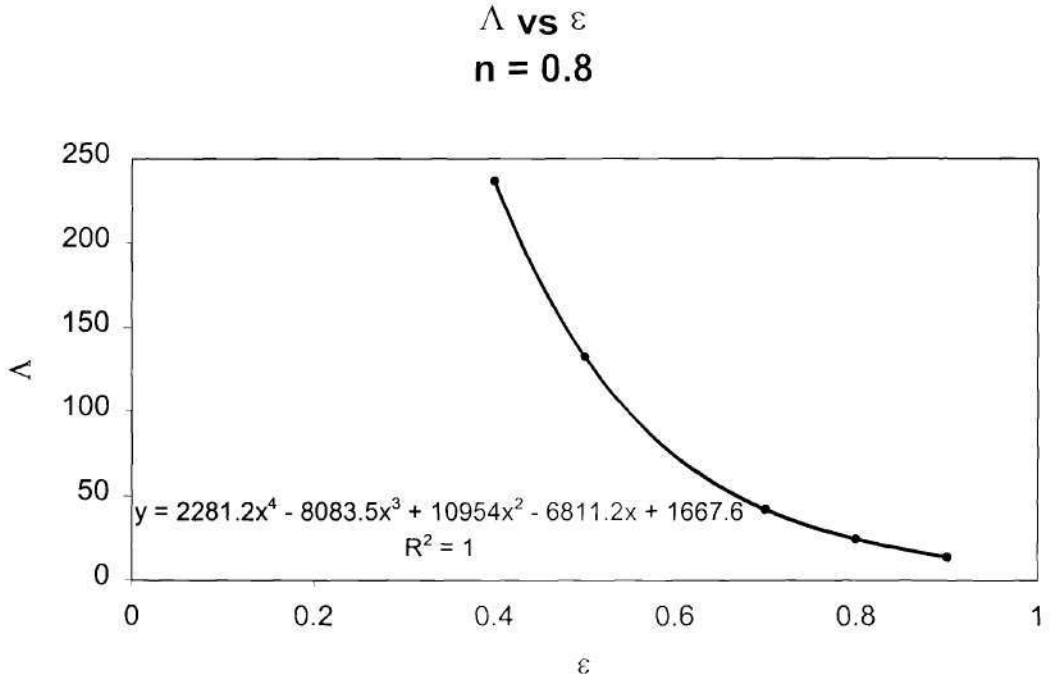

Figure C.3: Plot of Λ from Vijaysri et al., (1999) versus porosity. The power-law flow index is 0.8

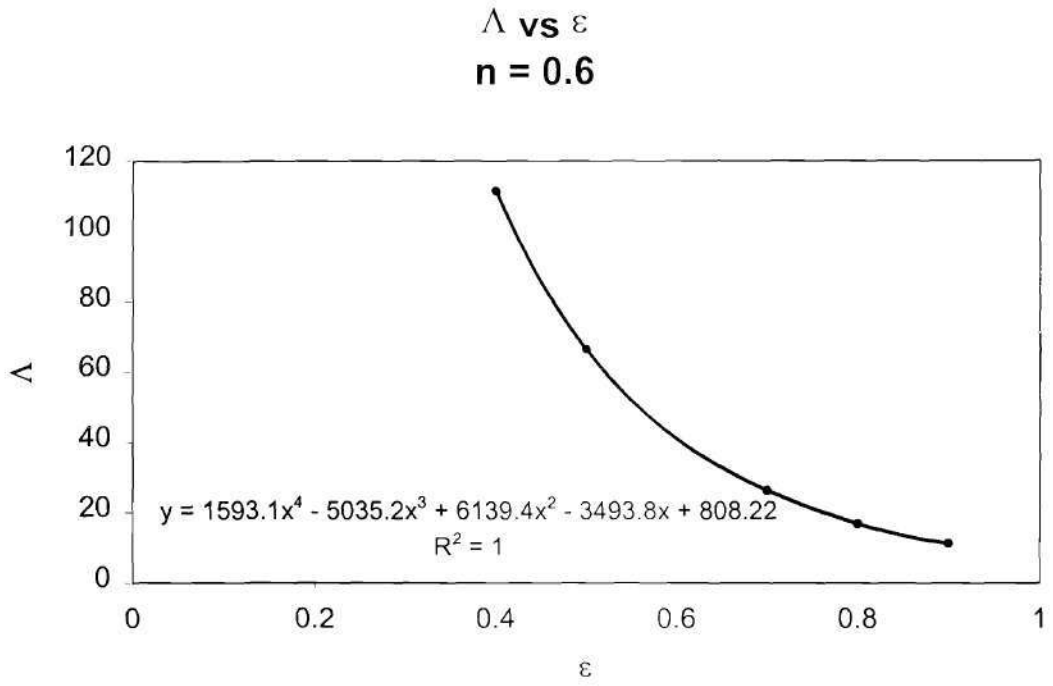

Figure C.4: Plot of Λ from Vijaysri et al., (1999) versus porosity. The power-law flow index is 0.6

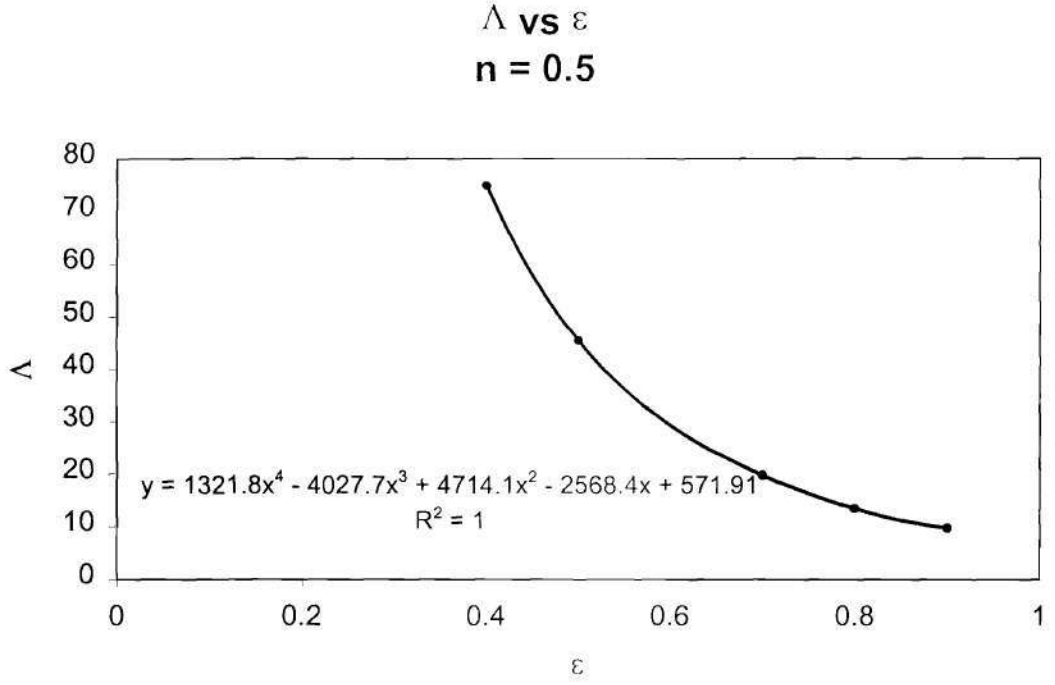

Figure C.5: Plot of Λ from Vijaysri et al., (1999) versus porosity. The power-law flow index is 0.5.

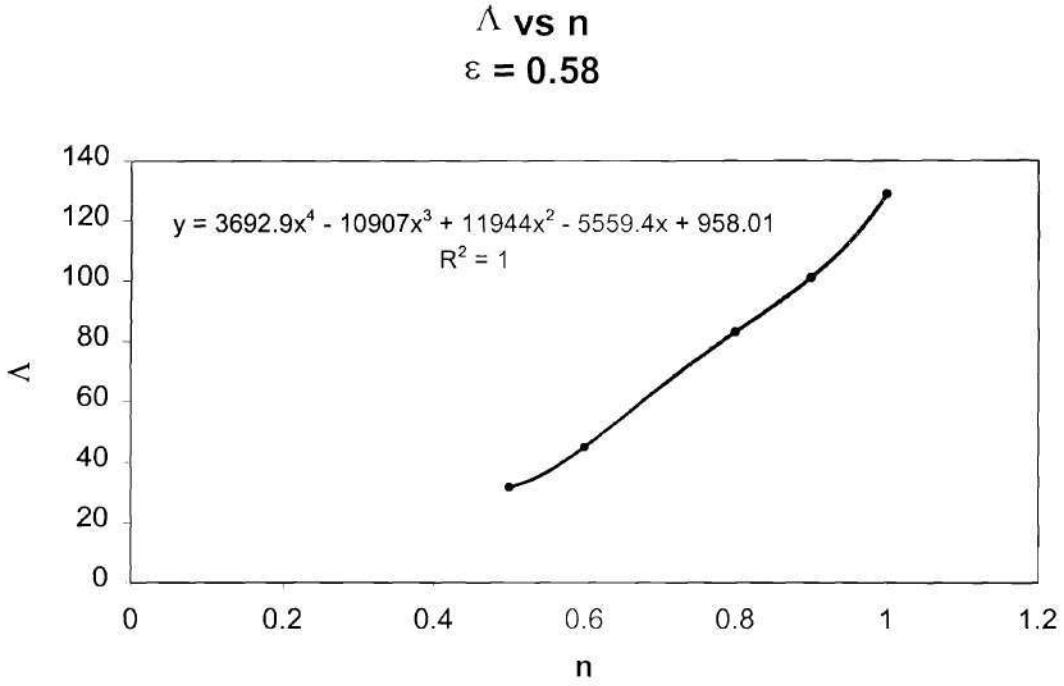

Figure C.6: Plot of Λ versus n. The porosity is 0.58.

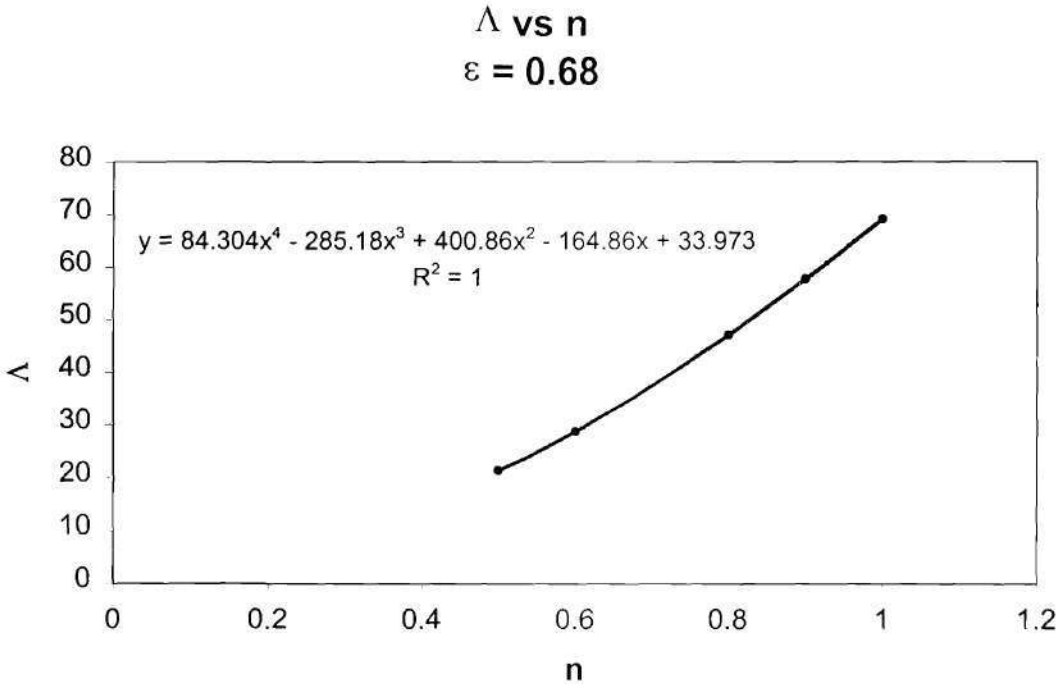

Figure C.7: Plot of Λ versus n. The porosity is 0.68.

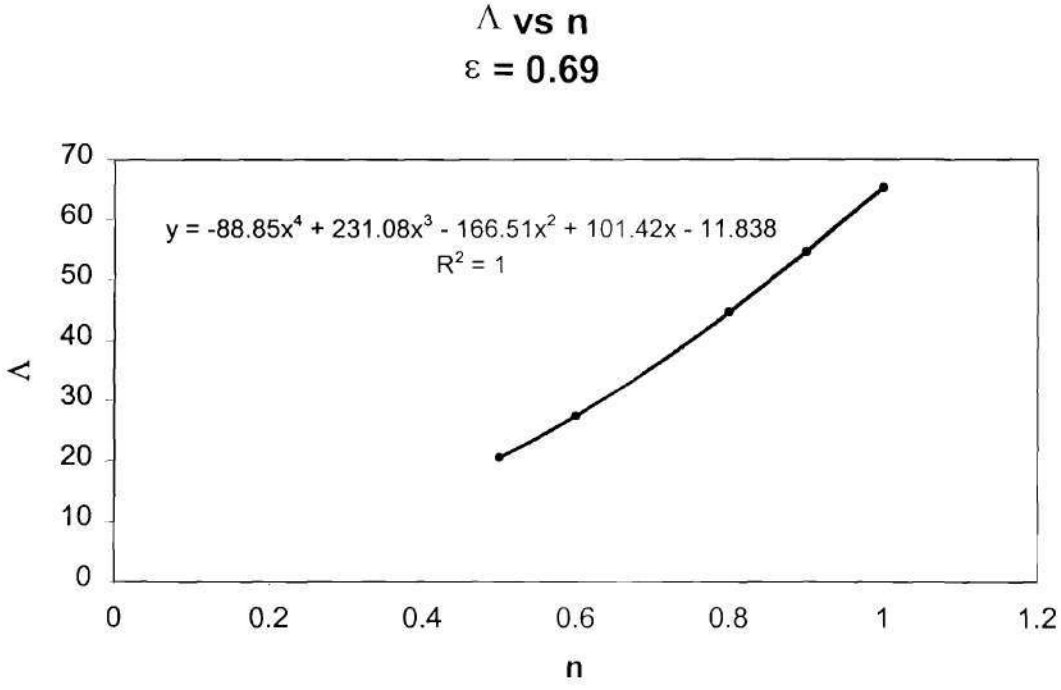

Figure C.8: Plot of Λ versus n. The porosity is 0.69.

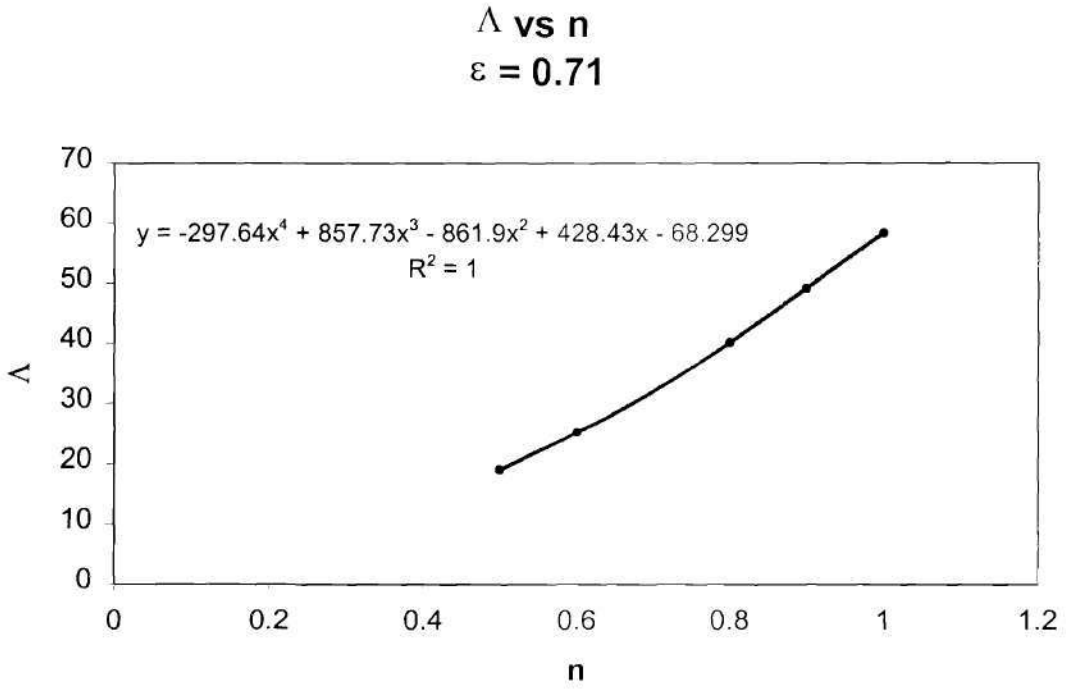

Figure C.9: Plot of Λ versus n. The porosity is 0.71.

C.2 Reference

Vijaysri et al., 1999: Vijaysri, M, Chhabra, R., Eswaran, V., "Power-law Fluid Flow Across an array of Infinite Circular Cylinders: A Numerical Study", *J. Non-Newtonian Fluid Mech.*, 1999, v 87, p 263-282.

APPENDIX D

SAS OUTPUT FOR KOZENY CONSTANT FROM MAT PREFORM PERMEATION

As discussed in Chapter V, SAS was used to non-linearly regress the experimental permeation data to obtain the tortuosity, K_1, which in turn was inserted into Equation 3.6 to calculate the Kozeny constant, K. The NLIN procedure in SAS was used to regress the data. This procedure fits nonlinear regression models using the least squares method. In this case, the nonlinear model was the Semi-empirical equation. Tables D.1-D.14 are the SAS output for each experimental condition for the mat preforms. Referring to Table D.1, the ratio of the regression's sum of square errors to the uncorrected total's sum of square errors is an indication of the fit of the data to the equation being regressed. This ratio is called the coefficient of determination or R^2. R^2 takes a value of between zero and one, with one indicating a good fit. As shown from the ratios in Tables D.1-D.14, the R^2 values are greater than 0.9. The experiments M1-M14 were described in Table 4.4.

Table D.1: SAS output for experiment M1

Non-Linear Least Squares Summary Statistics Dependent Variable X

Source	DF	Sum of Squares	Mean Square
Regression	1	0.00009394015	0.00009394015
Residual	286	0.00000010586	0.00000000037
Uncorrected Total	287	0.00009404601	
(Corrected Total)	286	0.00000938742	

Parameter	Estimate	Asymptotic Std. Error	Asymptotic 95 % Confidence Interval	
			Lower	Upper
K_1	1.974869686	0.00392011106	1.9671536541	1.9825857188

Table D.2: SAS output for experiment M2

Non-Linear Least Squares Summary Statistics Dependent Variable X

Source	DF	Sum of Squares	Mean Square
Regression	1	0.00010908910	0.00010908910
Residual	254	0.00000003025	0.00000000012
Uncorrected Total	255	0.00010911936	
(Corrected Total)	254	0.00000961592	

Parameter	Estimate	Asymptotic Std. Error	Asymptotic 95 % Confidence Interval	
			Lower	Upper
K_1	1.963595361	0.00205176015	1.9595546800	1.9676360421

Table D.3: SAS output for experiment M3

Non-Linear Least Squares Summary Statistics Dependent Variable X

Source	DF	Sum of Squares	Mean Square
Regression	1	0.00012837144	0.00012837144
Residual	263	0.00000007146	0.00000000027
Uncorrected Total	264	0.00012844290	
(Corrected Total)	263	0.00000905567	

Parameter	Estimate	Asymptotic Std. Error	Asymptotic 95 % Confidence Interval	
			Lower	Upper
K_1	2.037151756	0.00296372159	2.0313160377	2.0429874743

Table D.4: SAS output for experiment M4

Non-Linear Least Squares Summary Statistics Dependent Variable X

Source	DF	Sum of Squares	Mean Square
Regression	1	0.00023099306	0.00023099306
Residual	294	0.00000003325	0.00000000011
Uncorrected Total	295	0.00023102631	
(Corrected Total)	294	0.00001987249	

Parameter	Estimate	Asymptotic Std. Error	Asymptotic 95 % Confidence Interval	
			Lower	Upper
K_1	1.976707807	0.00138312041	1.9739856983	1.9794299161

Table D.5: SAS output for experiment M5

Non-Linear Least Squares Summary Statistics Dependent Variable X

Source	DF	Sum of Squares	Mean Square
Regression	1	0.00008930524	0.00008930524
Residual	229	0.00000049862	0.00000000218
Uncorrected Total	230	0.00008980385	
(Corrected Total)	229	0.00000561338	

Parameter	Estimate	Asymptotic Std. Error	Asymptotic 95 % Confidence Interval	
			Lower	Upper
K_1	2.035626542	0.01005137449	2.0158212963	2.0554317867

Table D.6: SAS output for experiment M6

Non-Linear Least Squares Summary Statistics Dependent Variable X

Source	DF	Sum of Squares	Mean Square
Regression	1	0.00006508690	0.00006508690
Residual	251	0.00000017781	0.00000000071
Uncorrected Total	252	0.00006526471	
(Corrected Total)	251	0.00000454568	

Parameter	Estimate	Asymptotic Std. Error	Asymptotic 95 % Confidence Interval	
			Lower	Upper
K_1	2.030424913	0.00669856729	2.0172321813	2.0436176446

Table D.7: SAS output for experiment M7

Non-Linear Least Squares Summary Statistics Dependent Variable X

Source	DF	Sum of Squares	Mean Square
Regression	1	0.00001063551	0.00001063551
Residual	184	0.00000000299	0.00000000002
Uncorrected Total	185	0.00001063850	
(Corrected Total)	184	0.00000097436	

Parameter	Estimate	Asymptotic Std. Error	Asymptotic 95 % Confidence Interval Lower	Upper
K_1	1.978969505	0.00244467363	1.9741462559	1.9837927540

Table D.8 SAS output for experiment M8

Non-Linear Least Squares Summary Statistics Dependent Variable X

Source	DF	Sum of Squares	Mean Square
Regression	1	0.00001501000	0.00001501000
Residual	180	0.00000001819	0.00000000010
Uncorrected Total	181	0.00001502818	
(Corrected Total)	180	0.00000149759	

Parameter	Estimate	Asymptotic Std. Error	Asymptotic 95 % Confidence Interval Lower	Upper
K_1	1.930733052	0.00500902415	1.9208489829	1.9406171204

Table D.9: SAS output for experiment M9

Non-Linear Least Squares Summary Statistics Dependent Variable X

Source	DF	Sum of Squares	Mean Square
Regression	1	0.00002074518	0.00002074518
Residual	182	0.00000003066	0.00000000017
Uncorrected Total	183	0.00002077584	
(Corrected Total)	182	0.00000218310	

Parameter	Estimate	Asymptotic Std. Error	Asymptotic 95 % Confidence Interval	
			Lower	Upper
K_1	1.927996694	0.00549437981	1.9171557011	1.9388376861

Table D10: SAS output for experiment M10

Non-Linear Least Squares Summary Statistics Dependent Variable X

Source	DF	Sum of Squares	Mean Square
Regression	1	0.00002871253	0.00002871253
Residual	186	0.00000003015	0.00000000016
Uncorrected Total	187	0.00002874268	
(Corrected Total)	186	0.00000278607	

Parameter	Estimate	Asymptotic Std. Error	Asymptotic 95 % Confidence Interval	
			Lower	Upper
K_1	1.968141464	0.00467619029	1.9589161727	1.9773667556

Table D.11 SAS output for experiment M11

Non-Linear Least Squares Summary Statistics Dependent Variable X

Source	DF	Sum of Squares	Mean Square
Regression	1	9.55355774E-6	9.55355774E-6
Residual	183	6.97851855E-9	3.8133981E-11
Uncorrected Total	184	9.56053626E-6	
(Corrected Total)	183	7.91951622E-7	

Parameter	Estimate	Asymptotic Std. Error	Asymptotic 95 % Confidence Interval	
			Lower	Upper
K_1	1.982938566	0.00396174288	1.9751219142	1.9907552184

Table D.12 SAS output for experiment M12

Non-Linear Least Squares Summary Statistics Dependent Variable X

Source	DF	Sum of Squares	Mean Square
Regression	1	0.00001656115	0.00001656115
Residual	178	0.00000002989	0.00000000017
Uncorrected Total	179	0.00001659104	
(Corrected Total)	178	0.00000119333	

Parameter	Estimate	Asymptotic Std. Error	Asymptotic 95 % Confidence Interval	
			Lower	Upper
K_1	1.976040319	0.00629205358	1.9636235663	1.9884570721

Table D.13: SAS output for experiment M13

Non-Linear Least Squares Summary Statistics Dependent Variable XE

Source	DF	Sum of Squares	Mean Square
Regression	1	0.00053356808	0.00053356808
Residual	187	0.00000054898	0.00000000294
Uncorrected Total	188	0.00053411706	
(Corrected Total)	187	0.00003588573	

Parameter	Estimate	Asymptotic Std. Error	Asymptotic 95 % Confidence Interval	
			Lower	Upper
K_1	1.998424081	0.00468757641	1.9891766498	2.0076715113

Table D.14: SAS output for experiment M14

Non-Linear Least Squares Summary Statistics Dependent Variable X

Source	DF	Sum of Squares	Mean Square
Regression	1	0.00076103596	0.00076103596
Residual	188	0.00000053005	0.00000000282
Uncorrected Total	189	0.00076156601	
(Corrected Total)	188	0.00007305744	

Parameter	Estimate	Asymptotic Std. Error	Asymptotic 95 % Confidence Interval	
			Lower	Upper
K_1	1.979082469	0.00380927026	1.9715679791	1.9865969581

APPENDIX E

ANOVA TABLES FOR KOZENY CONSTANT FROM MAT PREFORM PERMEATION

Minitab® was used to calculate ANOVA tables on the Kozeny constant. The factors were polymer, temperature, pressure, fiber, and porosity. The results are shown in Tables E.1-E.3.

Table E.1: Minitab® output of the ANOVA on the Kozeny constants from mat preform processing. The factor is porosity.

ANOVA: kozeny constant versus porosity

```
Factor     Type Levels Values
porosity   fixed      4  0.58  0.68  0.69  0.71

Analysis of Variance for kozeny c

Source      DF         SS         MS       F      P
porosity     3    0.33690    0.11230    1.74  0.222
Error       10    0.64470    0.06447
Total       13    0.98160
```

Table E.2: Minitab® output of the ANOVA on the Kozeny constants from mat preform processing. The factors are polymer and temperature.

ANOVA: kozeny constant versus polymer

```
Factor      Type Levels Values
polymer    fixed      2      1      2


Analysis of Variance for kozeny c

Source       DF         SS         MS        F      P
polymer       1    0.20284    0.20284     3.13  0.102
Error        12    0.77875    0.06490
Total        13    0.98160
```

ANOVA: kozeny constant versus temperature

```
Factor      Type Levels Values
temperat   fixed      3   170   190   230


Analysis of Variance for kozeny c

Source       DF         SS         MS        F      P
temperat      2    0.26672    0.13336     2.05  0.175
Error        11    0.71488    0.06499
Total        13    0.98160
```

Table E.3: Minitab® output of the ANOVA on the Kozeny constant for factors of pressure and fiber

ANOVA: kozeny constant versus pressure

```
Factor      Type Levels Values
pressure   fixed      3  0.34  1.38  2.76


Analysis of Variance for kozeny c

Source       DF         SS         MS       F      P
pressure      2    0.03162    0.01581    0.18  0.835
Error        11    0.94998    0.08636
Total        13    0.98160
```

ANOVA: kozeny constant versus fiber

```
Factor      Type Levels Values
fiber      fixed      3      1      2      3


Analysis of Variance for kozeny c

Source       DF         SS         MS       F      P
fiber         2    0.33569    0.16785    2.86  0.100
Error        11    0.64591    0.05872
Total        13    0.98160
```

APPENDIX F

RAW PERMEATION DATA FROM MAT PREFORM PROCESSING

The raw permeation data for the mat preform processing are located in Table F.1-F.14 on the following pages. In the tables, t is time and X is penetration depth. Refer to Table 4.4 for explanations of the experimental conditions M1-M14.

Table F.1: Raw permeation data for experiment M1. The standard deviation is ~70 μm.

t [s]	X [μm]	t [s]	X [μm]	t [s]	X [μm]	t [s]	X [μm]	t [s]	X [μm]	t [s]	X [μm]	t [s]	X [μm]	t [s]	X [μm]
0	0	42	303	84	408	126	485	168	557	209	612	252	664	294	715
1	44	43	306	86	409	127	488	169	558	212	613	253	665	295	715
2	71	45	308	87	410	128	487	170	559	213	614	255	666	296	716
3	89	46	310	88	411	130	501	172	560	214	615	256	679	297	716
5	96	47	311	89	426	131	502	174	561	215	616	257	680	299	717
7	114	49	313	90	426	132	503	175	562	216	629	258	681	300	731
8	133	50	328	91	429	133	505	176	563	218	630	259	682	301	732
9	138	51	330	93	430	135	506	177	564	219	631	260	683	303	732
10	143	52	331	94	431	137	506	178	577	220	632	262	683	304	733
12	160	53	333	96	432	138	507	179	578	221	632	264	684	306	734
13	165	54	334	97	434	139	508	181	579	222	633	265	685	307	734
14	182	56	335	98	435	140	509	182	580	223	634	266	686	308	735
15	185	57	338	100	436	141	510	183	581	226	635	267	687	309	736
16	188	59	353	101	436	142	511	184	582	227	636	269	687	310	737
17	205	60	355	102	439	144	512	186	583	228	637	270	688	311	737
20	208	61	355	103	453	145	526	188	584	229	637	271	689	313	738
21	211	63	358	104	454	147	527	189	585	230	639	272	690	314	739
22	215	64	359	105	455	148	528	190	586	231	639	273	690	316	739
23	230	65	361	106	455	149	530	191	586	233	640	274	691	317	740
24	233	66	363	109	457	150	530	192	587	234	654	277	692	318	741
25	236	67	364	110	458	152	531	193	588	235	655	278	705	319	741
27	238	68	378	111	459	153	533	194	589	237	655	279	706	321	742
28	241	69	380	112	460	154	533	196	603	238	656	280	707	322	743
29	256	72	381	113	462	155	534	197	604	240	657	281	707	323	743
31	258	73	383	115	463	156	535	199	604	241	657	282	709	324	744
32	260	74	384	116	476	157	536	200	605	242	658	284	709	325	757
34	264	75	385	117	477	160	538	201	606	243	659	285	710	326	758
35	279	76	388	118	480	161	539	203	607	244	660	286	710	329	758
36	280	78	388	119	481	162	552	204	608	245	660	287	711	330	760
37	283	79	402	120	481	163	553	205	609	247	661	289	712		
38	285	80	404	123	482	164	554	206	610	248	662	291	712		
39	287	81	405	124	483	166	555	207	611	249	663	292	714		
41	288	83	405	125	484	167	556	208	612	251	664	293	714		

Table F.2: Raw permeation data for experiment M2. The standard deviation is ~3 μm.

t [s]	X [mm]	t [s]	X [mm]	t [s]	X [mm]	t [s]	X [mm]	t [s]	X [mm]	t [s]	X [mm]	t [s]	X [mm]
0	0	52	410	102	540	150	633	198	712	247	783	295	847
1	60	53	414	103	541	152	634	199	715	248	785	296	849
3	91	54	417	104	545	153	637	200	717	249	786	297	850
5	122	56	421	105	547	154	639	203	718	250	787	299	852
6	144	58	424	106	551	155	641	204	720	251	790	300	854
7	162	59	429	108	553	156	643	205	723	253	792	301	855
8	179	60	433	109	555	157	646	206	725	255	794	302	857
9	193	61	437	110	558	159	648	207	726	256	795	304	858
10	206	63	441	111	560	160	650	208	728	257	797	306	860
12	219	64	446	113	562	161	653	209	730	258	799	307	862
13	228	65	448	115	565	163	654	211	732	259	801	308	863
14	240	67	454	116	569	164	657	212	734	260	802	309	865
16	249	68	457	117	570	166	659	214	736	262	804	310	866
17	258	69	461	118	573	167	661	215	737	263	806	311	867
19	267	71	464	119	575	168	664	216	739	264	808	313	869
20	276	72	467	120	578	169	665	218	742	266	810	314	872
21	282	73	470	122	581	170	667	219	743	267	811	315	873
22	291	74	475	123	584	171	670	220	746	269	813	317	874
23	297	75	477	125	586	172	672	221	747	270	816	318	876
24	304	78	480	126	588	174	675	222	748	271	816	319	878
25	311	79	484	127	590	176	676	223	750	272	818	321	878
27	317	80	486	128	593	177	678	225	752	273	820	322	880
29	324	81	491	130	597	178	680	227	754	274	822	323	882
30	329	82	494	131	597	179	682	228	757	275	823	324	883
32	337	83	496	132	601	181	684	229	758	277	825	325	885
34	343	84	500	133	602	182	686	230	760	279	826	326	886
35	347	86	502	134	605	183	688	231	762	280	828	328	888
36	354	87	506	135	607	184	691	233	763	281	830		
37	358	88	509	138	611	185	693	234	766	282	831		
38	364	90	512	139	613	186	694	235	767	284	833		
41	369	91	514	140	615	189	697	236	769	285	835		
42	375	93	516	141	617	190	698	237	771	286	836		
43	379	94	521	142	619	191	701	238	772	287	838		
44	386	95	523	144	621	192	703	241	774	288	839		
46	391	96	527	145	623	193	704	242	776	289	842		
47	396	97	530	146	625	194	707	243	778	292	843		
49	399	98	533	147	627	196	709	244	779	293	844		
50	404	100	536	149	630	197	711	245	781	294	846		

Table F.3 Raw permeation data for experiment M3. The standard deviation is ~3 μm.

t [s]	X [μm]	t [s]	X [μm]	t [s]	X [μm]	t [s]	X [μm]	t [s]	X [μm]	t [s]	X [μm]	t [s]	X [μm]
0	0	51	470	102	593	153	687	204	763	255	828	306	888
1	79	52	473	103	596	154	688	205	765	256	830	307	889
2	142	53	479	104	599	155	690	206	766	257	831	309	891
3	183	54	480	105	601	156	691	207	767	259	833	310	892
6	208	56	485	106	604	157	695	208	769	260	835	311	894
7	230	58	488	108	607	160	696	211	770	262	836	312	895
8	248	59	491	110	609	161	700	212	772	263	838	314	896
9	264	60	496	111	611	162	700	213	774	264	839	315	897
10	277	61	498	112	614	163	702	214	775	265	841	316	900
12	290	62	502	113	615	164	704	215	779	266	842	317	900
13	299	64	506	115	620	166	705	216	778	267	843	318	902
14	311	65	509	116	621	167	710	218	781	269	845	319	904
15	318	66	513	117	625	168	710	219	782	270	846	322	904
16	327	67	518	118	626	169	713	220	784	272	848	323	906
19	334	68	519	119	629	171	716	222	785	273	850	324	907
20	342	69	525	122	631	172	716	223	788	274	852	325	908
21	349	72	524	123	633	174	718	225	789	275	853	326	910
22	356	73	529	124	636	175	720	226	792	277	854	328	911
23	364	74	530	125	637	176	721	227	793	278	856	329	913
24	371	75	535	126	640	177	724	228	795	279	858	330	914
25	376	76	537	127	642	178	725	229	795	280	859		
27	383	78	540	128	644	179	728	230	798	281	861		
28	387	79	546	130	646	181	731	231	798	282	862		
29	394	80	546	131	649	182	732	234	800	285	863		
31	398	81	551	132	652	184	733	235	801	286	865		
32	405	82	552	133	655	185	735	236	803	287	866		
34	410	84	556	135	658	186	736	237	804	288	868		
35	416	86	559	137	658	187	739	238	807	289	870		
36	421	87	560	138	661	189	741	240	808	291	870		
37	425	88	565	139	662	190	741	241	810	292	872		
38	429	89	565	140	664	191	744	242	812	293	873		
39	432	90	569	141	667	192	745	243	814	294	875		
41	437	91	572	142	669	193	748	244	815	296	877		
42	440	93	573	144	670	194	748	247	817	297	878		
44	448	94	578	145	673	197	752	248	819	299	879		
45	450	95	579	146	676	198	754	249	820	300	881		
46	456	96	583	148	677	199	755	250	822	301	882		
47	458	98	586	149	680	200	757	251	824	302	883		

Table F.4: Raw permeation data for experiment M4. The standard deviation is ~4 μm.

t [s]	X [μm]	t [s]	X [μm]	t [s]	X [μm]	t [s]	X [μm]	t [s]	X [μm]	t [s]	X [μm]	t [s]	X [μm]
0	0	51	533	102	711	153	838	204	940	255	1016	306	1092
1	76	52	533	103	711	154	838	205	940	256	1016	307	1092
2	114	53	546	104	711	155	838	206	940	257	1016	308	1092
3	152	54	559	105	711	156	838	207	940	258	1016	310	1092
5	178	56	559	106	711	157	838	208	940	259	1016	311	1092
6	203	57	559	109	724	159	838	211	940	262	1029	313	1105
8	229	59	559	110	737	161	838	212	940	263	1029	314	1105
9	241	60	572	111	737	162	838	213	940	264	1029	315	1105
10	254	61	584	112	737	163	851	214	940	265	1041	316	1118
12	267	63	584	113	737	164	864	215	953	266	1041	317	1118
13	292	64	584	115	737	166	864	216	953	267	1041	318	1118
14	305	65	584	116	737	167	864	218	965	269	1041	319	1118
15	318	66	597	117	749	168	864	219	965	270	1041	321	1118
16	330	67	597	118	749	169	864	220	965	272	1041	323	1118
17	343	68	610	119	762	170	864	221	965	273	1041	324	1118
19	343	69	610	122	762	171	864	223	965	274	1041	325	1118
21	356	72	610	123	762	172	864	225	965	275	1041	326	1118
22	368	73	610	124	762	175	864	226	965	277	1041	328	1118
23	381	74	622	125	762	176	876	227	965	278	1054	329	1130
24	394	75	622	126	762	177	889	228	965	279	1054	330	1130
25	394	76	635	127	762	178	889	229	978	280	1067		
27	406	78	635	128	775	179	889	230	978	281	1067		
28	419	79	635	130	787	181	889	231	991	282	1067		
29	419	80	635	131	787	182	889	233	991	285	1067		
30	432	81	648	132	787	183	889	234	991	286	1067		
31	445	82	648	134	787	184	889	236	991	287	1067		
32	445	84	660	135	787	186	889	237	991	288	1067		
35	457	86	660	137	787	187	902	238	991	289	1067		
36	457	87	660	138	787	189	902	240	991	291	1067		
37	470	88	660	139	787	190	914	241	991	292	1067		
38	470	89	660	140	813	191	914	242	991	293	1067		
39	483	90	673	141	813	192	914	243	991	294	1080		
41	483	91	686	142	813	193	914	244	1003	295	1080		
42	495	93	686	144	813	194	914	245	1003	297	1092		
43	495	94	686	145	813	196	914	248	1016	299	1092		
44	508	96	686	147	813	198	914	249	1016	300	1092		
45	508	97	686	148	813	199	914	250	1016	301	1092		
47	508	98	686	149	813	200	914	251	1016	302	1092		

Table F.5: Raw permeation data for experiment M5. The standard deviation is ~62 μm.

t [s]	X [μm]	t [s]	X [μm]	t [s]	X [μm]	t [s]	X [μm]	t [s]	X [μm]	t [s]	X [μm]	t [s]	X [μm]
0	0	49	343	97	419	146	483	193	546	242	610	291	673
1	89	50	343	98	419	147	483	194	546	244	610	292	673
3	152	51	356	100	432	148	483	197	546	245	610	294	673
5	191	52	356	101	432	149	483	198	546	247	610	295	673
6	203	53	356	102	419	150	483	199	546	248	610	296	673
7	216	56	356	103	432	152	483	200	546	249	610	297	673
8	229	57	356	104	432	153	495	201	546	250	610	299	673
9	229	58	368	106	432	154	495	203	546	251	610	300	686
10	241	59	368	108	432	155	495	204	546	252	610	301	686
12	254	60	368	109	432	157	495	206	559	253	610	302	686
13	254	61	368	110	432	159	495	207	559	255	622	303	686
14	254	62	368	111	432	160	495	208	559	257	622	306	686
16	267	64	381	112	432	161	495	209	559	258	622	307	686
17	267	65	381	113	445	162	495	211	559	259	622	308	686
19	279	66	381	115	445	163	495	212	559	260	622	309	699
20	279	68	381	116	445	164	495	213	559	262	622	310	699
21	292	69	381	117	445	166	495	214	559	263	635	311	699
22	292	71	381	119	445	167	508	215	572	264	635	313	699
23	292	72	381	120	445	168	508	216	572	265	635	314	711
24	292	73	381	122	457	170	508	218	572	266	635	315	711
25	292	74	381	123	457	171	521	220	572	269	635	316	711
27	292	75	381	124	457	172	521	221	572	270	635	317	711
28	305	76	394	125	457	174	521	222	572	271	648	319	711
30	318	78	394	126	457	175	521	223	584	272	648	321	711
31	318	80	394	127	457	176	521	225	584	273	648	322	711
32	318	81	394	128	457	177	521	226	584	274	648	323	711
34	318	82	406	131	457	178	521	227	584	275	648	324	711
35	318	83	406	132	457	179	521	228	584	277	648	325	711
36	318	84	406	133	470	181	521	229	584	278	648	326	711
37	318	86	406	134	470	183	521	231	584	279	648	328	724
38	330	87	406	135	470	184	521	233	584	280	648	329	737
39	330	88	406	137	470	185	521	234	584	282	648		
41	343	89	406	138	470	186	521	235	584	284	648		
43	343	90	406	139	470	188	521	236	584	285	660		
44	343	93	406	140	470	189	533	237	584	286	673		
45	343	94	419	141	470	190	533	238	584	287	673		
46	343	95	419	142	470	191	533	240	610	288	673		
47	343	96	419	145	483	192	546	241	610	289	673		

Table F.6: Raw permeation data for experiment M6. The standard deviation is ~11 μm.

t [s]	X [μm]	t [s]	X [μm]	t [s]	X [μm]	t [s]	X [μm]	t [s]	X [μm]	t [s]	X [μm]	t [s]	X [μm]
0	0	49	445	100	533	149	610	198	699	249	787	307	876
1	203	50	445	101	533	150	610	199	699	250	787	308	889
2	229	52	445	102	533	152	610	201	699	251	800	309	889
3	292	53	457	103	533	153	610	203	699	252	800	310	889
5	292	54	457	104	533	154	622	204	699	253	800	311	902
6	318	56	457	106	533	155	622	205	699	255	800	314	902
7	318	57	470	108	533	156	622	206	711	257	800	315	902
8	343	59	470	109	533	157	622	207	711	258	800	316	902
9	343	60	470	110	546	160	635	208	724	259	800	317	902
10	343	61	470	111	559	161	635	209	724	260	800	318	902
13	368	62	470	112	559	162	635	211	724	262	813	319	914
14	368	64	470	113	559	163	635	213	724	263	813	321	914
15	368	65	470	115	559	164	635	214	724	264	826	322	914
16	368	66	470	116	559	166	635	215	724	265	826	323	914
17	368	67	483	117	559	167	635	216	724	266	826	325	914
19	381	69	483	118	559	168	648	218	724	269	826	326	927
20	394	71	483	120	559	169	648	219	737	270	826	328	927
21	394	72	483	122	559	170	648	220	737	271	826	329	927
22	394	73	483	123	559	171	648	221	737	272	826	330	927
23	394	74	495	124	572	174	648	222	749	273	826		
25	394	75	495	125	572	175	660	223	749	274	826		
27	394	76	495	126	584	176	660	225	749	275	838		
28	406	78	495	127	584	177	660	227	749	277	851		
29	419	79	495	128	584	178	660	228	749	278	851		
30	419	80	495	130	584	179	660	229	749	280	851		
31	419	82	508	131	584	181	660	230	749	281	851		
32	419	83	508	132	584	182	673	231	749	282	851		
34	419	84	508	134	584	183	673	233	762	284	851		
35	419	86	508	135	584	184	673	234	762	285	851		
36	419	87	508	137	584	185	673	235	762	286	851		
38	419	88	508	138	584	188	673	236	775	287	864		
39	432	89	508	139	597	189	673	237	775	288	864		
41	445	90	508	140	597	190	673	240	775	289	864		
42	445	91	521	141	597	191	686	241	775	291	876		
43	445	94	521	142	597	192	686	242	775	292	876		
44	445	95	521	144	597	193	686	243	775	302	876		
45	445	96	533	145	610	194	686	244	775	303	876		
46	445	97	533	146	610	196	699	245	775	304	876		

Table F.7: Raw permeation data for experiment M7. The standard deviation is ~20 μm.

t [s]	X [μm]	t [s]	X [μm]	t [s]	X [μm]	t [s]	X [μm]	t [s]	X [μm]
0	0	49	166	96	225	145	266	193	302
1	37	50	167	98	224	146	266	194	302
2	48	51	167	100	226	148	268	196	303
3	53	52	171	101	228	149	269	197	305
5	71	53	172	102	228	150	268	199	305
6	74	54	176	103	229	152	270	200	305
7	77	56	177	104	230	153	271	201	307
8	80	57	179	105	232	154	273	203	308
9	82	58	179	106	233	155	273	204	309
10	85	60	184	108	234	156	275	205	308
13	99	61	184	109	234	157	276	206	310
14	100	63	186	111	236	159	276	207	310
15	103	64	187	112	237	161	278	208	312
16	104	65	189	113	238	162	278	209	312
17	112	66	189	115	241	163	279	212	313
19	117	67	192	116	242	164	280	213	314
20	119	68	193	117	242	166	281	214	315
21	123	69	195	118	242	167	281	215	316
22	124	72	198	119	244	168	283	216	317
23	127	73	195	120	246	169	283	218	318
25	130	74	201	122	248	170	285	219	318
27	132	75	202	124	246	171	285	220	320
28	134	76	202	125	250	174	287	221	320
29	136	78	203	126	249	175	288	222	322
30	139	79	205	127	249	176	288	225	322
31	142	80	205	128	251	177	290	226	322
32	143	81	208	130	254	178	290	227	324
34	145	82	209	131	254	179	291	228	324
35	146	83	209	132	255	181	293	229	325
37	150	86	210	133	256	182	293	230	326
38	150	87	213	134	257	183	295	231	326
39	154	88	214	137	259	184	295	233	327
41	156	89	216	138	259	186	296	234	328
42	158	90	217	139	260	188	297	235	329
43	160	91	219	140	261	189	298	237	329
44	162	93	220	141	263	190	298	238	329
45	163	94	222	142	263	191	299	240	331
46	165	95	222	144	265	192	300		

Table F.8: Raw permeation data for experiment M8. The standard deviation is ~20 μm.

t [s]	X [μm]	t [s]	X [μm]	t [s]	X [μm]	t [s]	X [μm]	t [s]	X [μm]	t [s]	X [μm]
0	0	46	192	93	261	138	314	184	360	230	401
1	52	47	195	94	264	139	316	185	361	231	402
2	64	49	197	95	265	141	317	186	362	233	403
3	66	50	198	96	266	142	318	188	364	234	404
6	72	51	202	97	267	144	320	189	365		
7	80	52	203	98	269	145	321	191	366		
8	86	54	206	100	271	146	323	192	368		
9	92	56	207	101	272	147	324	193	369		
10	99	57	209	102	273	148	325	194	370		
12	104	58	210	104	275	149	327	196	371		
13	109	59	213	105	277	150	328	197	372		
14	114	60	216	106	278	153	329	198	373		
16	118	61	219	108	281	154	330	199	375		
17	122	63	219	109	282	155	332	200	376		
19	126	64	221	110	282	156	333	203	377		
20	131	65	224	111	283	157	334	204	378		
21	134	67	226	112	286	159	336	205	379		
22	138	68	228	113	286	160	337	206	380		
23	142	69	230	115	289	161	339	207	382		
24	144	71	231	117	291	162	339	208	382		
25	149	72	233	118	290	163	341	209	384		
27	151	73	235	119	293	166	342	211	384		
29	154	74	238	120	295	167	343	212	386		
30	157	75	238	122	296	168	344	214	387		
31	160	76	238	123	298	169	346	215	388		
32	162	79	243	124	299	170	346	216	389		
34	166	80	243	125	300	171	348	218	390		
35	169	81	246	126	301	172	350	219	391		
36	172	82	249	128	303	174	351	220	392		
37	173	83	248	130	305	175	352	221	393		
38	177	84	250	131	306	176	353	222	394		
39	179	86	253	132	308	178	354	223	396		
41	182	87	256	133	308	179	355	225	397		
43	183	88	256	134	310	181	357	226	398		
44	186	89	256	135	312	182	358	228	399		
45	188	91	260	137	314	183	359	229	400		

Table F.9: Raw permeation data for experiment M9. The standard deviation is ~4 μm.

t [s]	X [μm]	t [s]	X [μm]	t [s]	X [μm]	t [s]	X [μm]	t [s]	X [μm]	t [s]	X [μm]
0	0	47	224	95	312	142	372	190	423	237	464
1	27	49	226	97	313	144	374	191	425	238	466
2	44	50	230	98	315	146	378	192	425	240	466
3	54	51	233	100	318	147	378	193	427		
5	67	52	236	101	320	148	379	194	428		
6	78	54	238	102	320	149	381	197	431		
8	87	56	241	103	322	150	383	198	433		
9	92	57	245	104	326	152	383	199	432		
10	101	58	247	105	326	153	387	200	433		
12	106	59	250	106	328	154	386	201	434		
13	114	60	253	109	329	155	389	203	436		
14	119	63	257	110	332	156	389	204	437		
15	124	64	257	111	333	159	391	205	438		
16	131	65	261	112	336	160	393	206	438		
17	137	66	262	113	336	161	393	207	441		
19	142	67	266	115	340	162	396	209	441		
20	146	68	266	116	341	163	396	211	443		
22	151	69	271	117	342	164	399	212	443		
23	159	71	271	118	342	166	398	213	445		
24	161	73	274	120	346	167	400	214	446		
25	167	74	278	122	348	168	402	215	449		
27	170	75	278	123	347	169	404	216	447		
28	176	76	283	124	348	170	404	218	450		
29	179	78	283	125	353	172	404	219	452		
30	182	79	286	126	354	174	408	220	454		
31	185	80	289	127	355	175	409	221	453		
34	188	81	289	128	357	176	410	223	456		
35	194	82	291	130	359	177	410	225	455		
36	194	84	293	132	360	178	412	226	457		
37	199	86	295	133	361	179	414	227	457		
38	202	87	298	134	363	181	416	228	458		
39	208	88	299	135	365	182	415	229	459		
41	208	89	300	137	365	184	416	230	462		
42	213	90	304	138	368	185	418	231	461		
43	216	91	307	139	368	186	420	233	463		
44	220	93	307	140	371	188	419	234	462		
45	220	94	309	141	373	189	423	236	462		

Table F.10: Raw permeation data for experiment M10. The standard deviation is ~50 μm.

t [s]	X [μm]	t [s]	X [μm]	t [s]	X [μm]	t [s]	X [μm]	t [s]	X [μm]	t [s]	X [μm]
0	0	46	256	93	349	139	421	184	483	230	535
1	38	47	260	94	352	140	423	185	483	231	534
3	90	49	261	95	353	141	426	186	485	233	536
5	107	50	266	96	357	142	428	188	487	234	536
6	117	51	267	97	359	144	429	189	486	235	539
7	125	53	273	100	362	145	431	191	489	236	538
8	131	54	272	101	364	146	433	192	489	237	542
9	138	56	278	102	365	147	435	193	493		
10	146	57	280	103	368	148	437	194	494		
12	150	58	282	104	371	149	438	196	498		
14	158	59	286	105	372	150	440	197	498		
15	159	60	287	106	374	153	444	198	499		
16	165	61	291	108	377	154	444	199	500		
17	168	64	293	109	377	155	445	200	502		
19	173	65	297	110	380	156	447	201	504		
20	179	66	299	112	382	157	449	204	506		
21	182	67	303	113	384	159	450	205	507		
22	187	68	304	115	387	160	453	206	508		
23	193	69	309	116	388	161	454	207	509		
24	197	71	309	117	392	162	455	208	511		
27	201	72	312	118	393	163	458	209	511		
28	204	73	313	119	396	166	457	211	514		
29	208	75	316	120	397	167	461	212	515		
30	211	76	320	122	398	168	461	213	515		
31	217	78	322	123	401	169	465	214	518		
32	220	79	326	125	402	170	466	216	518		
34	224	80	326	126	404	171	468	218	521		
35	229	81	330	127	405	172	469	219	521		
36	230	82	331	128	407	174	470	220	522		
37	233	83	334	130	409	175	471	221	524		
39	235	84	337	131	412	176	472	222	526		
41	240	86	338	132	415	177	475	223	526		
42	242	88	342	133	417	179	477	225	529		
43	249	89	341	134	420	181	479	226	530		
44	250	90	345	135	420	182	479	227	532		
45	255	91	347	138	421	183	481	228	532		

Table F.11: Raw permeation data for experiment M11. The standard deviation is ~14 μm.

t [s]	X [μm]	t [s]	X [μm]	t [s]	X [μm]	t [s]	X [μm]	t [s]	X [μm]	t [s]	X [μm]
0	0	46	167	91	206	138	242	183	276	229	314
1	27	47	169	93	209	139	242	184	277	230	314
2	43	49	170	94	210	140	243	186	278	231	316
3	48	50	171	95	210	141	244	188	279	233	317
5	57	51	173	97	212	142	245	189	281	234	318
6	66	52	174	98	213	144	246	190	282	235	319
8	74	53	174	100	215	145	247	191	282	237	320
9	82	54	175	101	214	146	248	192	283	238	321
10	89	56	176	102	215	148	249	193	284	240	322
12	95	57	177	103	218	149	250	194	285		
13	100	59	180	104	218	150	251	196	286		
14	105	60	182	105	220	152	252	197	287		
15	110	61	182	106	220	153	253	199	288		
16	113	62	183	108	220	154	254	200	290		
17	118	64	185	110	221	155	255	201	291		
19	122	65	186	111	222	156	256	203	291		
21	124	66	188	112	223	157	256	204	293		
22	127	67	189	113	224	159	258	205	294		
23	130	68	189	115	225	161	258	206	295		
24	133	69	190	116	225	162	260	207	296		
25	137	72	191	117	226	163	261	208	296		
27	139	73	192	118	228	164	262	209	298		
28	141	74	194	119	230	166	263	212	299		
29	143	75	193	120	230	167	263	213	300		
30	145	76	195	123	229	168	264	214	301		
31	147	78	197	124	230	169	266	215	302		
34	149	79	198	125	232	170	267	216	303		
35	151	80	200	126	233	171	267	218	304		
36	153	81	200	127	235	174	268	219	305		
37	154	82	199	128	235	175	269	220	306		
38	157	84	201	130	236	176	270	221	307		
39	159	86	203	131	237	177	272	222	308		
41	160	87	204	132	237	178	272	225	309		
42	161	88	203	133	239	179	274	226	310		
43	163	89	204	135	241	181	274	227	311		
44	165	90	205	137	242	182	275	228	313		

Table F.12: Raw permeation data for experiment M12. The standard deviation is ~46 µm.

t [s]	X [µm]	t [s]	X [µm]	t [s]	X [µm]	t [s]	X [µm]	t [s]	X [µm]	t [s]	X [µm]
0	0	46	228	94	283	141	331	188	376	235	424
1	45	47	229	95	284	142	332	189	377	236	425
2	64	50	229	96	286	144	333	191	378		
3	102	51	231	97	288	145	334	192	380		
5	114	52	234	98	289	146	335	193	381		
6	132	53	235	101	290	147	338	194	383		
7	138	54	237	102	292	148	338	196	384		
8	144	56	239	103	293	149	338	197	385		
10	151	57	240	104	294	152	341	198	387		
12	154	58	242	105	296	153	342	199	388		
13	158	59	244	106	299	154	343	200	389		
14	163	60	245	108	299	155	344	203	391		
15	168	63	246	109	299	156	346	204	393		
16	170	64	249	110	301	157	346	205	394		
17	171	65	250	111	301	159	348	206	395		
19	174	66	253	113	303	160	351	207	396		
20	177	67	254	115	304	161	351	208	397		
21	181	68	257	116	306	162	352	209	398		
22	184	69	257	117	308	164	353	211	399		
24	187	71	258	118	310	166	355	212	400		
25	192	72	259	119	310	167	356	213	402		
27	194	73	260	120	311	168	356	215	404		
28	195	75	262	122	314	169	359	216	406		
29	197	76	263	123	314	170	361	218	406		
30	201	78	266	124	314	171	361	219	407		
31	203	79	267	126	317	172	362	220	409		
32	206	80	269	127	318	174	362	221	411		
34	209	81	271	128	318	175	365	222	411		
35	212	82	272	130	318	177	365	223	413		
37	213	83	273	131	320	178	365	225	415		
38	213	84	274	132	322	179	368	226	416		
39	214	86	276	133	325	181	370	228	418		
41	216	88	277	134	326	182	372	229	419		
42	219	89	278	135	328	183	372	230	420		
43	221	90	279	137	328	184	372	231	421		
44	223	91	279	138	327	185	374	233	424		
45	226	93	282	140	329	186	376	234	423		

Table F.13: Raw permeation data for experiment M13. The standard deviation is ~40 µm.

t [s]	X [µm]	t [s]	X [µm]	t [s]	X [µm]	t [s]	X [µm]	t [s]	X [µm]	t [s]	X [µm]
0	0	46	1221	93	1561	139	1817	184	2012	230	2165
1	307	47	1233	94	1568	140	1823	185	2016	231	2170
2	653	49	1241	95	1577	141	1828	186	2022	233	2172
5	681	50	1255	96	1585	142	1835	189	2026	234	2177
6	676	51	1266	98	1593	144	1841	190	2031	235	2180
7	714	52	1277	100	1601	145	1847	191	2035	236	2184
8	744	53	1286	101	1608	146	1853	192	2039	237	2188
9	772	56	1297	102	1616	147	1859	193	2044	240	2193
10	797	57	1309	103	1625	149	1865	194	2049		
12	821	58	1317	104	1631	150	1870	196	2053		
13	843	59	1328	105	1639	152	1877	197	2058		
14	861	60	1338	106	1647	153	1882	198	2062		
15	883	61	1348	108	1654	154	1887	200	2066		
17	900	62	1358	109	1661	155	1893	201	2070		
19	921	64	1368	111	1669	156	1899	203	2075		
20	939	65	1377	112	1676	157	1906	204	2079		
21	952	67	1387	113	1683	159	1910	205	2084		
22	973	68	1397	115	1690	160	1915	206	2088		
23	985	69	1406	116	1697	162	1921	207	2092		
24	1004	71	1415	117	1705	163	1926	208	2097		
25	1016	72	1424	118	1711	164	1933	209	2101		
27	1029	73	1434	119	1719	166	1937	211	2105		
28	1048	74	1442	120	1725	167	1942	213	2110		
30	1060	75	1452	122	1732	168	1948	214	2113		
31	1075	76	1461	124	1739	169	1954	215	2117		
32	1087	79	1469	125	1746	170	1959	216	2122		
34	1100	80	1477	126	1752	171	1963	218	2126		
35	1115	81	1486	127	1759	172	1967	219	2130		
36	1127	82	1495	128	1766	175	1973	220	2135		
37	1137	83	1503	130	1773	176	1978	221	2139		
38	1152	84	1511	131	1779	177	1983	222	2141		
39	1163	86	1521	132	1785	178	1989	223	2145		
41	1176	88	1528	133	1791	179	1992	226	2150		
43	1189	89	1537	134	1798	181	1998	227	2153		
44	1200	90	1544	135	1804	182	2002	228	2157		
45	1208	91	1553	138	1810	183	2007	229	2162		

Table F.14: Raw permeation data for experiment M14. The standard deviation is ~58 μm.

t [s]	X [μm]	t [s]	X [μm]	t [s]	X [μm]	t [s]	X [μm]	t [s]	X [μm]	t [s]	X [μm]
0	0	46	1325	93	1811	138	2175	184	2451	229	2672
1	267	47	1347	94	1829	139	2180	185	2468	231	2675
2	360	49	1356	95	1835	140	2184	186	2472	233	2678
5	450	50	1377	96	1840	141	2202	188	2475	234	2680
6	505	51	1385	97	1859	144	2205	189	2478	235	2696
7	558	52	1406	98	1865	145	2210	190	2495	236	2699
8	606	54	1414	100	1883	146	2227	191	2498	237	2702
9	639	56	1435	101	1889	147	2232	192	2502	238	2704
10	686	57	1455	102	1894	148	2236	194	2505	240	2707
12	716	58	1463	103	1912	149	2253	196	2509		
13	747	59	1483	105	1918	150	2258	197	2525		
14	788	60	1491	106	1936	152	2262	198	2528		
15	817	61	1512	108	1942	153	2279	199	2533		
17	845	63	1519	109	1947	154	2283	200	2536		
19	870	64	1540	110	1965	156	2287	201	2552		
20	899	65	1546	111	1970	157	2291	203	2555		
21	924	67	1567	112	1988	159	2308	204	2558		
22	950	68	1574	113	1994	160	2313	205	2562		
23	975	69	1593	115	1998	161	2317	207	2565		
24	999	71	1600	116	2016	162	2334	208	2581		
25	1013	72	1620	118	2022	163	2337	209	2585		
27	1036	73	1627	119	2027	164	2341	211	2588		
29	1061	74	1646	120	2045	166	2359	212	2591		
30	1083	75	1652	122	2049	167	2362	213	2594		
31	1108	76	1672	123	2067	169	2367	214	2610		
32	1119	78	1678	124	2072	170	2371	215	2613		
34	1142	80	1698	125	2077	171	2387	216	2616		
35	1164	81	1704	126	2095	172	2391	219	2619		
36	1188	82	1723	127	2100	174	2395	220	2622		
37	1197	83	1729	128	2104	175	2399	221	2638		
38	1220	84	1736	131	2121	176	2415	222	2641		
39	1243	86	1755	132	2126	177	2419	223	2645		
42	1252	87	1761	133	2132	178	2423	225	2647		
43	1272	88	1780	134	2149	179	2440	226	2650		
44	1295	89	1786	135	2154	182	2443	227	2666		
45	1304	90	1805	137	2158	183	2447	228	2668		

APPENDIX G

SAS OUTPUT FOR KOZENY CONSTANT FROM TOWPREG PREFORM PERMEATION

As discussed in Chapter V and Appendix D, SAS was used to non-linearly regress the experimental permeation data to obtain the tortuosity, K_1, which in turn was inserted into Equation 3.6 to calculate the Kozeny constant, K. The SAS procedure and output was discussed in greater detail in Appendix D. Tables G.1-G.20 are the SAS output for the towpreg preforms.

Table G1: SAS output for experiment T1

Non-Linear Least Squares Summary Statistics Dependent Variable X

Source	DF	Sum of Squares	Mean Square
Regression	1	6.71693376E-9	6.71693376E-9
Residual	111	7.9455744E-12	7.1581751E-14
Uncorrected Total	112	6.72487933E-9	
(Corrected Total)	111	7.1804957E-10	

Parameter	Estimate	Asymptotic Std. Error	Asymptotic 95 % Confidence Interval Lower	Upper
K_1	10.93646936	0.03571976873	10.865687756	11.007250964

Table G.2: SAS output for experiment T2

Non-Linear Least Squares Summary Statistics Dependent Variable X

Source	DF	Sum of Squares	Mean Square
Regression	1	1.29877235E-8	1.29877235E-8
Residual	119	6.1020036E-12	5.1277341E-14
Uncorrected Total	120	1.29938255E-8	
(Corrected Total)	119	1.43911122E-9	

Parameter	Estimate	Asymptotic Std. Error	Asymptotic 95 % Confidence Interval Lower	Upper
K_1	10.84277004	0.02154415074	10.800110141	10.885429936

Table G.3: SAS output for experiment T3

Non-Linear Least Squares Summary Statistics Dependent Variable X

Source	DF	Sum of Squares	Mean Square
Regression	1	1.56846823E-8	1.56846823E-8
Residual	118	3.146476E-11	2.666505E-13
Uncorrected Total	119	1.57161471E-8	
(Corrected Total)	118	1.39012406E-9	

Parameter	Estimate	Asymptotic Std. Error	Asymptotic 95 % Confidence Interval Lower	Upper
K_1	10.84926184	0.04473289130	10.760677859	10.937845812

Table G.4: SAS output for experiment T4

Non-Linear Least Squares Summary Statistics Dependent Variable X

Source	DF	Sum of Squares	Mean Square
Regression	1	2.70516072E-8	2.70516072E-8
Residual	120	2.664711E-11	2.2205925E-13
Uncorrected Total	121	2.70782543E-8	
(Corrected Total)	120	2.96972444E-9	

Parameter	Estimate	Asymptotic Std. Error	Asymptotic 95 % Confidence Interval Lower	Upper
K_1	10.84040928	0.031058 20008	10.778915726	10.901902828

Table G.5: SAS output for experiment T5

Non-Linear Least Squares Summary Statistics Dependent Variable X

Source	DF	Sum of Squares	Mean Square
Regression	1	6.63521489E-9	6.63521489E-9
Residual	114	1.0125085E-11	8.8816533E-14
Uncorrected Total	115	6.64533997E-9	
(Corrected Total)	114	7.6831198E-10	

Parameter	Estimate	Asymptotic Std. Error	Asymptotic 95 % Confidence Interval	
			Lower	Upper
K_1	11.27693222	0.04125539246	11.195205010	11.358659429

Table G.6: SAS output for experiment T6

Non-Linear Least Squares Summary Statistics Dependent Variable X

Source	DF	Sum of Squares	Mean Square
Regression	1	1.13933386E-8	1.13933386E-8
Residual	113	1.3298002E-11	1.1768143E-13
Uncorrected Total	114	1.14066366E-8	
(Corrected Total)	113	1.11050917E-9	

Parameter	Estimate	Asymptotic Std. Error	Asymptotic 95 % Confidence Interval	
			Lower	Upper
K_1	10.99789221	0.03534642358	10.927864067	11.067920355

Table G.7: SAS output for experiment T7

Non-Linear Least Squares Summary Statistics Dependent Variable X

Source	DF	Sum of Squares	Mean Square
Regression	1	1.5096915E-8	1.5096915E-8
Residual	116	2.9017875E-11	2.5015409E-13
Uncorrected Total	117	1.51259329E-8	
(Corrected Total)	116	1.84589552E-9	

Parameter	Estimate	Asymptotic Std. Error	Asymptotic 95 % Confidence Interval	
			Lower	Upper
K_1	10.88567929	0.04431097836	10.797915156	10.973443414

Table G.8: SAS output for experiment T8

Non-Linear Least Squares Summary Statistics Dependent Variable X

Source	DF	Sum of Squares	Mean Square
Regression	1	2.45381033E-8	2.45381033E-8
Residual	114	9.8382835E-11	8.6300732E-13
Uncorrected Total	115	2.46364862E-8	
(Corrected Total)	114	3.73225987E-9	

Parameter	Estimate	Asymptotic Std. Error	Asymptotic 95 % Confidence Interval	
			Lower	Upper
K_1	10.82899073	0.06421942838	10.701771614	10.956209853

Table G.9: SAS output for experiment T9

Non-Linear Least Squares Summary Statistics Dependent Variable X

Source	DF	Sum of Squares	Mean Square
Regression	1	3.85741339E-8	3.85741339E-8
Residual	115	9.5698019E-11	8.3215669E-13
Uncorrected Total	116	3.86698319E-8	
(Corrected Total)	115	3.40546647E-9	

Parameter	Estimate	Asymptotic Std. Error	Asymptotic 95 % Confidence Interval	
			Lower	Upper
K_1	10.76503483	0.04999829534	10.665997097	10.864072556

Table G.10: SAS output for experiment T10

Non-Linear Least Squares Summary Statistics Dependent Variable X

Source	DF	Sum of Squares	Mean Square
Regression	1	5.09125003E-8	5.09125003E-8
Residual	111	1.3004239E-10	1.1715531E-12
Uncorrected Total	112	5.10425426E-8	
(Corrected Total)	111	5.77377908E-9	

Parameter	Estimate	Asymptotic Std. Error	Asymptotic 95 % Confidence Interval	
			Lower	Upper
K_1	11.69574004	0.05610409484	11.584565244	11.806914826

Table G.11: SAS output for experiment T11

Non-Linear Least Squares Summary Statistics Dependent Variable XE

Source	DF	Sum of Squares	Mean Square
Regression	1	6.64625929E-8	6.64625929E-8
Residual	111	1.3299106E-10	1.1981177E-12
Uncorrected Total	112	6.6595584E-8	
(Corrected Total)	111	6.40951484E-9	

Parameter	Estimate	Asymptotic Std. Error	Asymptotic 95 % Confidence Interval	
			Lower	Upper
K_1	11.36243321	0.04823690697	11.266847887	11.458018534

Table G.12: SAS output for experiment T12

Non-Linear Least Squares Summary Statistics Dependent Variable X

Source	DF	Sum of Squares	Mean Square
Regression	1	6.71522389E-8	6.71522389E-8
Residual	115	1.96612307E-9	1.7096722E-11
Uncorrected Total	116	6.9118362E-8	
(Corrected Total)	115	2.41477868E-9	

Parameter	Estimate	Asymptotic Std. Error	Asymptotic 95 % Confidence Interval	
			Lower	Upper
K_1	15.15315471	0.24177022873	14.674250890	15.632058526

Table G.13: SAS output for experiment T13

Non-Linear Least Squares Summary Statistics Dependent Variable X

Source	DF	Sum of Squares	Mean Square
Regression	1	3.6355888E-8	3.6355888E-8
Residual	113	6.3459699E-11	5.6159026E-13
Uncorrected Total	114	3.64193477E-8	
(Corrected Total)	113	3.74593953E-9	

Parameter	Estimate	Asymptotic Std. Error	Asymptotic 95 % Confidence Interval Lower	Upper
K_1	10.91210572	0.04288729102	10.827137649	10.997073790

Table G.14: SAS output for experiment T14

Non-Linear Least Squares Summary Statistics Dependent Variable XE

Source	DF	Sum of Squares	Mean Square
Regression	1	6.21173335E-8	6.21173335E-8
Residual	112	9.6582708E-11	8.623456E-13
Uncorrected Total	113	6.22139162E-8	
(Corrected Total)	112	7.03840811E-9	

Parameter	Estimate	Asymptotic Std. Error	Asymptotic 95 % Confidence Interval Lower	Upper
K_1	10.82176437	0.04032026720	10.741874357	10.901654376

Table G.15: SAS output for experiment T15

Non-Linear Least Squares Summary Statistics Dependent Variable X

Source	DF	Sum of Squares	Mean Square
Regression	1	6.92656266E-8	6.92656266E-8
Residual	111	1.8858033E-10	1.6989219E-12
Uncorrected Total	112	6.94542069E-8	
(Corrected Total)	111	6.25123915E-9	

Parameter	Estimate	Asymptotic Std. Error	Asymptotic 95 % Confidence Interval	
			Lower	Upper
K_1	11.13768188	0.05515893313	11.028380003	11.246983757

Table G.16: SAS output for experiment T16

Non-Linear Least Squares Summary Statistics Dependent Variable X

Source	DF	Sum of Squares	Mean Square
Regression	1	1.07427185E-7	1.07427185E-7
Residual	115	9.6168924E-10	8.3625152E-12
Uncorrected Total	116	1.08388874E-7	
(Corrected Total)	115	7.24603554E-9	

Parameter	Estimate	Asymptotic Std. Error	Asymptotic 95 % Confidence Interval	
			Lower	Upper
K_1	11.88010478	0.10481591003	11.672483104	12.087726451

Table G.17: SAS output for experiment T17

Non-Linear Least Squares Summary Statistics Dependent Variable X

Source	DF	Sum of Squares	Mean Square
Regression	1	3.27707783E-8	3.27707783E-8
Residual	115	1.1149029E-10	9.6948078E-13
Uncorrected Total	116	3.28822686E-8	
(Corrected Total)	115	2.82203014E-9	

Parameter	Estimate	Asymptotic Std. Error	Asymptotic 95 % Confidence Interval	
			Lower	Upper
K_1	10.96663915	0.05966452419	10.848454340	11.084823959

Table G.18: SAS output for experiment T18

Non-Linear Least Squares Summary Statistics Dependent Variable X

Source	DF	Sum of Squares	Mean Square
Regression	1	6.50088038E-8	6.50088038E-8
Residual	117	3.8617391E-10	3.3006317E-12
Uncorrected Total	118	6.53949777E-8	
(Corrected Total)	117	5.37114285E-9	

Parameter	Estimate	Asymptotic Std. Error	Asymptotic 95 % Confidence Interval	
			Lower	Upper
K_1	11.26020476	0.08022925874	11.101313726	11.419095801

Table G.19: SAS output for experiment T19

Non-Linear Least Squares Summary Statistics Dependent Variable X

Source	DF	Sum of Squares	Mean Square
Regression	1	3.11471715E-8	3.11471715E-8
Residual	113	1.0097459E-10	8.9358045E-13
Uncorrected Total	114	3.1248146E-8	
(Corrected Total)	113	4.65392727E-9	

Parameter	Estimate	Asymptotic Std. Error	Asymptotic 95 % Confidence Interval Lower	Upper
K_1	11.04958857	0.05915866608	10.932383741	11.166793404

Table G.20: SAS output for experiment T20

Non-Linear Least Squares Summary Statistics Dependent Variable X

Source	DF	Sum of Squares	Mean Square
Regression	1	6.54645961E-8	6.54645961E-8
Residual	117	2.1049879E-10	1.799135E-12
Uncorrected Total	118	6.56750949E-8	
(Corrected Total)	117	5.96961663E-9	

Parameter	Estimate	Asymptotic Std. Error	Asymptotic 95 % Confidence Interval Lower	Upper
K_1	11.35764361	0.05953404349	11.239738667	11.475548547

APPENDIX H

ANOVA TABLES FOR KOZENY CONSTANT FROM TOWPREG PREFORM PERMEATION

Minitab® was used to calculate ANOVA tables on the Kozeny constant. The factors were polymer, temperature, pressure, fiber, and porosity. The results are shown in Tables H.1 and H.2.

Table H.1: Minitab® output of ANOVA table on Kozeny constants from towpreg processing. The factors are pressure and temperature.

ANOVA: kozeny constant versus pressure

```
Factor     Type Levels Values
pressure   fixed      2  0.52  1.03

Analysis of Variance for kozeny c

Source      DF         SS         MS        F      P
pressure     1       96.3       96.3     0.63  0.440
Error       14     2137.6      152.7
Total       15     2233.9
```

ANOVA: kozeny constant versus temperature

```
Factor     Type Levels Values
temperat   fixed      3   230   260   310

Analysis of Variance for kozeny c

Source      DF         SS         MS        F      P
temperat     2      874.0      437.0     4.18  0.040
Error       13     1359.9      104.6
Total       15     2233.9
```

Table H.2: Minitab® output of ANOVA table on Kozeny constants from towpreg processing. The factors are fiber, resin, and resin weight percent.

ANOVA: kozeny constant versus fiber

```
Factor     Type Levels Values
fiber     fixed      2     1     2


Analysis of Variance for kozeny c

Source      DF         SS         MS       F      P
fiber        1      126.8      126.8    0.84  0.374
Error       14     2107.1      150.5
Total       15     2233.9
```

ANOVA: kozeny constant versus resin

```
Factor     Type Levels Values
resin     fixed      2     1     2


Analysis of Variance for kozeny c

Source      DF         SS         MS       F      P
resin        1      749.1      749.1    7.06  0.019
Error       14     1484.8      106.1
Total       15     2233.9
```

ANOVA: kozeny constant versus resin weight percent

```
Factor     Type Levels Values
resin we  fixed      6    26    33    34    38    43    48


Analysis of Variance for kozeny c

Source      DF         SS         MS       F      P
resin we     5     1057.4      211.5    1.80  0.201
Error       10     1176.5      117.6
Total       15     2233.9
```

APPENDIX I

RAW PERMEATION DATA FROM TOWPREG PREFORM PROCESSING

The raw permeation data for the towpreg preform processing are located in Tables I.1-I.20 on the following pages. In the tables, t is time and X is penetration depth. Refer to Table 4.5 for explanations of experimental conditions T1-T20.

Table I.1: Raw permeation data for experiment T1. The standard deviation is ~1 μm.

t [s]	X [μm]	t [s]	X [μm]	t [s]	X [μm]	t [s]	X [μm]
0	0.0	42	5.7	82	8.1	123	10.0
1	1.9	43	5.9	83	8.0	124	10.0
3	2.1	44	6.3	84	8.4	125	10.4
5	1.9	45	6.3	86	8.8	126	10.0
6	2.6	46	6.1	87	8.0	128	10.4
7	2.3	47	6.6	88	8.9	130	10.3
8	2.9	49	6.9	89	8.2	131	10.5
9	2.8	50	6.3	91	8.6	132	10.6
10	2.9	51	7.2	93	9.2	133	10.5
12	2.8	52	7.1	94	8.9	134	10.6
13	3.8	54	7.2	95	8.7	135	10.7
14	3.9	56	6.9	96	8.4	137	10.4
16	3.7	57	6.6	97	8.9	138	10.6
17	3.7	58	7.4	98	9.0	140	10.7
19	4.2	59	7.1	100	9.3	141	10.7
20	4.6	60	6.9	101	9.1	142	10.8
21	4.1	61	7.0	102	9.6	144	10.8
22	4.0	63	6.9	103	9.5	145	10.9
23	4.2	64	7.8	105	9.4		
24	4.7	66	7.7	106	9.5		
25	4.4	67	7.1	108	9.4		
28	5.1	68	7.4	109	9.6		
29	5.2	69	7.8	110	9.6		
30	5.5	71	8.2	111	9.7		
31	5.2	72	8.1	112	9.8		
32	5.5	73	7.7	113	9.7		
34	5.8	74	7.9	115	10.0		
35	5.4	75	8.3	117	10.1		
36	5.5	76	7.7	118	9.9		
37	5.3	79	8.4	119	9.9		
38	6.0	80	8.4	120	9.9		
41	6.1	81	7.7	122	10.1		

Table I.2: Raw permeation data for experiment T2. The standard deviation is ~2 μm.

t [s]	X [μm]	t [s]	X [μm]	t [s]	X [μm]	t [s]	X [μm]
0	0.0	41	8.2	82	10.7	123	13.3
1	0.7	43	8.3	83	10.7	124	13.4
2	2.0	44	8.0	84	10.7	125	13.2
3	2.4	45	8.6	86	11.3	126	13.2
6	2.4	46	8.6	87	10.9	127	13.4
7	3.4	47	8.1	88	10.8	128	13.5
8	3.4	49	8.4	89	11.0	131	13.4
9	3.4	50	8.4	90	11.3	132	13.7
10	3.9	51	8.7	91	11.3	133	13.7
12	4.7	52	8.6	94	11.1	134	13.8
13	4.7	54	8.7	95	11.2	135	13.9
14	4.6	56	8.9	96	11.7	137	14.1
15	5.0	57	9.0	97	11.7	138	13.9
16	5.0	58	8.8	98	11.8	139	14.2
19	5.3	59	9.2	100	12.1	140	14.1
20	5.2	60	9.2	101	11.9	142	14.2
21	5.4	61	9.3	102	11.9	144	14.2
22	5.8	62	9.8	103	12.2	145	14.2
23	5.9	64	9.3	105	12.1	146	14.2
24	6.2	65	9.6	106	12.3	147	14.3
25	6.4	66	9.8	108	12.3	148	14.5
27	7.0	68	9.9	109	12.2	149	14.6
28	6.5	69	10.2	110	12.4	150	15.1
30	6.8	71	9.7	111	12.6		
31	7.0	72	9.8	112	12.6		
32	6.9	73	10.1	113	12.6		
34	7.3	74	10.1	115	12.9		
35	7.0	75	10.2	116	12.8		
36	7.5	76	10.3	118	12.7		
37	7.8	78	10.2	119	13.0		
38	7.6	79	10.6	120	13.2		
39	7.4	81	10.4	122	13.2		

Table I.3: Raw permeation data for experiment T3. The standard deviation is ~1 μm.

t [s]	X [μm]	t [s]	X [μm]	t [s]	X [μm]	t [s]	X [μm]
0	0.0	41	8.9	81	12.0	123	14.2
1	2.2	42	9.1	83	12.1	124	14.3
2	2.6	43	8.8	84	12.5	125	14.3
3	3.7	44	9.0	86	12.1	126	14.5
5	4.2	45	8.9	87	12.6	128	14.5
6	4.5	46	9.6	88	12.5	130	14.6
7	4.7	49	9.8	89	12.5	131	14.6
8	4.9	50	9.6	90	12.8	132	14.7
10	5.3	51	10.1	91	12.8	133	14.7
12	5.6	52	9.9	93	12.9	134	14.7
13	5.9	53	10.0	95	13.0	135	14.9
14	6.0	54	10.0	96	13.1	137	14.9
15	6.3	56	10.3	97	12.9	138	14.9
16	6.6	57	10.1	98	13.1	140	15.1
17	6.6	58	10.8	100	13.3	141	15.0
19	6.9	60	10.4	101	13.2	142	15.1
20	7.0	61	10.3	102	13.2	144	15.1
21	7.2	63	10.8	103	13.3	145	15.3
23	7.2	64	10.8	104	13.5	146	15.2
24	7.4	65	11.3	106	13.5	147	15.3
25	7.6	66	11.1	108	13.5	148	15.3
27	7.6	67	11.2	109	13.7	149	15.4
28	7.8	68	11.5	110	13.6	152	15.5
29	7.7	69	11.2	111	13.7		
30	8.2	72	11.6	112	13.8		
31	8.4	73	11.5	113	13.9		
32	8.3	74	11.4	115	14.0		
35	8.8	75	11.6	116	14.0		
36	8.7	76	11.6	118	13.9		
37	8.5	78	11.7	119	14.2		
38	8.4	79	12.0	120	14.2		
39	8.3	80	12.1	122	14.2		

Table I.4: Raw permeation data for experiment T4. The standard deviation is ~2 μm.

t [s]	X [μm]	t [s]	X [μm]	t [s]	X [μm]	t [s]	X [μm]
0	0.0	41	10.9	82	15.3	123	19.0
1	4.5	42	11.1	83	15.6	124	19.0
3	3.6	44	11.5	84	15.6	125	19.1
5	4.2	45	12.0	86	15.8	126	19.0
6	4.8	46	12.3	87	15.9	127	19.3
7	5.3	47	12.1	88	16.0	128	19.4
8	6.6	49	12.6	89	16.2	130	19.3
9	6.2	50	12.5	90	16.3	131	19.4
10	4.1	51	12.6	91	16.3	133	19.7
12	4.9	52	12.6	93	16.5	134	19.6
13	4.9	53	13.1	95	16.7	135	19.8
14	5.4	54	13.2	96	16.8	137	19.6
15	6.1	57	13.2	97	16.8	138	20.0
17	6.3	58	13.3	98	17.0	139	19.7
19	6.6	59	13.2	100	17.1	140	19.8
20	7.2	60	13.4	101	17.3	141	20.0
21	7.4	61	13.5	102	17.3	142	20.2
22	7.6	62	14.0	103	17.5	144	20.6
23	7.8	64	13.8	104	17.6	146	20.7
24	8.3	65	13.9	105	17.7	147	20.6
25	8.5	66	14.3	108	18.0	148	20.5
27	8.8	67	14.2	109	17.9	149	20.5
28	9.1	69	14.2	110	17.8	150	20.5
30	9.6	71	14.2	111	18.1		
31	9.7	72	14.5	112	18.2		
32	10.0	73	14.4	113	18.4		
34	10.3	74	14.5	115	18.5		
35	10.1	75	14.7	116	18.6		
36	10.6	76	14.8	117	18.2		
37	10.5	78	15.0	118	18.3		
38	11.0	79	15.1	120	18.8		
39	10.9	80	15.3	122	18.9		

Table I.5: Raw permeation data for experiment T5. The standard deviation is ~0.5 μm.

t [s]	X [μm]	t [s]	X [μm]	t [s]	X [μm]	t [s]	X [μm]
0	0.0	41	5.6	82	7.3	123	10.0
1	0.8	43	6.3	83	8.6	124	9.9
2	1.0	44	6.2	84	7.7	125	10.0
3	1.4	45	5.5	86	8.3	126	10.0
5	1.6	46	6.8	87	8.8	127	9.9
6	1.8	47	6.4	88	8.6	128	10.0
8	2.8	49	6.5	89	8.3	131	10.1
9	3.1	50	6.4	93	8.4	132	10.2
10	3.0	52	6.9	94	8.5	133	10.3
12	3.0	54	6.7	95	8.7	134	10.3
13	3.4	56	6.5	96	8.3	135	10.3
14	4.0	58	6.3	97	8.9	137	10.2
15	3.3	59	7.1	98	9.0	138	10.5
16	3.2	60	7.3	100	9.0	139	10.4
17	3.4	61	6.4	101	8.9	140	10.5
20	4.0	62	7.0	102	9.2	142	10.4
21	3.8	64	7.3	103	9.0	144	10.6
22	4.2	65	7.5	105	9.3	145	10.6
23	4.3	66	7.8	106	9.2	146	10.7
24	4.8	68	7.1	108	9.3		
25	4.4	69	7.2	109	9.1		
27	4.8	71	7.7	110	9.2		
28	5.0	72	7.3	111	9.3		
29	5.0	73	7.6	112	9.6		
31	4.9	74	8.1	113	9.6		
34	5.5	75	7.2	115	9.6		
35	6.0	76	7.4	116	9.6		
38	6.2	78	7.3	118	9.8		
39	6.0	80	7.9	119	9.8		

Table I.6: Raw permeation data for experiment T6. The standard deviation is ~0.7 μm.

t [s]	X [μm]	t [s]	X [μm]	t [s]	X [μm]	t [s]	X [μm]
0	0.0	41	7.8	82	10.5	123	12.6
1	1.4	43	8.0	83	11.2	124	12.6
2	1.8	44	8.7	84	11.0	125	12.9
3	2.4	45	8.4	86	10.8	126	13.0
5	3.1	46	8.8	87	11.2	127	12.8
6	3.4	47	8.5	88	10.8	128	12.8
7	4.0	49	8.6	89	11.1	131	13.1
8	3.7	50	8.8	90	11.1	132	12.9
9	4.4	51	8.5	91	11.2	133	13.2
12	4.4	52	8.8	94	11.3	134	13.0
13	4.9	53	8.8	95	11.4	135	13.1
14	4.7	56	8.9	96	11.2	137	13.5
15	4.9	57	9.1	97	11.6	138	13.4
16	5.2	58	9.4	98	11.6	139	13.4
17	5.3	59	9.4	100	11.5	140	13.4
20	5.7	60	9.3	101	11.7	141	13.3
21	5.7	61	9.6	102	12.1	144	13.4
22	6.2	62	9.7	103	11.9	145	13.5
23	6.2	64	10.1	104	11.7		
24	6.7	65	9.7	105	11.8		
25	6.8	66	10.0	108	11.9		
27	6.8	68	9.7	109	12.0		
28	6.8	69	9.9	110	12.2		
29	6.6	71	10.3	111	12.0		
31	7.0	72	10.3	112	12.5		
32	7.2	73	10.1	113	12.4		
34	7.3	74	10.3	115	12.5		
35	7.3	75	10.2	116	12.3		
36	7.4	76	10.3	117	12.3		
37	7.8	78	10.7	119	12.8		
38	8.0	79	10.5	120	12.5		
39	7.8	81	11.0	122	12.7		

Table I.7: Raw permeation data for experiment T7. The standard deviation is ~1 μm.

t [s]	X [μm]	t [s]	X [μm]	t [s]	X [μm]	t [s]	X [μm]
0	0.0	41	8.3	82	11.9	123	14.7
1	2.9	42	8.5	83	11.9	124	14.8
2	4.9	44	8.6	84	12.4	125	14.8
3	3.4	45	8.6	86	12.4	126	14.9
5	2.8	46	8.9	87	12.4	128	15.0
7	2.9	47	8.8	88	12.5	130	15.2
8	3.9	49	9.0	89	12.7	131	15.2
9	2.5	50	9.0	90	12.5	132	15.1
10	3.1	51	9.2	91	12.6	133	15.1
12	3.7	52	9.2	93	12.9	134	15.3
13	4.0	53	9.4	95	13.0	135	15.5
14	4.1	54	9.5	96	12.9	137	15.5
15	4.3	57	9.7	97	13.5	138	15.5
16	4.5	58	10.1	98	13.3	139	15.6
17	5.1	59	10.1	100	13.5	141	15.7
20	5.5	60	10.1	101	13.5	142	15.8
21	5.3	61	10.2	102	13.7	144	15.8
22	5.9	62	10.2	103	13.8	145	15.9
23	5.9	64	10.3	104	13.6	146	16.0
24	6.1	65	10.8	105	13.7	147	15.9
25	6.3	66	10.7	108	14.0	148	15.9
27	6.6	67	11.1	109	14.0		
28	6.9	69	10.6	110	14.1		
29	7.0	71	10.8	111	13.9		
31	7.3	72	11.1	112	14.2		
32	7.2	73	11.2	113	14.1		
34	7.4	74	11.4	115	14.4		
35	7.6	75	11.6	116	14.5		
36	7.8	76	11.8	118	14.4		
37	7.9	78	11.5	119	14.7		
38	8.1	79	11.9	120	14.5		
39	8.1	80	12.0	122	14.8		

Table I.8: Raw permeation data for experiment T8. The standard deviation is ~0.9 μm.

t [s]	X [μm]	t [s]	X [μm]	t [s]	X [μm]	t [s]	X [μm]
0	0.0	41	10.2	82	15.4	123	19.5
1	0.2	42	10.4	83	15.6	124	19.5
2	1.2	43	11.0	84	15.6	125	19.5
3	0.8	45	10.8	86	15.9	126	19.8
5	1.5	46	11.4	87	15.9	128	20.0
6	2.0	47	11.5	88	16.1	130	20.1
7	2.2	49	11.6	89	16.3	131	20.3
9	3.1	50	11.7	90	16.4	132	20.0
10	3.6	51	11.9	93	16.6	133	20.2
12	3.7	52	12.1	94	16.7	134	20.2
13	4.5	53	12.5	95	17.0	135	20.6
14	4.8	54	12.6	96	17.2	137	20.5
15	5.1	56	12.7	97	17.2	138	20.8
16	5.4	58	12.6	98	17.3	139	20.8
17	5.6	59	12.8	100	17.4	141	20.7
19	6.3	60	13.1	101	17.5	142	20.9
21	6.5	61	13.4	102	17.9	144	20.9
22	6.5	62	13.5	103	17.8	145	20.9
23	7.3	64	13.7	105	18.0	146	20.9
24	7.4	65	13.9	106	18.2		
25	7.6	66	13.8	108	18.3		
27	8.0	67	13.8	109	18.4		
28	8.1	69	13.8	110	18.4		
29	8.4	71	13.9	111	18.4		
31	8.8	72	14.3	112	18.6		
32	8.9	73	14.3	113	18.9		
34	9.3	74	14.6	115	18.7		
35	9.6	75	14.7	117	18.9		
36	9.9	76	14.8	118	19.2		
37	9.7	78	14.9	119	19.1		
38	10.0	79	15.1	120	19.2		
39	10.4	81	15.3	122	19.2		

Table I.9: Raw permeation data for experiment T9. The standard deviation is ~3 μm.

t [s]	X [μm]	t [s]	X [μm]	t [s]	X [μm]	t [s]	X [μm]
0	0.0	41	15.2	82	19.9	123	22.6
1	3.1	42	15.3	83	19.2	124	22.8
2	4.3	43	15.0	84	19.9	125	22.9
3	4.8	44	15.7	86	20.4	126	23.0
5	5.5	45	15.8	87	20.0	127	23.0
6	7.0	47	16.1	88	19.9	128	23.1
7	7.1	49	16.1	89	19.6	131	23.1
8	7.6	50	15.5	90	20.3	132	23.3
9	7.8	51	16.6	91	20.5	133	23.4
12	9.0	52	16.3	94	20.7	134	23.4
13	9.4	53	16.3	95	20.3	135	23.6
14	9.6	54	16.1	96	21.0	137	23.6
15	9.4	56	16.5	97	21.1	138	23.6
16	9.7	57	17.2	98	20.9	139	23.7
17	10.3	58	17.4	100	21.2	140	23.8
19	10.5	60	17.0	101	21.2	142	24.0
20	11.1	61	17.0	102	21.4	144	24.0
21	11.1	63	17.7	103	21.5	145	24.1
23	12.0	64	18.1	104	21.5	146	24.2
24	12.0	65	18.3	106	21.5		
25	12.3	66	17.8	108	21.6		
27	12.7	67	17.9	109	21.6		
28	12.6	69	18.5	110	21.9		
29	12.9	71	18.0	111	21.9		
30	12.8	72	18.8	112	22.0		
31	13.5	73	18.7	113	22.0		
32	14.2	74	18.2	115	22.2		
34	13.6	75	18.8	116	22.3		
35	13.9	76	18.6	118	22.3		
37	14.7	78	18.8	119	22.5		
38	14.6	79	19.7	120	22.5		
39	14.2	80	19.0	122	22.7		

Table I.10: Raw permeation data for experiment T10. The standard deviation is ~0.7 μm.

t [s]	X [μm]	t [s]	X [μm]	t [s]	X [μm]	t [s]	X [μm]
0	0.0	41	17.5	81	23.5	124	27.0
1	0.3	42	17.7	82	23.7	125	27.2
2	0.5	43	18.1	84	23.4	126	27.3
3	1.4	44	18.4	86	24.1	127	27.4
5	2.8	46	18.5	87	23.7	128	27.5
6	4.0	47	18.5	88	24.0	130	27.6
8	4.9	49	19.3	89	24.1	132	27.6
9	5.9	50	19.1	90	24.3	133	27.7
10	7.2	51	19.7	91	24.5	134	27.9
12	7.9	52	20.0	93	24.3	135	27.8
13	8.9	53	19.7	94	24.5	137	28.0
14	9.4	54	20.4	96	24.5	138	28.1
15	10.2	56	20.0	97	24.9	139	28.1
16	10.9	57	20.2	98	25.1	140	28.4
17	11.2	59	20.3	100	25.4	141	28.3
19	11.5	60	20.3	101	25.3	142	28.4
21	11.9	61	20.8	102	25.5	145	28.5
22	12.3	63	21.1	103	25.5	146	28.6
23	12.7	64	21.3	104	25.7	147	28.7
24	13.3	65	21.7	105	25.7		
25	13.9	66	21.3	108	25.9		
27	14.7	67	22.0	109	26.1		
28	14.4	68	22.1	111	26.2		
29	15.4	69	22.3	112	26.2		
30	15.4	72	22.1	113	26.3		
31	15.6	73	22.4	115	26.4		
34	15.9	74	22.4	116	26.5		
35	15.9	75	22.8	117	26.5		
36	16.4	76	22.7	119	26.7		
37	16.7	78	22.5	120	26.8		
38	16.9	79	23.3	122	26.9		
39	17.2	80	22.8	123	26.9		

Table I.11: Raw permeation data for experiment T11. The standard deviation is ~2 μm.

t [s]	X [μm]	t [s]	X [μm]	t [s]	X [μm]	t [s]	X [μm]
0	0.0	41	20.1	82	26.3	123	30.7
1	1.6	42	20.7	83	26.5	124	30.9
2	3.7	44	20.9	84	26.6	125	30.9
3	4.8	45	20.8	86	26.9	127	31.1
5	6.3	46	21.5	87	27.0	128	31.2
6	7.2	47	21.7	88	27.2	130	31.3
7	8.4	49	21.7	89	27.4	131	31.4
8	9.2	50	22.1	90	27.6	132	31.5
9	10.1	51	22.3	93	27.7	133	31.6
12	10.7	52	22.4	94	27.7	134	32.0
13	11.5	53	22.7	95	28.1	135	31.9
14	12.4	56	23.1	96	28.1	137	32.2
15	12.6	57	22.9	97	28.4	138	32.2
16	13.3	58	23.2	98	28.4	140	32.2
17	13.7	59	23.2	100	28.3	141	32.4
19	14.6	60	23.6	101	28.9	142	32.5
20	14.8	61	23.9	102	28.7	144	30.5
21	15.3	63	23.8	104	28.9	145	33.5
23	15.7	64	24.2	105	28.9	146	33.7
24	15.9	65	24.3	106	29.0	147	33.5
25	16.4	67	24.4	108	29.5	148	33.7
27	16.9	68	24.4	109	29.5	149	33.6
28	17.3	69	24.4	110	29.7		
29	17.7	71	24.8	111	29.7		
30	18.0	72	24.9	112	29.8		
31	18.2	73	25.1	113	30.1		
34	18.5	74	25.3	116	30.2		
35	18.9	75	25.4	117	30.1		
36	19.2	76	25.6	118	30.2		
37	19.6	78	25.8	119	30.4		
38	20.0	80	26.1	120	30.6		
39	20.2	81	26.1	122	30.6		

Table I.12: Raw permeation data for experiment T12. The standard deviation is ~7 μm.

t [s]	X [μm]	t [s]	X [μm]	t [s]	X [μm]	t [s]	X [μm]
0	0.0	41	22.7	80	25.2	119	27.9
1	11.4	42	22.6	81	25.5	120	27.7
3	11.3	43	22.7	82	25.3	122	27.5
5	11.3	44	23.3	83	25.5	124	27.8
6	12.8	45	23.4	86	25.7	125	27.8
7	14.1	46	23.3	87	25.9	126	27.9
8	14.9	47	23.3	88	25.9	127	28.1
9	16.0	49	23.8	89	26.0	128	27.9
10	16.4	50	23.8	90	26.0	130	27.9
12	17.3	52	23.7	91	26.1	131	28.2
13	18.1	53	23.8	93	26.1	132	28.1
14	18.4	54	23.8	94	26.5	133	28.3
16	18.7	56	24.0	95	26.6	134	28.2
17	19.1	57	24.0	96	26.4	137	28.2
19	19.5	58	24.4	98	26.7	138	28.3
20	20.0	59	24.1	100	26.5	139	28.3
21	20.1	60	24.4	101	26.8	140	28.4
22	20.4	63	24.2	102	27.0	141	28.4
23	20.7	64	24.3	103	26.6	142	28.6
24	20.6	65	24.6	104	26.7	144	28.7
25	21.1	66	24.6	105	26.9	145	28.5
28	21.3	67	24.7	106	27.1	146	28.6
29	21.5	68	24.9	108	27.2	148	28.5
30	21.7	69	24.9	109	26.9		
31	21.7	71	24.8	111	27.3		
32	21.9	73	24.9	112	27.1		
34	22.5	74	24.9	113	27.1		
35	22.0	75	25.0	115	27.3		
36	22.5	76	25.2	116	27.4		
37	22.7	78	25.1	117	27.4		
39	22.6	79	25.1	118	27.4		

Table I.13: Raw permeation data for experiment T13. The standard deviation is ~2 μm.

t [s]	X [μm]	t [s]	X [μm]	t [s]	X [μm]	t [s]	X [μm]
0	0.0	41	13.8	82	19.5	123	22.8
1	2.8	42	14.4	83	19.3	124	23.0
2	6.1	44	14.4	84	19.2	125	23.0
3	7.5	45	14.4	86	19.3	126	23.2
6	8.4	46	14.9	87	19.3	127	23.3
7	4.4	47	15.2	88	20.0	128	23.4
8	9.4	49	15.2	89	19.9	131	23.6
9	5.7	50	15.3	90	20.2	132	23.5
10	5.8	51	15.9	91	20.3	133	23.7
12	6.3	52	15.8	94	20.1	134	23.8
13	6.8	53	16.0	95	20.6	135	23.9
14	7.3	54	16.5	96	21.0	137	24.1
15	7.8	57	16.3	97	20.6	138	23.9
16	8.8	58	16.7	98	20.4	139	23.9
19	8.7	59	16.5	100	20.6	140	24.0
20	9.0	60	16.8	101	21.1	141	24.3
21	9.9	61	16.8	102	21.3	144	24.3
22	10.2	63	17.1	103	21.3	145	24.4
23	10.5	64	16.9	104	21.5	146	24.4
24	10.5	65	17.2	106	21.6	147	24.4
25	10.4	66	17.3	108	21.6	148	24.4
27	10.8	67	17.8	109	21.7	149	24.5
28	11.1	69	18.0	110	21.9	150	24.5
29	11.6	71	17.6	111	22.0	152	24.5
30	12.0	72	17.8	112	22.2		
32	12.5	73	18.8	113	22.3		
34	12.7	74	18.9	115	22.4		
35	12.9	75	18.7	116	22.4		
36	13.3	76	18.7	117	22.5		
37	13.4	78	18.8	119	22.7		
38	13.3	79	18.9	120	22.8		
39	13.5	80	19.3	122	22.8		

Table I.14: Raw permeation data for experiment T14. The standard deviation is ~1 μm.

t [s]	X [μm]	t [s]	X [μm]	t [s]	X [μm]	t [s]	X [μm]
0	0.0	41	17.7	81	24.8	123	29.6
1	0.6	42	19.3	82	25.6	124	29.4
2	2.8	43	19.3	84	25.8	125	29.6
5	4.0	45	19.2	86	25.4	126	29.9
6	4.9	46	19.3	87	25.7	127	30.0
7	5.3	47	20.0	88	25.7	128	30.5
8	6.4	49	20.4	89	26.2	131	30.2
9	7.2	50	20.4	90	26.7	132	30.5
10	7.5	51	20.5	91	26.1	133	30.5
12	8.2	52	21.4	94	27.1	134	30.9
14	9.3	53	20.9	95	26.7	135	30.7
15	9.5	56	21.8	96	26.8	137	30.6
16	11.1	57	22.0	97	27.5	138	30.9
17	11.5	58	22.1	98	27.7	139	31.2
19	11.6	59	22.3	100	27.0	140	31.0
20	12.2	60	21.8	101	27.0	142	31.3
21	13.2	61	22.8	102	27.6	144	31.4
22	13.7	63	22.7	104	28.0	145	31.2
24	13.8	64	22.6	105	28.2	146	30.9
25	13.6	65	22.5	106	28.1	147	30.7
27	14.2	67	23.0	108	28.8		
28	14.8	68	23.8	109	28.4		
29	15.1	69	23.9	110	28.8		
30	15.9	71	23.3	111	28.3		
31	16.1	72	23.6	113	29.0		
32	17.0	73	24.3	115	28.6		
34	16.9	75	24.8	116	29.0		
36	17.5	76	24.9	117	29.5		
37	18.2	78	24.6	118	29.4		
38	18.0	79	24.9	119	29.4		
39	18.3	80	25.4	122	29.5		

Table I.15: Raw permeation data for experiment T15. The standard deviation is ~3 μm.

t [s]	X [μm]	t [s]	X [μm]	t [s]	X [μm]	t [s]	X [μm]
0	0.0	41	20.9	82	26.8	123	31.4
1	3.2	42	20.9	83	26.9	124	31.6
2	2.9	44	21.2	84	27.2	125	31.3
5	4.5	45	21.6	86	27.0	126	31.5
6	6.6	46	21.9	87	27.7	127	31.6
7	8.4	47	22.1	88	27.5	130	31.7
8	9.4	49	22.3	89	27.6	131	32.3
9	10.4	50	22.6	90	28.1	132	32.2
10	11.4	51	22.9	93	27.9	133	32.0
12	12.1	52	22.8	94	28.1	134	32.6
13	12.8	53	23.1	95	28.5	135	32.3
14	13.3	54	23.0	96	28.3	137	32.5
15	13.9	57	23.5	97	28.5	138	32.7
17	14.5	58	23.6	98	28.6	140	33.1
19	14.7	59	24.0	100	29.1	141	33.0
20	15.5	60	24.1	101	29.3	142	32.9
21	15.7	61	24.3	102	29.4	144	33.0
22	16.2	62	24.2	104	29.4	145	33.1
23	16.7	64	24.4	105	29.6	146	33.2
24	16.8	65	24.8	106	29.8	147	33.6
25	17.4	67	24.8	108	29.7	149	33.7
27	17.9	68	25.0	109	29.9	150	33.7
28	18.1	69	25.2	110	29.9		
30	18.4	71	25.3	111	30.0		
31	18.8	72	25.5	112	30.4		
32	19.2	73	25.4	113	30.6		
34	19.5	74	25.5	115	30.6		
35	19.4	75	25.9	117	30.7		
36	19.8	76	26.1	118	31.0		
37	20.3	78	26.0	119	30.9		
38	20.2	80	26.4	120	31.4		
39	20.7	81	26.7	122	31.3		

Table I.16: Raw permeation data for experiment T16. The standard deviation is ~2 μm.

t [s]	X [μm]	t [s]	X [μm]	t [s]	X [μm]	t [s]	X [μm]
0	0.0	41	26.7	81	32.2	122	37.3
1	4.2	42	26.7	82	32.3	123	36.9
2	8.1	43	27.0	83	32.5	125	37.5
3	10.1	44	27.2	84	32.7	126	37.4
5	12.1	45	27.4	87	32.9	127	37.2
6	13.2	46	27.7	88	33.0	128	37.8
7	14.3	47	28.0	89	33.2	130	37.9
8	15.7	50	27.9	90	33.3	131	37.8
9	16.6	51	28.4	91	33.6	132	38.0
10	17.2	52	28.4	93	33.8	133	38.2
13	18.1	53	28.5	94	33.9	134	38.1
14	18.5	54	28.9	95	34.0	135	38.2
15	19.4	56	28.8	96	34.1	138	38.5
16	19.8	57	29.3	97	34.6	139	38.5
17	20.4	58	29.3	98	34.6	140	38.7
19	20.7	59	29.5	101	34.4	141	38.9
20	21.4	60	29.8	102	34.6	142	38.8
21	21.9	62	29.9	103	34.9	144	39.0
22	22.1	64	30.0	104	34.9	145	39.1
24	22.5	65	30.1	105	35.1	146	39.1
25	23.0	66	30.2	106	35.4		
27	23.3	67	30.5	108	35.7		
28	23.7	68	30.3	109	35.5		
29	24.1	69	30.6	110	35.8		
30	24.4	71	30.8	112	36.1		
31	24.6	72	31.0	113	35.9		
32	24.9	73	31.0	115	36.3		
34	25.2	75	31.3	116	36.4		
35	25.5	76	31.5	117	36.4		
37	25.8	78	31.6	118	36.3		
38	26.0	79	31.8	119	36.7		
39	26.2	80	32.0	120	36.7		

Table I.17: Raw permeation data for experiment T17. The standard deviation is ~2 μm.

t [s]	X [μm]	t [s]	X [μm]	t [s]	X [μm]	t [s]	X [μm]
0	0.0	41	14.0	82	17.8	123	20.6
1	1.7	42	14.5	83	18.3	124	21.1
2	3.4	44	14.5	84	18.3	126	21.2
3	4.8	45	14.4	86	18.1	127	21.1
5	5.6	46	14.5	87	18.3	128	21.4
7	6.0	47	14.8	88	18.1	130	21.3
8	6.7	49	14.7	89	18.7	131	21.5
9	6.9	50	15.2	91	18.8	132	21.4
10	7.8	51	15.2	93	18.7	133	21.3
12	8.7	52	15.5	94	18.4	134	21.5
13	8.7	53	15.0	95	18.6	135	21.4
14	8.8	56	15.5	96	19.0	138	21.4
15	9.2	57	15.8	97	19.2	139	21.6
16	9.8	58	15.8	98	19.2	140	21.7
19	10.2	59	15.5	100	19.4	141	21.9
20	9.7	60	15.9	101	19.8	142	21.9
21	9.9	61	16.0	102	19.8	144	22.0
22	10.4	62	16.7	104	19.7	145	21.9
23	10.6	64	16.5	105	19.8	146	22.1
24	11.2	65	16.2	106	19.8	147	22.3
25	11.6	67	16.7	108	19.9		
27	11.8	68	17.0	109	20.0		
28	12.1	69	17.3	110	20.0		
29	12.2	71	17.1	111	20.3		
30	12.6	72	16.9	112	20.4		
32	12.5	73	17.3	113	20.5		
34	12.6	74	17.3	116	20.2		
35	12.7	75	17.5	117	20.4		
36	12.9	76	17.7	118	20.4		
37	13.5	79	17.7	119	20.7		
38	13.5	80	17.5	120	20.4		
39	13.4	81	17.7	122	20.5		

Table I.18: Raw permeation data for experiment T18. The standard deviation is ~2 μm.

t [s]	X [μm]	t [s]	X [μm]	t [s]	X [μm]	t [s]	X [μm]
0	0.0	41	20.0	82	25.1	123	28.6
1	3.3	42	20.0	83	25.8	124	28.7
2	4.1	44	20.4	84	25.5	125	28.8
3	4.7	45	20.3	86	25.7	126	28.5
6	6.3	46	20.7	87	26.1	127	28.5
7	7.2	47	20.9	88	26.0	128	28.6
8	8.3	49	20.9	89	25.9	130	28.9
9	9.3	50	21.2	90	26.4	131	28.8
10	10.2	51	21.4	91	26.4	133	29.2
12	10.8	52	21.6	93	26.4	134	28.9
13	11.9	53	21.8	95	26.3	135	29.2
14	12.1	54	22.1	96	26.8	137	29.2
15	12.8	57	22.2	97	27.0	138	29.4
16	13.5	58	22.5	98	26.8	139	29.2
19	14.2	59	22.7	100	26.9	140	29.3
20	14.8	60	22.9	101	27.1	141	29.6
21	15.1	61	23.1	102	27.3	142	29.5
22	15.7	63	23.1	103	27.3	144	29.5
23	15.9	64	23.4	104	27.2	146	29.7
24	16.5	65	23.5	105	27.6	147	29.8
25	16.6	66	23.7	108	27.5	148	29.4
27	17.1	67	23.9	109	27.5	149	29.4
28	17.2	69	23.9	110	27.8		
29	17.7	71	24.5	111	27.7		
31	18.2	72	24.4	112	27.9		
32	18.1	73	24.5	113	27.9		
34	18.3	74	24.6	115	27.8		
35	18.6	75	24.8	116	28.0		
36	19.0	76	25.0	117	28.2		
37	19.3	78	24.7	118	28.4		
38	19.7	79	25.0	120	28.5		
39	19.7	80	25.2	122	28.5		

Table I.19: Raw permeation data for experiment T19. The standard deviation is ~0.2 µm.

t [s]	X [µm]	t [s]	X [µm]	t [s]	X [µm]	t [s]	X [µm]
0	0.0	41	11.8	82	17.8	123	22.1
1	0.7	42	11.8	83	17.9	124	22.3
2	0.8	44	12.3	84	17.9	125	22.3
3	1.5	45	12.7	86	18.2	126	22.2
5	1.9	46	12.4	87	18.0	128	22.5
7	2.4	47	12.6	88	18.6	130	23.0
8	3.4	49	13.3	89	18.9	131	23.1
9	4.0	50	13.8	90	18.6	132	23.1
10	4.6	51	13.8	93	18.6	133	23.2
12	5.2	52	13.6	94	18.7	134	23.1
13	5.0	53	13.8	95	19.0	135	23.5
14	5.8	54	14.2	96	19.4	137	23.2
15	6.4	57	14.3	97	19.3	138	23.4
16	6.7	58	14.0	98	19.4	140	23.2
17	6.4	59	14.3	100	19.8	141	23.6
20	6.7	60	14.7	101	20.2	142	23.8
21	7.3	61	15.4	102	20.2	144	24.2
22	7.7	62	15.1	104	20.3	145	24.2
23	8.1	64	15.0	105	20.3	147	24.2
24	8.4	65	15.3	106	20.4	148	24.2
25	8.8	66	15.9	108	20.6	149	24.2
27	9.2	68	15.9	109	20.7		
28	9.3	69	16.0	110	20.6		
29	9.8	71	16.1	111	20.9		
31	9.8	72	16.4	112	21.1		
32	10.2	73	16.3	113	21.2		
34	10.0	74	16.7	116	21.4		
35	10.6	75	17.1	117	21.7		
36	11.1	76	17.0	118	21.7		
37	10.9	78	16.9	119	21.8		
38	11.3	80	16.9	120	22.0		
39	11.7	81	17.1	122	21.7		

Table I.20: Raw permeation data for experiment T20. The standard deviation is ~2 μm.

t [s]	X [μm]	t [s]	X [μm]	t [s]	X [μm]	t [s]	X [μm]
0	0.0	41	19.1	81	25.1	122	28.7
1	1.6	42	19.1	82	25.0	124	28.7
2	3.4	43	19.4	83	25.4	125	28.9
3	5.0	44	19.6	84	25.3	126	28.9
5	6.5	46	19.7	86	25.6	127	29.1
7	7.6	47	20.3	88	25.5	128	29.0
8	8.1	49	20.2	89	25.7	130	29.2
9	9.0	50	20.7	90	26.2	131	29.4
10	10.0	51	20.9	91	25.9	132	29.5
12	10.7	52	20.8	93	26.4	134	29.6
13	11.3	53	21.0	94	26.5	135	29.6
14	11.6	54	21.5	96	26.3	137	29.8
15	12.4	57	21.7	97	26.7	138	29.7
16	13.1	58	21.8	98	26.7	139	30.0
19	13.4	59	22.2	100	26.8	140	30.0
20	14.1	60	22.5	101	26.8	141	30.1
21	14.5	61	22.6	102	27.1	142	30.4
22	14.8	62	22.5	103	27.2	145	30.4
23	15.4	64	22.8	104	27.3	146	30.4
24	15.5	65	22.9	106	27.4	147	30.5
25	15.9	67	23.4	108	27.5	148	30.5
27	15.9	68	23.3	109	27.7	149	30.7
29	16.7	69	23.7	110	27.8	150	30.8
30	17.0	71	23.9	111	27.8	152	30.8
31	17.3	72	23.6	112	27.9	153	30.8
32	17.7	73	23.9	115	28.1		
34	17.7	74	24.3	116	28.1		
35	17.9	76	24.3	117	28.3		
37	18.4	78	24.5	118	28.4		
38	18.4	79	24.5	119	28.5		
39	18.8	80	24.9	120	28.6		

APPENDIX J

EXPERIMENTAL DENSITY AND FIBER WEIGHT PERCENTAGES TO CALCULATE EXPERIMENTAL VOID CONTENTS

As discussed in Chapter IV, the experimental densities and the fiber weight percentages of the composites were needed to calculate the experimental void content of the composites. The results for the composites made from towpreg are in Table J.1 and the results for the composites made from commingled fibers are in Table J.2. The conditions of experiments T1-T16 and T21-T30 are listed in Table 4.5. The conditions of experiments C1-C12 are listed in Table 4.6.

Table J.1: Experimental densities and fiber weight percentages of composites made from towpreg

Experiment	Experimental Density [g/cm^3]	Fiber Weight Percent [%]
T1	1.39±0.02	58±2
T2	1.41±0.02	58±2
T3	1.42±0.01	58±2
T4	1.45±0.03	62±2
T5	1.46±0.02	68±1
T6	1.51±0.02	71±4
T7	1.48±0.01	69±2
T8	1.52±0.02	72±2
T9	1.77±0.03	65±2
T10	1.83±0.06	66±3
T11	1.81±0.03	66±2
T12	1.78±0.02	65±1
T13	1.90±0.05	74±2
T14	1.94±0.03	74±3
T15	1.90±0.04	73±1
T16	1.94±0.07	75±2
T21	1.35±0.03	56±3
T22	1.38±0.02	57±2
T23	1.44±0.03	69±2
T24	1.48±0.03	71±3
T25	1.78±0.02	68±1
T26	1.79±0.02	67±2
T27	1.76±0.04	69±2
T28	1.83±0.01	73±2

Table J.2: Experimental densities and fiber weight percentages of composites made from commingled fibers

Experiment	Experimental Density [g/cm^3]	Fiber Weight Percent [%]
C1	1.78±0.04	77±2
C2	1.79±0.03	76±1
C3	1.80±0.06	77±2
C4	1.75±0.03	75±1
C5	1.49±0.01	62±1
C6	1.54±0.04	64±2
C7	1.54±0.03	64±2
C8	1.56±0.06	65±1
C9	1.73±0.05	76±2
C10	1.75±0.03	76±2
C11	1.48±0.03	62±2
C12	1.49±0.02	62±1

APPENDIX K

RAW PERMEATION DATA FROM COMMINGLED FIBER PREFORM PROCESSING

The raw permeation data for the commingled fiber preform processing are located in Table K.1-K.8 on the following pages. In the tables, t is time and X is penetration depth. The conditions of experiments C1-C8 are listed in Table 4.6.

Table K.1: Raw permeation data for experiment C1. The standard deviation is ~1 µm.

t [s]	X [µm]	t [s]	X [µm]
0	0.0	41	7.8
2	0.5	42	7.8
3	0.5	43	8.0
5	1.4	44	8.0
6	2.0	45	8.1
7	2.4	46	8.5
8	2.8	47	8.6
9	3.1	49	8.7
10	3.5	50	8.8
12	3.9	52	9.0
13	4.1	53	9.2
14	4.4	54	9.2
16	4.5	56	9.2
17	4.9	57	9.4
19	5.1	58	9.5
20	5.3	59	9.5
21	5.5	60	9.7
22	5.6	63	9.7
23	5.8	64	9.9
24	6.2	65	10.1
25	6.3	66	10.1
28	6.3	67	10.1
29	6.5	68	10.2
30	6.7	69	10.3
31	7.0	71	10.4
32	7.0	72	10.6
34	7.3	73	10.6
35	7.4	75	10.8
36	7.3	76	10.8
37	7.6	78	10.9
39	7.8		

Table K.2: Raw permeation data for experiment C2. The standard deviation is ~0.7 μm.

t [s]	X [μm]	t [s]	X [μm]
0	0.0	41	5.5
1	1.2	42	5.7
2	1.8	43	5.4
3	2.5	44	5.9
5	4.0	45	6.0
6	2.9	46	6.0
7	3.3	47	6.1
8	3.3	49	6.1
9	3.7	51	6.1
10	3.7	52	6.2
13	3.9	53	6.2
14	4.3	54	6.3
15	4.1	56	6.2
16	4.5	57	6.4
17	4.2	58	6.5
19	4.4	59	6.5
20	4.6	60	6.4
21	4.4	61	6.6
22	4.8	64	6.6
23	4.9	65	6.6
25	5.0	66	6.9
27	4.8	67	6.7
28	5.0	68	6.8
29	5.3	69	6.9
30	5.2	71	7.0
31	5.0	72	7.0
32	5.4	73	7.1
34	5.4	74	7.0
35	5.4	76	7.2
36	5.7	78	7.1
38	5.8	79	7.1
39	5.4		

Table K.3: Raw permeation data for experiment C3. The standard deviation is ~1 μm.

t [s]	X [μm]	t [s]	X [μm]
0	0.0	41	11.2
1	4.2	43	11.2
2	2.5	44	11.4
5	2.8	45	11.4
6	3.7	46	11.7
7	4.0	47	11.7
8	4.7	49	11.8
9	5.1	50	12.0
10	5.7	52	12.1
12	6.1	53	12.3
13	6.5	54	12.5
15	6.8	56	12.4
16	7.1	57	12.7
17	7.4	59	12.7
19	7.7	60	12.8
20	7.8	61	13.0
21	8.3	62	13.1
22	8.3	64	13.2
24	8.8	66	13.2
25	8.9	69	13.4
27	9.3	71	13.6
28	9.4	72	13.7
29	9.5	73	13.8
30	9.8	75	13.8
31	9.8	76	14.0
34	10.1	78	14.1
35	10.3	79	14.1
36	10.5	80	14.2
37	10.5		
38	10.6		
39	10.9		

Table K.4: Raw permeation data for experiment C4. The standard deviation is ~4 μm.

t [s]	X [μm]	t [s]	X [μm]
0	0.0	41	7.7
1	0.6	42	7.8
2	1.0	44	8.1
5	1.5	45	8.2
6	2.0	46	8.4
7	2.2	47	8.6
8	2.7	49	8.5
9	2.9	50	8.6
10	3.1	51	9.0
12	3.4	52	9.0
13	3.9	54	9.0
15	4.2	56	9.2
16	4.2	57	9.3
17	4.6	58	9.4
19	4.6	59	9.6
20	5.1	60	9.7
21	5.2	61	10.0
22	5.2	62	10.1
23	5.7	65	10.1
25	5.8	66	10.2
27	6.1	67	10.3
28	6.0	68	10.3
29	6.3	69	10.3
30	6.5	71	10.4
31	6.8	72	10.7
32	6.8	73	10.6
35	7.1		
36	7.2		
37	7.4		
38	7.6		
39	7.8		

Table K.5: Raw permeation data for experiment C5. The standard deviation is ~1 μm.

t [s]	X [μm]	t [s]	X [μm]
0	0.0	41	7.8
1	0.6	42	7.9
2	1.1	43	7.9
3	1.2	44	8.1
5	1.9	46	8.2
6	2.4	47	8.4
8	2.8	49	8.5
9	3.0	50	8.6
10	3.4	51	8.7
12	3.6	52	8.9
13	4.0	53	8.9
14	4.2	54	9.1
15	4.4	56	9.2
16	4.7	57	9.2
17	4.8	59	9.3
19	5.2	60	9.5
21	5.3	61	9.5
22	5.5	62	9.7
23	5.7	64	9.7
24	5.8	65	9.9
25	6.1	66	9.9
27	6.1	67	10.0
28	6.3	68	10.1
29	6.5	69	10.3
30	6.7	72	10.3
31	6.7	73	10.4
34	7.0	74	10.5
35	7.0	75	10.6
36	7.3	76	10.7
37	7.4	78	10.8
38	7.5	79	10.9
39	7.6	80	10.9

Table K.6: Raw permeation data for experiment C6. The standard deviation is ~0.5 μm.

t [s]	X [μm]	t [s]	X [μm]
0	0.0	42	6.6
1	0.3	43	6.6
2	0.6	44	6.9
5	0.9	46	7.0
6	1.1	47	7.1
7	1.5	49	7.3
8	1.7	50	7.4
9	2.1	51	7.6
10	2.3	52	7.7
12	2.5	53	7.8
13	2.8	54	8.0
15	2.9	57	8.1
16	3.2	58	8.2
17	3.3	59	8.4
19	3.6	60	8.4
20	3.8	61	8.6
21	3.9	62	8.6
22	4.2	65	8.8
23	4.3	66	8.8
24	4.5	67	9.1
27	4.6	68	9.1
28	4.9	69	9.2
29	5.0	71	9.3
30	5.2	72	9.5
31	5.3	73	9.5
32	5.6	75	9.7
34	5.7	76	9.8
35	5.9	78	9.9
37	6.0	79	10.0
38	6.2		
39	6.3		
41	6.3		

Table K.7: Raw permeation data for experiment C7. The standard deviation is ~0.6 μm.

t [s]	X [μm]	t [s]	X [μm]
0	0.0	41	10.4
1	1.6	42	10.7
2	2.4	43	10.8
3	2.8	44	11.0
5	3.5	45	11.2
6	3.9	46	11.4
7	4.4	47	11.6
8	4.7	50	11.6
9	5.1	51	11.8
12	5.4	52	12.0
13	5.7	53	12.2
14	5.9	54	12.3
15	6.3	56	12.5
16	6.6	57	12.6
17	6.8	58	12.8
19	7.0	59	13.0
20	7.3	60	13.1
21	7.5	62	13.3
22	7.8	64	13.4
23	7.9	65	13.6
25	8.2	66	13.7
27	8.4	67	13.9
28	8.6	68	14.0
29	8.8	69	14.1
30	9.0	71	14.3
31	9.2	72	14.5
32	9.4	73	14.6
34	9.6	75	14.6
35	9.8	76	14.8
36	9.9	78	14.9
38	10.1	79	15.0
39	10.3	80	15.0

Table K.8: Raw permeation data for experiment C8. The standard deviation is ~0.4 μm.

t [s]	X [μm]	t [s]	X [μm]
0	0.0	41	9.4
1	0.7	42	9.6
2	1.3	43	9.7
3	1.8	45	9.9
5	2.3	46	10.1
7	2.7	47	10.3
8	3.2	49	10.5
9	3.5	50	10.6
10	3.8	51	10.9
12	4.1	53	10.9
13	4.4	54	11.2
14	4.7	56	11.3
15	5.0	57	11.5
17	5.3	58	11.8
19	5.6	59	11.8
20	5.7	60	12.0
21	6.1	61	12.2
22	6.3	64	12.4
23	6.5	65	12.5
24	6.7	66	12.7
27	7.0	67	12.9
28	7.2	68	13.0
29	7.5	69	13.2
30	7.8	71	13.4
31	8.0	73	13.6
32	8.1	74	13.6
34	8.3		
36	8.5		
37	8.7		
38	8.9		
39	9.2		

VITA

Jurron Bradley was born February 8, 1973, in Mobile, Alabama. He graduated from Vanderbilt University in May 1995 with a Bachelor of Engineering degree in Chemical Engineering. He enrolled in the School of Chemical Engineering at the Georgia Institute of Technology in September 1995. He earned a Master of Science Degree in Chemical Engineering in December 1997 and a Doctor of Philosophy Degree in Chemical Engineering in May 2001. Currently, he is employed by Praxair, Inc.